

**THE ROLE OF QUORUM SENSING REGULATORS IN VIBRIO  
PARAHAEMOLYTICUS**

by

Sai Siddarth Kalburge

A dissertation submitted to the Faculty of the University of Delaware in partial fulfillment of the requirements for the degree of Doctor of Philosophy in Biological Sciences

Winter 2017

©2017 Sai Siddarth Kalburge  
All Rights Reserved

ProQuest Number: 10254180

All rights reserved

INFORMATION TO ALL USERS

The quality of this reproduction is dependent upon the quality of the copy submitted.

In the unlikely event that the author did not send a complete manuscript and there are missing pages, these will be noted. Also, if material had to be removed, a note will indicate the deletion.



ProQuest 10254180

Published by ProQuest LLC (2017). Copyright of the Dissertation is held by the Author.

All rights reserved.

This work is protected against unauthorized copying under Title 17, United States Code  
Microform Edition © ProQuest LLC.

ProQuest LLC.  
789 East Eisenhower Parkway  
P.O. Box 1346  
Ann Arbor, MI 48106 – 1346

**THE ROLE OF QUORUM SENSING REGULATORS IN VIBRIO  
PARAHAEMOLYTICUS**

by

Sai Siddarth Kalburge

Approved: \_\_\_\_\_  
Robin W. Morgan, Ph.D.  
Chair of the Department of Department of Biological Sciences

Approved: \_\_\_\_\_  
George H. Watson, Ph.D.  
Dean of the College of Arts and Sciences

Approved: \_\_\_\_\_  
Ann L. Ardis, Ph.D.  
Senior Vice Provost for Graduate and Professional Education

I certify that I have read this dissertation and that in my opinion it meets the academic and professional standard required by the University as a dissertation for the degree of Doctor of Philosophy.

Signed:

---

E. Fidelma Boyd, Ph.D.  
Professor in charge of dissertation

I certify that I have read this dissertation and that in my opinion it meets the academic and professional standard required by the University as a dissertation for the degree of Doctor of Philosophy.

Signed:

---

Diane S. Herson, Ph.D.  
Member of dissertation committee

I certify that I have read this dissertation and that in my opinion it meets the academic and professional standard required by the University as a dissertation for the degree of Doctor of Philosophy.

Signed:

---

Thomas E. Hanson, Ph.D.  
Member of dissertation committee

I certify that I have read this dissertation and that in my opinion it meets the academic and professional standard required by the University as a dissertation for the degree of Doctor of Philosophy.

Signed:

---

Shawn W. Polson, Ph.D.  
Member of dissertation committee

I certify that I have read this dissertation and that in my opinion it meets the academic and professional standard required by the University as a dissertation for the degree of Doctor of Philosophy.

Signed:

---

Salil A. Lachke, Ph.D.  
Member of dissertation committee

## **ACKNOWLEDGMENTS**

I owe a debt of gratitude to my advisor Prof. E. Fidelma Boyd. To say that she “guided” me through my PhD would be a gross understatement. Her contribution to my development as a researcher and an individual has been immense. Her constant support throughout my graduate career has been a great source of strength and motivation. Her earnestness in prepping me for presentations, meetings, exams and writing manuscripts, and her belief that my success is a reflection upon her has always inspired me to perform better. I am proud to have been advised by Fidelma and sincerely feel she is an Outstanding Mentor and truly a great friend. I hope that I can make her proud of me someday.

Ever since my preliminary exam in the graduate program, Dr. Diane Herson and Dr. Tom Hanson have been constant sources of support. As members of my committee they have challenged my thought process and guided my project, providing helpful insights at all meetings. Dr Shawn Polson, who I rotated with, has been a great mentor for all my bioinformatics projects. I thank him and Dr Salil Lachke for providing me valuable feedback that has guided my projects towards success.

The Boyd lab has been family throughout my graduate career. I would like to thank every member, past and present, who in one way or another, big or small, have contributed to the success of my projects. Their readiness to help with experiments

and to be involved in preparation for presentations and meetings has been invaluable. My eternal thanks to Serge Ongagna, Nithyananda Chowdhury and Brian Whitaker, who have each, at various stages mentored and trained me; Discussions with them about experiments and results have helped shape my ability to think, plan and critically analyze experiments. I would also like to thank Megan Carpenter for not just being a great colleague but for also being a great friend. As any true friend would be, she was also my biggest critic and always provided suggestions for improvement. I would also like to thank JB Lubin, Brandy Menges, Abish Regmi and Nathan McDonald who have all been great friends and sounding boards through my graduate career.

A number of individuals in the Biological sciences department have made immense contributions to my graduate career. I would like to thank Dr Melinda Duncan for being extremely supportive of me during my time here. Dr Erica Selva has been ever so helpful throughout my graduate career. I cannot thank Betty Cowgill enough for making the administrative part of graduate school a breeze. She always kept every document ready even before I needed it. Special thanks to Dr Carlton Cooper and Tisa Della-Volpe for making my teaching experience so wonderful.

Words cannot do justice to the contribution of my parents, Ashok and Shailaja Anand towards everything that I ever achieve in life. I would like to thank them for all the unconditional love and support they have provided me all through my life. I would also like to thank my sister Rohini for being my best 'buddy'. My fiancé Neethu has

been a big pillar of strength throughout my entire time in graduate school. I am grateful to all the support that I have received from her and her family.

Last but not least by any stretch of imagination, I would like to thank all my friends. Being away from home in a different country is hard enough but when you guys have made this journey so enjoyable. Special thanks to Vignesh, Vimal, Praveen, Adithya (Boddu), Manju (Montu), Pratima, Hemanth and Srinivas. It was great to have you guys on this journey!

## RESULTING PUBLICATIONS FROM DISSERTATION

**Quorum Sensing Regulators are required for Metabolic Fitness in *Vibrio parahaemolyticus*.**

Kalburge, S.S., Carpenter, M.R., Rozovsky, S., Boyd, E.F.

Accepted to be published in Infection and Immunity journal. 2017

**Complete genome sequence of *Vibrio parahaemolyticus* environmental strain UCM-V493.**

Kalburge, S.S., Polson, S.W., Boyd Crotty, K., Katz, L., Turnsek, M., Tarr, C.L., Martinez-Urtaza, J., Boyd, E.F.

Genome Announc. 2014 Mar 13;2(2). pii: e00159-14. doi: 10.1128/genomeA.00159-14.

**High-salt preadaptation of *Vibrio parahaemolyticus* enhances survival in response to lethal environmental stresses.**

Kalburge, S.S. Whitaker, W.B., Boyd, E.F.

J Food Prot. 2014 Feb;77(2):246-53. doi: 10.4315/0362-028X.JFP-13-241

## TABLE OF CONTENTS

LIST OF TABLES .....	xiv
LIST OF FIGURES .....	xvi
ABSTRACT .....	xx

### Chapter

1. INTRODUCTION .....	1
<i>Vibrio parahaemolyticus</i> : Epidemiology and Pathogenesis .....	1
Quorum Sensing in Bacteria .....	7
Quorum Sensing in Vibrios .....	8
Quorum response regulator LuxO and its interaction with sigma 54, RpoN .....	13
Quorum Regulatory RNAs (Qrrs) .....	13
Quorum sensing master output regulators AphA and OpaR .....	17
Quorum sensing and Metabolism .....	19
Dissertation Work .....	21
2. QUORUM SENSING REGULATORS ARE REQUIRED FOR METABOLIC FITNESS IN <i>VIBRIO PARAHAEMOLYTICUS</i> .....	25
Introduction .....	25
Material and Methods .....	32
Bacterial strains, media and culture conditions. ....	32
Construction of <i>V. parahaemolyticus</i> RIMD2210633 quorum sensing deletion mutants .....	32
<i>In vivo</i> competition assays .....	33
Capsule polysaccharide (CPS) production, motility and biofilm assays .....	35
RNA extraction, Illumina sequencing and quantitative real time PCR (qPCR) .....	35
RNA-Seq analysis. ....	37
Growth analysis and <i>in vitro</i> competition assays. ....	38
Bioinformatics analysis of OpaR and AphA binding sites .....	39
Purification of OpaR .....	40
Electrophoretic Mobility Shift Assays . ....	42

Results .....	42
Deletion of <i>luxO</i> or <i>aphA</i> leads to a defect in intestinal colonization. ....	42
RNA-seq data and comparative analysis of gene expression in mouse intestinal mucus. ....	49
Metabolism and transporter genes are downregulated in the <i>luxO</i> mutant. ....	54
Growth comparisons of wild-type and mutant strains on different carbon sources. ....	57
Deletion of <i>opaR</i> leads to increased metabolic fitness in intestinal mucus and its components. ....	61
OpaR binding sites in the promoter regions of carbon transport and metabolism genes. ....	63
Discussion.....	67
3. RNA-SEQ TRANSCRIPTOME ANALYSIS OF THE SIGMA-54 REGULON OF <i>VIBRIO PARAHAEMOLYTICUS</i> RIMD2210633. ....	90
Introduction .....	90
Materials and Methods .....	94
RNA extraction.....	94
Illumina sequencing.....	94
RNA-Seq analysis. ....	95
Binding site analysis. ....	96
Results and Discussion.....	97
RNA-seq analysis of <i>V. parahaemolyticus</i> wild-type and $\Delta rpoN$ strains. .	97
Genes induced in the <i>rpoN</i> mutant when grown in minimal media supplemented with glucose.....	101
Genes repressed in the <i>rpoN</i> mutant when grown in minimal media supplemented with glucose.....	107
Genes induced in the <i>rpoN</i> mutant when grown in minimal media supplemented with intestinal mucus.....	110
Genes repressed in the <i>rpoN</i> mutant when grown in minimal media supplemented with intestinal mucus.....	115
Genes differentially regulated in the <i>rpoN</i> mutant in both glucose and mouse intestinal mucus.....	116
OpaR was not induced in the <i>rpoN</i> mutant under the conditions examined.....	119
OpaR binding sites in the promoter regions of ribosomal proteins.....	123

4.	COMPLETE GENOME SEQUENCE OF <i>VIBRIO PARAHAEMOLYTICUS</i> ENVIRONMENTAL STRAIN UCM-V493.....	161
	Introduction .....	161
	Materials and Methods .....	162
	Results and Discussion.....	163
5.	HIGH SALT PRE-ADAPTATION OF <i>VIBRIO PARAHAEMOLYTICUS</i> ENHANCES SURVIVAL TO LETHAL ENVIRONMENTAL STRESSES	164
	Introduction .....	164
	Materials and Methods .....	169
	Bacterial strains, plasmids and growth conditions. ....	169
	Construction of the $\Delta cadA$ deletion mutant.....	170
	Acid survivability assays.....	171
	High salinity pre-adapted acid survivability assays. ....	171
	High salinity pre-adapted temperature survivability assays. ....	172
	High salinity pre-adapted acid survivability assays in other <i>Vibrio</i> species.....	173
	Statistical analysis. ....	173
	Results .....	173
	Pre-adaptation in mild acid condition increases survival under lethal acid stress conditions.....	173
	High salt adaptation increases survival under lethal acid stress conditions. ....	175
	High salt concentration cross-protects against cold shock but does not protect against heat. ....	178
	Increased survival under lethal acid stress upon high salt adaptation is consistent among other pathogenic <i>Vibrio</i> species. ....	180
	Discussion.....	182
6.	PERSPECTIVES AND FUTURE DIRECTIONS .....	188
	Quorum Sensing and Metabolism .....	188
	Role of metabolism in <i>V. parahaemolyticus</i> <i>in vivo</i> colonization.....	190
	Investigation of <i>V. parahaemolyticus</i> small RNAs .....	191
	REFERENCES .....	193

## Appendix

A.	EFFECT OF LOW SALT ON LETHAL ACID STRESS SURVIVAL OF <i>VIBRIO PARAHAEMOLYTICUS</i> . .....	220
B.	EFFECT OF ORGANIC ACID AND BILE STRESS ON <i>VIBRIO PARAHAEMOLYTICUS</i> . .....	223
C.	GROWTH IN HIGH SALT PROVIDES COMPETITIVE ADVANTAGE <i>IN VIVO</i> . .....	227
D.	<i>IN VIVO</i> COLONIZATION ABILITY OF ENVIRONMENTAL ISOLATE UCM-V493 AND GALACTOSE UTILIZATION IN THE STRAIN. ....	228
E.	ADDITIONAL <i>IN VITRO</i> AND <i>IN SILICO</i> ANALYSIS OF <i>VIBRIO PARAHAEMOLYTICUS</i> QUORUM SENSING MUTANTS. ....	232
F.	RNASEQ EXPRESSION ANALYSIS OF THE WILD-TYPE AND THE <i>LUXO</i> MUTANT IN GLUCOSE. ....	250
G.	ROLE OF QUORUM SENSING IN OSMOTIC STRESS RESPONSE IN <i>VIBRIO PARAHAEMOLYTICUS</i> . ....	262
H.	BACTERIOPHAGE f237 IS REGULATED BY QUORUM SENSING .....	266
I.	IMPORTANT <i>VIBRIO CHOLERAE</i> COLONIZATION FACTOR, GbpA DOES NOT PLAY A ROLE IN <i>VIBRIO PARAHAEMOLYTICUS IN VIVO</i> COLONIZATION. ....	267
	Introduction .....	267
	Materials and Methods .....	269
	Bacterial strains, media and culture conditions. ....	269
	Construction of <i>V. parahaemolyticus</i> RIMD2210633 <i>gbpA</i> deletion mutant. ....	270
	Motility and biofilm assays. ....	270
	<i>In vivo</i> competition assays. ....	270
	Results and Discussion .....	272
	$\Delta$ <i>gbpA</i> mutant behaves similar to wild-type <i>in vitro</i> . ....	272
	Deletion of <i>gbpA</i> does not cause any defect in <i>in vivo</i> colonization. ....	273
	Conclusions .....	275
J.	CHARACTERIZATION OF <i>VIBRIO PARAHAEMOLYTICUS</i> TYPE 6 SECRETION SYSTEM MUTANTS <i>IN VITRO</i> AND <i>IN VIVO</i> .....	278

K.	RNASEQ ANALYSIS STEP-BY-STEP PROTOCOL .....	281
L.	ANIMAL WORK APPROVAL.....	287
M.	PERMISSIONS RIGHTS LINK .....	290

## LIST OF TABLES

Table 1	The key gene systems in the OpaR regulon. ....	19
Table 2	Bacterial strains and plasmids used in this study .....	73
Table 3	Primers used in this study.....	74
Table 4	Differential expressed genes induced in the <i>luxO</i> mutant compared to wild-type.....	76
Table 5	Differential expressed genes repressed in the <i>luxO</i> mutant compared to wild-type.....	80
Table 6	Putative OpaR binding sites identified by the MOODS algorithm. ....	84
Table 7	Putative AphA binding sites identified by the MOODS algorithm.....	89
Table 8	Bacterial strains used in this study .....	124
Table 9	Primers used in this study.....	124
Table 10	Genes upregulated in the <i>rpoN</i> mutant in glucose .....	125
Table 11	Genes downregulated in the <i>rpoN</i> mutant in glucose.....	137
Table 12	Genes upregulated in the <i>rpoN</i> mutant in mouse intestinal mucus .....	151
Table 13	Genes downregulated in the <i>rpoN</i> mutant in mouse intestinal mucus ..	155
Table 14	Putative OpaR binding sites identified using the MOODS algorithm ..	160
Table 15	Bacterial strains and plasmids used in this study .....	186
Table 16	Primers used in this study.....	187
Table 17	Primers used in this study.....	231
Table 18	Biolog phenotype microarray data for wild-type and quorum sensing mutants. ....	244

Table 19	Summary of quorum sensing biolog data. Numbers indicate carbon sources with significant difference in AUC compared to wild-type. ....	249
Table 20	Genes upregulated in the <i>luxO</i> mutant in glucose.....	253
Table 21	Genes downregulated in the <i>luxO</i> mutant in glucose .....	257
Table 22	Putative binding sites in the Ectoine biosynthesis regulatory region identified using the MOODS algorithm. Start and End indicate number of base pairs upstream of the ATG start codon. ....	262
Table 23	Putative OpaR binding sites in the identified using the MOODS algorithm. Start and End indicate number of base pairs upstream of the ATG start codon. ....	263
Table 24	Putative AphA binding sites in the identified using the MOODS algorithm. Start and End indicate number of base pairs upstream of the ATG start codon. ....	264
Table 25	Putative BetI binding sites in the identified using the MOODS algorithm. Start and End indicate number of base pairs upstream of the ATG start codon. ....	265
Table 26	Putative OpaR binding sites identified using the MOODS algorithm. Start and End indicate number of base pairs upstream of the ATG start codon. ....	266
Table 27	Bacterial strains and plasmids used in this study .....	276
Table 28	Primers used in this study.....	277

## LIST OF FIGURES

Figure 1	An overview of the quorum sensing pathway in <i>V. parahaemolyticus</i> ... 12
Figure 2	Sequence homology between the five quorum regulatory RNAs (Qrrs) in <i>V. parahaemolyticus</i> RIMD2210633. .... 15
Figure 3	Qrr interaction with quorum sensing master regulator OpaR and LCD regulator AphA..... 16
Figure 4	Regulatory interactions among the components of the quorum sensing pathway in <i>V. parahaemolyticus</i> . .... 29
Figure 5	<i>In vivo</i> competition assays between the wild-type and each QS mutant. 44
Figure 6	Expression analysis of quorum sensing master regulators and <i>qrrs</i> . ..... 46
Figure 7	<i>In vitro</i> phenotypic analysis of <i>V. parahaemolyticus</i> RIMD2210633 and the QS mutants. .... 48
Figure 8	RNA-seq sequencing yield and RNA classification..... 50
Figure 9	RNA Seq MA-plot showing expression in the <i>luxO</i> mutant relative to wild-type..... 51
Figure 10	Cluster of Orthologous Groups (COG) classification of differentially expressed genes in the <i>luxO</i> mutant. .... 52
Figure 11	qPCR validations of RNA Seq Expression in the <i>luxO</i> mutant relative to wild-type..... 56
Figure 12	Carbon phenotypic microarrays of <i>V. parahaemolyticus</i> wild-type and QS regulator mutants..... 59
Figure 13	Growth characteristics of <i>V. parahaemolyticus</i> wild-type and QS regulator mutants in various sugars and amino acids..... 60
Figure 14	<i>In vitro</i> competition assays of <i>V. parahaemolyticus</i> wild-type and the QS mutants <i>luxO</i> , <i>opaR</i> and <i>aphA</i> . .... 63

Figure 15	OpaR binding sites in the regulatory regions of metabolism and transporter genes.....	66
Figure 16	$\Delta rpoN$ vs wild-type RNA-seq sequencing yield and RNA classification in glucose and mucus. (A&C). .....	99
Figure 17	RNA Seq MA-plots showing expression in the <i>rpoN</i> mutant relative to wild-type.....	100
Figure 18	Circos plot showing classification of differentially expressed genes between the <i>rpoN</i> mutant and the wild-type in glucose into Cluster of Orthologous Groups (COG). .....	105
Figure 19	Cluster of Orthologous Groups (COG) classification of differentially expressed genes in the <i>rpoN</i> mutant when grown in glucose.....	106
Figure 20	Circos plot showing classification of differentially expressed genes between the <i>rpoN</i> mutant and the wild-type in mucus into Cluster of Orthologous Groups (COG). .....	113
Figure 21	Cluster of Orthologous Groups (COG) classification of differentially expressed genes in the <i>rpoN</i> mutant when grown in mucus. ....	114
Figure 22	Differentially Expressed Genes in the <i>rpoN</i> mutant. ....	118
Figure 23	qPCR Expression of Secretion System Effectors in the <i>rpoN</i> mutant grown in mouse intestinal mucus as sole carbon source. ....	119
Figure 24	Expression of Quorum Sensing Master Regulators. ....	121
Figure 25	Expression of Quorum Regulatory RNAs ( <i>qrrs</i> ). ....	122
Figure 26	The lysine decarboxylase pathway.....	168
Figure 27	Effect of lethal acid stress on the <i>cadA</i> deletion mutant. ....	175
Figure 28	Effect of high salt adaptation on survival in lethal acid stress. ....	177
Figure 29	Effect of high salt concentration on survival under high-temperature stress and cold stress.....	179
Figure 30	Effect of high salt adaptation on the survival of other <i>Vibrio</i> species under lethal acid stress. ....	181

Figure 31	Effect of low salt, lethal acid stress on <i>V. parahaemolyticus</i> cells pre-adapted in LB media supplemented with (A) 1% NaCl (B) 3% NaCl and (C) 6% NaCl.....	221
Figure 32	Effect of low salt, lethal acid stress on <i>V. parahaemolyticus</i> cells pre-adapted in LB media acidified to mild acid pH 5.5 and supplemented with (A) 1% NaCl (B) 3% NaCl and (C) 6% NaCl.....	222
Figure 33	Effect of lethal organic acid stress on <i>V. parahaemolyticus</i> . ....	225
Figure 34	Effect of bile salt stress on <i>V. parahaemolyticus</i> . ....	226
Figure 35	<i>In vivo</i> competition assay between WBWlacZ and WT RIMD2210633 and WBWlacZ and WT RIMD2210633 grown in 6% NaCl. ....	227
Figure 36	<i>In vivo</i> persistence competition assay of UCM-V493 vs WBWlacZ. ....	229
Figure 37	Growth of RIMD2210633, UCM-V493 and UCM-V493 $\Delta$ galK on LB, M9 glucose and M9 galactose. ....	230
Figure 38	Analysis of biofilm formation using the crystal violet assay. ....	232
Figure 39	Analysis of motility of the quorum sensing mutants.....	233
Figure 40	Analysis of Capsule Polysaccharide (CPS) production using the Congo red assay. ....	234
Figure 41	Growth analysis of the $\Delta$ luxO mutant in mucus and individual mucus components.....	235
Figure 42	Growth analysis of the $\Delta$ aphA mutant in mucus and individual mucus components.....	236
Figure 43	Growth analysis of the $\Delta$ opaR mutant in mucus and individual mucus components.....	237
Figure 44	Doubling times of strains grown in mucus and individual mucus components.....	238
Figure 45	Colony Forming Units (CFUs) counts for <i>V. parahaemolyticus</i> .....	239
Figure 46	COG Classification of differentially expressed genes between the luxO mutant and the wild-type cells grown in mucus.....	241
Figure 47	Coverage across downregulated gene clusters. ....	242

Figure 48	Pathway analysis using KEGG colorizer. ....	243
Figure 49	COG Classification of differentially expressed genes between the <i>luxO</i> mutant and the wild-type cells grown in glucose. ....	252
Figure 50	<i>In vitro</i> characterization of the <i>gbpA</i> deletion mutant. (A) Growth in LB and M9 minimal medium supplemented with glucose (B) Swarming motility (C) Biofilm formation.....	273
Figure 51	<i>In vivo</i> colonization competition using streptomycin pre-treated adult mouse model. Competition assay was performed between $\Delta gbpA$ and WBWlacZ.....	274
Figure 52	Growth analysis of the T6SS mutants in (A) LB 3% NaCl (B) M9 minimal media supplemented with 10mM glucose and (C) M9 minimal media supplemented with 30 $\mu$ g/ml cecal mucus.....	279
Figure 53	<i>In vitro</i> colonization competition assay between POR1 $\Delta hcp1\Delta hcp2$ and WBWlacZ.....	280

## ABSTRACT

*Vibrio parahaemolyticus* is the leading cause of bacterial seafood-borne gastroenteritis worldwide as well as a significant pathogen of shellfish and fish. In addition, the geographic range of this species and others within the genus is spreading globally due to climate change. Our knowledge of how this pathogen colonizes the human intestine, the first step in its pathogenesis, is limited. Some of the most influential factors for survival and pathogenesis of bacteria in changing environments include stress response mechanisms, motility, production of virulence factors and formation of a biofilm. Bacteria possess a communication mechanism, where they synchronize actions with other bacteria in the population by regulating the expression of genes that control these actions. Bacteria do this by secreting molecules called autoinducers that act as extracellular signals that other bacteria in the environment can respond to. This process of bacterial cell to cell communication is called quorum sensing. The work in this dissertation examined the role of the downstream regulators of the quorum sensing pathway in *V. parahaemolyticus* colonization and fitness. By examining single and double deletion mutants of the three downstream regulators of the quorum sensing pathway, the response regulator *luxO* and the two quorum sensing master regulators *opaR* and *aphA*, we determined that the low cell density master regulator AphA is important for *in vivo* fitness and that over-expression of the high

cell density master regulator *opaR* is detrimental to *in vivo* fitness. We then performed RNASeq transcriptome analysis on the wild-type and the *luxO* mutant, which was found to be defective *in vivo* and over-expressed the high cell density regulator *opaR*. The transcriptome analysis revealed that 60% of genes downregulated in the *luxO* mutant were involved in metabolism and transport, suggesting that the mutant could have a metabolic disadvantage compared to wild-type. This was indeed confirmed by carbon phenotype microarrays, which revealed that the *luxO* mutant was significantly defective in growth compared to the wild-type when grown in a number of carbon sources. Additionally, the *aphA* mutant, which was also defective *in vivo*, exhibited similar growth defects compared to wild-type. Both *luxO* and *aphA* mutant strains were defective in 25 carbon sources compared to wild-type. By bioinformatics and biochemical analysis, we further showed that OpaR binds directly to the regulatory regions of genes and operons involved in carbon transport and metabolism thereby indicating a role for this regulator in metabolism in the bacteria.

In Chapter 3, we perform comparative transcriptome analysis of wild-type versus the super-colonizer *rpoN* mutant. RpoN is a sigma factor that is involved in the transcription of 100s of genes but requires an activator protein to be functional. We examined this regulator since one of its activators is LuxO and together they regulate the expression of the quorum sensing master regulators OpaR and AphA. We found a number of genes were differentially regulated between the wild-type and the *rpoN* mutant including a number of genes encoding for ribosomal proteins and tRNAs that were upregulated in the *rpoN* mutant. This was in keeping with the fact that we had

previously found the mutant to be metabolically more fit than the wild-type. Expression of the QS master regulators in the *rpoN* mutant did not match the expression pattern seen in the *luxO* mutant. We speculate that these differences in expression between the *luxO* and *rpoN* mutants might be due to increased expression of one of the quorum regulatory small RNA, *qrr2* in the *rpoN* mutant.

Other work in this dissertation focuses on the acid and osmotic stress response mechanisms in *V. parahaemolyticus*. As a marine bacteria and a gastrointestinal pathogen, *V. parahaemolyticus* constantly encounters various salt gradients and is subjected to acid stresses within the gastrointestinal tract. We examined the effect of lethal acid stress on the bacteria under varying degrees of salt concentration. We found that preadaptation of the bacteria to high salt is beneficial for the bacteria as it leads to improved survival under lethal acid stress and other lethal environmental stresses.

Finally, we performed whole genome sequencing on an environmental isolate of *V. parahaemolyticus*, strain UCM-V493. UCM-V493 was isolated from a sediment sample in Spain in 2002. We were interested in determining differences between pathogenic and non-pathogenic strains. We sequenced this strain to completion and closed both circular chromosomes with a combination of Illumina and Pacbio sequencing. Comparative genomic analysis uncovered many regions of difference between UCM-V493 and RIMD2210633, the canonical clinical isolate.

## Chapter 1

### INTRODUCTION

#### ***Vibrio parahaemolyticus*: Epidemiology and Pathogenesis**

*Vibrio parahaemolyticus* is a Gram-negative, rod-shaped, halophilic bacterium that inhabits a wide range of marine ecosystems (Colwell, Kaper, and Joseph 1977; Fujino et al. 1972; Joseph, Colwell, and Kaper 1982; Kaneko and Colwell 1973; Krantz, Colwell, and Lovelace 1969; Thompson et al. 2004). It is the leading bacterial cause for seafood-related gastroenteritis worldwide (Scallan et al. 2011; Su and Liu 2007; Letchumanan, Chan, and Lee 2014). It belongs to the family Vibrionaceae that also includes other human pathogens such as *V. cholerae* and *V. vulnificus*. The first reported outbreak of *V. parahaemolyticus* occurred in Japan in 1950 and was caused by consumption of contaminated sardines (Fujino 1953). The majorities of infections today are mainly associated with consumption of raw or undercooked shellfish and in the United States particularly oysters (Daniels et al. 2000; Iwamoto et al. 2010; McLaughlin et al. 2005). In healthy individuals, *V. parahaemolyticus* infection causes mild, self-limited gastroenteritis with watery diarrhea lasting up to 3 days (Daniels 2000; Honda 2008; Nair et al. 2007; O'Boyle and Boyd 2014). In immunocompromised individuals, however, the infection can result in severe inflammatory diarrhea leading to septicemia and death (Honda 2008; O'Boyle and Boyd 2014). In

some instances, *V. parahaemolyticus* has also been reported to cause wound infections resulting in necrotizing fasciitis (Ralph and Currie 2007; Tena et al. 2010).

In a 2015 Food Safety Report the Center for Disease Control and Prevention (CDC) reported a 34% increase in *Vibrio* infections in the United States as compared to 2006-2008 infection rates. *Vibrio parahaemolyticus* accounted for 65% of all speciated isolates from these infections (CDC 2016; Jennifer 2016). Also in 2015, the Public Health Agency of Canada reported 82 cases of *V. parahaemolyticus* infection caused by to consumption of raw oysters (PHAC 2015). The geographical range of *V. parahaemolyticus* has extended into unexpected areas such as Canada and Alaska where Ocean temperatures are much colder (McLaughlin et al. 2005) (PHAC 2015).

Once inside the human host, *V. parahaemolyticus* is known to attach to the columnar epithelial cells of the intestine (Finn et al. 2013). Pathogenic strains of *V. parahaemolyticus* are characterized by the presence of *tdh* and *trh* genes, coding for the thermostable Direct Hemolysin (TDH) and TDH-related hemolysin (TRH) respectively (DePaola et al. ; Johnson et al. 2012; Johnson et al. 2009; Paranjpye et al. 2012; Parvathi et al. 2006). For a number of years it was believed that TDH was the main virulence factor required for pathogenesis (Miyamoto et al. 1969). The contribution of TDH had come into question when a number of TDH –ve strains were isolated from infected patients. It was discovered that these isolates contain TRH (Nishibuchi et al. 1992). In 2003, the first *V. parahaemolyticus* genome was sequenced, a serogroup O3:K6 clinical strain RIMD2210633. Genome analysis of this sequenced strain revealed the presence of two type-three-secretion-systems (T3SSs),

one on each chromosome named T3SS-1 and T3SS-2 (Makino et al. 2003). Bacterial T3SSs are contact dependent secretion systems that span the bacterial inner and outer membranes and when in contact with a eukaryotic cell can pierce its membrane and deliver proteins directly into the eukaryotic cytosol. T3SS are complex structures composed of over 40 proteins that are classified as “structural proteins”, “translocator proteins” and “effector proteins”. The effector proteins are delivered into the cytosol and have been implicated in disrupting a variety of cells structures, cell signaling and regulation pathways (Coburn, Sekirov, and Finlay 2007). The T3SS-1 of *V. parahaemolyticus* is present in both clinical and non-clinical isolates and was shown to be important for cytotoxicity (Broberg et al. 2010; Burdette, Seemann, and Orth 2009; Burdette, Yarbrough, and Orth 2009; Gode-Potratz, Chodur, and McCarter 2010; Hiyoshi et al. 2010). The T3SS-2 was shown in several studies to be the major contributing factor towards enterotoxicity and is only present on pathogenic strains (Hiyoshi et al. 2010; Park et al. 2004; Pineyro et al. 2010; Ritchie et al. 2012). Studies of both these systems have led to the identification of several effector proteins associated with inflammatory diarrhea (Makino et al. 2003; Boyd et al. 2008; Hurley et al. 2006; Ham and Orth 2012; O'Boyle and Boyd 2014).

Two type-six-secretion-systems (T6SSs) named T6SS-1 and T6SS-2 have been identified on chromosome 1 and 2 respectively of *V. parahaemolyticus* RIMD2210633 (Yu et al. 2012). T6SS are also contact dependent secretion systems that interact with both bacterial and eukaryotic cells. They are structurally similar but have evolutionarily distinct structures from T3SSs. T6SS2 is present in both clinical and

non-clinical isolates, whereas T6SS-1 was found mainly in clinical isolates. The T6SS-1 was found to be an anti-microbial secretion system involved in competing with other bacterial species (Salomon et al. 2013; Yu et al. 2012; Ceccarelli et al. 2013). The role for T6SSs in *V. parahaemolyticus* pathogenesis has not yet been determined.

Our knowledge of how *V. parahaemolyticus* initially colonizes and survives within the host gastrointestinal tract is much less well known. This lack of knowledge is in part due to a lack of animal models to study colonization and infection *in vivo*. The development of a streptomycin pretreated adult mouse model that removes microbiota colonization resistance and allows *V. parahaemolyticus* to colonize has uncovered a number of bacterial colonization factors (Whitaker et al. 2012; Whitaker, Richards, and Boyd 2014; Haines-Menges, Whitaker, and Boyd 2014). Adult mice are pretreated with streptomycin 24 h prior to bacterial inoculation, which removes a large portion of the mouse intestinal microbiota, allowing *V. parahaemolyticus* to colonize. Untreated mice are not susceptible to *V. parahaemolyticus* colonization (Whitaker 2012).

The *Vibrio* specific global regulator ToxRS has been shown to be a key requirement for colonization of *V. cholerae*, the causative agent of cholera. Examination of a *V. parahaemolyticus toxR* mutant demonstrated a significant defect in intestinal colonization compared to the wild-type (Whitaker et al. 2012). This study showed that ToxR was a negative regulator of T3SS-1 gene expression and a positive regulator of the global regulator LeuO and the major outer membrane porin OmpU

(Whitaker et al. 2012). In the *toxR* mutant, both *leuO* and *ompU* expression was repressed and T3SS-1 gene expression was induced. It was shown that *leuO* is a negative regulator of T3SS-1 expression. OmpU was shown to be essential for resistance and tolerance to acid and bile salts, important abiotic stresses *in vivo* (Whitaker et al. 2012). The role of the two T3SSs was also examined *in vivo* and it was shown that the T3SS-1 mutant showed no defect in *in vivo* colonization but the T3SS-2 showed a defect with a competitive index of 0.7 (Whitaker et al. 2012). Recently, the importance of ToxR for *V. parahaemolyticus* *in vivo* survival was also demonstrated in an infant rabbit model of infection and in this study ToxR was proposed to be involved in expression of T3SS-2 (Hubbard et al. 2016).

The alternative sigma factor RpoE, required for the cell envelope stress response, was shown to be essential for *in vivo* survival (Haines-Menges, Whitaker, and Boyd 2014; Haines-Menges 2015) It was demonstrated that deletion of the *rpoE* gene resulted in attenuation of mouse colonization compared to wild-type with a competitive index of 0.3 (Haines-Menges, Whitaker, and Boyd 2014). It was shown that RpoE is required for resistance to antimicrobial peptides, an important protective barrier *in vivo*.

Sigma-54 encoded by *rpoN* is transcriptional factor that controls the expression of 100s of genes and was first recognized as an important regulator of nitrogen assimilation. Sigma-54 was also shown to be required for cell motility and biofilm formation important *in vivo* phenotypes. RpoN is a direct regulator of two additional sigma factors that control flagella synthesis, FliAP required for polar flagellum

synthesis and FliAL required for lateral flagella synthesis. RpoN mutants are non-motile and have a defect in nitrogen assimilation. Analysis of a deletion mutant of sigma-54 *rpoN* in *V. parahaemolyticus* showed that in *in vivo* colonization competition assays, the mutant colonized significantly more proficiently than the wild-type strain. Thus motility and biofilm formation were not important phenotypes for colonization by *V. parahaemolyticus*. The mechanism for the enhanced colonization of the *rpoN* mutant is unknown; however, it was shown that the *rpoN* mutant had a metabolic advantage over wild-type when grown in intestinal mucus and its components. Expression analysis showed that genes required for gluconate, ribose and arabinose catabolism were induced in the *rpoN* mutant. These data suggested that specific carbon metabolism genes are negatively regulated by RpoN and that competitive carbon utilization could be an important colonization factor (Whitaker, Richards, and Boyd 2014).

Interestingly, RpoN was shown to play an important role in quorum sensing in *V. harveyi* since along with the sigma-54 activator protein LuxO, it is required for transcription of the quorum small regulatory RNAs (*qrrs*) that regulate the expression of the quorum sensing master regulators (Lilley and Bassler 2000). RpoN binding sites in the *qrr* genes were identified for both *V. harveyi* and *V. parahaemolyticus* suggesting a similar mechanism in both species (Lilley and Bassler 2000).

## Quorum Sensing in Bacteria

Quorum sensing is a process by which bacteria modulate gene expression in response to cell density changes and is mediated by autoinducers (AIs) such as acyl homoserine lactone that act as extracellular signals. (Kuo, Blough, and Dunlap 1994; Salmond et al. 1995; Swift, Bainton, and Winson 1994; Zhang et al. 1993; Bassler, Greenberg, and Stevens 1997; Fuqua, Winans, and Greenberg 1996; Fuqua, Winans, and Greenberg 1994; Gray et al. 1994; Bassler 1999; Bassler et al. 1993; Bassler, Wright, and Silverman 1994). Quorum sensing AI molecules are of two major types: Acyl-homoserine lactones (AHLs) and autoinducing peptides (AIPs) (Waters and Bassler 2005). AHLs are the major class of autoinducer molecules in Gram-negative bacteria (Fuqua and Greenberg 1998; Hanzelka et al. 1997; Kuo, Blough, and Dunlap 1994; Swift, Bainton, and Winson 1994; Winson et al. 1995; Zhang et al. 1993; Fuqua, Parsek, and Greenberg 2001; Ng and Bassler 2009). AIPs are the autoinducer molecules used by Gram-positive bacteria (Ji, Beavis, and Novick 1995; Novick et al. 1995; Saenz et al. 2000).

There are three basic steps involved in the QS mechanism. Firstly, bacteria synthesize the AI molecules (AHLs/ AIPs) intracellularly. Next, these AI molecules are transported outside the cell into the extracellular environment. The transport occurs either through passive release or they are actively secreted out of the cell. Finally, when the concentration of the AIs in the external environment goes beyond a certain threshold, associated cell surface receptors bind the AIs and activate signal cascades resulting in cell density based gene expression changes (Ng and Bassler

2009). Bacterial gene expression can be classified into two distinct patterns based on cell density changes (Novick and Geisinger 2008; Waters and Bassler 2006; Ng and Bassler 2009). At low cell density (LCD), when the extracellular concentration of the AIs is low, bacteria regulate gene expression to favor an asocial individual behavior, and at high cell density (HCD), when there is considerable accumulation of the AIs in the extracellular environment, bacterial gene expression favors a social group behavior (Bassler 1999; Bassler et al. 1993; Chapon-Herve et al. 1997; Ng and Bassler 2009; Schaefer et al. 1996).

### **Quorum Sensing in Vibrios**

The genus *Vibrio* contains over 60 species that encounter various ecological challenges from the external environment and within the host (Sawabe, Kita-Tsukamoto, and Thompson 2007; Sawabe et al. 2013; Thompson et al. 2009; Thompson et al. 2005; Thompson et al. 2004). The bacteria interact with the host as either part of the normal flora as a symbiont or as a pathogen (Reen and Boyd 2005). Quorum sensing is an integral part of how the bacteria coordinate their response to the broad spectrum of activities they undertake (Milton 2006). Within the genus, QS has been widely studied in the two bioluminescent species, *Vibrio fischeri*, a symbiont of squid, *Vibrio harveyi*, a pathogen in fish and humans, and also in the human pathogen *Vibrio cholerae* (Ng et al. 2012; Bassler, Greenberg, and Stevens 1997; Bassler et al. 1993; Bassler, Wright, and Silverman 1994; Gray et al. 1994; Shao et al. 2013; Stevens and Greenberg 1997; van Kessel, Rutherford et al. 2013; van Kessel, Ulrich et

al. 2013; Zhu et al. 2002; Miller and Bassler 2001; Miller et al. 2002; Milton 2006). The basic QS system is analogous in all three species but they differ substantially in the composition of the output regulons. A signature phenotype of QS is bioluminescence in *V. fischeri* and *V. harveyi*, whereas virulence and biofilm formation are signature phenotypes in *V. cholerae* (Bassler, Wright, and Silverman 1994; Stevens and Greenberg 1997; Zhu et al. 2002). In *V. cholerae*, a deletion in the QS response regulator, *luxO* was found to be defective in production of cholera toxin and the toxin coregulated pilus. The mutant strain also showed a severe defect in *in vivo* colonization in an infant mouse model (Zhu et al. 2002).

Also, the regulation of gene expression is not always in the same direction among species. For example, QS induces the expression of extracellular polysaccharide in *V. fischeri*; it represses the same in *V. cholerae* (Yildiz and Visick 2009).

Quorum Sensing has also been examined in *V. parahaemolyticus* (Gode-Potratz and McCarter 2011; Henke and Bassler 2004; Wang, Ling et al. 2013; Wang, Zhou et al. 2013; Zhang et al. 2012; Zhou et al. 2013). Quorum sensing was shown to regulate 100s of genes in this species, which included the T3SS-1 and the two T6SSs expression along with biofilm formation and motility (Gode-Potratz and McCarter 2011; Wang, Ling et al. 2013; Ma et al. 2012; Salomon et al. 2013; Salomon, Klimko, and Orth 2014). Much of the understanding of the QS pathway in *V. parahaemolyticus* is derived from the high similarity it shares with *V. harveyi*, a species in which the pathway has been well elucidated (McCarter 1998; Henke and Bassler 2004; Liu,

Srinivas et al. 2013; Zhang et al. 2012). Similar to *V. harveyi*, *V. parahaemolyticus* contains a three-channel QS system (Henke and Bassler 2004). *V. parahaemolyticus* produces three different types of AI molecules that enter a shared signal transduction cascade that includes the LuxO response regulator. AI-1, is synthesized by LuxM and detected by histidine kinase LuxN, AI-2 which is produced by LuxS and recognized by the histidine kinase complex LuxPQ, and CAI-1, produced by CqsA and recognized by histidine kinase CqsS (Henke and Bassler 2004; Ng and Bassler 2009; Rutherford and Bassler 2012). The membrane bound histidine kinases act as cognate receptors for AI molecules. At LCD the cell surface receptors are devoid of the autoinducer molecules and in this mode their kinase activity predominates and a phosphate group from the receptor is transferred to LuxU which then transfers the phosphate to response regulator LuxO (**Figure 1**) (Ng and Bassler 2009). Together with sigma factor 54 (aka  $\sigma^{54}$  /RpoN) – loaded RNA polymerase LuxO activates the transcription of genes encoding the 5 small quorum regulatory RNAs (Qrrs) (**Figure 1**). The Qrrs bind to the mRNA of the central QS output regulators AphA and OpaR. Binding of the Qrrs promotes the translation of the LCD master regulator AphA while it destabilizes the mRNA of the HCD master regulator OpaR. At HCD, when the concentration of the autoinducer molecules is high, the receptors bind autoinducers, which switches to its phosphatase activity and becomes a LuxO phosphatase, resulting in deactivation of LuxO. The *qrr* genes are not transcribed, ceasing the promotion of *aphA* mRNA translation and allowing for the *opaR* mRNA to be translated (**Figure 1**) (Ng and Bassler 2009; Zhang et al. 2012; Gode-Potratz and McCarter 2011; Lenz et

al. 2004; Shao and Bassler 2012; Shao et al. 2013; van Kessel, Rutherford et al. 2013; Rutherford and Bassler 2012; Rutherford et al. 2011; Tu and Bassler 2007). This regulatory architecture ensures that the LCD master regulator AphA is up-regulated at LCD conditions and an up-regulation of HCD master regulator OpaR as cell density increases (Rutherford et al. 2011; Shao and Bassler 2012). In *V. parahaemolyticus*, AphA has been shown to be required for biofilm formation and motility. An *aphA* defective mutant strain exhibited reduced lethality in mice and reduced cytotoxic and hemolytic activity (Wang, Ling et al. 2013). OpaR has been shown to regulate capsule polysaccharide (CPS) formation, T3SS-1 expression, expression of both T6SSs, surface sensing and motility (Gode-Potratz and McCarter 2011; Kernell Burke et al. 2015; Ma et al. 2012; McCarter 1998; Salomon, Klimko, and Orth 2014; Zhang et al. 2012; Zhang et al. 2016; Zhou et al. 2013).

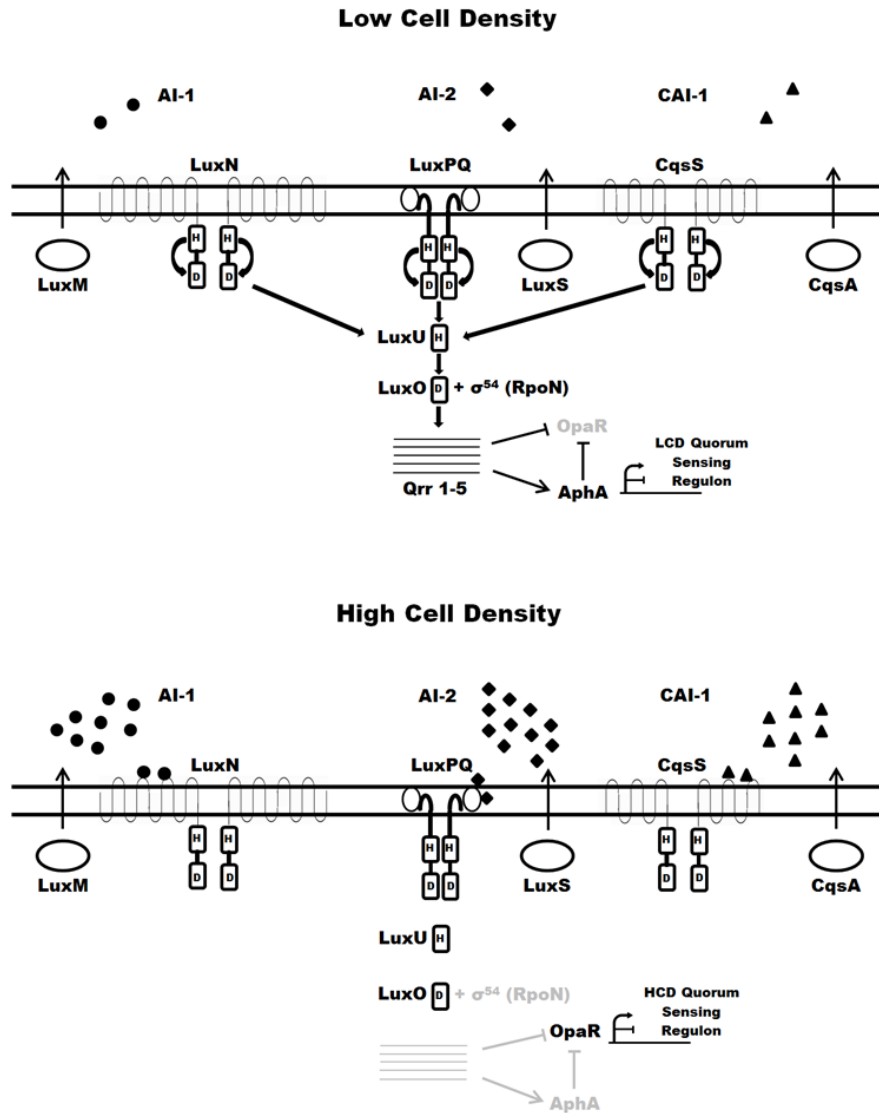


**Figure 1** An overview of the quorum sensing pathway in *V. parahaemolyticus*. AI-1, AI-2, and CAI-1 are synthesized by LuxM, LuxS, and CqsA, respectively. At low cell density, the 5 quorum regulatory RNAs (Qrrs) are transcribed and activate AphaA and repress OpaR. At high cell density, the Qrrs are no longer transcribed and OpaR is constitutively expressed and AphaA is repressed.

### **Quorum response regulator LuxO and its interaction with sigma 54, RpoN**

The QS response regulator, LuxO is a member of the NtrC family of response regulators (Bassler, Wright, and Silverman 1994). The members of this family of regulators act together with the sigma factor RpoN ( $\sigma^{54}$ ) to activate gene expression. The NtrC proteins contain a conserved central domain that is involved in ATP hydrolysis. The ATP hydrolysis activity is essential in the role of these proteins in protein unfolding, DNA unwinding and transcriptional regulation (Bush and Dixon 2012; Erzberger and Berger 2006; Joly et al. 2012). LuxO and other NtrC proteins drive the conversion of the RNA polymerase holoenzyme-promoter closed complexes into active open complexes (Lilley and Bassler 2000; Popham et al. 1989; Weiss et al. 1991; Ng et al. 2012; Rombel et al. 1998; Studholme and Dixon 2003; Shingler 1996; Boyaci et al. 2016). Phosphorylation of LuxO activates the ATPase domain for ATP hydrolysis (Freeman and Bassler 1999; Boyaci et al. 2016). The active LuxO initiates transcription of *qrr 1* to *qrr5* through its interaction with the RpoN-loaded RNA polymerase bound to DNA (Lenz et al. 2004; Lilley and Bassler 2000; Tu and Bassler 2007).

### **Quorum Regulatory RNAs (Qrrs)**

The Qrrs are a group of bacterial sRNAs that are partially complimentary to their target mRNA regulating gene expression post-transcriptional. They require the sRNA chaperone Hfq for their activity. Hfq binding to the sRNA remodels the RNA

tertiary structure such that it allows the binding of the sRNA to its mRNA target (Vogel and Luisi 2011; Waters and Storz 2009; Lenz et al. 2004). Qrrs were identified first in *V. cholerae* where they were shown to repress HapR (the LuxR homologue) through direct base pairing (Lenz et al. 2004). As a repressor, the Qrrs base pair directly to the 5' UTR of the mRNA. They base pair to the ribosome binding site and prevent the ribosomal binding, thus preventing translation of the mRNA (Bardill, Zhao, and Hammer 2011; Lenz et al. 2004; Tu and Bassler 2007). As an activator, the Qrrs bind to the 5' UTR of the mRNA, release the inhibitory secondary structure preventing ribosome binding, and thus promote translation (Shao and Bassler 2012).

Five *qrr* genes have been identified in *V. parahaemolyticus* compared to four in *V. cholerae* (Lenz et al. 2004). The sequence of the five *qrrs* is conserved in *V. parahaemolyticus* (**Figure 2**). The *qrrs* share > 70% sequence identity. *qrr1* is located adjacent to *luxO* and has been thought to be the ancestral *qrr*. It is proposed that the others were generated through gene duplication events (Tu and Bassler 2007). The secondary structure of each *qrr* contains four main stem loops (**Figure 3**). The first two stem loops are responsible for base pairing with the mRNA targets. The most 5' loop contains the terminator sequence and protects the *qrr* from RNase E mediated degradation. The third loop plays a role in stabilizing the binding of the Qrr to the mRNA (**Figure 3**). The Qrrs repress the translation of OpaR and promote the translation of AphA by direct base pairing with the 5' UTR of the *opaR* and *aphA* mRNA (**Figure 3**).

*Vibrio cholerae* encodes four Qrrs that are redundant in function. Any one of the four Qrrs was found to be sufficient to repress HapR, the OpaR homologue in this species (Lenz et al. 2004). *Vibrio harveyi*, like in *V. parahaemolyticus*, encodes five Qrrs. The Qrrs in *V. harveyi* are not redundant in function but acted additively. The strength of repression of the OpaR homologue, LuxR followed the order: Qrr4 > Qrr2 > Qrr3 > Qrr1 > Qrr5, meaning that Qrr4 was able to repress LuxR the most followed by the other Qrrs (Tu and Bassler 2007).

The Qrrs in *V. harveyi* have also been shown to regulate targets that are outside the quorum sensing pathway. Microarray analysis revealed 16 novel targets for the Qrrs which included virulence factors, metabolic enzymes and chemotaxis receptor (Shao et al. 2013).



**Figure 2** Sequence homology between the five quorum regulatory RNAs (Qrrs) in *V. parahaemolyticus* RIMD2210633. The size of each Qrr and location within the genome are included in the parentheses.

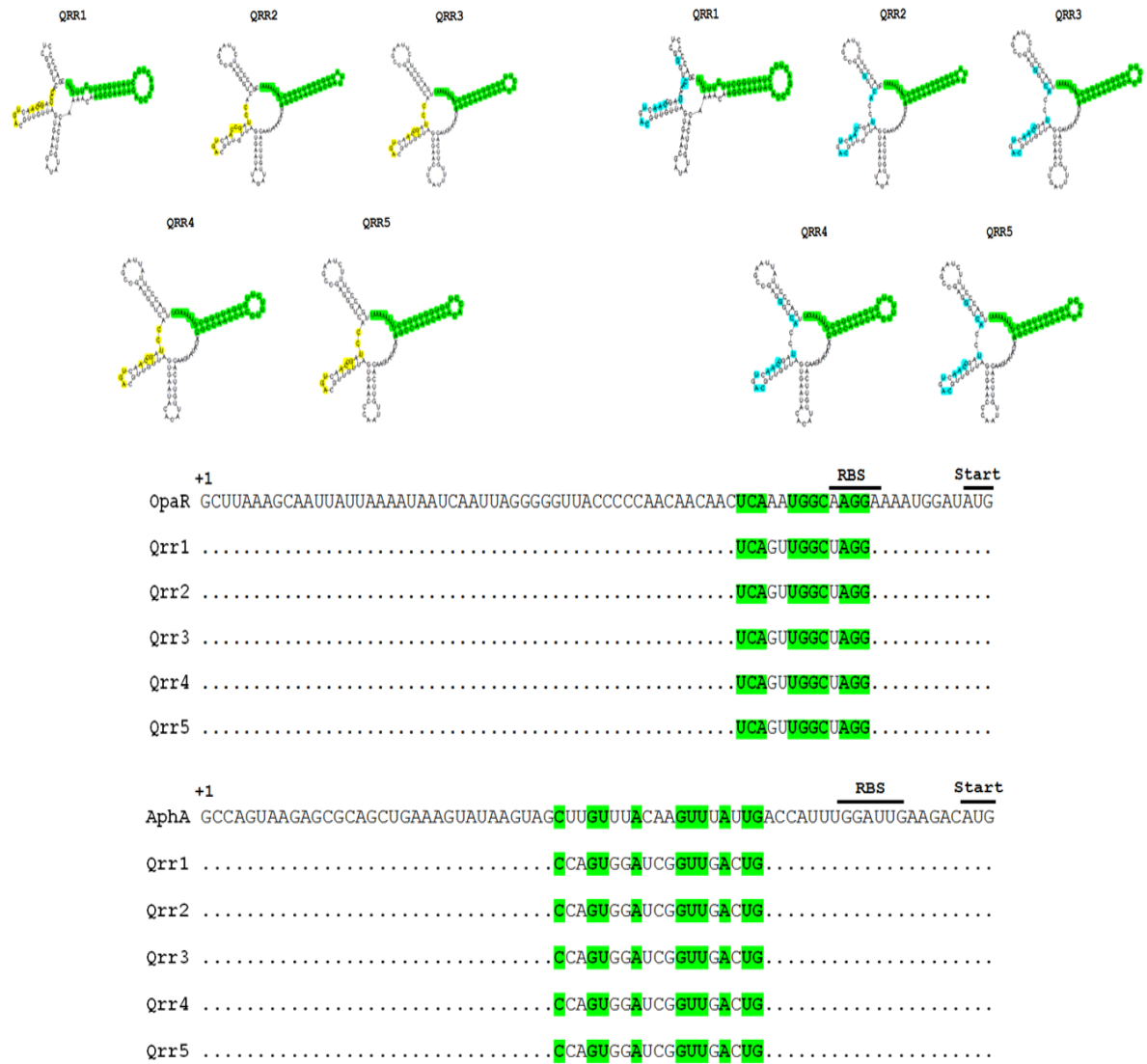


**Figure 3 Qrr interaction with quorum sensing master regulator OpaR and LCD regulator Apha.** First shown are the lowest energy secondary structures of the five quorum regulatory RNAs (Qrrs) showing OpaR (yellow) and Apha binding sequence (blue) and terminator sequence (green). Shown below that are the sequence alignments of the five Qrrs with *opaR* and *aphA* generated using CLUSTALW. The transcriptional start site (+1), Ribosome binding site (RBS) and translational start site (Start) are indicated.

### **Quorum sensing master output regulators AphA and OpaR**

The low cell density (LCD) master output regulator AphA belongs to the PadR family of transcriptional regulators. AphA was initially identified in *V. cholerae* as the transcriptional activator of the *tcpPH* operon (De Silva et al. 2005; Skorupski and Taylor 1999; Kovacicova, Lin, and Skorupski 2003). In *V. harveyi*, AphA was shown to control 296 genes, activating 99 and repressing 197 of those genes (Rutherford et al. 2011). Genes repressed by AphA included *luxR* and three *qrrs*. Genes found to be regulated by AphA included the T3SS, genes involved in metabolism, oxidoreductases, motility and pilus-related genes (Rutherford et al. 2011). Another study in *V. harveyi* showed that AphA regulated 167 genes. That same study discovered that the HCD master output regulator LuxR regulated 625 genes. A comparison of both the AphA and OpaR regulons showed that 77 genes were controlled by both regulators of which 18 were differentially regulated by the two regulators (van Kessel, Rutherford et al. 2013). In *V. parahaemolyticus*, AphA has been shown to be required for biofilm formation, motility and virulence. A deletion of the *aphA* gene locus resulted in decreased hemolytic activity, cytotoxicity and reduced lethality in mice (Sun et al. 2012; Wang, Ling et al. 2013). No global gene expression studies have been performed to examine the regulon of AphA in *V. parahaemolyticus*.

The high cell density (HCD) master output regulator OpaR belongs to the TetR family of transcriptional regulators (Jaques and McCarter 2006). LuxR of *V. harveyi* is the founding member of the TetR-family of QS regulatory proteins in vibrios (Pompeani et al. 2008). Like other members of the TetR family, LuxR-type proteins

including OpaR can activate as well repress transcription of its targets (Gode-Potratz and McCarter 2011; Martin, Showalter, and Silverman 1989; Pompeani et al. 2008; Showalter, Martin, and Silverman 1990; Ramos et al. 2005). The *V. parahaemolyticus* LuxR-homologue, OpaR shows 96% identity to the *V. harveyi* protein. The hallmark target of OpaR in *V. parahaemolyticus* is CPS production that determines colony opacity (McCarter 1998). Deletion or mutation of the *opaR* gene locus leads to significantly reduced levels of CPS and hence, results in a translucent colony morphology (Gode-Potratz and McCarter 2011; Guvener and McCarter 2003; Kernell Burke et al. 2015). Besides CPS gene expression, OpaR has also been shown to regulate biofilm formation and motility in *V. parahaemolyticus* (Enos-Berlage et al. 2005; Gode-Potratz and McCarter 2011; Jaques and McCarter 2006). Global transcriptome analysis has revealed that OpaR regulates nearly 500 genes including those involved in virulence and metabolism (**Table 1**) (Kernell Burke et al. 2015; Gode-Potratz and McCarter 2011).

**Table 1 The key gene systems in the OpaR regulon.** (as determined by Gode-Potratz et al, 2011)

<b>Genes repressed by OpaR</b>	<b>Genes induced by OpaR</b>
Polar Flagella	Capsular polysaccharide
Lateral Flagella	T6SS-2
Surface sensing regulon	C-di-GMP modulation
T3SS-1	Competence
T6SS-1	PHA synthesis
MCP's	Sodium/ Solute symporter
Iron Transporter	Iron Siderophores
Amino Acid Transporters	Cation efflux system

### **Quorum sensing and Metabolism**

Bacteria encounter a wide range of environments, and compete with each other to fight for the same pool of resources. In densely populated environments where cell densities are very high, nutrients are limited and the environment becomes unfavorable for growth. Yet, bacteria are able to compete, coexist and survive (Hibbing et al. 2010). In order to coexist and compete, bacterial cells have developed QS regulatory controls to coordinate nutrient utilization and metabolism in a cooperative population (Goo et al. 2015; Hibbing et al. 2010). For example, in *Burkholderia glumae*, a Gram-negative Proteobacteria, QS regulates glucose utilization and primary metabolism to ensure homeostasis of individual cells in a population (An et al. 2014). Quorum sensing control of metabolism has also been shown to be important in other *Burkholderia* species, where mutations in QS regulators lead to uncontrolled nutrient consumption and toxicity in cells (Goo et al.

2015; Goo et al. 2012). Regulation of metabolic genes by QS regulators has also been shown in other bacteria including *Pseudomonas aeruginosa* and *Yersinia pestis* (Chugani et al. 2012; LaRock et al. 2013; Schuster et al. 2003; Wagner et al. 2003). Quorum sensing based regulation of metabolism is not always in the same direction in all bacteria. While QS serves as a metabolic brake in *Burkholderia* species and *P. aeruginosa*, it upregulates metabolism in *Yersinia pestis* (Chugani et al. 2012; LaRock et al. 2013; Schuster et al. 2003; Wagner et al. 2003).

Another group of bacteria that confront a varied range of environments are members of the family *Vibrionaceae*. These heterotrophs are found free-living in aquatic environments or in association with a eukaryotic host as symbionts or pathogens. Vibrios are metabolically versatile and have been shown to utilize a wide range of carbon sources (Boyd et al. 2015; Farmer 2006; Farmer and Hickman-Brenner 2006). Although very little is known about QS control of metabolism in vibrios, cell density based regulators have been shown to play a role in regulation of metabolism genes in different species. The QS master regulator in *V. fischeri*, LitR has been shown to regulate acetate utilization and has been proposed to play an important role in utilization of nutrients under different conditions (Studer, Mandel, and Ruby 2008). In *V. cholerae*, utilization of chitin, an important carbon source for the bacteria in the marine environment, has been shown to be regulated by quorum sensing (Sun et al. 2015). Quorum sensing in *V. harveyi* has been shown to regulate the arginine biosynthetic pathway, biosynthesis of purines and amino acid efflux proteins (Miyamoto and Meighen 2006). In *V. parahaemolyticus*, although regulation of

metabolism has never been studied directly, transcriptome analysis has revealed the quorum sensing based regulation of amino acid transporters (Gode-Potratz and McCarter 2011; Kernell Burke et al. 2015). In this dissertation, we have elucidated further the role of quorum sensing in regulation of metabolism in *V. parahaemolyticus*.

### **Dissertation Work**

*Vibrio parahaemolyticus* is the leading cause of bacterial seafood-borne gastroenteritis worldwide as well as a significant pathogen of shellfish and fish. In addition, the geographic range of this species and others within the genus is spreading globally due to climate change. Our knowledge of how this pathogen colonizes the human intestine, which is the first step in pathogenesis, is limited. Much less is known about how *V. parahaemolyticus* initially colonizes and survives within the host gastrointestinal tract. This lack of knowledge is in part due to a lack of animal models to study colonization and infection *in vivo*. Previously we developed a streptomycin pre-treated adult mouse model in which the streptomycin pre-treatment removes microbiota colonization resistance and allows *V. parahaemolyticus* colonization. It has allowed us to uncover a number of bacterial colonization factors required for colonization (Whitaker et al. 2012; Whitaker, Richards, and Boyd 2014; Haines-Menges, Whitaker, and Boyd 2014). Quorum sensing is a process by which bacteria modulate gene expression in response to cell density changes and is mediated by autoinducers such as acyl homoserine lactone that act as extracellular signals (Fuqua,

Winans, and Greenberg 1994; Hardman, Stewart, and Williams 1998; Hastings and Nealson 1977; Bassler 1999; Bassler et al. 1993; Ng and Bassler 2009). The role of the quorum sensing regulators in the *in vivo* colonization fitness of the bacteria largely remains unknown. Here, we set out to determine the importance and contribution of the QS regulators in *in vivo* and *in vitro* fitness.

First, we constructed single and double deletion mutants of the three downstream regulators of the quorum sensing pathway, the response regulator *luxO* and the two quorum sensing master regulators *opaR* and *aphA*. We examined these mutants in our streptomycin pretreated adult mouse model for colonization. The *luxO* and *aphA* mutants were found to be defective in *in vivo* colonization competition assays with the wild-type strain. These experiments suggested that the low cell density master regulator AphA is important for *in vivo* fitness likely in part through its negative regulation of the high cell density master regulator *opaR*. Our data also suggested that over-expression of *opaR* is detrimental to *in vivo* fitness. In order to determine the cause for the *in vivo* colonization defects, we performed comparative RNA-Seq transcriptome analysis of wild-type versus the *luxO* mutant cells grown in intestinal mucus as a sole carbon source. The transcriptome analysis showed that 60% of genes downregulated in the *luxO* mutant were involved in metabolism and transport. This indicated to us that the *in vivo* defect observed with the *luxO* mutant might be due to a metabolic defect in the mutant compared to the wild-type. In order to further examine this, we performed global growth assays using carbon phenotype microarrays. We found that there were significant differences in growth between the

wild-type and *luxO* mutant in a number of carbon sources. We also found that the *aphA* mutant which was also defective *in vivo*, exhibited similar growth differences compared to wild-type. Both strains were defective in 25 carbon sources compared to wild-type. In order to determine whether the observed defects were due to the absence of *aphA* or over-expression of *opaR*, we performed bioinformatics analysis to identify putative OpaR and/or AphA binding sites in the regulatory regions of 89 genes/operons involved in carbon metabolism and transport. This analysis identified putative OpaR binding sites in 55 of the 89 regulatory regions examined. In contrast, we only found 9 putative AphA binding sites. This strongly suggested that OpaR plays a significant role in metabolism. In order to confirm our bioinformatic findings, we performed biochemical analysis using electrophoretic mobility shift assays and showed direct binding to five representative regulatory regions. Overall, we demonstrated a direct role for the high cell density master quorum sensing regulator OpaR in cell metabolism, and suggest a mechanism for the *in vivo* colonization defect of the *luxO* and *aphA* mutants.

In Chapter 3, we perform comparative transcriptome analysis of wild-type versus an *rpoN* deletion mutant. LuxO and RpoN act synergistically to activate Qrr expression, which in turn control *aphA* and *opaR* expression. We wanted to determine the differences in expression in the *rpoN* mutant compared to the *luxO* mutant in order to understand *in vivo* and *in vitro* phenotypic differences. Unlike in the *luxO* mutant, *opaR* was not constitutively induced in the *rpoN* mutant, which was not expected. We took a step back and asked whether there were differences in expression of the *qrr*

genes between these mutants. Quantitative PCR analysis showed that in the *rpoN* mutant *qrr2* was highly expressed, which likely explains the difference in *opaR* expression. The *rpoN* mutant is metabolically more fit than wild-type and expression analysis showed that many gene clusters encoding ribosomal proteins and tRNA genes were upregulated in the *rpoN* mutant, which would explain its growth advantage but not the mechanism. In order to determine if RpoN had a direct role in regulation of these genes, we performed bioinformatics analysis of the regulatory regions of two large operons encoding ribosomal proteins. We did not find any RpoN binding sites, however, we identified one strong OpaR binding site in one of the regulatory regions examined. This needs to be examined further.

In chapter 4, we describe the sequencing of an environmental *V. parahaemolyticus* strain UCM-V493 and performed comparative analysis with the clinical isolate RIMD2210633. The final chapter describes the investigation of salt and acid stress response mechanisms in *V. parahaemolyticus*. These studies showed that pre-adaptation to high salt is beneficial for the bacteria for survival in acid and other environmental stress conditions.

## Chapter 2

### **QUORUM SENSING REGULATORS ARE REQUIRED FOR METABOLIC FITNESS IN *VIBRIO PARAHAEMOLYTICUS***

The work in this chapter has been accepted to be published in the journal of *Infection and Immunity*.

#### **Quorum Sensing Regulators are required for Metabolic Fitness in *Vibrio parahaemolyticus***

Kalburge, S.S., Carpenter, M.R., Rozovsky, S., Boyd, E.F.

#### **Introduction**

*Vibrio parahaemolyticus* is the leading cause of bacterial seafood borne gastroenteritis worldwide resulting in mild to severe inflammatory gastroenteritis (Hondo et al. 1987; Daniels et al. 2000; McLaughlin et al. 2005; Nair et al. 2007; Qadri et al. 2003). The completed genome sequence of *V. parahaemolyticus* RIMD2210633, an O3:K6 serotype associated with pandemic disease, demonstrated the presence of two type III secretion systems (T3SSs) one on each chromosome, which led to the identification of several effector proteins associated with inflammatory diarrhea (Makino et al. 2003; Ham and Orth 2012; O'Boyle and Boyd 2014). Studies have shown that T3SS-2 is the major contributing factor towards enterotoxicity and that inflammatory diarrhea and intestinal epithelial cell disruption

are dependent upon a functional T3SS-2 (Hiyoshi et al. 2010; Park et al. 2004; Pineyro et al. 2010; Ritchie et al. 2012).

Much less is known about how *V. parahaemolyticus* initially colonizes and survives within the host gastrointestinal tract. This lack of knowledge is in part due to a lack of animal models to study colonization and infection *in vivo*. The development of a streptomycin pretreated adult mouse model that removes microbiota colonization resistance and allows *V. parahaemolyticus* to colonize has uncovered a number of bacterial colonization factors required for colonization (Whitaker et al. 2012; Whitaker, Richards, and Boyd 2014; Haines-Menges, Whitaker, and Boyd 2014). Examination of a mutant deficient in the global regulator ToxR demonstrated a significant defect in intestinal colonization compared to the wild-type (Whitaker et al. 2012). This study showed that ToxR was a negative regulator of the global regulator LeuO and a positive regulator of T3SS-1 and the major outer membrane porin OmpU (Whitaker et al. 2012). OmpU was shown to be essential for resistance and tolerance to acid and bile salts, important abiotic stresses *in vivo* (Whitaker et al. 2012). The importance of ToxR for *in vivo* survival was also demonstrated in an infant rabbit model of infection (Hubbard et al. 2016). The alternative sigma factor RpoE, required for the cell envelope stress response, was shown to be essential for *in vivo* survival, as deletion of the *rpoE* gene resulted in attenuation of mouse colonization (Haines-Menges, Whitaker, and Boyd 2014). In contrast, analysis of a deletion mutant of sigma-54, *rpoN* showed that in *in vivo* competition assays, the mutant colonized significantly more proficiently than the wild-type strain. The mechanism for the

enhanced colonization of the *rpoN* mutant is unknown, however, it was shown that the *rpoN* mutant had a metabolic advantage over wild-type when grown in intestinal mucus and its components. Expression analysis showed that genes required for gluconate, ribose and arabinose catabolism were induced in the *rpoN* mutant. These data suggested that specific carbon metabolism genes are negatively regulated by RpoN and that competitive carbon utilization could be an important colonization factor (Whitaker, Richards, and Boyd 2014).

Quorum sensing is a process by which bacteria modulate gene expression in response to cell density changes and is mediated by autoinducers such as acyl homoserine lactone that act as extracellular signals (Fuqua, Winans, and Greenberg 1994; Hardman, Stewart, and Williams 1998; Hastings and Nealson 1977; Bassler 1999; Bassler et al. 1993; Ng and Bassler 2009). Quorum sensing has been studied in a number of *Vibrio* species including *V. parahaemolyticus*, which contains the central conserved components of the quorum sensing pathway identified in *V. harveyi* (**Figure 4**) (Miyamoto et al. 2003; Gray et al. 1994; McCarter 1998; Miller et al. 2002; Jaques and McCarter 2006; Milton 2006; Ng and Bassler 2009; Hammer and Bassler 2003; Gode-Potratz and McCarter 2011; Henke and Bassler 2004; Wang, Ling et al. 2013; Zhang et al. 2012; Zhou et al. 2013). In *V. harveyi*, quorum sensing regulation of gene expression is carried out by two quorum sensing master regulators, the low cell density (LCD) regulator AphA and the high cell density (HCD) regulator, LuxR. At LCD, when the autoinducer concentration is low, LuxO, the QS response regulator is active and functions as an activator for sigma factor RpoN ( $\delta^{54}$ ) that then aids in the

transcription of five small RNAs termed quorum regulatory RNAs (*qrr*) 1-5 (Lilley and Bassler 2000; Tu and Bassler 2007). Qrrs are bacterial sRNAs that are partially complementary to their target mRNA and thereby regulate gene expression post-transcriptionally. They require the sRNA chaperone Hfq for their activity (Lenz et al. 2004; Bardill, Zhao, and Hammer 2011; Tu and Bassler 2007). Qrrs were identified first in *V. cholerae* where they were shown to repress HapR (the LuxR homologue) through direct base pairing (Lenz et al. 2004). The Qrrs stabilize the mRNA of *aphA* and destabilize the mRNA of *luxR*. In addition, AphA represses *luxR* transcription, independent of the Qrrs (Tu and Bassler 2007; van Kessel, Ulrich et al. 2013; Rutherford et al. 2011). At HCD, LuxO is not active, the *qrrs* are not transcribed, leading to a constitutively expressed LuxR, which in turn represses the transcription of *aphA* (**Figure 4**) (Tu and Bassler 2007; Rutherford et al. 2011; van Kessel, Ulrich et al. 2013).

### Quorum sensing pathway

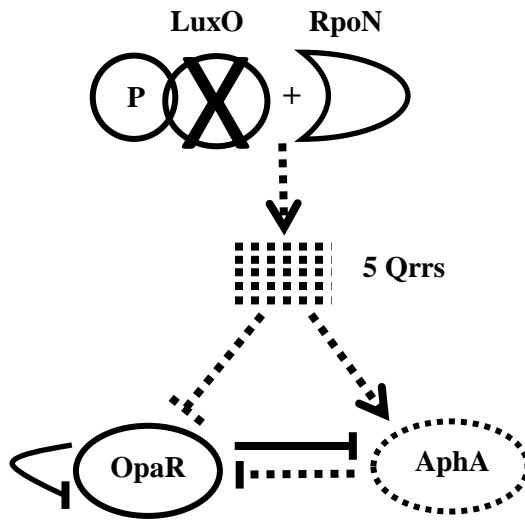


**Figure 4** Regulatory interactions among the components of the quorum sensing pathway in *V. parahaemolyticus*. The sigma 54-dependent response regulator LuxO activates the transcription of the quorum regulatory RNAs (*qrrs*) 1-5. These Qrrs bind to the mRNA of the QS master regulators, blocking the translation of OpaR and promoting the translation of AphA. OpaR and AphA repress the transcription of each other. In a *luxO* mutant indicated by X, no *qrrs* are transcribed and this results in constitutive activation of OpaR and repression of *aphA*. Dashed lines indicate no transcripts made and dashed arrows indicate no regulation, solid lines indicate regulation, arrows indicate positive regulation and hammers indicate negative regulation.

The *V. parahaemolyticus* genome contains each of the components described above, *luxO*, *qrr1* to *qrr5*, *aphA* and *opaR*, the *luxR* homologue in this species (Lenz et al. 2004; McCarter 1998; Gode-Potratz and McCarter 2011; Wang, Ling et al. 2013; Kernell Burke et al. 2015 Zhang, 2012 #25). LuxR and OpaR regulate 100s of genes in *V. harveyi* and *V. parahaemolyticus*, respectively (Gode-Potratz and McCarter 2011; Kernell Burke et al. 2015; van Kessel, Rutherford et al. 2013). OpaR was shown to positively regulate capsule polysaccharide (CPS) production, competence, and type VI secretion system-2 (T6SS-2) production and negatively regulate motility, biofilm, and T3SS-1 and T6SS-1 production (Gode-Potratz and McCarter 2011; Kernell Burke et al. 2015; Salomon, Klimko, and Orth 2014; Wang, Ling et al. 2013; Wang, Zhou et al. 2013; Zhang et al. 2012; Zhou et al. 2013). AphA has been shown to regulate several genes in various *Vibrio* species including genes involved in biofilm formation, motility and virulence (Gu et al. 2016; Skorupski and Taylor 1999; van Kessel, Rutherford et al. 2013; Yang et al. 2010). In *V. harveyi*, AphA coregulated a number of genes including the T3SS apparatus along with LuxR (van Kessel, Rutherford et al. 2013). In *V. parahaemolyticus*, AphA is required for motility, biofilm formation and an *aphA* mutant strain is avirulent in a murine infection model (Wang, Ling et al. 2013).

In this study, we determined the role of the QS regulators in *V. parahaemolyticus* intestinal colonization, the first step in pathogenesis. We constructed a *luxO* deletion mutant and *in vivo* analysis showed that the mutant had a significant defect in a streptomycin pretreated adult mouse model of colonization. We

determined whether the defect in the *luxO* mutant was through its regulation of the QS regulators OpaR or AphA by constructing deletions in each of these genes as well as double deletion mutants and examined the *in vivo* phenotypes. The *aphA* mutant was attenuated for colonization similar to the *luxO* mutant, whereas the *opaR* mutant showed no defect in colonization. Double deletion mutants *luxO/opaR* and *opaR/aphA* showed significantly increased colonization abilities compared to the single *luxO* or *aphA* deletion mutants. These results suggested that AphA is important for *in vivo* fitness likely in part through its negative regulation of *opaR* and that over expression of *opaR* is detrimental. Comparative transcriptome analysis of wild-type versus the *luxO* mutant grown in mouse intestinal mucus showed 60% of genes downregulated in the *luxO* mutant were involved in metabolism. Using phenotype microarrays, we found significant differences in growth between the wild-type and *luxO* and *aphA* mutant strains in 25 carbon sources. Bioinformatics analysis identified putative OpaR binding sites in the regulatory regions of carbon metabolism and transporter genes. By using electrophoretic mobility shift assays, we show direct binding to five of these regulatory regions. Overall, the data demonstrate a direct role for the QS regulator OpaR in cell metabolism and suggests a mechanism for the *in vivo* phenotypes of the *luxO* and *aphA* mutants.

## Material and Methods

### Bacterial strains, media and culture conditions.

All the strains and plasmids used in this study are listed in **Table 2**. A streptomycin-resistant strain of *V. parahaemolyticus* O3:K6 clinical isolate RIMD2210633 was used throughout this study (Whitaker et al. 2010; Whitaker et al. 2012). For competition experiments a  $\beta$ -galactosidase-positive strain of RIMD2210633, named WBWlacZ was used, which was previously shown to behave identical to wild-type *in vitro* and *in vivo* (Whitaker et al. 2012; Whitaker, Richards, and Boyd 2014). Unless stated otherwise, all *V. parahaemolyticus* strains were grown in Lysogeny Broth (LB) containing 3% NaCl (LBS) (Fischer Scientific, Pittsburgh, PA) at 37°C with aeration. For growth studies, M9 medium (Sigma Aldrich, St. Louis, MO) supplemented with 3% NaCl was used to which different carbon sources were added. For genetic manipulations, an *Escherichia coli* diaminopimelic acid (DAP) auxotroph  $\beta$ 2155  $\lambda$ pir was used. The *E. coli*  $\beta$ 2155  $\lambda$ pir strain was cultured in LB medium supplemented with 0.3 mM DAP (Sigma Aldrich). When required, antibiotics were used at the following concentrations: streptomycin, 200  $\mu$ g/ml; chloramphenicol, 25  $\mu$ g/ml; ampicillin 100  $\mu$ g/ml.

### Construction of *V. parahaemolyticus* RIMD2210633 quorum sensing deletion mutants.

Splicing by overlap extension (SOE) PCR with homologous recombination (Horton et al. 1989) was used to construct in-frame nonpolar deletions in VP2099

(*luxO*), VP2762 (*aphA*), VP2516 (*opaR*) and double deletion mutants *luxO/opaR* and *opaR/aphA* as previously described by this group (Whitaker et al. 2010; Whitaker et al. 2012; Whitaker, Richards, and Boyd 2014; Haines-Menges, Whitaker, and Boyd 2014; Kalburge, Whitaker, and Boyd 2014). Primers were designed to the QS response regulator *luxO* and the two QS master regulators *opaR* and *aphA* using the *V. parahaemolyticus* RIMD2210633 genome sequence as the template. All primers used in the study are listed in **Table 3** and SOE PCR was performed to obtain a 75-bp truncated version of the 1,362-bp *luxO* gene, a 39-bp truncated version of the 615-bp *opaR* gene and a 48-bp truncated version of the 540-bp *aphA* gene. All mutants were confirmed by PCR analysis and were verified to be in-frame by sequencing.

#### ***In vivo* competition assays.**

All experiments involving mice were approved by the University of Delaware Institutional Animal Care and Use Committee. Male C57BL/6 mice, aged 6 to 10 wk were housed under specific-pathogen-free conditions in standard cages in groups (4 or 5 per group) and provided standard mouse feed and water *ad libitum*. Streptomycin pre-treatment and inoculations were performed as previously described (Whitaker et al. 2012; Whitaker, Richards, and Boyd 2014). Briefly, 24 h before bacterial inoculations by oral gavage, mice were fasted for 4 h and then administered 20 mg streptomycin per animal orogastrically and then food and water were immediately returned. Four hours prior to inoculation food and water were removed. Water was restored immediately upon inoculation and food was restored 2 h post-infection. The

*V. parahaemolyticus* strain used for *in vivo* experiments is the  $\beta$ -galactosidase knock-in designated WBWlacZ, which allows for a blue: white colony screening (Whitaker et al. 2012; Whitaker, Richards, and Boyd 2014; Haines-Menges, Whitaker, and Boyd 2014). Overnight cultures were diluted 1:50 with LBS streptomycin media and grown for 4 h at 37°C with aeration. An aliquot of the 4 h culture was pelleted and resuspended in PBS to a final concentration of  $\sim 1 \times 10^{10}$  CFU/ml. A 1 ml aliquot of each deletion mutant strain was combined with 1 ml of the WBWlacZ strain, yielding a bacterial suspension of  $\sim 1 \times 10^{10}$  CFU/ml with a ratio of 1:1 CFU of mutant to WBWlacZ strain. Mice were inoculated with 100  $\mu$ l of the appropriate bacterial suspension. An aliquot of the inoculum was serially diluted and plated onto LBS plates with streptomycin and X-gal in order to determine the exact ratio of CFUs in the inoculum. For *in vitro* competition assays, a 100  $\mu$ l aliquot of the *in vivo* inoculum was added to 5 ml of LBS, grown at 37°C with aeration for 24 h and serially diluted and plated. The mice were sacrificed 24 h post infection and the gastrointestinal tract was harvested and suspended in 8 ml of sterile PBS, homogenized mechanically, serially diluted and plated on LBS plates containing 120  $\mu$ g/ml X-gal and incubated at 37°C overnight. The competitive index (CI) for the *in vivo* and *in vitro* assays was determined with the following equation:  $CI = \text{ratio out}_{(\text{mutant/wild-type})} / \text{ratio in}_{(\text{mutant/wild-type})}$ . A CI >1 indicates that the test strain has the ability to out-compete the wild-type strain, while a CI <1 indicates that the test strain is less fit than the wild-type strain.

### **Capsule polysaccharide (CPS) production, motility and biofilm assays.**

CPS production was examined using heart infusion (HI) (Remel, Lenexa, KS) plates containing 1.5% agar, 2.5 mM CaCl<sub>2</sub>, and 0.25% Congo red dye. Single colonies were inoculated onto the surface of the plates and were incubated at 30°C for 36 h before images were taken. Biofilm formation was examined using the crystal violet assay. Briefly, overnight cultures of *V. parahaemolyticus* were diluted 1:40 into LBS and grown statically in 96-well strip plates at 37°C for 3, 6, 12 and 24h. After static incubation, the culture was decanted from each well and the well was washed once with sterile phosphate buffered saline (PBS). Crystal violet was added into each well and the plate was incubated at room temperature for 30 min. The crystal violet was decanted out and the well was washed with sterile PBS. The PBS was then decanted out and crystal violet that had stained the adherent cells was solubilized completely in dimethylsulfoxide (DMSO) and the OD<sub>595</sub> was measured to quantify the amount of biofilm formed.

### **RNA extraction, Illumina sequencing and quantitative real time PCR (qPCR).**

*Vibrio parahaemolyticus* wild-type and mutant strains were grown for 4 h in LBS and then diluted 1:50 into M9 medium supplemented with mouse intestinal mucus as the sole carbon source and the cells were grown statically. We examined early-exponential-phase cultures that were grown for 1.5 h, considering the low cell density condition would restrict *opaR* levels in the wild-type, thereby allowing us to observe the greatest difference in *opaR* levels between the *luxO* mutant and wild-type.

Total RNA was extracted from cells obtained by centrifugation at the end of 1.5 h using Trizol (Invitrogen, Carlsbad, CA) according to manufacturer's protocol. The RNA samples were then quantified using a Nanodrop spectrophotometer (Thermo Scientific, Waltham, MA). The samples were treated with Turbo DNase (Invitrogen) according to manufacturer's instructions. For each sample of the wild-type and mutant, RNA samples from two independent cultures were pooled together. Nanodrop quantifications were used to ensure equal representation of RNA from both biological replicates. Then, 3  $\mu$ g of RNA was used for rRNA depletion using the Ribo-Zero rRNA removal kit for Gram-negative bacteria (Illumina, San Diego, CA). Libraries for each sample were prepared from 100ng of rRNA-depleted-RNA using the Illumina TruSeq Stranded mRNA kit (Illumina). Sequencing was performed at the University of Delaware Sequencing and Genotyping Center on the HiSeq 2500 platform to yield 51-base single-end reads.

For qPCR validations of the RNA-Seq, 500 ng of pre-ribozero treated RNA was used as a template for cDNA synthesis. cDNA was synthesized using Superscript III reverse transcriptase (RT) (Invitrogen) following manufacturer instructions using 500 ng of RNA template and priming with 200 ng of random hexamers. cDNA samples were then diluted 1:25 and used for quantitative-real time PCR (qPCR). To analyze expression of the wild-type and mutant strains at HCD, cells were grown for 4 h in LBS medium and were then diluted 1:50 into M9 medium containing 3% NaCl and supplemented with glucose (M9G) and grown to an OD of 1.0. Total RNA was extracted using the Trizol extraction protocol detailed above. 500 ng of the DNase

treated RNA samples were used as template for cDNA synthesis. cDNA samples were then diluted 1:25 or 1:10 and used for quantitative-real time PCR (qPCR). Fast SYBR Green master mix or PowerUp SYBR Green master mix (Life Technologies, Carlsbad, CA) was used for qPCR and samples were run on an Applied Biosystems 7500 fast real-time PCR system or QuantStudio 6 Flex real-time PCR system (Applied Biosystems, Foster City, CA). Primers used for the qPCR reactions are listed in **Table 3**. Data was analyzed using Applied Biosystems software. Expression levels of each gene as determined by their cycle threshold ( $C_T$ ) values, were normalized using the 16s rRNA housekeeping gene to correct for sampling errors. Differences in the ratios of gene expression were determined using the  $\Delta\Delta C_T$  method (Pfaffl 2001).

### **RNA-Seq analysis.**

Raw 51-base reads were filtered to remove adaptor only sequences and low quality reads using the FASTX Toolkit. Filtered reads were aligned to the *V. parahaemolyticus* RIMD2210633 genome (Refseq ID NC\_004603.1 Chromosome 1 and NC\_004605.1 Chromosome 2) using Burrows-Wheeler Aligner (BWA.aln) version 0.7.7. Gene annotations were obtained from Ensembl bacteria, Rfam, Bacterial Small Regulatory RNA database and RAST. Number of reads aligning to each genomic position were calculated using Htseq version 0.6.1. Differential expression analysis was performed on obtained read counts using DESeq2 version 1.4.5. Differential expressed genes were categorized into Cluster of orthologous groups (COG) obtained from Integrated Microbial Genomes (IMG) database.

### **Growth analysis and *in vitro* competition assays.**

Strains were grown overnight in M9G at 37°C with aeration. For the Biolog PM1 and PM2A phenotype microarrays (Biolog Inc., Hayward, CA), overnight cultures were then diluted 1:50 into fresh M9G and allowed to grow for 4 h. These cultures were pelleted by centrifugation for 10 min at  $4,000 \times g$ , washed twice with PBS and then diluted 1:50 into fresh M9 media supplemented with 3% NaCl and 100µl was then added to each well of the Biolog plate. Plates were incubated at 37°C with intermittent shaking for 1 min. during every hour. Optical densities at 595 nm were taken hourly for a total of 24 h using a Tecan Sunrise microplate reader and Magellan plate reader software (Tecan Systems Inc., San Jose, CA). Growth characteristics were analyzed by calculating Area under the curve using the Origin 8.5 software. The Area under the curve for the blank well was subtracted from each well to perform the analysis. For growth curves in individual mucus sugars and amino acids, 4 h cultures were pelleted, washed and were diluted 1:40 in M9G (10 mM), M9 D-Gluconate (10 mM), D-Mannose (10 mM), D-Ribose (10 mM), L-Arabinose (10 mM), D-Galactose (10 mM), D-Glucosamine (10 mM), Pyruvic acid (10 mM), D-Trehalose (10 mM), Fructose (10 mM), L-Glutamic acid (5 mM), or L-Aspartic acid (30 mM). Mouse intestinal mucus was extracted as described previously (Haines-Menges, Whitaker, and Boyd 2014; Whitaker, Richards, and Boyd 2014). Mice gastrointestinal tracts were harvested and then flushed with PBS to remove intestinal contents. Mucus was collected and pooled by gently scraping the surface walls of the intestine using a spatula or blunted blade. The collected mucus was suspended in PBS

and vortexed until homogenized. The mucus solution was then centrifuged at 500 x *g* for 10 min and the supernatant collected. Protein concentration was determined using a Bradford assay. Approximately 30 µg/ml of protein was used in M9 medium for experiments involving mucus (Cohen and Laux 1995; Leatham et al. 2005; Whitaker, Richards, and Boyd 2014). Each experiment was performed in triplicate with at least two biological replicates. *In vitro* competition assays in mucus and mucus sugars were performed with inoculums prepared as described for *in vivo* competition assays. 100 µl aliquot of the inoculum was added to 5 ml of M9 minimal media supplemented with 10mM of individual mucus sugars or 30 µg/ml of intestinal mucus and grown at 37°C with aeration for 24 h, serially diluted and plated. Competitive index for each assay was calculated as detailed above.

#### **Bioinformatics analysis of OpaR and AphA binding sites.**

The consensus binding sequence and position frequency matrix was obtained for OpaR (Zhang et al. 2012) and AphA (Sun et al. 2012). The position frequency matrix was then used to identify potential binding sites using the MOODS (Motif Occurrence Detection Suite) algorithm (Version 1.0.2.1) (Korhonen et al. 2009; Pizzi, Rastas, and Ukkonen 2011). The upstream intergenic sequence for the first gene of each operon was obtained from the NCBI database and used to identify putative binding sites. Operon information was obtained from the DOOR2 prokaryotic operon database (Mao et al. 2009) and was confirmed using the IGV viewer (Thorvaldsdottir, Robinson, and Mesirov 2013) with the RNASeq sequence data. The MOODS tool returned a Log-

odds score for each putative binding site that was then used to assess probability of binding.

### **Purification of OpaR.**

OpaR was purified using a method previously described (Carpenter, Rozovsky, and Boyd 2015). Briefly, *opaR* was cloned into the pProEXHTa expression plasmid (Invitrogen) in which an N-terminal 6x His tag is fused to *opaR*, separated by a Tobacco Etch Virus (TEV) protease cleavage site. The primer pair SfoIVP2516Fwd/SacIVP2516Rev (**Table 3**) was used to amplify *opaR* (VP2516) from the *V. parahaemolyticus* RIMD2210633 genome using Accura HiFidelity Polymerase (Lucigen, Middleton, WI) following manufacturer's instruction. The *opaR* PCR product was gel cut purified using the Nucleospin Gel and PCR cleanup kit (Macherey-Nagel) and cloned into pJET1.2 using the blunt end ligation protocol. This was transformed into *E. coli* Dh5 $\alpha$  using standard CaCl<sub>2</sub> transformation protocol. Plasmid DNA was isolated, restriction digested and ligated into pProEXHTa plasmid. The ligation product was transformed into *E. coli* DH5 $\alpha$  and plasmid DNA was isolated and confirmed by sequencing before being transformed into *E. coli* BL21(DE3) using standard CaCl<sub>2</sub> method. The pProExHtaOpaR plasmid was expressed in *E. coli* BL21(DE3). Ten milliliters of overnight culture was inoculated into 1 L LB broth at 37°C and induced with 0.5 mM isopropyl-1-thio- $\beta$ -D-galactopyranoside (IPTG) at OD<sub>600</sub> 0.5. Growth continued overnight at 18°C. Cells were harvested by centrifugation (5,000 x g for 20 min at 4°C) and were re-suspended

in immobilized metal affinity chromatography (IMAC) Wash Buffer (50 mM sodium phosphate, 200 mM NaCl, 20 mM imidazole pH 7.6) supplemented with the protease inhibitors, 1 mM phenylmethanesulfonyl fluoride (PMSF) and 1 mM benzimidazole. Bacterial cells were lysed on ice using a high-pressure homogenizer (EmulsiFlex-C5, Avestin, Ottawa, Canada). Cell debris was removed by centrifugation (15,000 x g for 1 h at 4°C). The supernatant was passed through a column containing 5 ml Profinity IMAC resin (Bio-Rad Laboratories, Hercules, CA). The column was washed with 10 column volumes (CV) of IMAC Wash Buffer. The fusion protein, 6xHis-OpaR was eluted with 3 CV IMAC Elution Buffer (50 mM sodium phosphate, 200 mM NaCl, 500 mM imidazole, pH 7.6). A hexahistidine-tagged TEV protease was added to the eluent in a 1:10 molar ratio (TEV: 6xHis-OpaR) and the cleavage reaction proceeded overnight at 4°C. The cleavage mixture was centrifuged, adjusted to 20 mM imidazole and subject to IMAC using Profinity IMAC resin to remove the His-tagged TEV and any remaining un-cleaved fusion protein. The flow through and one CV of wash with IMAC Wash Buffer contained OpaR. The fractions were combined, concentrated and the buffer exchanged to that of the electrophoretic mobility shifts assays binding buffer (10 mM Tris, 150 mM KCl, 0.1 mM dithiothreitol, 0.1 mM EDTA, 5% PEG, pH 7.4). The protein identity was confirmed by mass spectrometry and its purity was determined to be higher than 95% by SDS-PAGE.

### **Electrophoretic Mobility Shift Assays.**

DNA probes VP0008 (amino acid transport), VP1779 (putrescine metabolism), VPA1087 (ribose transport), VPA0500 (mannitol PTS transporter), VPA1424 (mannose metabolism) and negative control VPA1667 (Glucose-specific PTS transporter), were PCR amplified using Accura HiFidelity Polymerase in 50  $\mu$ l reactions using corresponding primer sets in **Table 3** with *V. parahaemolyticus* DNA as template. PCR products were separated on a 1% agarose gel and bands excised from the gel were purified using NucleoSpin Gel and PCR clean-up kit (Macherey-Nagel, Bethlehem, PA). Purified DNA probes were quantified using a Nanodrop spectrophotometer. Varying concentrations of purified OpaR were incubated with 30 ng of target DNA in binding buffer (10 mM Tris, 150 mM KCl, 0.1 mM dithiothreitol, 0.1 mM EDTA, 5% PEG, pH 7.4) for 20 min at room temperature and 10  $\mu$ L were loaded onto a pre-run (200 V for 2 h at 4°C) 6% native acrylamide gel. The gel was run at 200 V for 3 h in 1x Tris-acetate-EDTA (TAE) buffer at 4°C. Following electrophoresis, gels were stained in an ethidium bromide bath (0.5  $\mu$ g/ml) for 20 min, washed with water and imaged.

### **Results**

#### **Deletion of *luxO* or *aphA* leads to a defect in intestinal colonization.**

To determine the role of the QS regulators in *V. parahaemolyticus* pathogenesis, we examined each of the QS mutants for their ability to colonize the adult mouse intestine. We examined *luxO*, *aphA* and *opaR* deletion mutant strains as

well as double deletion mutants *luxO/opaR* and *opaR/aphA* in *in vivo* competition assays with wild-type using the streptomycin pretreated adult mouse model of intestinal colonization (Whitaker et al. 2012; Whitaker, Richards, and Boyd 2014). Mice pretreated with streptomycin were orogastrically co-inoculated with an equal mixture of WBWlacZ (wild-type marked with *lacZ*) and each of the mutants. In these assays, the WBWlacZ strain significantly out-competed the *luxO* mutant, which had a competitive index (CI) of 0.27 indicating that deletion of *luxO* leads to reduced fitness *in vivo* (**Figure 5**). In order to investigate if the defect in the *luxO* mutant was through its regulation of the QS regulators AphA or OpaR, we constructed deletion mutants in each of these genes. The *aphA* mutant showed a significant defect in colonization similar to the *luxO* mutant with a CI of 0.39 (Fig 2). Both the *luxO* and *aphA* mutant strains grew similar to wild-type in *in vitro* competition assays in LBS, with CIs of 0.9 and 1.01 respectively. These data show that deletion of *luxO* or *aphA* affects colonization ability specifically (**Figure 5**). The *opaR* mutant behaved similar to the wild-type in both *in vitro* and *in vivo* assays with a CI of ~1. In order to determine further, the importance of each of these regulators in colonization, we examined double deletion mutants, *luxO/opaR* and *opaR/aphA*. Interestingly, deletion of *opaR* in the *luxO* and *aphA* mutant resulted in a significant increase in colonization ability compared to the single mutants. Colonization was restored to wild-type levels in the *luxO/opaR* double mutant which had a CI of 1.4. The *opaR/aphA* mutant also had increased colonization compared to the *aphA* single mutant with a CI of 0.7, however, this mutant still showed a defect in colonization compared to wild-type, indicating that

AphA is required for colonization *in vivo* (Figure 5). Taken together, these data demonstrate that over-expression of OpaR is detrimental and AphA is required for *in vivo* colonization.

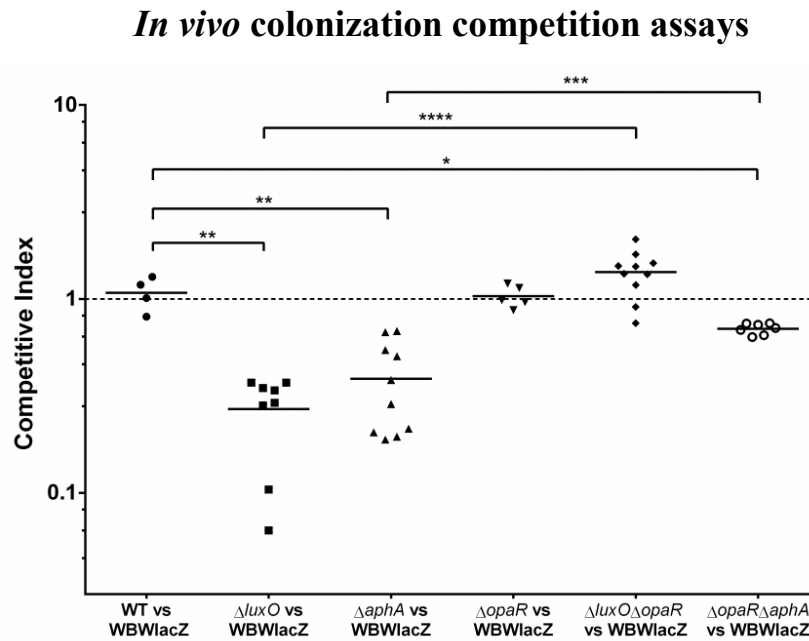
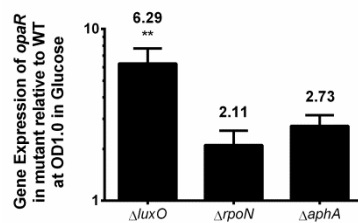


**Figure 5** *In vivo* competition assays between the wild-type and each QS mutant. A 1:1 mixed culture of WBWlacZ and each deletion mutant was used to orogastrically infect streptomycin-pretreated adult mice. CFUs were calculated 24 h post infection from the entire gastrointestinal tracts using a blue/white colony selection. Data are pooled from two separate experiments and reported as competitive index (CI) for the *luxO* (n=8), *aphA* (n=10), *opaR* (n=5), *luxO/opaR* (n=10), and *opaR/aphA* (n=7) mutants. The solid line indicates the means. *P* values were calculated using a Welch's unpaired t-test with a 95% confidence interval. Asterisks denote significant differences between the CI of the mutant strains compared with the wild-type strain. \*, *P* < 0.05; \*\*, *P* < 0.01; \*\*\*, *P* <= 0.001 \*\*\*\*, *P* < 0.0001.

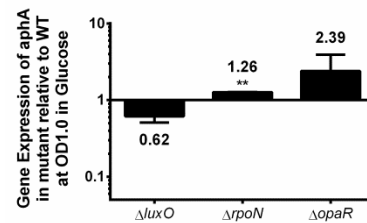
The *in vivo* defect observed for the *luxO* mutant is unlike the superior colonization phenotype that we had previously showed for an *rpoN* deletion mutant (Whitaker, Richards, and Boyd 2014). According to the quorum sensing pathway in *V. parahaemolyticus*, deletion of both *luxO* and *rpoN* should have the same effect on the expression of the two master regulators *aphA* and *opaR*. In order to investigate this, we determined the expression patterns of *aphA* and *opaR* in *luxO*, *opaR*, *aphA* and *rpoN* mutant strains grown to OD 1.0 in M9G. Expression of *opaR* was significantly induced in the *luxO* mutant with a 6.3-fold change in expression relative to wild-type. The expression of *opaR* was increased in both the *rpoN* and the *aphA* mutants, but not to the same level as in the *luxO* mutant (**Figure 6A**). Expression of *aphA*, although not significant, was reduced in the *luxO* mutant and was induced in the *opaR* mutant. The expression of *aphA* was not repressed in the *rpoN* mutant (**Figure 6B**). Both RpoN and its activator LuxO are required for the *qrrs* expression since *qrr1* to *qrr5* each contain a conserved RpoN -12 and -24 promoter binding sequence indicating this sigma factor is required for expression (Lilley and Bassler 2000). To address why *aphA* was not repressed and *opaR* is not as highly expressed in the *rpoN* mutant compared to the *luxO* mutant, we examined the expression patterns of *qrr1* to *qrr5* in both these mutants under the same conditions as *opaR* expression. QPCR analysis showed that in the *luxO* mutant compared to wild-type, *qrr2*, *qrr3* and *qrr5* were repressed, while *qrr1* was unchanged (**Figure 6C**). In the *rpoN* mutant, qPCR analysis showed that *qrr1*, *qrr3* and *qrr5* were repressed, however *qrr2* was induced compared to wild-type (**Figure 6D**). In both cases, no *qrr4* expression was either very low or

altogether not detected. The most notable difference in expression patterns between the *luxO* and *rpoN* mutants was in *qrr2*. While *qrr2* was significantly downregulated in the *luxO* mutant, its expression was induced in the *rpoN* mutant. We speculate that the induction of *qrr2* in the *rpoN* mutant may explain the reduced level of *opaR* compared to the *luxO* mutant.

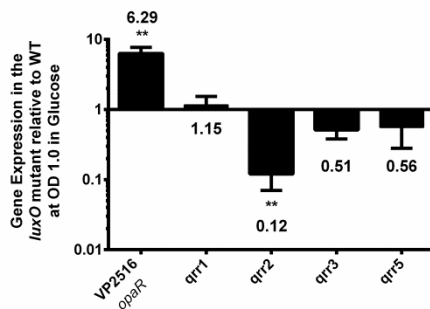
### A. Relative expression of *opaR*



### B. Relative expression of *aphA*



### C. Relative expression of *qrrs* in $\Delta luxO$



### D. Relative expression of *qrrs* in $\Delta rpoN$

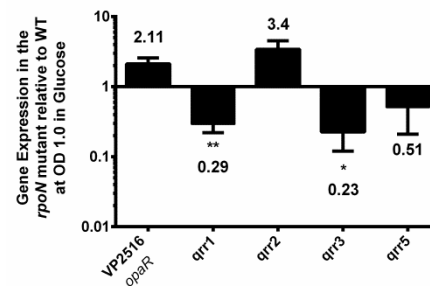


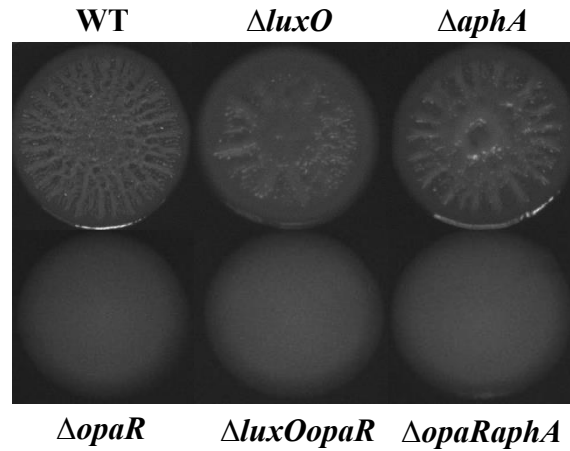
## Figure 6 Expression analysis of quorum sensing master regulators and *qrrs*.

RNA was extracted from wild-type and mutant strains grown in M9 media supplemented with glucose (M9G) to OD 1.0 and analyzed by qPCR in duplicate for each biological replicate. A. Bars represent the expression of *opaR* normalized to 16S rRNA in the *luxO*, *rpoN* and *aphA* mutants relative to wild-type cells. B. Bars represent the expression of the *aphA* normalized to 16S rRNA in the *luxO*, *rpoN*, and *opaR* mutants relative to wild-type cells. C. Bars represent the expression of *qrr 1*, *qrr2*, *qrr3* and *qrr5* normalized to 16S rRNA in  $\Delta luxO$ . D. Bars represent the expression of the *qrr 1*, *qrr2*, *qrr3* and *qrr5* normalized to 16S rRNA in  $\Delta rpoN$ . *P* values were calculated using an unpaired Student's t-test with a 95%

confidence interval. Asterisks denote significant differences in relative gene expression between mutant and wild-type. \*,  $P < 0.05$ ; \*\*,  $P < 0.01$

The *V. parahaemolyticus* quorum sensing master regulators OpaR and AphA have been shown to regulate CPS production and biofilm formation (McCarter 1998; Enos-Berlage et al. 2005; Guvener and McCarter 2003; Gode-Potratz and McCarter 2011; Wang, Ling et al. 2013). We examined these phenotypes in the QS regulator mutants examined in this study. The *luxO* and *aphA* mutants produced rugose colonies similar to wild-type indicating CPS production, which indicates that CPS production is not involved in the *in vivo* phenotype of these mutants (**Figure 7A**). The *luxO* and *aphA* mutants produced similar amount of biofilm as wild-type at the initial time points but were found to be defective at 24 h (**Figure 7B**). Previously, we showed that an *rpoN* mutant had a defective in biofilm formation but had a superior colonization phenotype suggesting this is not the cause of the *luxO* and *aphA* mutant *in vivo* phenotypes.

### A. Capsule polysaccharide (CPS) production



### B. Quantitative analysis of biofilm formation among QS regulator mutants

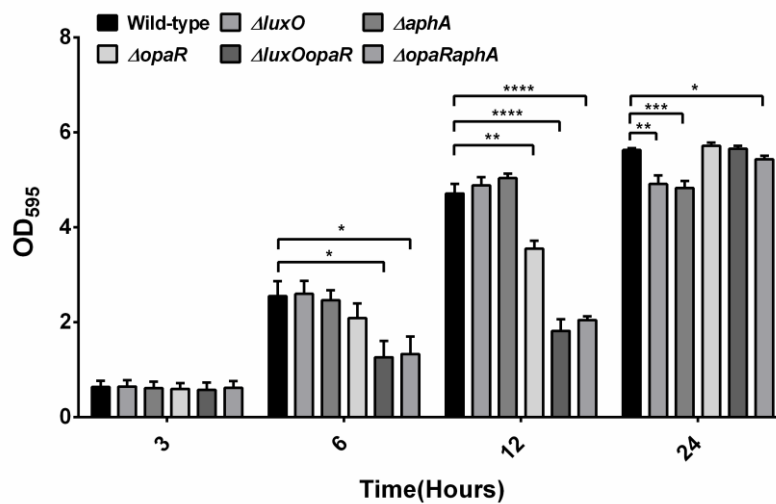


**Figure 7** *In vitro* phenotypic analysis of *V. parahaemolyticus* RIMD2210633 and the QS mutants. **A.** Capsule polysaccharide production on Congo red plates, **B.** Biofilm formation using the crystal violet assay at 3, 6, 12 and 24 h. *P* values were calculated using an unpaired Student's t-test with a 95% confidence interval. Asterisks denote significant differences in biofilm production between the mutant strains and the wild-type. \*, *P* < 0.05 \*\*, *P* < 0.01, \*\*\*, *P* < 0.001, \*\*\*\*, *P* < 0.0001

### **RNA-seq data and comparative analysis of gene expression in mouse intestinal mucus.**

To begin to determine the mechanism of the *in vivo luxO* mutant colonization defect, we performed RNA-Seq expression analysis of wild-type and the *luxO* mutant grown in mouse intestinal mucus as a sole carbon source. RNA was isolated from the wild-type and *luxO* mutant strains grown to early exponential phase in M9 supplemented with mouse intestinal mucus as the sole carbon source. The LCD time point was chosen since it should show maximum differences in *opaR* expression between the wild-type (low OpaR levels) and the *luxO* mutant (high OpaR levels). Sequencing resulted in greater than 10 million sequence reads obtained for each sample (**Figure 8A**). Over 98% of the reads aligned to genomic features including mRNA, tRNA, sRNA or to unannotated regions of the genome. The rRNA depletion procedure resulted in less than 0.5% of the reads aligning to these features in the genome (**Figure 8A and 8B**). Differential expression analysis revealed that 106 genomic features and 102 features were downregulated and upregulated ( $> 2$ -fold,  $P_{\text{adj}} < 1 \times 10^{-4}$ ) respectively in the *luxO* mutant compared to wild-type (**Figure 9, Figure 10A and B, Table 4 and Table 5**).

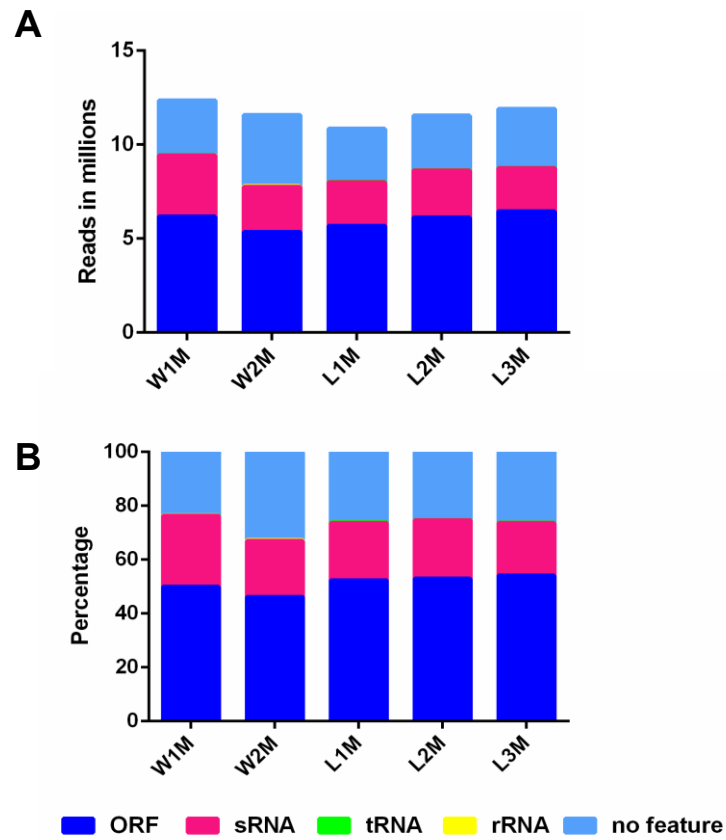


**Figure 8 RNA-seq sequencing yield and RNA classification. A.** Total number of reads sequenced per sample indicated to corresponding RNA-feature. **B.** Total percentage of reads mapping to various RNA features. Table indicates numbers in millions of reads for each sample.

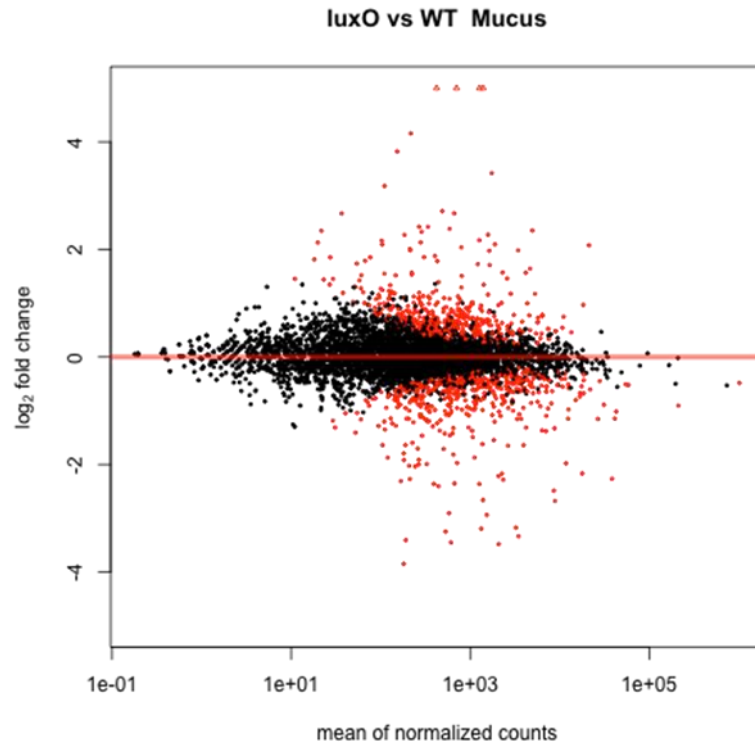


**Figure 9 RNA Seq MA-plot showing expression in the *luxO* mutant relative to wild-type.** Plot showing the log<sub>2</sub> fold changes in the *luxO* mutant over the mean of the normalized counts. Dots represent log<sub>2</sub> fold change in expression for each genomic feature. Red dots represent all genes with an adjusted *P* value of  $\leq 0.0001$ . Genes with a log<sub>2</sub> fold change of  $> 1$  or  $< -1$  were considered as being differentially expressed between the mutant and the wild-type.

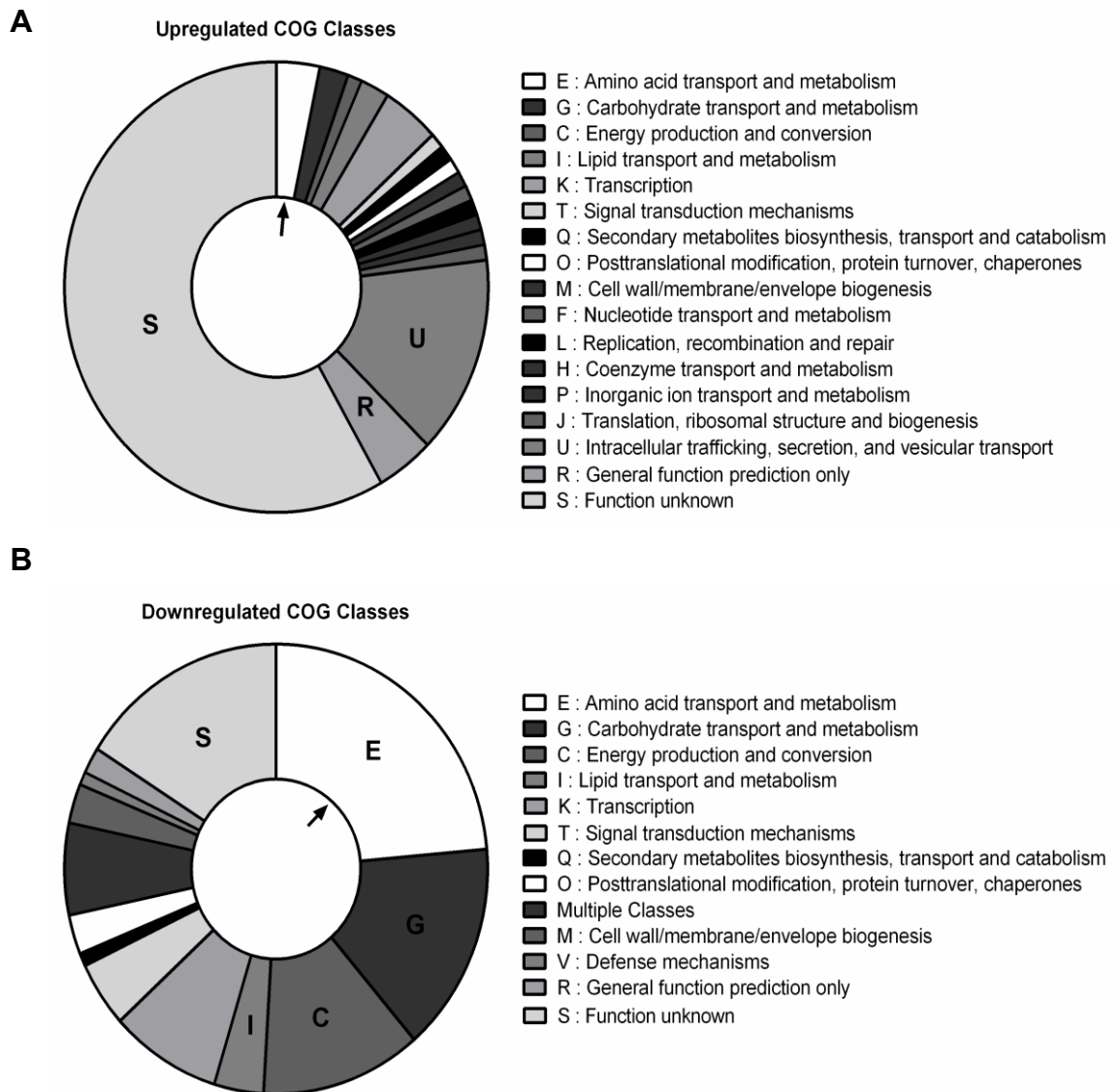


**Figure 10 Cluster of Orthologous Groups (COG) classification of differentially expressed genes in the *luxO* mutant. A. Upregulated COG classes. The T6SS2, f237 phage and integron region are classified into the COG classes S, R and U and are indicated within the chart. B. Downregulated COG classes. The letters E, G, C and I within the chart, indicate the COG categories involved in metabolism. The first COG class in each chart is indicated by an arrow. Following COG classes are represented in a clockwise arrangement.**

Of the total 208 differentially regulated features, 134 were from chromosome I and 74 were from chromosome II (**Table 4 and Table 5**). The 106 downregulated features were all annotated ORFs. The 102 upregulated features included 93 annotated ORFs, 3 small RNAs and 6 tRNAs. The *opaR* gene was induced and *aphA* was repressed in the *luxO* mutant compared to wild-type and this was confirmed by qPCR (**Figure 11A**). Expression analysis of the *qrrs* by qPCR showed that *qrr5* was significantly downregulated in the *luxO* mutant (**Figure 11A**). Twenty-one of the genes upregulated in the *luxO* mutant belonged to the T6SS-2 region on chromosome II (VPA1024 - 44), which was previously shown to be positively regulated by OpaR (Gode-Potratz and McCarter 2011). QPCR analysis of VPA1027 (*hcp2*) from the T6SS-2 cluster confirmed that in the *luxO* mutant this gene was induced (**Figure 11C**). Furthermore, qPCR analysis of *hcp1* (VP1393) from the T6SS-1 cluster and *yopD* (VP1656) from the T3SS-1 cluster showed their expression was reduced compared to wild-type (**Figure 11C**). The most highly upregulated genes in the *luxO* mutant were genes for the replication and synthesis of the filamentous phage f237 (VP1550-VP1562). Many genes within the class-1 integron region on chromosome I (VP1790-VP1851) were also induced in the *luxO* mutant compared to wild-type (Table S3A). The majority of the genes within the f237 phage and the class-1 integron were categorized into the COG classes S: Function unknown and R: General function prediction only (**Figure 10A**). The T6SS-2 genes were classified into the COG class U: Intracellular trafficking, secretion and vesicular transport (**Figure 10A**). Among the downregulated COG classes, most interesting to note was that 60% of the genes were classified into

categories involved in metabolism and transport (**Figure 10B**).

**Metabolism and transporter genes are downregulated in the *luxO* mutant.**

Of the 106 genomic features downregulated in the *luxO* mutant, 64 genes were involved in transport and metabolism of amino acids, carbohydrate and lipids (**Figure 10B and Table 5**). Downregulated gene clusters that comprised amino acid transport and metabolism included arginine biosynthesis (VP2756-VP2760) and transport (VPA0637-VPA0639) (Fig 3A), phenylalanine/ tyrosine biosynthesis (VP0546-VP0547, VP0555) and histidine biosynthesis (VP1137-VP1138). QPCR analysis confirmed the downregulation of VP2756 (*argH*), an ORF in the arginine biosynthesis (VP2756-VP2760) pathway (**Figure 11B**). The carbohydrate metabolism and transport genes downregulated in the *luxO* mutant included genes involved in D-mannitol metabolism (VPA0501-0502), D-galactose degradation (VP2397-VP2400) and L-arabinose transport and metabolism (VPA1671-VP1677) (**Table 5**). QPCR analysis confirmed the downregulation of VPA1674 (*araB*), an ORF in the arabinose catabolism pathway (**Figure 11B**). A region required for tetrathionate reductase synthesis (VP2012-VP2016) was also repressed in the *luxO* mutant compared to wild-type. Tetrathionate can be used as an electron donor that is produced in vertebrate intestinal mucosa from thiosulphate by the action of tetrathionate reductase (Liu, Denkmann et al. 2013). VP1771-VP1779 and VP1781-VP1782 are two operons involved in the polyamine putrescine utilization and all ORFs within this region were downregulated in the *luxO* mutant, which was confirmed by qPCR analysis of VP1779

(*puuD*) (**Figure 11B**). ORFs VP1447 to VP1451 are homologs of genes required for the synthesis of a putative anaerobic dimethyl sulfoxide reductase and these genes were all downregulated in the *luxO* mutant. There were eight putative transcription regulators downregulated in the *luxO* mutant compared to wild-type, VP0358 (DeoR), VP1778 (PuuR), VP3009 (AraC/XylS family), VPA0053 (TetR family), VPA0251 (LysR family), VPA0717 (LysR family), VPA0883 (LysR family), and VPA1678 (AraC/XylS family). In addition, genes for compatible solute biosynthesis were also downregulated, two genes in the ectoine biosynthesis pathway (VP1721-VP1720) and two genes involved in betaine biosynthesis (VPA1112) and transport (VPA1111) operon (**Table 5**).

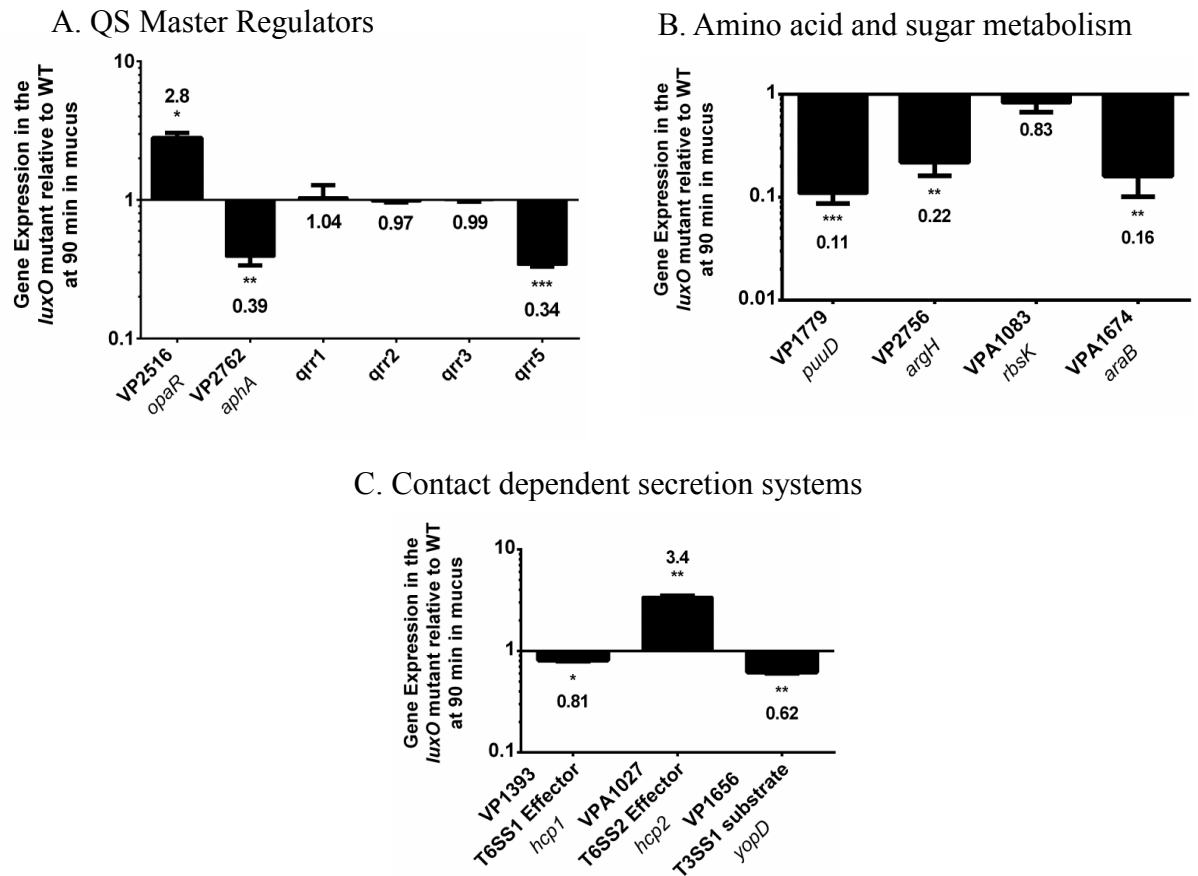


**Figure 11** qPCR validations of RNA Seq Expression in the *luxO* mutant relative to wild-type. Pre-ribozero treated RNA from the wild-type and the *luxO* mutant was used for cDNA synthesis and expression analyzed by qPCR in duplicate for each biological replicate. **A.** Bars represent the expression of the *opaR*, *aphA*, *qrr1*, *qrr2*, *qrr3* and *qrr5* normalized to 16S rRNA in the *luxO* mutant relative to wild-type cells. **B.** Bars represent the expression of four metabolism genes normalized to 16S rRNA in the *luxO* mutant relative to wild-type. **C.** Bars represent relative expression of T3SS and T6SS genes normalized to 16S rRNA in the *luxO* mutant relative to wild-type cells. *P* values were calculated using an unpaired Student's t-test with a 95% confidence interval. Asterisks denote significant differences in relative gene expression between mutant and wild-type. \*,  $P < 0.05$ ; \*\*,  $P < 0.01$ ; \*\*\*,  $P < 0.001$ .

### **Growth comparisons of wild-type and mutant strains on different carbon sources.**

Our RNA-seq data suggests that *luxO* could be at a metabolic disadvantage given the down regulation of many metabolism and transporter genes. We examined the growth patterns of the wild-type and QS mutants in 190 carbon sources to determine whether there were differences among the strains. A total of 71 different carbon sources were utilized by wild-type *V. parahaemolyticus* (**Figure 12**). There was a total of 33 substrates that the *luxO* mutant showed a defect in compared to the wild-type, seven substrates of which showed a defect only in the *luxO* mutant. The *aphA* mutant showed a significant defect in 30 substrates, five of which were unique to the mutant while 13 carbon sources showed defects also in the *luxO* (**Figure 12**). Thus, there were 25 carbon substrates that the *luxO* and *aphA* mutants showed a defect in growth in whereas the *opaR* mutant did not show a defect in these substrates. These 25 carbon sources included 6 amino acids or their derivatives, 4 dipeptides, 7 sugars, 2 nucleosides, 1 TCA cycle metabolite and 5 miscellaneous carbon sources. The most significant growth defects in the *luxO* mutant were growth on amino acids and their dipeptide derivatives; L-Aspartic acid, Glycyl-L-Aspartic acid, Glycyl-L-Glutamic, Glycyl L- Proline acid, L-Serine and L-Threonine (**Figure 12**). The *luxO* and *aphA* mutants also showed notable defects in L-Glutamic acid and L-Arginine, 2 TCA cycle metabolites (Pyruvic acid and  $\alpha$ -Keto-Glutamic acid) and 2 polysaccharides (Glycogen and inulin). We confirmed many of these growth defects by examining the growth pattern of the QS mutants in 12 of the carbon sources (**Figure 13**). The *opaR* mutant

did not show a defect in these carbon sources and grew similar to wild-type. These data suggest that the QS regulators may play a key role in regulation of cell metabolism. In addition, considering many of these carbon sources are components of intestinal mucus, which is the primary carbon source available for the bacteria *in vivo*, this disadvantage could contribute to these mutants being out-competed by the wild-type *in vivo*.

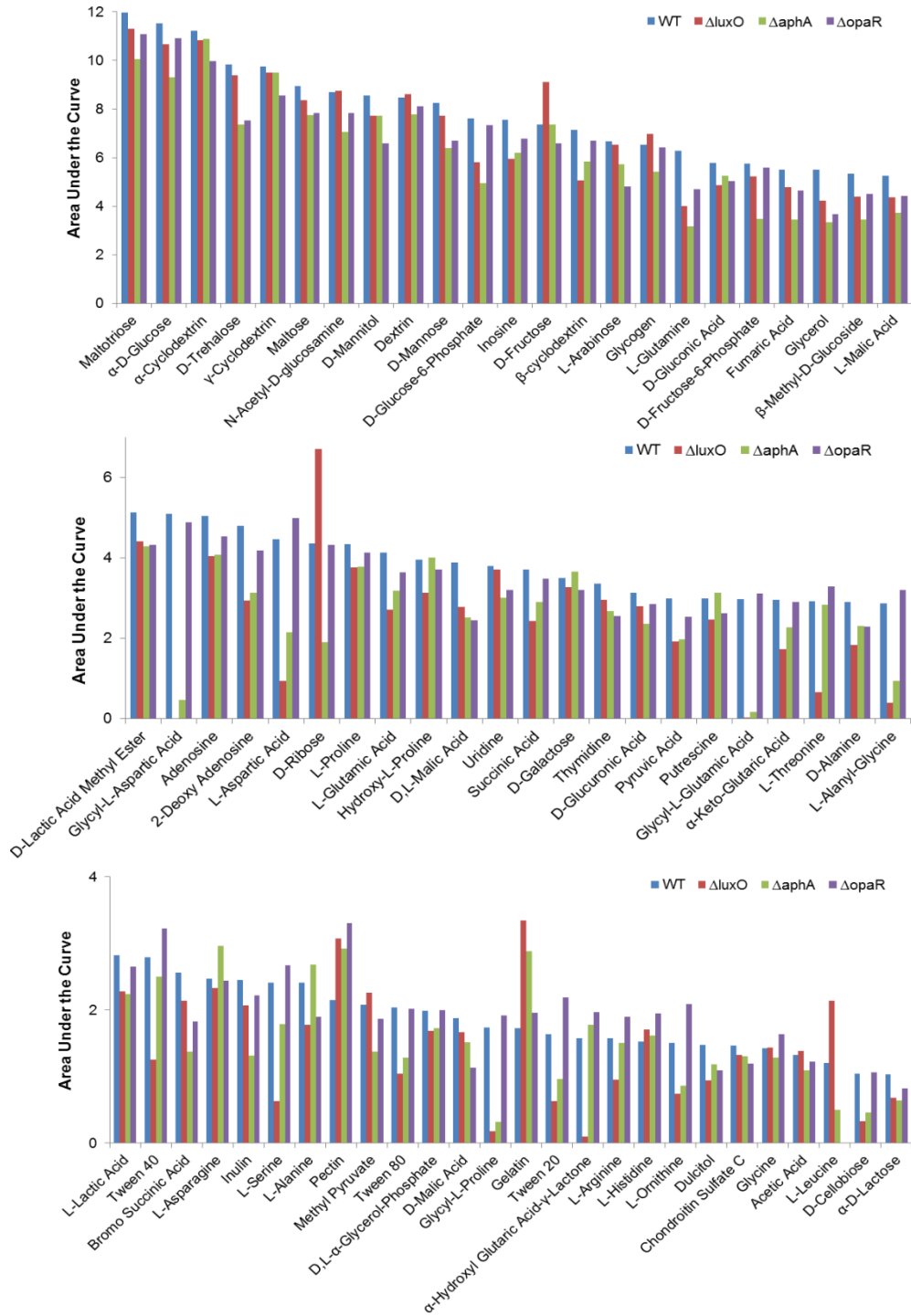


**Figure 12 Carbon phenotypic microarrays of *V. parahaemolyticus* wild-type and QS regulator mutants.** Bars represent Area Under the Growth Curve values for each strain in the carbon source.

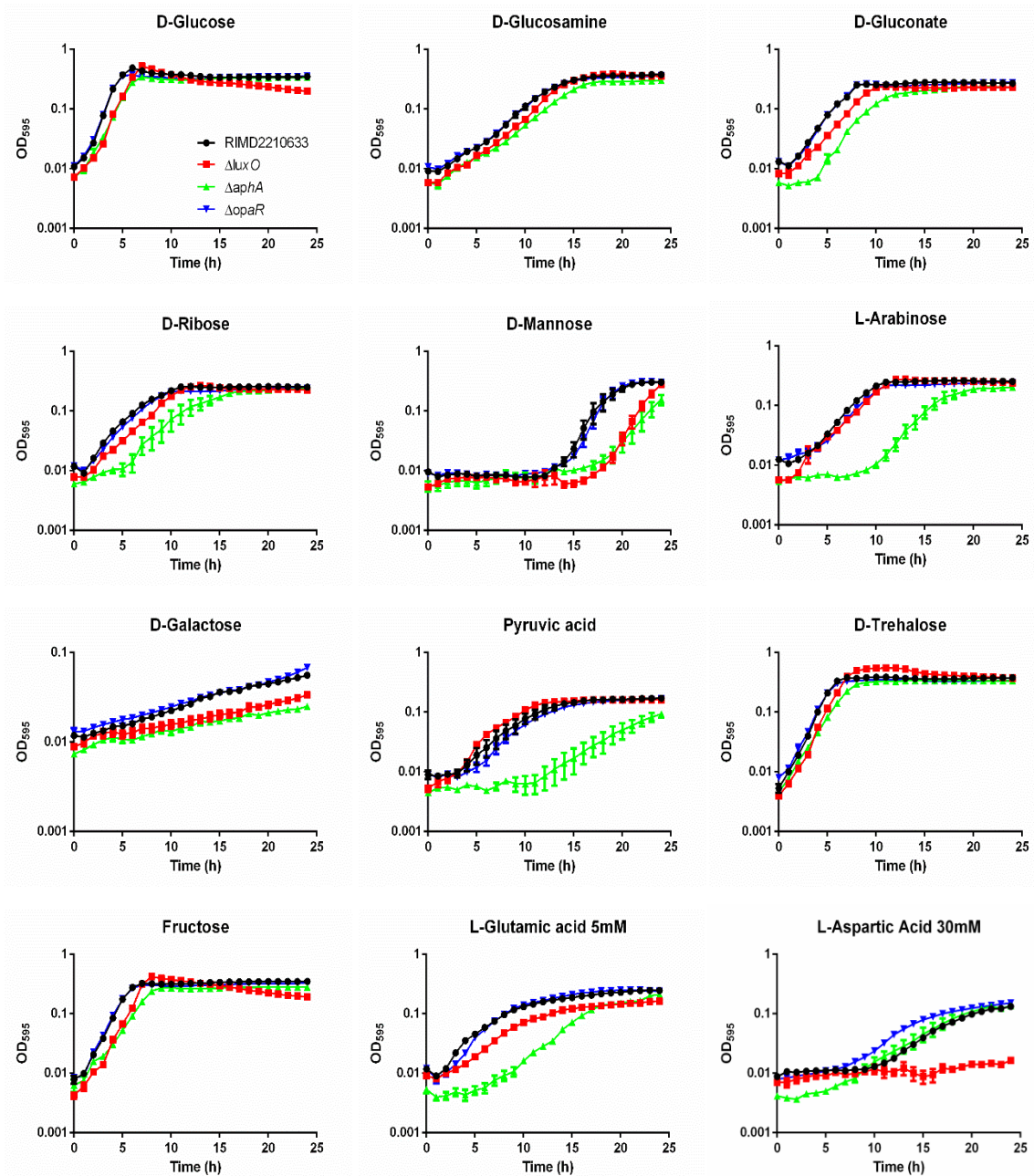


**Figure 13 Growth characteristics of *V. parahaemolyticus* wild-type and QS regulator mutants in various sugars and amino acids.** Strains were grown in M9 minimal media supplemented with 10mM of each carbon source unless otherwise specified.

### **Deletion of *opaR* leads to increased metabolic fitness in intestinal mucus and its components.**

Intestinal mucus is composed of glycoproteins known as mucins that are comprised of 80% oligosaccharide and 20% protein. The main sugars in mucin include fucose, galactose, mannose, sialic acid, N-acetyl glucosamine, and N-acetyl galactosamine, as well as arabinose, ribose, gluconate, galacturonate, and glucuronate. The three main amino acids that make up the protein core of mucin are serine, threonine and proline (Chang et al. 2004; Clamp, Fraser, and Read 1981; Conway, Krogfelt, and Cohen 2004; Corazziari 2009; Fabich et al. 2008). From genomic analysis, we know that *V. parahaemolyticus* cannot utilize fucose, sialic acid, or galacturonate, and only clinical strains can utilize arabinose. We examined growth of the *luxO*, *aphA* and *opaR* mutants on M9 supplemented individual mucus sugars as the sole carbon source (**Figure 13**). These data demonstrate that the *luxO* and *aphA* mutants had significantly longer lag phases than wild-type when grown on these substrates (**Figure 13**). These longer lag phases indicate that these mutants would be at a significant disadvantage at utilizing mucus as a carbon source in comparison to the wild-type strain.

In order to assess whether the metabolic fitness effects could account for the defect of the *luxO* and *aphA* mutant *in vivo*, we performed *in vitro* competition assays in M9 supplemented with mucus (M9M) or M9 with individual mucus sugars as sole carbon sources (**Figure 14**). We observed that the *luxO* mutant was out-competed in intestinal mucus with a CI of 0.6 (**Figure 14**) and mucus sugars gluconate, ribose and

arabinose with a CI of 0.3, 0.24 and 0.25 (**Figure 14**). The *aphA* mutant was also significantly out-competed by the wild-type in intestinal mucus with a CI of 0.59 and mucus sugars ribose and arabinose with a CI of 0.67 and 0.66 respectively (**Figure 14**). In addition, the competitive indices for the *opaR* mutant in *in vitro* competition assays showed the mutant significantly out-competed the wild-type in intestinal mucus with a CI of 1.6 (**Figure 14**). The *opaR* mutant also significantly out-competed wild-type in individual mucus sugars; mannose, ribose and arabinose with a CI of 1.6, 1.6 and 1.5 respectively (**Figure 14**). Overall, the *in vitro* metabolic assays suggest that not only is the presence of *aphA* important to the cells, in part due to its regulation of *opaR*, but also induced expression of *opaR* can have a detrimental effect. In contrast constitutive expression of *opaR* results in a fitness defect (*luxO* mutant), deletion of *opaR* provides a fitness advantage (*opaR* mutant) *in vitro*.

## *In vitro* competition assays

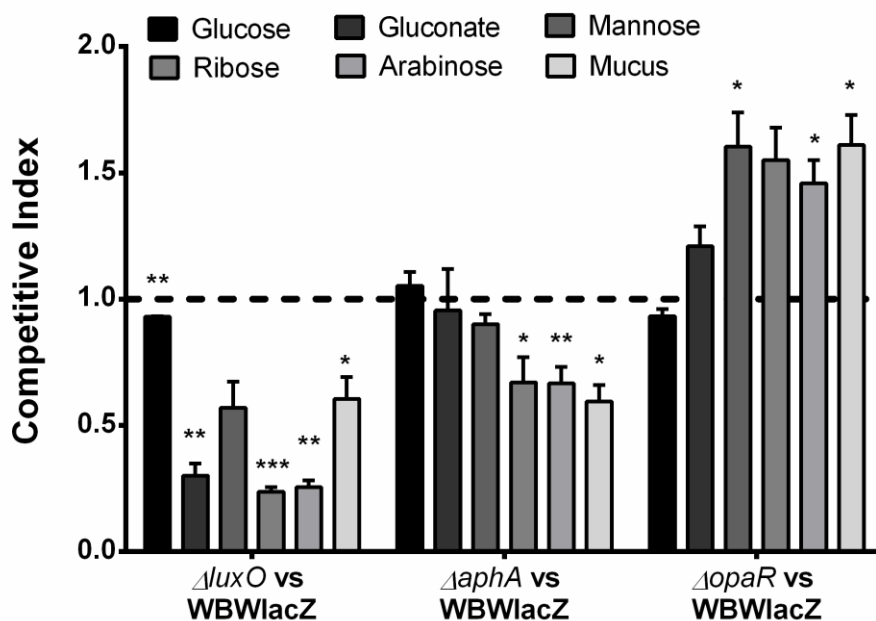


**Figure 14** *In vitro* competition assays of *V. parahaemolyticus* wild-type and the QS mutants *luxO*, *opaR* and *aphA*. *In vitro* competition assays between the WBWlacZ strain and the mutant strains in mucus and individual mucus sugars. *P* values were calculated using an unpaired Student's t-test with a 95% confidence interval. Asterisks denote significant differences in CI between the mutant strains and the wild-type. \*, *P* < 0.05, \*\*, *P* < 0.01, \*\*\*, *P* < 0.001

### **OpaR binding sites in the promoter regions of carbon transport and metabolism genes.**

Both the *luxO* and *aphA* mutants have a constitutively expressed *opaR* and a repressed *aphA*. We wanted to determine if the observed *in vitro* growth phenotypes were due to direct or indirect regulation of metabolism and transporter genes by OpaR. First, we performed bioinformatics analysis to identify putative binding sites for OpaR

in the promoter regions of 89 metabolism and transporter genes. We choose genes that were involved in the transport and metabolism of carbon sources that showed different growth patterns between wild-type and mutants in the phenotypic arrays. The MOODS tool was used to identify OpaR and AphA binding sites using the consensus sequence and position frequency matrix identified by Zhang et al (Zhang et al. 2012) and Sun et al (Sun et al. 2012). In this analysis, we identified 55 promoter regions with strong binding sites ( $P \leq 0.005$  and  $>90\%$  probability) for OpaR (**Table 6**). Interestingly the same analysis for AphA consensus binding sequence only identified 9 putative AphA binding sites suggesting that OpaR is the main QS regulator of metabolism (**Table 7**). Of the 55 putative OpaR binding sites, 28 OpaR binding sites were in promoter regions of operons and 27 binding sites were in single gene promoter regions. These included genes for arabinose, ribose, glucose, maltose, trehalose, mannitol, mannose, glycogen, glycerol, cellobiose and sperimidine/putrescine transport and/or metabolism. Putative OpaR binding sites were identified also in genes for a general amino acid transport (ORFs VP0008-VP0006, VP1620), thymidine, uridine, serine, aspartate, fumarate, glutarate, arginine, histidine, phenylalanine, tyrosine and tryptophan transport and/or metabolism. In contrast, of the 89 promoter regions examined for AphA binding sites only 9 promoter regions showed strong binding sites (probability  $>90\%$ ), which included mannose (VPA1424-VPA1425), arabinose (VPA1673-VPA1671), and glycogen (VPA1620) transport and/or metabolism genes (**Table 7**).

In order to validate the bioinformatics analysis of putative OpaR binding sites, we purified OpaR to homogeneity and performed EMSAs on five representative target promoter regions. The five targets were comprised of an amino acid transporter promoter region VP0008-VP0006, the polyamine putrescine cluster VP1779-VP1771, two sugar transporter promoter regions, mannitol (VPA0500-VPA0501) and ribose (VPA1087-VPA1084) and a promoter region for mannose transport and metabolism cluster (VPA1424-VPA1425). The glucose-specific PTS VPA1667 probe, was included as a negative control as it did not have any predicted OpaR binding sites. (**Figure 15**). For the *PVP0008*, OpaR bound to the 323-bp DNA probe with increasing concentration of OpaR protein (0-2.7  $\mu$ M). Similarly, promoter regions, *PVP1779* (244-bp), *PVPA1087* (333-bp), *PVPA0500* (360-bp) and *PVPA1424* (350-bp) were bound by OpaR in a concentration dependent manner (**Figure 15**). The negative DNA control target remained unbound by OpaR at the highest concentrations tested (**Figure 15**). These data demonstrate that OpaR binding is specific and that OpaR directly regulates the expression of these targets indicating that it plays a direct role in cell metabolism.

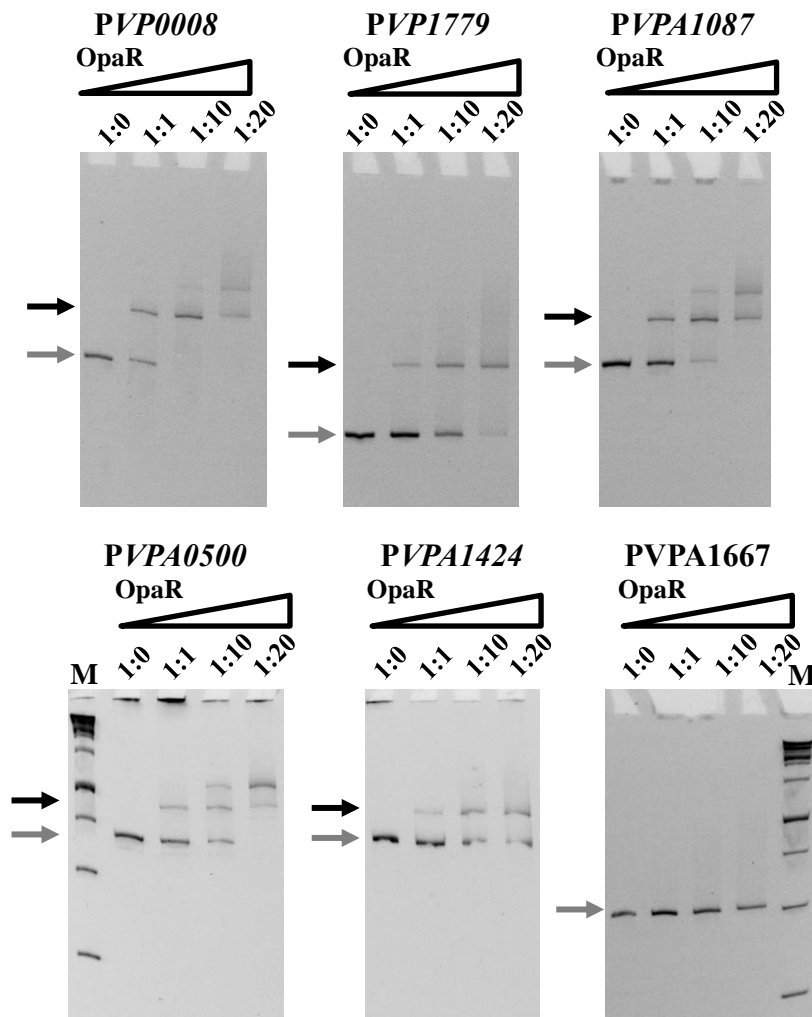


**Figure 15 OpaR binding sites in regulatory regions of metabolism and transporter genes.** Electrophoretic mobility shift assays (EMSAs) of the DNA fragments of promoter regions for VP0008, VP1779, VPA1087, VPA0500, and VPA1424. Varying concentrations of OpaR (0 -3.7  $\mu$ M) were incubated with DNA substrates corresponding to the promoter region of the following genes starting upstream of the translational ATG start site; VP0008 (PVP0008: DNA probe 323-bp), VP1779 (PVP1779: DNA probe 244-bp), VPA1087 (PVPA1087: DNA probe 333-bp), VPA0500 (PVPA0500): DNA probe 360-bp), and VPA1424 (PVPA1424: DNA probe 350-bp). Also included is the negative control DNA fragment from ORF VPA1667 (PVPA1667: DNA probe 308-bp). Binding of OpaR was shown for all sites chosen with putative OpaR binding sites. Grey arrows represent unbound DNA and black arrows represent bound DNA. M=marker.

## Discussion

In this study, we examined the role of QS regulators in *V. parahaemolyticus* pathogenesis, specifically their role in intestinal colonization. The *in vivo* colonization data show that the QS regulators are essential for efficient colonization. RNA-Seq transcriptome data between the *luxO* mutant and wild-type cells showed global gene expression differences. A striking feature of this data is the number of genes involved in cell metabolism and transport that were downregulated in the *luxO* mutant compared to wild-type. These included genes required for carbon transport and metabolism of substrates present in intestinal mucus, one of the main nutrient sources *in vivo*. The gene expression data suggested that the *luxO* mutant could have metabolic defects based on the down regulation of key metabolism genes. Competition for intestinal nutrients and the ability to utilize intestinal mucus as a carbon and energy source has been shown to be important for successful colonization of intestinal bacteria (Conway and Cohen 2015; Maltby et al. 2013; Stecher and Hardt 2011; Donaldson, Lee, and Mazmanian 2015). Phenotypic array data showed that the deletion of *luxO* resulted in metabolic defects, with the mutant demonstrating a defect in growth on a number of carbon sources. This was also showed to be the case for the *aphA* mutant, which showed a growth defect compared to wild-type in 25 carbon sources. The carbon substrates in which the mutants showed defects were comprised of nearly equal number of sugars, organic acids and peptides indicating that not just one pathway was affected. Some of the most significant growth defects were in the utilization of amino acids and amino acid derivatives, key intermediates in central

metabolism. The *luxO* mutant also had a defect in *in vitro* competition assays in mucus. This is not too surprising given that mucus is made of mainly the glycoprotein mucin and is therefore rich in amino acids as well as sugars (Clamp, Fraser, and Read 1981; Conway, Krogfelt, and Cohen 2004; Corazziari 2009; Fabich et al. 2008). Neither the single *aphA* nor the *opaR* mutants demonstrated a dramatic *in vitro* metabolic fitness effects compared to the *luxO* mutant although each had slightly different growth patterns in one or two carbon sources. One scenario to explain these differences is that in the *luxO* mutant, *aphA* expression is down as is *qrr* expression and *opaR* expression is highly induced. In the *aphA* mutant, *opaR* is induced, but so too should be the *qrrs*, which are negatively regulated by AphA in *V. harveyi*. Thus knocking out both *aphA* and *qrr* expression is more detrimental than just knocking out *aphA* alone. This suggests that there may be dual regulation of genes involved in metabolism and/or additional roles for the Qrrs.

A transcriptome study of *Pseudomonas aeruginosa* over 10 years ago demonstrated that the QS activated regulon was over represented by genes involved in intermediate central metabolism. They showed that the QS repressed regulon showed carbohydrate utilization and nutrient transport genes were the most abundant representatives (Schuster et al. 2003). A more recent study in the same species demonstrated a global impact of QS on the metabolome and proposed that QS plays a key role in metabolic rewiring of the cell under certain conditions (Davenport, Griffin, and Welch 2015). A study examining the targets of LuxR homologues in *Brucella* an intracellular pathogen, identified a large number of proteins involved in metabolic

pathways such as central metabolism or amino acid metabolism, respiration, transport of amino acids and sugars that were under the control of QS regulators (Uzureau et al. 2010). QS control of metabolic pathways that affects fitness has also been shown in *Burkholderia* species (Goo et al. 2012). Hwang and colleagues showed that QS regulates oxalate synthesis to counteract alkalization of the growth medium and was essential for fitness (Goo et al. 2012; An et al. 2014). More recently this same group has demonstrated that the QS master regulator QsmR down regulates glucose transport, substrate-level and oxidative phosphorylation and nucleotide biosynthesis acting as a metabolic brake on individuals as the population increases (An et al. 2014). Evidence for a role for LuxR in metabolism also comes from *Vibrio* species. In *V. harveyi*, it was demonstrated that the *argA*, *purM*, *lysE*, and *rluA* promoter regions were LuxR dependent, genes involved in arginine and purine biosynthesis, amino acid efflux, and pseudouridine synthesis, respectively (Miyamoto and Meighen 2006). In addition, it was demonstrated in *V. fischeri* that QS AinS signaling is essential for control of the acetate switch and this regulation is mediated through the LuxR homolog LitR (Studer, Mandel, and Ruby 2008). A recent study in *V. cholerae* showed that the QS LuxR homolog HapR regulated chitin metabolism that provided predator grazing resistance in biofilms. They showed that 19 of 22 genes involved in GlcNAc catabolism were repressed in a *hapR* mutant compared to wild-type (Sun et al. 2015).

QS regulation is required for both population level and individual control of gene expression, which corresponds to stationary phase and early exponential growth phases respectively, during which availability of the type and amount of nutrients is very different. Thus, the involvement of QS regulators controlling expression of transporter and metabolism genes makes biological sense. The *luxO* and *aphA* mutants had an *in vivo* defect that correlates to reduced metabolic fitness. In both these mutants OpaR is highly expressed, which suggests that OpaR could be a direct or indirect negative regulator of cell metabolism. Our RNA-seq data revealed that in the *luxO* mutant of the 106 genes that were downregulated 64 genes were involved in transport and metabolism. In addition, in the *luxO* mutant a number of regulators that could be involved in regulation of metabolism were also downregulated. These included genes belonging to the LysR family of proteins, which have been shown to regulate a diverse set of genes including those involved in metabolism (Maddocks and Oyston 2008), the AraC/XylS family of transcriptional regulators, which are predominantly involved in the regulation of carbon metabolism (Gallegos et al. 1997). Interestingly, we also found that the DNA-binding protein Fis (VP2885) was slightly upregulated in the *luxO* mutant (1.62-fold,  $P_{adj} < 0.0001$ ). Fis is a known global regulator of metabolism. In *Salmonella enterica*, Fis was shown to negatively regulate genes contributing to metabolism in the mammalian gut (Kelly et al. 2004). In addition, the Hfq-binding sRNA Spot 42 was upregulated in the *V. parahaemolyticus luxO* mutant. In *E. coli*, Spot 42 plays an essential role as a regulator in carbohydrate metabolism and uptake, and its expression is activated by glucose and inhibited by CRP. Spot 42

was shown to be a negative regulator of metabolism of many sugars in both *E. coli* and *Vibrio (Allivibrio) salmonicida* (Beisel and Storz 2011, 2012; Hansen et al. 2012; Moller et al. 2002). A second sRNA, VrrA was also induced in the *V. parahaemolyticus luxO* mutant. In *V. cholerae*, studies showed that a *vrrA* mutant had a 5 fold increased ability to colonize infant mice (Song et al. 2008). VrrA downregulates outer membrane proteins, OmpA and OmpT, the stationary phase survival factor Vrp and biofilm matrix protein RbmC in *V. cholerae* (Sabharwal et al. 2015; Song, Sabharwal, and Wai 2010).

To determine the possible extent of direct regulation of cell metabolism and transport by the QS regulators we performed bioinformatics analysis and examined 89 genes and operons for the presence of putative OpaR and AphA binding sites. We identified 55 loci that contained strong putative OpaR binding sites and only 9 AphA putative binding sites. From the 55 loci with putative OpaR binding sites, we chose five of these loci to examine further using EMSAs; a general amino acid transporter (VP0008-VP0006), ribose (VPA1087-VPA1084) and mannose (VPA1424-VPA1425) metabolism and transporter, mannitol (VPA0500-VPA0501) and putrescine metabolism (VP1771-VP1779) regulatory regions. EMSA analysis demonstrated binding to all five regulatory regions and no binding to the negative control using the highest concentration of OpaR. These data demonstrate a direct role for OpaR in cell metabolism and suggest that this role may be more prevalent than previously appreciated. We investigated the general amino acid transporter regulatory since both microarray and RNA seq analysis showed repression by OpaR (Gode-Potratz and

McCarter 2011; Kernell Burke et al. 2015). Our data agree with these findings. We examined the ribose and mannose regulatory regions since these sugars are important mucus sugars and we observed growth defects in these sugars in the *luxO* and *aphA* mutants compared to wild-type. We investigated binding to the regulatory region of the transporter of sugar alcohol mannitol because it had one of the strongest putative OpaR binding sites. The polyamine putrescine cluster VP1779-VP1771 is involved in putrescine metabolism and contains genes that shuttle into multiple metabolic pathways. All the genes in this pathway were downregulated in the *luxO* mutant compared to wild-type, and this was confirmed by qPCR and EMSA analysis showed binding of OpaR to the regulatory region. These data indicate that OpaR is a negative regulator of putrescine metabolism.

**Table 2 Bacterial strains and plasmids used in this study**

Strain	Genotype/ Strain Description	Reference
<i>Vibrio parahaemolyticus</i>		
RIMD2210633	O3:K6 clinical isolate, StrR	(Makino et al. 2003; Whitaker et al. 2010)
WBWlacZ	RIMD2210633, StrR, lacZ	(Whitaker et al. 2012)
SSK2099 ( $\Delta luxO$ )	RIMD2210633 $\Delta luxO$ (VP2099), StrR	This study
SSK2516 ( $\Delta opaR$ )	RIMD2210633 $\Delta opaR$ (VP2516), StrR	This study
SSK2762 ( $\Delta aphA$ )	RIMD2210633 $\Delta aphA$ (VP2762), StrR	This study
SSK9916 ( $\Delta luxO\Delta opaR$ )	RIMD2210633 $\Delta luxO \Delta opaR$ , StrR	This study
SSK1662 ( $\Delta opaR\Delta aphA$ )	RIMD2210633 $\Delta opaR \Delta aphA$ , StrR	This study
<i>Escherichia coli</i>		
DH5 $\alpha$ $\lambda$ pir	$\Delta lac$ <i>pir</i>	Laboratory strain
$\beta$ 2155 $\lambda$ pir	$\Delta dapA::erm$ <i>pir</i> for bacterial conjugation	Laboratory strain
BL21(DE3)	Expression strain	Laboratory strain
$\beta$ 2155 $\lambda$ pir $\Delta luxO$	$\beta$ 2155 $\lambda$ pir containing pDS132 $\Delta luxO$	This study
$\beta$ 2155 $\lambda$ pir $\Delta opaR$	$\beta$ 2155 $\lambda$ pir containing pDS132 $\Delta opaR$	This study
$\beta$ 2155 $\lambda$ pir $\Delta aphA$	$\beta$ 2155 $\lambda$ pir containing pDS132 $\Delta aphA$	This study
Plasmids		
pDS132	Suicide plasmid; Cmr; SacB	(Philippe et al. 2004)
pDS132 $\Delta luxO$	pDS132 harboring truncated <i>luxO</i> (VP2099)	This study
pDS132 $\Delta opaR$	pDS132 harboring truncated <i>opaR</i> (VP2516)	This study
pDS132 $\Delta aphA$	pDS132 harboring truncated <i>aphA</i> (VP2762)	This study
pJET1.2	Cloning vector, AmR	Fermentas
pJET1.2 OpaR	pJET1.2 harboring OpaR	This study
pProExHta	Expression vector, TEV site; AmR	Invitrogen
pProOpaR	pProExHta harboring OpaR; AmR	This study

**Table 3 Primers used in this study**

Use and primer	Sequence (5'-3')	T <sub>m</sub>	Product size (bp)
<b>Splice Overlap Extension PCR</b>			
SOEVP2099A	<u>TCT AGA</u> ACT AGA AGC GGC GAT GTA CC	60	493
SOEVP2099B	CGG CGT GAG GTA CGA ACG GTA T	65	
SOEVP2099C	ATA CCG TTC GTA CCT CAC GCC GGA AGA GCG GCA GAA GGT GTA A	60	496
SOEVP2099D	<u>GAG CTC</u> GCG TCA CGA CCG AGA TAA GT	60	
SOEVP2099FL For	ACG AGA AAA TGG GCA TTA CG	57	1356
SOEVP2099FL Rev	TGC TAA CCT CAG CCC TGA ATA CG	62	
SOEVP2516A	<u>TCT AGA</u> TGA GTC AGT TCA ATA GCA CGC	58	509
SOEVP2516B	TGC AAT TGA GTC CAT ATC C	52	
SOEVP2516C	GGA TAT GGA CTC AAT TGC ATG CAT CTA CAA TCG CGA ACA C	59	509
SOEVP2516D	<u>GAG CTC</u> GGC TTG GGT TGG TAA GAC AG	59	
SOEVP2516FL For	CGC TAA GCC ACA AAA TCT GA	56	1702
SOEVP2516FL Rev	ACC AAA CGG CAA ACT TAT CG	57	
SOEVP2762A	<u>TCT AGA</u> CAT GCT TCA AGC TGA ATT GC	56	561
SOEVP2762B	CAT GTC TTC AAT CCA AAT GGT	54	
SOEVP2762C	GAC CAT TTG GAT TGA AGA CAT GAC TTG GGC AGA AGA AGT CCT	66	569
SOEVP2762D	<u>GAG CTC</u> GGC TTT TCC AGA AGT GCA TC	62	
SOEVP2762FL For	ACA CCA AGT GCA ACA TGG AA	55	1511
SOEVP2762FL Rev	CGA TGC AAC ACG TTC AGA GT	56	

Table 3 Continued

<b>qPCR primers</b>			
VP2516For	TCA TGG AAA TCG CGT TAG AA	55	123
VP2516Rev	CTT CGC GAG TTG GGA AGT AG	58	
VP2762For	AGC CAC CAA CAA GTT TAC CG	59	140
VP2762Rev	CAT TCT CCA AGA GCG CTA CG	59	
<i>qrr1</i> For	CTC GGG TCA CCT AGC CAA CT	61	85
<i>qrr1</i> Rev	AAG AAG CCA ATA GGC AGT CG	58	
<i>qrr2</i> For	CTT AAG CCG AGG GTC ACC TA	59	95
<i>qrr2</i> Rev	ATA GCC AAC CGC AAT AAT CG	56	
<i>qrr3</i> For	CTT AAG CCG AGG GTC ACC TA	59	95
<i>qrr3</i> Rev	ATA GCC AAC CGC AAA GAG TG	50	
<i>qrr5</i> For	TCT AAG CCG AGG GTC ACC TA	59	95
<i>qrr5</i> Rev	AAA AGC CAA CCA CAA GGT GT	58	
VP1779For	GAG ACG ACG TTG CCA CCA TA	60	156
VP1779Rev	CCG CGT GAC GAA TTA ACG TC	60	
VP2756For	TCT CGT AAC GAC CAA GTG GC	60	192
VP2756Rev	CGC CAA ACA CCA ATG AGC AA	60	
VPA1083For	CCT TTT GCA CCG AGA GTG AT	55	222
VPA1083Rev	TGT GGC AAA AGA TGC AAA AA	52	
VPA1674For	ATG CCT GGT TCA AAA ACG T	53	211
VPA1674Rev	CCT TTA AGA CGC TGG TTT GC	55	
VP1393For	CGG TGA AAC TCA AGG TCA CA	58	135
VP1393Rev	TGT GGA TCA CGT GGA ACA GT	59	
VPA1027For	ACC GAT TGT TGC TTC CTT GA	58	142
VPA1027Rev	TTG GAG TGT TGG TCG TGA AA	58	
VP1656For	CAC TTG GTA AAG CAG CGT CA	55	196
VP1656Rev	TCA ATT AGA TGG GCC GAA AG	52	
16sRNA_FWD	ACC GCC TGG GGA GTA CGG TC	66	234
16sRNA_REV	TTG CGC TCG TTG CGG GAC TT	66	
<b>OpaR cloning</b>			
SfoIVP2516Fwd	<u>TAC GGC</u> GCC ATG GAC TCA ATT GCA AAG AG	54	615
SacIVP2516Rev	CAC GAG CTC TTA GTG TTC GCG ATT GTA GA	52	

Table 3 Continued

<b>EMSA Primers</b>			
VP0008_EMSA_For	GCG AGA TCG ACA GAT TGG TGA	57	323
VP0008_EMSA_Rev	AGA CAT GCC CAC CTT GAC TT	57	
VPA1087_EMSA_For	TGT GGC AGA TTT CCT TCC CG	58	333
VPA1087_EMSA_Rev	CAT CTC ATC GAC CTT TCG GT	58	
VP1779_EMSA_For	GCT TTT GGT GTT TAA CGA CTG GT	60	244
VP1779_EMSA_Rev	CCA ATG ATG GGT TTG CGT GTT	60	
VPA0500_EMSA_For	TAC GTT TGA GTG CGA GCC AT	57	360
VPA0500_EMSA_Rev	TGG TCG ATT AAC TCG TAC AGC A	56	
VPA1424_EMSA_For	CCG GAC TGG ACT TTT GTG CT	56	350
VPA1424_EMSA_Rev	TTA GTT TGG TGA TCA TTG TCG AAC C	57	
VPA1667_EMSA_For	GCA GGT CGA GGT TGT CAT CG	56	308
VPA1667_EMSA_Rev	TGC AAA CAT GGT TTC CTC CTG	58	

**Table 4 Differential expressed genes induced in the *luxO* mutant compared to wild-type.**

<b>Locus Tag</b>	<b>baseMean</b>	<b>log2FoldChange</b>	<b>lfcSE</b>	<b>stat</b>	<b>pvalue</b>	<b>padj</b>
VP0023	269.42	1.10	0.128	8.612	7.18E-18	1.55E-16
EBG00000020412	102.57	2.14	0.295	7.257	3.96E-13	5.50E-12
svpa117.1	18.14	1.79	0.316	5.669	1.44E-08	1.17E-07
VP0161	1060.62	1.01	0.094	10.822	2.70E-27	1.13E-25
VP0348	57.86	1.42	0.246	5.763	8.27E-09	6.94E-08
VP0394	1581.60	1.16	0.077	15.152	7.36E-52	8.22E-50
VP0586	403.27	1.88	0.104	17.997	2.06E-72	4.09E-70
VP0593	1037.14	1.00	0.161	6.238	4.43E-10	4.37E-09
VP1070	184.64	2.26	0.249	9.054	1.38E-19	3.30E-18
svpa1295.1	54.15	1.73	0.238	7.241	4.44E-13	6.09E-12
VP1252	1412.33	1.34	0.092	14.604	2.64E-48	2.42E-46
VP1253	5293.07	1.17	0.050	23.340	1.75E-120	8.01E-118
VP1276	143.68	1.18	0.187	6.295	3.07E-10	3.07E-09

Table 4 Continued

VP1302	353.19	1.09	0.106	10.241	1.30E-24	4.63E-23
VP1423	443.06	1.39	0.185	7.493	6.71E-14	1.01E-12
VP1429	96.79	1.10	0.207	5.332	9.71E-08	7.19E-07
VP1434	63.72	1.20	0.207	5.783	7.33E-09	6.24E-08
VP1534	11.03	1.43	0.328	4.362	1.29E-05	6.76E-05
VP1550	36.60	2.63	0.324	8.108	5.16E-16	9.57E-15
VP1551	702.75	5.40	0.206	26.224	1.41E-151	1.08E-148
VP1552	420.82	5.08	0.229	22.137	1.38E-108	5.28E-106
VP1553	217.10	4.13	0.263	15.690	1.78E-55	2.21E-53
VP1554	1268.13	5.10	0.183	27.851	1.04E-170	1.58E-167
VP1555	1392.19	5.10	0.216	23.591	4.76E-123	2.73E-120
VP1556	153.03	3.80	0.235	16.152	1.09E-58	1.67E-56
VP1557	21.76	2.32	0.322	7.199	6.07E-13	8.18E-12
VP1558	110.53	3.16	0.240	13.153	1.64E-39	1.16E-37
VP1562	76.48	1.85	0.210	8.788	1.52E-18	3.49E-17
VP1790	137.27	1.07	0.158	6.751	1.47E-11	1.67E-10
VP1794	234.00	1.01	0.142	7.093	1.31E-12	1.68E-11
VP1796	275.36	1.02	0.131	7.790	6.71E-15	1.09E-13
VP1798	100.51	1.27	0.178	7.112	1.14E-12	1.49E-11
VP1803	37.90	1.18	0.249	4.754	1.99E-06	1.21E-05
VP1810	133.70	1.21	0.150	8.049	8.37E-16	1.50E-14
VP1826	234.28	1.12	0.129	8.716	2.89E-18	6.42E-17
VP1848	266.38	1.08	0.174	6.233	4.58E-10	4.50E-09
VP1849	104.49	1.24	0.173	7.163	7.91E-13	1.05E-11
VP1850	431.49	1.01	0.172	5.902	3.60E-09	3.17E-08
VP1851	2237.22	1.00	0.125	8.002	1.22E-15	2.17E-14
VP1888	1264.44	2.16	0.217	9.962	2.24E-23	7.03E-22
VP1889	4936.65	2.35	0.176	13.369	9.14E-41	6.76E-39
VP1890	21222.11	2.07	0.200	10.360	3.78E-25	1.40E-23
VP1987	730.75	1.13	0.076	14.849	7.06E-50	7.03E-48
VP1992	298.33	1.13	0.157	7.166	7.72E-13	1.03E-11
VP2000	26.91	1.34	0.280	4.768	1.86E-06	1.14E-05
VP2001	52.07	1.30	0.226	5.724	1.04E-08	8.64E-08
VP2002	127.82	1.33	0.208	6.373	1.85E-10	1.92E-09

Table 4 Continued

VP2003	147.06	1.51	0.159	9.526	1.64E-21	4.60E-20
VP2020	587.89	1.08	0.094	11.469	1.89E-30	9.30E-29
VP2021	184.83	1.10	0.144	7.630	2.35E-14	3.67E-13
VP2098	1737.62	3.42	0.080	42.677	0	0
VP2388	766.77	1.07	0.070	15.272	1.18E-52	1.38E-50
EBG00000020405	88.63	1.07	0.219	4.897	9.75E-07	6.23E-06
VP2516	4164.54	1.57	0.107	14.646	1.43E-48	1.37E-46
VP2520	797.42	1.29	0.192	6.726	1.75E-11	1.96E-10
VP2581	340.12	1.12	0.110	10.214	1.71E-24	5.99E-23
EBG00000020371	19.83	2.09	0.327	6.412	1.43E-10	1.49E-09
EBG00000020402	94.63	1.15	0.219	5.252	1.50E-07	1.08E-06
VP2636	123.34	1.08	0.153	7.036	1.98E-12	2.49E-11
VP2638	416.36	1.23	0.107	11.519	1.06E-30	5.46E-29
EBG00000020331	27.34	1.83	0.321	5.687	1.30E-08	1.07E-07
EBG00000020307	23.17	1.42	0.323	4.392	1.13E-05	5.94E-05
VPA0010	381.18	1.20	0.096	12.511	6.47E-36	3.95E-34
VPA0029	124.73	1.10	0.215	5.103	3.35E-07	2.30E-06
VPA0347	4661.35	1.64	0.203	8.069	7.07E-16	1.29E-14
VPA0348	2300.27	1.57	0.223	7.015	2.31E-12	2.89E-11
VPA0459	221.70	1.53	0.137	11.195	4.32E-29	2.02E-27
VPA0568	127.30	1.16	0.163	7.121	1.07E-12	1.41E-11
VPA0653	49.12	1.02	0.221	4.623	3.79E-06	2.19E-05
VPA0659	29.33	1.44	0.280	5.149	2.62E-07	1.83E-06
VPA0914	511.60	1.10	0.084	13.027	8.61E-39	5.98E-37
VPA1024	222.12	1.57	0.127	12.293	9.91E-35	5.67E-33
VPA1025	123.83	1.23	0.182	6.742	1.56E-11	1.76E-10
VPA1026	803.11	1.50	0.194	7.760	8.52E-15	1.36E-13
VPA1027	1886.78	2.09	0.124	16.906	4.04E-64	7.13E-62
VPA1028	191.74	1.05	0.262	4.002	6.28E-05	0.000287
VPA1029	60.88	1.51	0.240	6.299	2.99E-10	3.01E-09
VPA1030	211.89	2.00	0.183	10.951	6.55E-28	2.91E-26
VPA1031	66.97	1.78	0.250	7.102	1.23E-12	1.59E-11
VPA1032	104.14	2.08	0.224	9.291	1.53E-20	4.10E-19
VPA1033	279.58	2.12	0.234	9.072	1.17E-19	2.84E-18

Table 4 Continued

VPA1034	796.61	2.03	0.186	10.945	7.06E-28	3.11E-26
VPA1035	305.19	1.85	0.210	8.809	1.26E-18	2.91E-17
VPA1036	337.45	2.41	0.219	11.005	3.62E-28	1.64E-26
VPA1037	268.97	2.41	0.210	11.475	1.76E-30	8.84E-29
VPA1038	286.57	2.32	0.195	11.881	1.49E-32	8.15E-31
VPA1039	1583.29	2.27	0.206	11.013	3.31E-28	1.52E-26
VPA1040	487.62	2.70	0.200	13.503	1.50E-41	1.15E-39
VPA1041	663.05	2.66	0.167	15.970	2.08E-57	3.08E-55
VPA1042	213.60	1.97	0.230	8.589	8.80E-18	1.89E-16
VPA1043	589.01	2.38	0.211	11.255	2.19E-29	1.04E-27
VPA1044	428.83	1.78	0.171	10.392	2.69E-25	1.00E-23
VPA1202	3427.85	1.98	0.088	22.580	6.84E-113	2.85E-110
VPA1203	1632.97	1.97	0.125	15.812	2.58E-56	3.29E-54
VPA1204	1650.13	1.71	0.163	10.475	1.13E-25	4.35E-24
VPA1205	1215.47	1.73	0.136	12.731	3.99E-37	2.54E-35
VPA1291	110.23	1.55	0.180	8.569	1.04E-17	2.23E-16
svpa1370.1	60.36	1.27	0.212	5.999	1.99E-09	1.82E-08
VPA1505	65.91	1.00	0.213	4.700	2.60E-06	1.54E-05
VPA1572	2582.44	1.46	0.069	21.031	3.40E-98	1.11E-95
VPA1612	269.28	1.19	0.145	8.247	1.62E-16	3.14E-15
VPA1648	2832.55	1.18	0.071	16.590	8.26E-62	1.35E-59

**Table 5 Differential expressed genes repressed in the *luxO* mutant compared to wild-type.**

<b>Locus Tag</b>	<b>baseMean</b>	<b>log2FoldChange</b>	<b>lfcSE</b>	<b>stat</b>	<b>pvalue</b>	<b>padj</b>
VP0048	12401.97	-1.15	0.066	17.443	3.89E-68	7.12E-66
VP0060	208.48	-1.00	0.178	-5.589	2.28E-08	1.81E-07
VP0061	278.88	-1.12	0.161	-6.926	4.32E-12	5.25E-11
VP0074	130.01	-1.14	0.145	-7.885	3.15E-15	5.22E-14
VP0287	54.49	-1.03	0.221	-4.683	2.83E-06	1.67E-05
VP0358	1068.91	-1.49	0.107	13.913	5.30E-44	4.41E-42
VP0369	537.67	-1.07	0.085	12.527	5.29E-36	3.28E-34
VP0484	6997.60	-1.38	0.150	-9.196	3.71E-20	9.56E-19
VP0546	957.39	-1.30	0.302	-4.311	1.62E-05	8.37E-05
VP0547	578.81	-1.08	0.089	12.223	2.33E-34	1.32E-32
VP0555	1831.68	-1.55	0.102	15.233	2.12E-52	2.43E-50
VP0583	42849.75	-1.01	0.102	-9.960	2.29E-23	7.13E-22
VP0618	1266.72	-2.35	0.257	-9.145	5.95E-20	1.49E-18
VP0699	426.45	-1.23	0.134	-9.187	4.03E-20	1.03E-18
VP0826	3937.76	-1.64	0.179	-9.173	4.58E-20	1.17E-18
VP1008	2254.84	-2.17	0.080	26.999	1.52E-160	1.74E-157
VP1053	3706.95	-1.15	0.142	-8.113	4.93E-16	9.22E-15
VP1137	4205.23	-1.31	0.111	11.844	2.32E-32	1.25E-30
VP1138	3526.88	-1.06	0.116	-9.159	5.22E-20	1.32E-18
VP1254	352.73	-1.02	0.094	10.858	1.83E-27	7.91E-26
VP1284	2178.50	-1.10	0.086	12.763	2.65E-37	1.76E-35
VP1315	608.62	-1.04	0.115	-9.058	1.33E-19	3.19E-18
VP1379	1052.03	-1.37	0.087	15.823	2.16E-56	2.83E-54

Table 5 Continued

VP1447	637.16	-1.42	0.133	-10.628	2.21E-26	8.88E-25
VP1448	182.31	-1.91	0.148	-12.897	4.69E-38	3.20E-36
VP1449	259.46	-1.70	0.113	-15.061	2.90E-51	3.02E-49
VP1450	180.69	-1.79	0.133	-13.514	1.29E-41	1.01E-39
VP1451	119.84	-1.87	0.184	-10.158	3.04E-24	1.03E-22
VP1506	329.14	-1.19	0.178	-6.702	2.06E-11	2.27E-10
VP1647	963.77	-1.09	0.156	-6.967	3.23E-12	3.97E-11
VP1651	226.16	-1.59	0.173	-9.223	2.88E-20	7.59E-19
VP1720	7064.58	-1.09	0.103	-10.623	2.32E-26	9.26E-25
VP1721	26662.90	-1.15	0.101	-11.390	4.69E-30	2.26E-28
VP1771	519.26	-1.42	0.166	-8.539	1.36E-17	2.90E-16
VP1772	347.19	-1.19	0.114	-10.421	1.98E-25	7.57E-24
VP1773	232.00	-1.22	0.114	-10.674	1.35E-26	5.54E-25
VP1774	290.15	-1.46	0.114	-12.813	1.39E-37	9.38E-36
VP1775	647.82	-1.81	0.114	-15.879	8.80E-57	1.22E-54
VP1776	211.76	-2.27	0.154	-14.742	3.46E-49	3.37E-47
VP1777	1390.62	-2.66	0.131	-20.288	1.66E-91	4.74E-89
VP1778	1527.98	-2.93	0.163	-17.992	2.26E-72	4.32E-70
VP1779	3239.51	-3.17	0.146	-21.665	4.43E-104	1.56E-101
VP1781	3456.28	-3.33	0.142	-23.382	6.56E-121	3.34E-118
VP1782	1117.31	-1.87	0.162	-11.517	1.08E-30	5.52E-29
VP1966	282.55	-1.07	0.106	-10.103	5.34E-24	1.76E-22
VP2012	309.39	-2.03	0.300	-6.769	1.30E-11	1.49E-10
VP2013	124.25	-1.28	0.283	-4.523	6.10E-06	3.39E-05
VP2014	304.63	-1.13	0.256	-4.420	9.87E-06	5.26E-05
VP2015	180.67	-3.83	0.209	-18.319	5.86E-75	1.28E-72
VP2016	112.18	-2.11	0.312	-6.747	1.51E-11	1.71E-10
VP2099	610.61	-3.42	0.292	-11.732	8.71E-32	4.64E-30
VP2159	111.36	-1.35	0.153	-8.778	1.66E-18	3.79E-17
VP2212	456.57	-1.37	0.098	-13.937	3.78E-44	3.21E-42
VP2321	614.70	-1.01	0.086	-11.656	2.14E-31	1.11E-29
VP2371	2336.03	-2.27	0.225	-10.117	4.66E-24	1.56E-22
VP2397	266.26	-1.91	0.191	-9.998	1.55E-23	4.90E-22
VP2398	327.25	-1.99	0.148	-13.400	6.01E-41	4.51E-39

Table 5 Continued

VP2399	188.86	-1.63	0.209	-7.817	5.39E-15	8.76E-14
VP2400	241.72	-2.03	0.146	-13.937	3.76E-44	3.21E-42
VP2403	134.72	-1.23	0.168	-7.354	1.93E-13	2.80E-12
VP2653	38313.97	-2.26	0.237	-9.498	2.14E-21	5.95E-20
VP2756	17766.15	-2.16	0.211	-10.259	1.08E-24	3.88E-23
VP2757	8582.22	-2.47	0.297	-8.313	9.32E-17	1.82E-15
VP2758	8851.43	-2.67	0.177	-15.067	2.65E-51	2.83E-49
VP2759	11779.83	-1.97	0.267	-7.357	1.88E-13	2.74E-12
VP2760	2065.00	-2.21	0.174	-12.733	3.90E-37	2.51E-35
VP2876	8762.37	-1.33	0.104	-12.757	2.83E-37	1.85E-35
VP2878	41256.68	-1.15	0.112	-10.238	1.34E-24	4.74E-23
VP2920	6338.76	-1.37	0.071	-19.135	1.28E-81	3.46E-79
VP3009	382.29	-1.29	0.142	-9.074	1.14E-19	2.80E-18
VP3064	593.29	-1.45	0.200	-7.273	3.51E-13	4.93E-12
VPA0053	273.59	-1.07	0.103	-10.356	3.92E-25	1.44E-23
VPA0196	3008.27	-1.00	0.068	-14.606	2.56E-48	2.39E-46
VPA0198	109.96	-1.20	0.163	-7.349	2.00E-13	2.90E-12
VPA0229	194.39	-1.15	0.116	-9.929	3.13E-23	9.62E-22
VPA0251	52.36	-1.40	0.204	-6.868	6.51E-12	7.73E-11
VPA0279	327.37	-1.16	0.138	-8.448	2.96E-17	6.06E-16
VPA0318	1875.43	-1.20	0.153	-7.851	4.12E-15	6.74E-14
VPA0501	60.28	-1.16	0.187	-6.186	6.17E-10	5.94E-09
VPA0502	94.66	-1.28	0.160	-7.981	1.46E-15	2.54E-14
VPA0511	504.93	-1.71	0.091	-18.843	3.35E-79	8.09E-77
VPA0637	1368.87	-1.62	0.191	-8.485	2.16E-17	4.44E-16
VPA0638	712.36	-1.96	0.233	-8.431	3.43E-17	6.95E-16
VPA0639	441.73	-2.39	0.225	-10.655	1.65E-26	6.71E-25
VPA0640	29.26	-1.18	0.261	-4.502	6.72E-06	3.70E-05
VPA0656	30.95	-1.30	0.246	-5.302	1.14E-07	8.40E-07
VPA0693	205.55	-1.15	0.115	-10.024	1.20E-23	3.81E-22
VPA0707	1758.52	-1.08	0.100	-10.853	1.94E-27	8.31E-26
VPA0717	148.11	-1.28	0.135	-9.481	2.52E-21	6.96E-20
VPA0883	466.03	-1.18	0.145	-8.090	5.97E-16	1.10E-14
VPA0957	646.94	-1.32	0.126	-10.495	9.11E-26	3.54E-24

Table 5 Continued

VPA1111	2097.44	-1.02	0.099	-10.257	1.11E-24	3.96E-23
VPA1112	3352.47	-1.15	0.071	-16.374	2.96E-60	4.67E-58
VPA1120	523.45	-1.00	0.226	-4.437	9.12E-06	4.89E-05
VPA1417	907.33	-1.06	0.110	-9.627	6.12E-22	1.76E-20
VPA1570	105.10	-1.64	0.161	-10.190	2.20E-24	7.59E-23
VPA1638	2642.96	-1.65	0.091	-18.180	7.37E-74	1.54E-71
VPA1670	40.46	-1.04	0.217	-4.805	1.55E-06	9.65E-06
VPA1671	580.23	-2.90	0.158	-18.350	3.32E-75	7.61E-73
VPA1672	1328.77	-3.19	0.102	-31.166	3.04E-213	6.97E-210
VPA1673	2077.28	-3.48	0.139	-24.939	2.81E-137	1.84E-134
VPA1674	392.81	-2.36	0.190	-12.421	2.01E-35	1.18E-33
VPA1675	168.27	-2.30	0.159	-14.514	9.93E-48	8.92E-46
VPA1676	668.74	-2.35	0.153	-15.308	6.73E-53	8.12E-51
VPA1677	208.27	-2.02	0.149	-13.592	4.47E-42	3.53E-40
VPA1678	349.17	-1.01	0.123	-8.213	2.16E-16	4.11E-15

**Table 6 Putative OpaR binding sites identified by the MOODS algorithm.**

Operon	Function	OpaR Binding Site Prediction				
		Upstream ATG		Log odds score	Probability	P-Value
		Start	End			
VP2046	Glucose specific PTS	270	251	7.696	1.000	0.00006
		261	242	6.008	0.998	0.0004
		28	9	5.993	0.998	0.0004
VP2038	ROK family transcriptional regulator glucokinase	166	147	4.305	0.987	0.002
		69	50	3.827	0.979	0.002
		65	46	3.442	0.969	0.003
		124	105	2.613	0.932	0.004
		181	162	2.590	0.930	0.004
		72	53	2.322	0.911	0.005
VP2158	Glucose-6-phosphate 1-epimerase	85	66	3.359	0.966	0.002
VPA0038	NagB	51	32	4.117	0.984	0.002
		248	229	3.380	0.967	0.003
VPA1619	4-alpha-glucanotransferase (Maltose -> α-D-Glucose)	66	47	3.405	0.968	0.002
VP0710-0711	Trehalose specific PTS and Trehalose-6-P hydrolase	146	127	7.620	1.000	0.00007
VP0370-0368	PTS Subunit IIABC	237	218	6.644	0.999	0.0002
		204	185	4.763	0.992	0.001
		208	189	4.712	0.991	0.001
		281	262	3.664	0.975	0.003
		246	227	3.218	0.962	0.003
VPA0500-0501	PTS	47	28	6.705	0.999	0.0002
		210	191	3.317	0.965	0.003
		186	167	2.995	0.952	0.004
VPA1424-1425	PTS system fructose-specific transporter subunit IIABC Mannose-6-phosphate isomerase	315	296	3.989	0.982	0.002
		31	12	3.907	0.980	0.002
		250	231	3.100	0.957	0.003

Table 6 Continued

VPA1620	Maltodextrin Phosphorylase	153	134	4.729	0.991	0.0007
VPA1645		426	407	4.882	0.992	0.0006
		26	7	2.492	0.924	0.004
VPA1673-1671	Arabinose transport	245	226	4.271	0.986	0.002
		233	214	3.239	0.962	0.003
		291	272	3.000	0.953	0.003
VPA1674-1677	Arabinose degradation	146	127	4.271	0.986	0.002
		158	139	3.239	0.962	0.003
		100	81	3.000	0.953	0.003
VPA1087-1084	D-Ribose transport	73	54	5.030	0.994	0.0006
		82	63	2.544	0.927	0.003
VPA1083	Ribokinase	112	93	2.350	0.913	0.005
VP2398-97	Galactose	27	8	2.749	0.940	0.003
VP2400-2399	Galactose	348	329	2.612	0.932	0.003
VP1207	Xanthosine 5-P -> Xanthosine	87	68	3.760	0.977	0.002
VP0748	Xanthosine 5-P -> Xanthosine	133	114	4.039	0.983	0.002
		97	78	2.953	0.950	0.004
VPA0813-0811		246	227	2.574	0.929	0.004
		56	37	2.526	0.926	0.004
		135	116	2.310	0.910	0.005
VPA1420		266	247	2.960	0.951	0.003
VPA1421-1422		21	3	2.960	0.951	0.003
VPA1423		90	71	3.989	0.982	0.002
		155	136	3.907	0.980	0.002
		374	355	3.100	0.957	0.003
VPA0298-0297		166	147	4.676	0.991	0.001

Table 6 Continued

VP2385-2386	Glycerol uptake facilitator protein and Glycerol kinase	182	163	6.206	0.998	0.0003
		128	109	3.948	0.981	0.002
		311	292	3.010	0.953	0.003
VP2382-2381		142	123	2.483	0.923	0.004
		145	126	2.342	0.912	0.005
VP0843-46	Fumarate <-> Succinate	200	181	3.434	0.969	0.003
VP2872-2873	Fumarate hydratase	41	22	4.405	0.988	0.001
		34	15	3.260	0.963	0.003
		50	31	2.436	0.920	0.004
VP2637-2633	Cellobiose-specific PTS	227	208	6.848	0.999	0.0002
		201	182	5.338	0.995	0.0006
VP2636	Cellobiose-specific PTS	87	68	5.094	0.994	0.0007
VP2767	Malate oxidoreductase	202	183	2.411	0.918	0.005
VP0325	Malate dehydrogenase	199	180	3.553	0.972	0.002
VP1258	Malate dehydrogenase	210	191	2.645	0.934	0.004
VPA1292	Adenosine deaminase	205	186	7.875	1.000	0.00005
		213	194	3.264	0.963	0.002
VP1525	Spermidine/putrescine ABC transporter	181	162	4.073	0.983	0.002
		106	87	3.803	0.978	0.002
		185	166	3.398	0.968	0.003
VP1529-26	Spermidine/putrescine ABC transporter	353	334	4.413	0.988	0.002
		92	73	2.562	0.928	0.005
VPA0354-49	ABC transporter	137	118	2.238	0.904	0.004
VP2436-34	VP2435 - deoA thymidine phosphorylase	108	89	7.334	0.999	0.00009
		328	309	3.016	0.953	0.003

Table 6 Continued

VP0960	Uridine phosphorylase	46	27	4.294	0.987	0.002
		37	18	3.599	0.973	0.002
		249	230	3.473	0.970	0.002
		41	22	3.337	0.966	0.003
		135	116	2.767	0.941	0.003
		53	34	2.332	0.911	0.004
VPA0190	(S)-2-hydroxyglutarate + oxygen -> 2-oxoglutarate + H2O2	502	483	6.410	0.998	0.0003
		123	104	2.991	0.952	0.003
VP0008-06	Amino acid ABC transporters	53	34	7.733	1.000	0.00006
		44	25	2.877	0.947	0.004
VP1620	Amino acid ABC transporter periplasmic substrate binding protein	333	314	8.261	1.000	0.00004
		126	107	4.202	0.985	0.002
		69	50	3.936	0.981	0.002
		314	295	3.698	0.976	0.003
		169	150	3.370	0.967	0.003
VP1392	putative ClpA/B-type protease	439	420	2.595	0.931	0.005
VP0070	oligopeptidase A	187	168	2.510	0.925	0.003
VP1879-80	Serine transporter and dehydratase	119	100	6.668	0.999	0.0002
		225	206	4.370	0.988	0.002
		259	240	4.284	0.986	0.002
		307	288	2.588	0.930	0.005
VP0470-71	carbamoyl-phosphate synthase small subunit and large subunit	98	79	2.654	0.934	0.004
		440	421	2.461	0.921	0.005
VP0826	asparagine synthetase B	125	106	4.672	0.991	0.002
		133	114	3.159	0.959	0.004
		210	191	2.938	0.950	0.004
VP0927	aspartate aminotransferase	80	61	3.449	0.969	0.003
		76	57	3.366	0.967	0.003
VPA0636-39	Arginine transport	93	74	4.139	0.984	0.002

Table 6 Continued

VP2756	Bifunctional argininosuccinate lyase	135	116	5.042	0.994	0.0007
VP2759-57	Arginine biosynthesis	79	60	2.659	0.935	0.006
VP2760	Acetyl ornithine deacetylase	85	66	2.659	0.935	0.006
VP1779-71	Polyamine Putrescine	88	69	7.474	0.999	0.00007
		79	60	4.054	0.983	0.0009
		87	68	3.972	0.982	0.0009
		95	76	3.377	0.967	0.002
		193	174	3.266	0.963	0.002
		91	72	3.002	0.953	0.002
		68	49	2.833	0.944	0.002
VP1137-38	Histidine metabolism	463	444	6.987	0.999	0.0002
		220	201	4.784	0.992	0.0009
		21	2	4.307	0.987	0.002
		32	13	4.021	0.982	0.002
		232	213	2.656	0.934	0.004
		24	5	2.642	0.934	0.004
VP0546-47	Phenylalanine, tyrosine and tryptophan biosynthesis	207	188	6.158	0.998	0.0003

**Table 7 Putative AphA binding sites identified by the MOODS algorithm**

Operon	Function	AphA Binding Site Prediction				
		Upstream ATG		Log odds score	Probability	P-Value
		Start	End			
VP0370-0368	PTS Subunit IIABC	44	25	2.364	0.914	0.0005
VPA1424-1425	PTS system fructose-specific transporter subunit IIABC	204	185	5.127	0.994	0.0002
VPA1620	Glycogene	217	198	3.674	0.975	0.0002
VPA1673-1671	Arabinose transport	53	34	3.605	0.974	0.0003
VP1207	Xanthosine 5-P -> Xanthosine	239	220	2.298	0.909	0.0006
VP2382-81	Glycerol-3-Phosphate Transporter	129	110	7.889	1.000	0.00002
VP2840-43	Fumarate -> Succinate	165	146	2.392	0.916	0.0005
VP0960	Uridine phosphorylase	62	43	3.944	0.981	0.0002
		308	289	2.920	0.949	0.0004
VPA0190	(S)-2-hydroxyglutarate + oxygen -> 2-oxoglutarate + H2O2	294	275	4.606	0.990	0.0002
		194	175	2.919	0.949	0.0003
		160	141	2.724	0.938	0.0004

Column Guide	
Start	Binding site start position relative of ATG
End	Binding site end position relative of ATG
Log odds score	Natural log of Odds
Probability	Probability of binding
P-Value	Significance of binding site prediction. According to program documentation, $P < \text{or} = 0.001$ is considered as strong, significant binding

## Chapter 3

### **RNA-SEQ TRANSCRIPTOME ANALYSIS OF THE SIGMA-54 REGULON OF *VIBRIO PARAHAEMOLYTICUS* RIMD2210633.**

#### **Introduction**

Sigma factors are subunits of the bacterial RNA polymerase (RNAP) holoenzyme and are required for promoter recognition. The core RNAP alone is incapable of transcription initiation and recognition of specific promoter sequences. Sigma factors have helix-turn-helix domains that recognize and direct RNAP to specific promoter sequences upstream of the transcriptional start. There are two major families of sigma factors: the sigma-70 family, which has multiple members and the sigma-54 family which has one member. Sigma-54 encoded by *rpoN* (ORF VP2670) is one of the eleven sigma factors present in *Vibrio parahaemolyticus* (Haines-Menges, Whitaker, and Boyd 2014; Haines-Menges 2015). Historically, from its function in *E.coli*, Sigma-54 was categorized as a regulator of the nitrogen assimilation genes and was critical under nitrogen-limiting conditions (Reitzer and Schneider 2001). It is now known that RpoN is a global regulator and plays an important role in a wide range of cellular functions in *E. coli* and most other bacteria (Reitzer and Schneider 2001; Francke et al. 2011). RpoN has been characterized in many species of the *Vibrio* genus; *V. alginolyticus*, *V. anguillarum*, *V. cholerae*, *V. harveyi*, *V. fischeri*, and *V. parahaemolyticus* (Dong and Mekalanos 2012; Hao et al.

2012; Ishikawa et al. 2009; Kawagishi et al. 1997; Lilley and Bassler 2000; O'Toole et al. 1997; Whitaker, Richards, and Boyd 2014; Wolfe et al. 2004). In *V. cholerae*, the RpoN regulon includes more than 500 genes including genes encoding for nitrogen metabolism, polar flagellum synthesis, biofilm formation, quorum sensing small regulatory RNAs, dicarboxylic acid transport, type 6 secretion system synthesis, and virulence (Dong and Mekalanos 2012; Klose and Mekalanos 1998, 1998; Klose, Novik, and Mekalanos 1998; Prouty, Correa, and Klose 2001; Syed et al. 2009). It was also shown that RpoN is required for colonization in an infant mouse model of cholera (Klose and Mekalanos 1998). RpoN was shown to be required for motility and biofilm formation in other *Vibrio* species including *V. anguillarum*, *V. alginolyticus* and *V. fischeri* (Hao et al. 2012; Kawagishi et al. 1997; Millikan and Ruby 2003; O'Toole et al. 1997; Wolfe et al. 2004). Additionally in *V. fischeri*, RpoN was shown to be a negative regulator of bioluminescence as the *rpoN* mutant was produced significantly higher levels of bioluminescence compared to wild-type (Millikan and Ruby 2003; Wolfe et al. 2004).

In *V. parahaemolyticus* RIMD2210633, RpoN was demonstrated to be required for the synthesis of both polar and lateral flagellum as well as biofilm formation. In *in vivo* colonization experiments, the *rpoN* mutant was shown to be a superior colonizer compared to the wild-type strain and it was suggested that this could be due to the increased metabolic fitness exhibited by the mutant strain. The *rpoN* mutant had faster doubling times than wild-type when grown on mouse intestinal mucus or mucus sugars as sole carbon sources (Whitaker, Richards, and Boyd 2014).

RpoN also plays an important role in *Vibrio* quorum sensing. The quorum sensing response regulator LuxO is an activator for RpoN and together they are required for expression of the *qrr* genes, which are in turn responsible for the activation or repression of the low cell density (LCD) and high cell density (HCD) quorum sensing master regulators, *aphA* and *opaR* respectively (Ng and Bassler 2009; Zhang et al. 2012; Gode-Potratz and McCarter 2011; Lenz et al. 2004; Shao and Bassler 2012; Shao et al. 2013; van Kessel, Rutherford et al. 2013; Rutherford and Bassler 2012; Rutherford et al. 2011; Tu and Bassler 2007; Lilley and Bassler 2000). The activation and repression of the *aphA* and *opaR* master regulators is brought about as a result of post-transcriptional regulation by the Qrrs (Lenz et al. 2004; Lilley and Bassler 2000; Tu and Bassler 2007). In *V. parahaemolyticus*, the LCD master regulator, AphA has been shown to be required for biofilm formation and motility. An *aphA* defective mutant strain exhibited reduced lethality in mice and reduced cytotoxic and hemolytic activity (Wang, Ling et al. 2013). The HCD master regulator OpaR has been shown to regulate capsule polysaccharide formation, Type 3 Secretion System-1, the two Type 6 Secretion Systems, surface sensing and motility (Gode-Potratz and McCarter 2011; Kernell Burke et al. 2015; Ma et al. 2012; McCarter 1998; Salomon, Klimko, and Orth 2014; Zhang et al. 2012; Zhang et al. 2016; Zhou et al. 2013).

We have also determined that deletion of the quorum sensing response regulator LuxO resulted in a defect in *in vivo* colonization. The *luxO* mutant strain also exhibited a defect in metabolic fitness compared to the wild-type. Both of these phenotypes are the opposite of what occurs in the *rpoN* mutant strain. LuxO and RpoN

act in conjunction in the quorum sensing pathway, yet they exhibit different phenotypes with respect to *in vivo* and metabolic fitness. We know RpoN regulates other gene systems independent of the quorum sensing pathway and we speculate that this contributes to its superior *in vivo* and metabolic fitness. In this study, we performed RNA-Seq transcriptome analysis to determine the RpoN regulon in *V. parahaemolyticus*. We compare the expression of the *rpoN* mutant and the wild-type strains grown in minimal media supplemented with glucose or mouse intestinal mucus as sole carbon sources. These analyses identified 596 genes that were differentially regulated between the mutant and the wild-type when grown in glucose. Analysis of wild-type and the *rpoN* mutant grown in mouse intestinal mucus identified 191 differentially regulated genes. Transcriptome analysis revealed a number of gene systems involved in pathogenesis that were differentially regulated in the *rpoN* mutant including motility, T3SS1 and the two T6SSs. We found that genes encoding for tRNAs and ribosomal proteins were upregulated in the *rpoN* mutant, providing a possible explanation for the increased growth rate of the mutant compared to wild-type. One interesting finding was that the expression of the two quorum sensing regulators *opaR* and *aphA* was opposite to the expression patterns observed in the *luxO* mutant. Unlike the *luxO* mutant, the high cell density master regulator *opaR* was not constitutively induced in the *rpoN* mutant. We found that this might be due to the highly induced quorum regulatory RNA, *qrr2*. Also, by bioinformatic analysis of the promoter regions of two major ribosomal protein operons we identified a strong OpaR binding site in one of the ribosomal operons examined.

## Materials and Methods

### RNA extraction.

*Vibrio parahaemolyticus* wild-type and mutant strains used in this study are listed in **Table 8**. Strains were grown for 4 h in LB 3% NaCl and then diluted 1:50 into M9 medium supplemented with glucose or mouse cecal mucus as the sole carbon source. In order to best mimic the limited oxygen *in vivo* conditions the cells were grown statically without any shaking (Chang et al. 2004; He et al. 1999). To determine expression patterns upon initial exposure to glucose or mucus, we examined early-exponential-phase cell cultures that were grown for 90 mins. Total RNA was extracted from cells obtained by centrifugation using Trizol (Invitrogen, Carlsbad, CA) according to manufacturer's protocol. The RNA samples were then quantified using a Nanodrop spectrophotometer (Thermo Scientific, Waltham, MA). The samples were treated with Turbo DNase (Invitrogen) according to manufacturer's instructions. For the wild-type and mutant, RNA samples from two independent cultures were pooled together. Nanodrop quantifications were used to ensure equal representation of RNA from both biological replicates. Then, 3 µg of RNA was used for rRNA depletion using the Ribo-Zero rRNA removal kit for Gram-negative bacteria (Illumina).

### Illumina sequencing.

Libraries for each sample were prepared from 100ng of rRNA-depleted-RNA using the Illumina TruSeq Stranded mRNA kit (Illumina). Sequencing was performed

at the University of Delaware Sequencing and Genotyping Center on the HiSeq 2500 platform to yield 51-base single-end reads.

### **RNA-Seq analysis.**

Raw 51-base reads were filtered to remove adaptor only sequences and low quality reads using the FASTX Toolkit. Filtered reads were aligned to the *Vibrio parahaemolyticus* RIMD2210633 genome (Refseq ID NC\_004603.1 Chromosome 1 and NC\_004605.1 Chromosome 2) using Burrows-Wheeler Aligner (BWA.aln) version 0.7.7. Gene annotations were obtained from Ensembl bacteria, Rfam, Bacterial Small Regulatory RNA database and RAST. Number of reads aligning to each genomic position was calculated using Htseq version 0.6.1. Differential expression analysis was performed on obtained read counts using DESeq2 version 1.4.5. Differential expressed genes were categorized into Cluster of orthologous groups (COG) obtained from Integrated Microbial Genomes (IMG) database.

### **Quantitative real time PCR (qPCR) analysis.**

For qPCR validations of the RNA-Seq, 500 ng of pre-ribozero treated RNA was used as a template for cDNA synthesis. cDNA was synthesized using Superscript III reverse transcriptase (RT) (Invitrogen) following manufacturer instructions using 500 ng of RNA template and priming with 200 ng of random hexamers. cDNA samples were then diluted 1:25 and used for quantitative-real time PCR (qPCR). Fast SYBR Green master mix or PowerUp SYBR Green master mix (Life Technologies,

Carlsbad, CA) was used for qPCR and samples were run on an Applied Biosystems 7500 fast real-time PCR system or QuantStudio 6 Flex real-time PCR system (Applied Biosystems, Foster City, CA). Primers used for the qPCR reactions are listed in **Table 9**. Data was analyzed using Applied Biosystems software. Expression levels of each gene as determined by their cycle threshold ( $C_T$ ) values, were normalized using the 16s rRNA housekeeping gene to correct for sampling errors. Differences in the ratios of gene expression were determined using the  $\Delta\Delta C_T$  method (Pfaffl 2001).

### **Binding site analysis.**

The consensus binding sequence and position frequency matrix was obtained for OpaR (Zhang et al. 2012) and AphA (Sun et al. 2012). The consensus -12 and -24 binding sequence and position frequency matrix for RpoN was constructed using the alignment of 36 RpoN binding sites predicted by BPROM promoter prediction tool from Softberry. The position frequency matrices were then used to identify potential binding sites using the MOODS (Motif Occurrence Detection Suite) algorithm (Version 1.0.2.1) (Korhonen et al. 2009; Pizzi, Rastas, and Ukkonen 2011). The upstream intergenic sequence for the first gene of each operon was obtained from the NCBI database and used to identify putative binding sites. Operon information was obtained from the DOOR2 prokaryotic operon database (Mao et al. 2009) and was confirmed using the IGV viewer (Thorvaldsdottir, Robinson, and Mesirov 2013) with the RNASeq sequence data. The MOODS tool returned a Log-odds score for each putative binding site that was then used to assess probability of binding.

**Accession numbers for data.** The read data for the *V. parahaemolyticus* wild type and mutant strains, will be deposited in the NCBI Sequence Read Archive (SRA) An Excel file summarizing the differential gene expression in total counts and normalized RPM, will be deposited in the NCBI Gene Expression Omnibus (GEO) database.

## Results and Discussion

### RNA-seq analysis of *V. parahaemolyticus* wild-type and $\Delta rpoN$ strains.

Previously it was demonstrated that an *rpoN* mutant exhibited superior colonization ability compared to wild-type *in vivo* and this correlated with an increased metabolic fitness when cells were grown in intestinal mucus and in individual mucus sugar components (Whitaker, Richards, and Boyd 2014). To investigate this further, we performed RNA-Seq expression analysis of *rpoN* mutant cells grown in M9 minimal media supplemented with either glucose or intestinal mucus as the sole carbon sources. We isolated RNA from the wild-type and mutant cells grown to early exponential phase (OD 0.1). Sequencing resulted in greater than 10 million sequence reads obtained for each sample. Over 98% of the reads aligned to genomic features including mRNA, tRNA, sRNA or to unannotated regions of the genome. The rRNA depletion procedure resulted in less than 0.5% of the reads aligning to these features in the genome (**Figure 16**). Differential expression analysis between the wild-type and the mutant strain revealed a number of genes that were up-regulated or down-regulated ( $> 2$ -fold,  $P_{\text{adj}} < 1 \times 10^{-3}$ ) in the *rpoN* mutant compared to

wild-type under both conditions (**Figure 17**). For analysis of genes differentially expressed between wild-type and mutant we took a stringent approach and only discuss genes that showed a base mean expression level of 100 or greater and showed a log<sub>2</sub>-fold change of 1.5 or greater in expression.

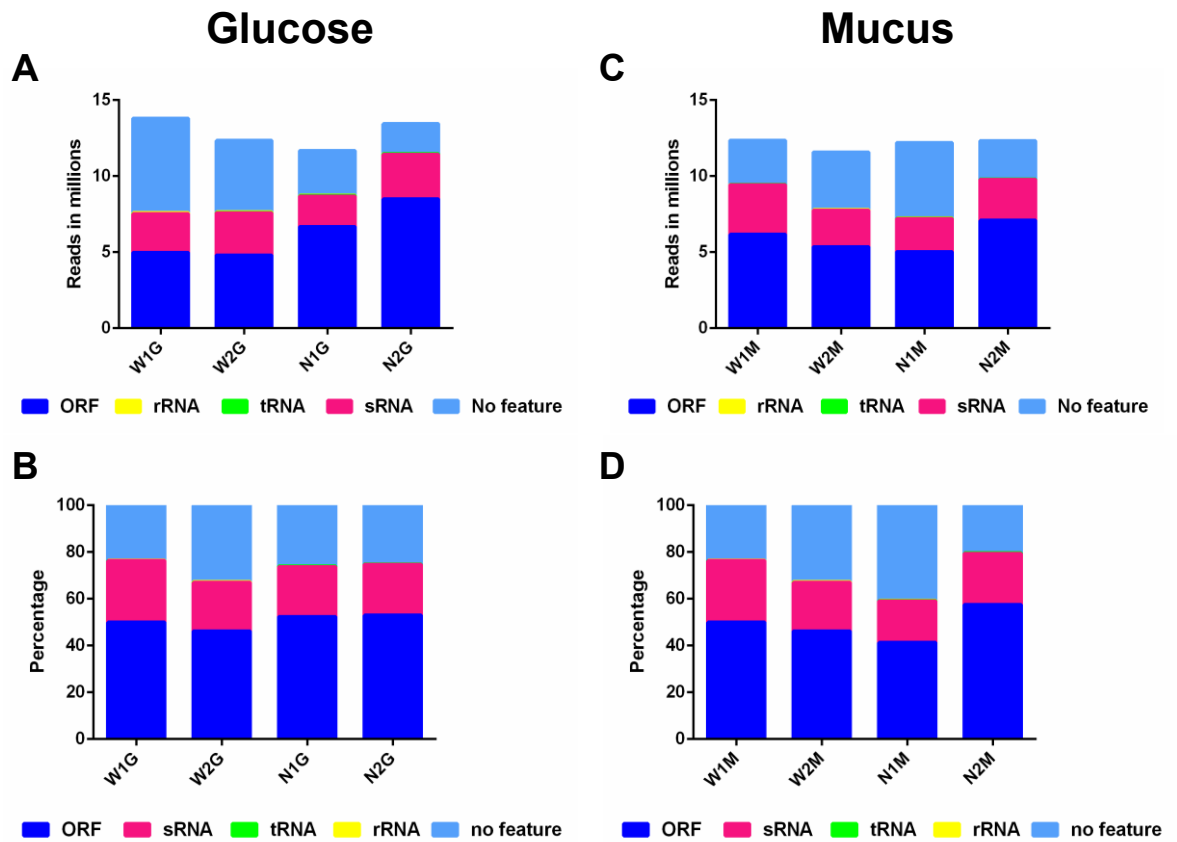


**Figure 16** *ΔrpoN* vs wild-type RNA-seq sequencing yield and RNA classification in glucose and mucus. (A&C). Total number of reads sequenced indicated to corresponding to RNA-feature obtained from samples grown in (A) Glucose and (C) Mucus. (B&D) Total percentage of reads mapping to various RNA features for samples grown in (B) Glucose and (D) Mucus.

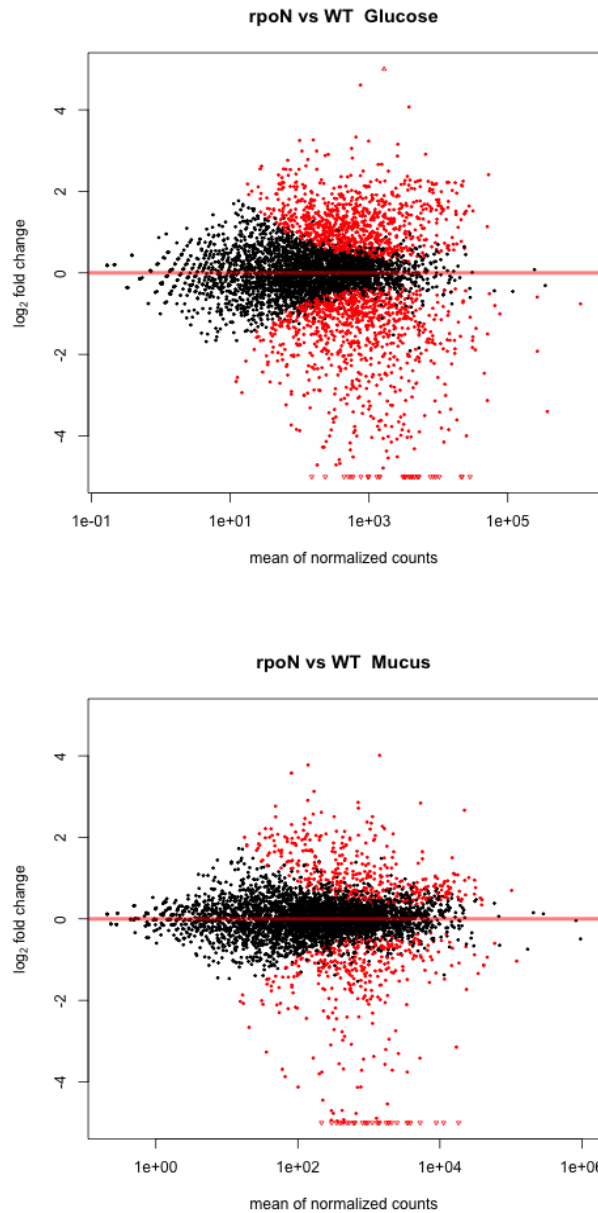


**Figure 17 RNA Seq MA-plots showing expression in the *rpoN* mutant relative to wild-type.** Plots showing the log<sub>2</sub> fold changes in the *rpoN* mutant over the mean of the normalized counts. Dots represent log<sub>2</sub> fold change in expression for each genomic feature. Red dots represent all genes with an adjusted *P* value of  $\leq 0.0001$ . Genes with a log<sub>2</sub> fold change of  $> 1$  or  $< -1$  were considered as being differentially expressed between the mutant and the wild-type.

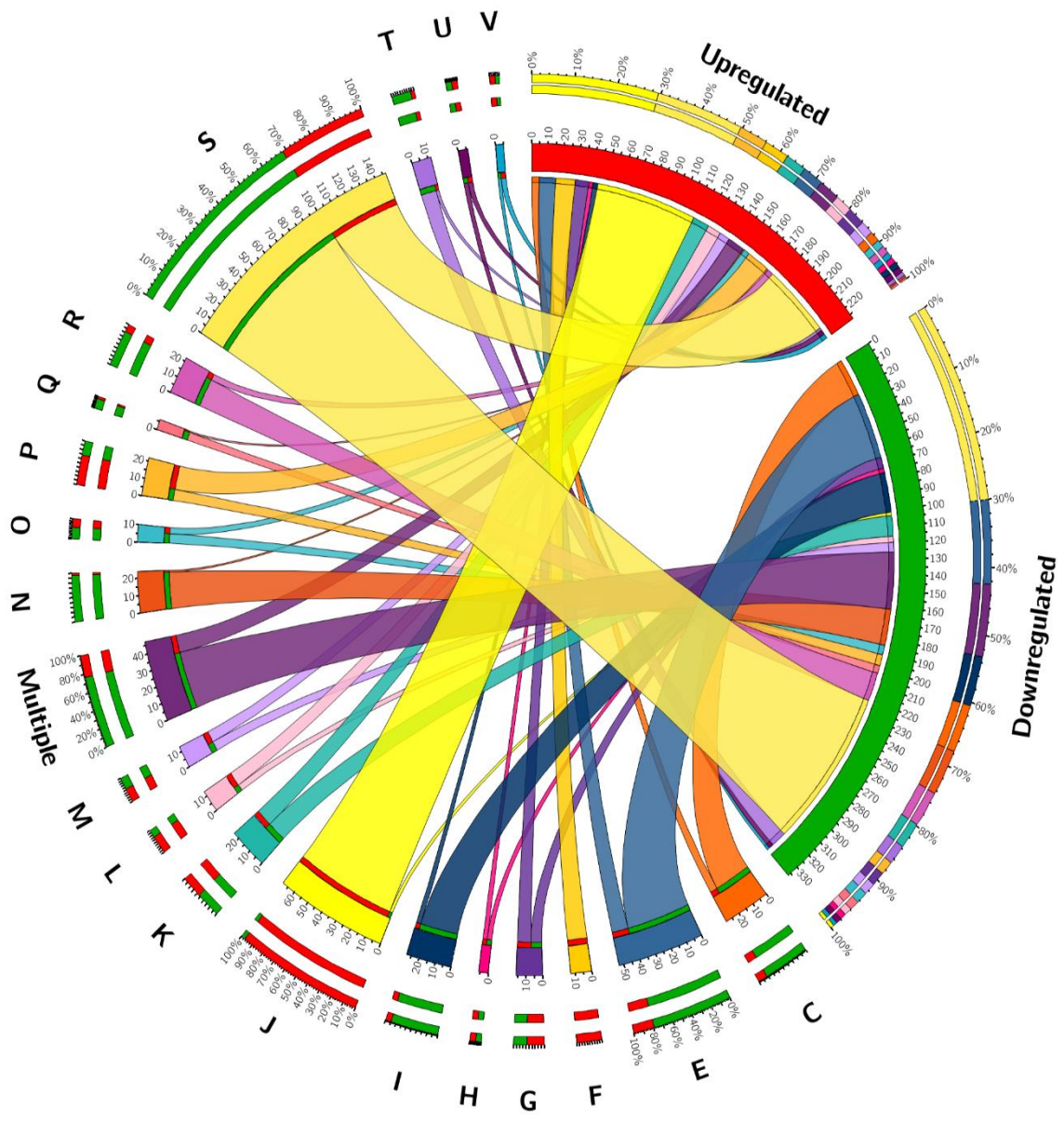
**Genes induced in the *rpoN* mutant when grown in minimal media supplemented with glucose.**

When grown in glucose, the *rpoN* mutant compared to wild-type had 596 differentially expressed genes, 255 genomic features were upregulated and 341 were downregulated. Upregulated features included 19 genes encoding tRNAs and 7 small RNAs (**Table 10**). Of the ORFs that encoded proteins that were upregulated, 169 belonged to chromosome I and 60 were from chromosome II. Interestingly, along with the 19 tRNA loci, 48 genes encoding ribosomal proteins were upregulated in the *rpoN* mutant (**Table 10**). These along with other genes categorized into COG class J: Translation, ribosomal structure and biogenesis, were overall one of the most induced gene categories (**Figure 18 and Figure 19**). It has been known for some time that the number of ribosomes in a cell is proportional to the growth rate of the cell, in fast growing cell there are more than 70,000 ribosomes whereas in a slower growing cell about 20,000 ribosomes are present (Bremer and Dennis 1996). Thus induction of ribosomal genes in the *rpoN* mutant provides a possible explanation for the faster growth rates seen in this strain. Also noteworthy was the induction of the six structural subunits of the NADH-quinone reductase (NqrA-F, VP2346-2351), which functions as the primary Na<sup>+</sup> pump in Gram-negative halophilic marine bacteria (Unemoto and Hayashi 1979; Hayashi, Nakayama, and Unemoto 2001). The sodium motive force generated by the Na<sup>+</sup> pumping NQR has been shown to be essential for the uptake of nutrients (Drapeau and Macleod 1963; Hayashi, Nakayama, and Unemoto 2001; Tokuda, Sugasawa, and Unemoto 1982).

Six annotated putative transcriptional regulators were upregulated in the *rpoN* mutant, VPA0148 (*cpxR*), VPA1701 (*uxuR*), VP1889 and VPA1289 (*cspA*), VP2396 (*lacI*) and VP2520 (*pdhR*) (**Table 10**). The CpxR protein belongs to the OmpR family of regulators. UxuR is a member of the GntR family of regulators and UxuR clusters with genes required for glucuronate TRAP transport (UxuPQM) and catabolism ORFs VPA1700 to VPA1709. The *cspA* encodes a major cold shock protein and there are a total of five copies on the *V. parahaemolyticus* genome, which share between 74% to 30% amino acid homology. CSP proteins are involved in the cold shock response and were shown to regulate flagella gene expression and metabolism in *E. coli* (Phadtare and Inouye 2004). ORF VP2396 although induced is expressed at very low levels, this gene clusters with genes required for galactose transporter and metabolism, ORFs VP2394-VP2400. The PdhR regulator is significantly induced as is an adjacent gene VP2519 that encodes pyruvate dehydrogenase component E. It is of interest to note that VP1890, which encodes a putative cold shock ribonuclease with two S1-RNase domains similar to those present in CSP proteins. This gene annotated as *vacB* clusters with *cspA* (VP1889), which are transcribed as an operon. The DNA-binding protein Fis, a nucleoid-associated protein transiently produced at high numbers in early exponential growth was upregulated in the *rpoN* mutant. Fis is a known regulator of ribosomal genes as well as genes involved in virulence (Gonzalez-Gil, Bringmann, and Kahmann 1996; Kelly et al. 2004).

Genes encoding the type 3 secretion system-1 (T3SS-1) on chromosome 1 were upregulated in the *rpoN* mutant, however many of these genes were expressed at low levels including the transcriptional activator ExsA (VP1699). The transcriptional regulator ExsA is a member of the AraC/XylS family and has been shown to be a positive regulator of T3SS-1 expression in *V. parahaemolyticus* (Brutinel, Vakulskas, and Yahr 2009; Gode-Potratz, Chodur, and McCarter 2010; Zhou, Konkell, and Call 2010; Zhou et al. 2008). Other upregulated gene systems included iron-complex ABC transporters (VP2489-VP2491, VPA0657- VPA 0660, and VPA1434- VPA1435). Iron is an essential component for cell physiology and has been shown to be a negative regulator of swarming motility in *V. parahaemolyticus* (Gode-Potratz, Chodur, and McCarter 2010).

Seven small RNAs were induced in the *rpoN* mutant (**Table 10**). Three of these, t44, S15, and rimP are regulatory RNAs that regulate the expression of ribosomal proteins (Chao et al. 2013; Toffano-Nioche et al. 2012). Three small RNAs were riboswitches, which are RNA elements that are encoded in the 5' UTRs of several bacterial operons and regulate their expression (Henkin 2008; Nudler and Mironov 2004). The second copy of *groESEL* (VPA0286-VP0287) present on chromosome II were also significantly induced in the *rpoN* mutant, which would reflect an increased requirement for chaperone proteins in cells at high growth rates.



■ Upregulated genes     ■ Downregulated genes

- |   |  |  |  |
|---|--|--|--|
| <span style="color: orange;">■</span> C: Energy production and conversion         | <span style="color: blue;">■</span> E: Amino acid transport and metabolism           | <span style="color: yellow;">■</span> F: Nucleotide transport and metabolism   | <span style="color: purple;">■</span> G: Carbohydrate transport and metabolism |
| <span style="color: pink;">■</span> H: Coenzyme transport and metabolism          | <span style="color: darkblue;">■</span> I: Lipid transport and metabolism            | <span style="color: lightyellow;">■</span> J: Translation, ribosomal structure | <span style="color: teal;">■</span> K: Transcription                           |
| <span style="color: lightpink;">■</span> L: Replication, recombination and repair | <span style="color: lightpurple;">■</span> M: Cell wall/membrane/envelope biogenesis | <span style="color: darkpurple;">■</span> Multiple Classes                     | <span style="color: brown;">■</span> N: Cell motility                          |
| <span style="color: cyan;">■</span> O: Posttranslational modification             | <span style="color: orange;">■</span> P: Inorganic ion transport and metabolism      | <span style="color: lightcoral;">■</span> Q: Secondary metabolites catabolism  | <span style="color: magenta;">■</span> R: General function prediction only     |
| <span style="color: yellow;">■</span> S: Function unknown                         | <span style="color: purple;">■</span> T: Signal transduction mechanisms              | <span style="color: darkred;">■</span> U: Intracellular trafficking, secretion | <span style="color: lightblue;">■</span> V: Defense mechanisms                 |

**Figure 18** Circos plot showing classification of differentially expressed genes between the *rpoN* mutant and the wild-type in glucose into Cluster of Orthologous Groups (COG). Segments of the Circos Plot occur in a clockwise manner. The first two segments indicated in Red and Green represent the sum total of Upregulated and Downregulated genes respectively. Each following colored segment represents each COG class and is labelled with the letter assigned for the COG class. The size of the colored segment is representative of the number of differentially expressed genes within the segment. Colored COG classes are linked to the Red and Green segments by Ribbons. The size of the ribbon indicates the number of up or downregulated genes within each class. The outermost segment for the Upregulated and Downregulated genes indicates the percentage of genes represented by each COG class. The outermost segment for each COG class indicates the percentage of up or downregulated genes within each COG class.

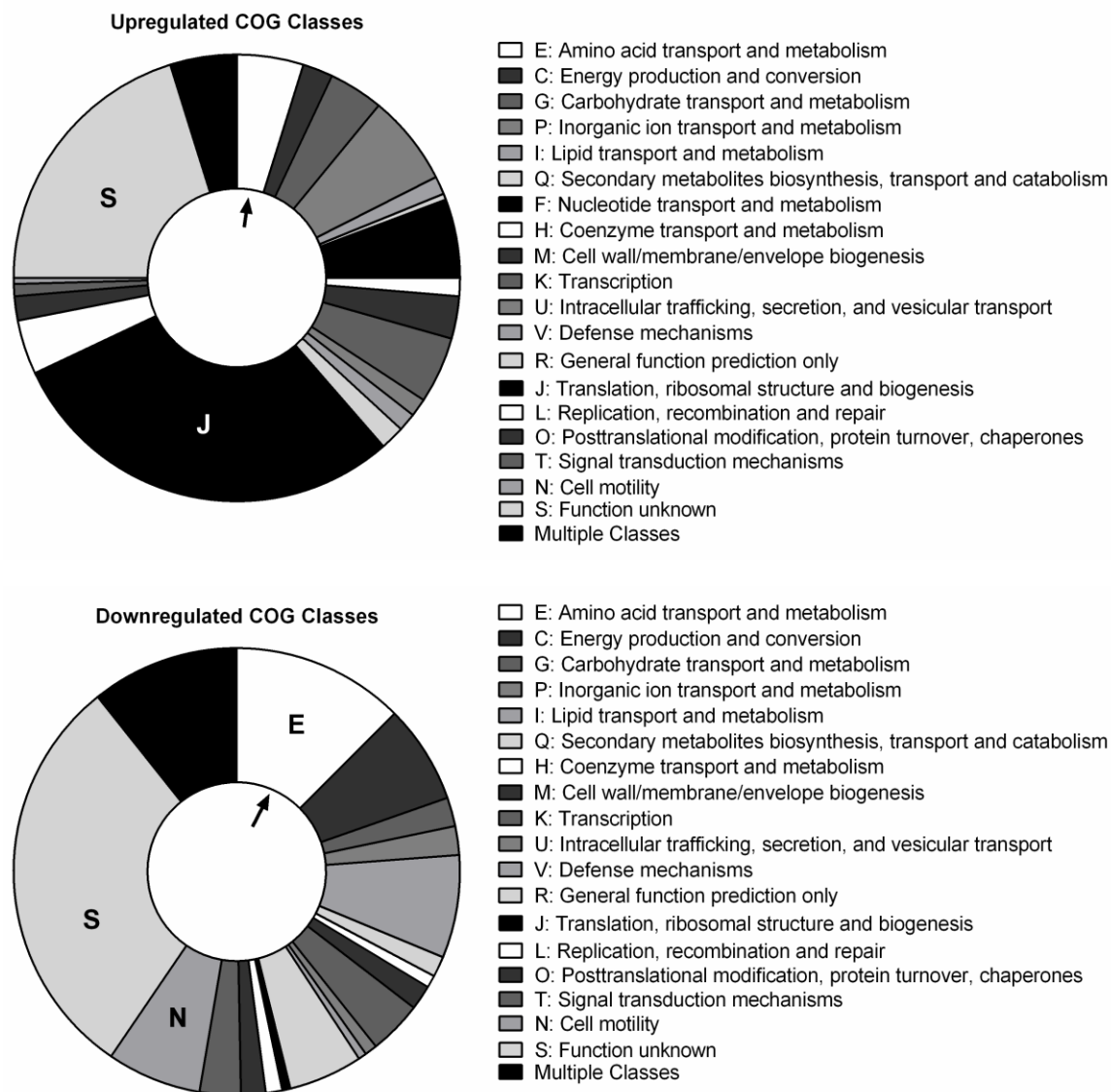


**Figure 19 Cluster of Orthologous Groups (COG) classification of differentially expressed genes in the *rpoN* mutant when grown in glucose. **A.** Upregulated COG classes. The ribosomal proteins are classified into the COG class J and is indicated within the chart. **B.** Downregulated COG classes. Genes encoding motility proteins are classified into the COG class N. The most enriched COG class S is indicated within both charts. The first COG class in each chart is indicated by an arrow. Following COG classes are represented in a clockwise arrangement.**

### **Genes repressed in the *rpoN* mutant when grown in minimal media supplemented with glucose.**

There were 341 downregulated genomic features in the *rpoN* mutant when grown in minimal media supplemented with glucose. These included 231 annotated ORFs on chromosome 1 and 106 ORFs on chromosome 2, 3 small RNAs and 1 unannotated ORF (**Table 11**). Gene clusters encoding nitrogen regulatory response proteins and proteins involved in glutamine synthesis (VP0118-0121, VP0481-0484) were downregulated in the mutant. This is consistent with the function of RpoN as an important regulator of the nitrogen assimilation and as a critical factor for the bacteria under nitrogen-limiting conditions (Reitzer and Schneider 2001). RpoN has also been shown to play a role in regulation of motility in various Vibrios including *V. parahaemolyticus* (Dong and Mekalanos 2012; Moisi et al. 2009; Hao et al. 2012; Kawagishi et al. 1997; Millikan and Ruby 2003; O'Toole et al. 1997; Wolfe et al. 2004; Whitaker, Richards, and Boyd 2014). In agreement with that, we found that a number of genes encoding proteins involved in chemotaxis, polar and lateral flagellum biosynthesis (VP0689-0690, VP0770-0790, and VP2228-2231, VP2827, VPA0554, VPA0596, VPA1449) were downregulated in the mutant (**Figure 18 and Figure 19**).

The most highly repressed gene was a hyperosmotically inducible periplasmic ORF VP0081, an OsmY homologue, which contains two BON domains that are present in osmotic shock protection proteins. The *osmY* gene in *E. coli* has been shown to be RpoS-dependent and is also osmotically controlled (Lange, Barth, and Hengge-

Aronis 1993). VP0081 encompassed an operon VP0081 to VP0091, which were all highly repressed in the mutant.

There were a number of metabolic gene cluster that were highly downregulated in the *rpoN* mutant when grown in glucose (**Table 11**). These included ORFs VP1644 to VP1655, which are involved in the tricarboxylic cycle and tricarboxylic transport. In addition, a number of enzymes required for TCA intermediate conversion were also down regulated. ORFs VP1771 to VP1781 is a large gene cluster required for the regulation and utilization of putrescine, were all down regulated in the *rpoN* mutant. The gene cluster (VP1722-VP1719) required for the *de novo* synthesis of ectoine, a compatible solute, and VP1726-VP1728 a putative compatible solute transporter were all down regulated. VPA1117-VPA1129 is a gene cluster that contains enoyl-CoA hydratases, enoyl-CoA dehydrogenase, enoyl-CoA carboxyltransferase, and acyl-CoA dehydrogenases and carboxylase enzymes putatively involved in fatty acid metabolism which were all repressed. Also present within the same genomic region is VPA1147-VPA1158 ORFs that encode fatty acid transporters and catabolism genes that are also downregulated in the *rpoN* mutant. Several peptide and amino acid transporters are also repressed (ORFs VP0170-VP0174, VP0998-VP1001, VP1620-VP1623 and VPA1148-VPA1153).

There were 18 regulators downregulated in the *rpoN* mutant, which included two two-component systems, VP0361- VP0362 and VPA1515- VPA1516 (**Table 11**). The 18 regulators belonged to a number of regulator families, which included the LysR family, MetR family and the GntR family. Three sigma factors were repressed in

the *rpoN* mutant, the polar flagellum biosynthesis Sigma-28 encoded by *fliA* (VP2232), an alternative sigma factor (VP2358) of unknown function, and the stationary-phase stress response Sigma-S encoded by *rpoS* (VP2553). Previously, others have shown that RpoN is a positive regulator of the *fliA* expression and an indirect positive regulator of *rpoS* (Dong, Yu, and Schellhorn 2011; Dong and Mekalanos 2012). Genes encoding the outer membrane protein OmpA (VP0636, VPA1186) were repressed in the mutant. Also downregulated was the gene encoding the ribonuclease activity regulator protein RraA, which was shown to be an inhibitor of RNase E, an endoribonuclease that plays a major role in degradation and processing of RNAs in *V. vulnificus* and *E. coli* (Kim et al. 2016; Lee et al. 2009). The phage shock proteins *pspABC* (VP1173-1175) and *pspG* (VP2725) were also downregulated in the mutant and are important for cell membrane stress. These proteins maintain proton-motive force under extracytoplasmic stress conditions and have been shown to be regulated by *rpoN* in *E. coli* and *V. cholerae*. PspG has been shown to play a role in iron utilization (Dong and Mekalanos 2012; Jovanovic et al. 2010).

Three small RNAs were downregulated in the *rpoN* mutant (**Table 11**). These included the quorum regulatory RNAs *qrr4*, which is involved in the quorum sensing pathway, and two of the three Csr small RNAs. The Csr small RNAs have been shown to regulate quorum sensing in *V. cholerae* and were shown to be functionally redundant. Deletion of all the Csr sRNAs resulted in overexpression of Qrrs and hence, led to repression of the high cell density regulator HapR (Lenz et al. 2005). About 146 of the differentially regulated genes, were categorized into the COG class

S: Function Unknown with a majority of the gene annotated as hypothetical proteins (**Figure 18 and Figure 19**).

**Genes induced in the *rpoN* mutant when grown in minimal media supplemented with intestinal mucus.**

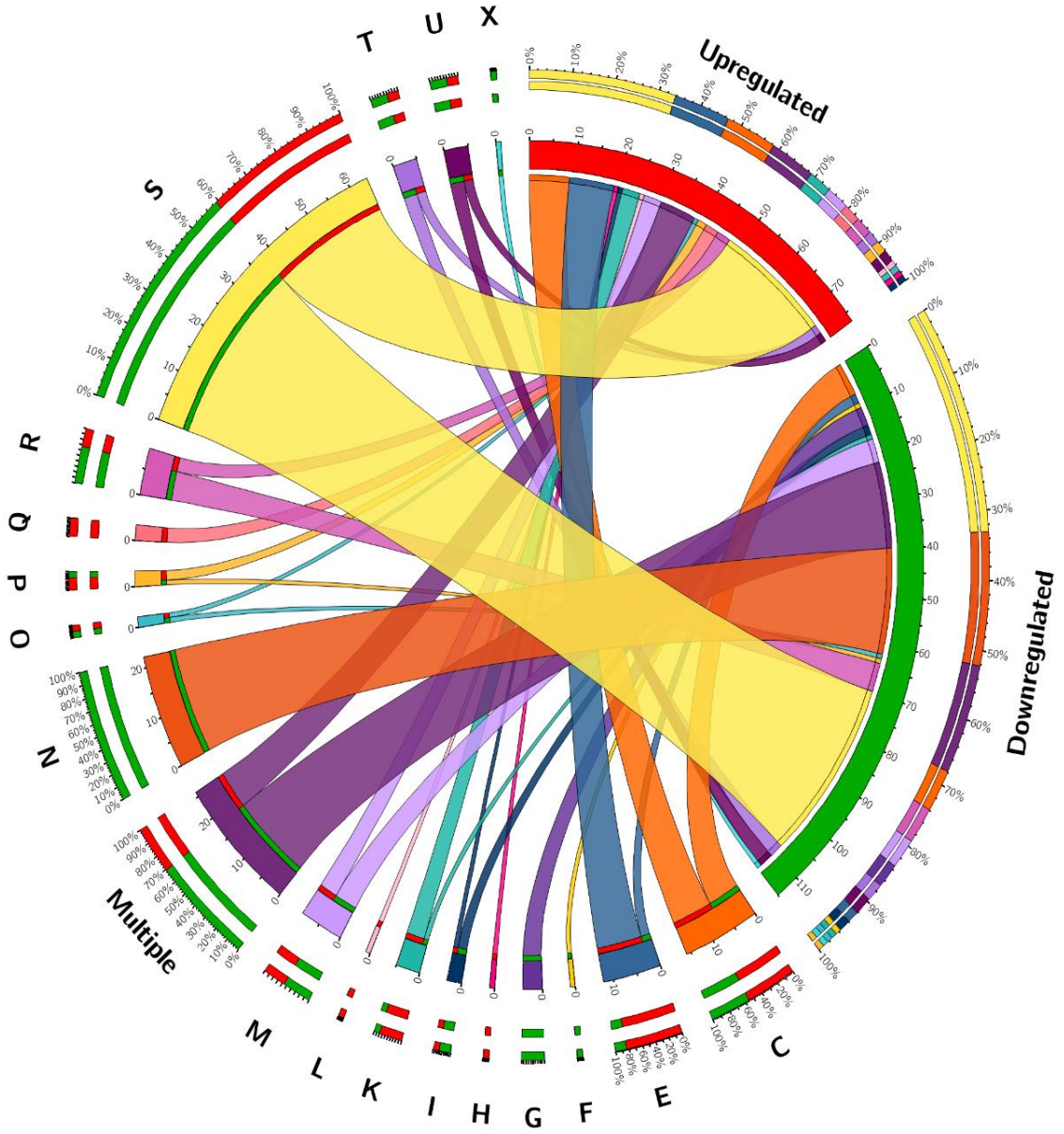
Differential expression analysis of cells grown in mucus revealed that a total of 191 genomic features were differentially regulated in the *rpoN* mutant in comparison to wild-type. Of those, 77 genomic features were upregulated and 114 were downregulated in the mutant. Upregulated genomic features comprised of 77 annotated ORFs (**Table 12, Figure 20 and Figure 21**).

Four transcriptional regulators were upregulated in the *rpoN* mutant in mucus (**Table 12**). These included two genes (VP1889 and VPA1289) encoding the major cold shock protein CspA, which are also induced in the *rpoN* mutant when grown in glucose. A LysR family transcriptional regulator (VPA0251) and *vacB* that clusters with *cspA* (VP1889) were also induced. The DNA repair protein RecN (VP0648) was also upregulated in the *rpoN* mutant. RecN belongs to the SMC family of proteins. These proteins have been shown to play a critical role in DNA damage response and repair of double stranded breaks (Reyes et al. 2010; Strom et al. 2004).

Several genes encoding structural and secretory components of the T6SS-1 and T3SS-1 were upregulated in the *rpoN* mutant when grown in mucus (**Table 12**). Genes including those encoding the T3SS-1 ATPase VscN1 (VP1668), the secretin VscC (VP1696) and outer membrane protein YopN (VP1667), structural proteins of the

T6SS-1 (VP1400, VP1408-1409) including the inner membrane protein IcmF1 (VP1408) and structural protein VasL (VP1409) were all upregulated. However, the secreted protein T6SS-1 Hcp1 (VP1393) was downregulated with an l2fc of -1.8. These results were validated by qPCR (**Figure 23**). Previously published research in *V. cholerae* has shown that RpoN controls the expression of *hcp* but does not control the expression of other genes in the T6SS gene cluster (Dong and Mekalanos 2012). It will be interesting to investigate this further to see if perhaps T6SS structural and effector proteins are regulated by two separate mechanisms.

A number of genes encoding for proteins involved in metabolism were induced in the *rpoN* mutant cells when grown in intestinal mucus (**Table 12**). ORFs VP1771-1775, which are involved in putrescine transport and utilization were induced. These genes were downregulated in the *rpoN* mutant when grown in M9 glucose. Also upregulated was the tricarboxylic acid transporter gene cluster *tctABC* (VP1651-1653) and pyruvate dehydrogenase components. These genes were highly repressed in the *rpoN* mutant when grown in glucose. Genes encoding proteins of the periplasmic nitrate reductase (*nap*) complex (VP1197-1199) were induced in the mutant. The Nap proteins have been shown to play an important role during anaerobic respiration in *E. coli* (Brondijk et al. 2002; Potter et al. 1999; Stewart, Lu, and Darwin 2002). The *scrABC* operon (VPA1511-VPA1513) was also upregulated in the *rpoN* mutant, a locus that induces swarming motility and inhibits CPS production in *V. parahaemolyticus* (Boles and McCarter 2002).



■ Upregulated genes     ■ Downregulated genes

- |   |  |   |  |
|---|--|---|--|
| <span style="color: orange;">■</span> C: Energy production and conversion         | <span style="color: blue;">■</span> E: Amino acid transport and metabolism           | <span style="color: yellow;">■</span> F: Nucleotide transport and metabolism      | <span style="color: purple;">■</span> G: Carbohydrate transport and metabolism |
| <span style="color: pink;">■</span> H: Coenzyme transport and metabolism          | <span style="color: darkblue;">■</span> I: Lipid transport and metabolism            | <span style="color: lightyellow;">■</span> J: Translation, ribosomal structure    | <span style="color: teal;">■</span> K: Transcription                           |
| <span style="color: lightpink;">■</span> L: Replication, recombination and repair | <span style="color: lightpurple;">■</span> M: Cell wall/membrane/envelope biogenesis | <span style="color: darkpurple;">■</span> Multiple Classes                        | <span style="color: brown;">■</span> N: Cell motility                          |
| <span style="color: cyan;">■</span> O: Posttranslational modification             | <span style="color: orange;">■</span> P: Inorganic ion transport and metabolism      | <span style="color: lightpink;">■</span> Q: Secondary metabolites catabolism      | <span style="color: magenta;">■</span> R: General function prediction only     |
| <span style="color: yellow;">■</span> S: Function unknown                         | <span style="color: lightpurple;">■</span> T: Signal transduction mechanisms         | <span style="color: darkpurple;">■</span> U: Intracellular trafficking, secretion | <span style="color: lightblue;">■</span> V: Defense mechanisms                 |

**Figure 20** Circos plot showing classification of differentially expressed genes between the *rpoN* mutant and the wild-type in mucus into Cluster of Orthologous Groups (COG). Segments of the Circos Plot occur in a clockwise manner. The first two segments indicated in Red and Green represent the sum total of Upregulated and Downregulated genes respectively. Each following colored segment represents each COG class and is labelled with the letter assigned for the COG class. The size of the colored segment is representative of the number of differentially expressed genes within the segment. Colored COG classes are linked to the Red and Green segments by Ribbons. The size of the ribbon indicates the number of up or downregulated genes within each class. The outermost segment for the Upregulated and Downregulated genes indicates the percentage of genes represented by each COG class. The outermost segment for each COG class indicates the percentage of up or downregulated genes within each COG class.

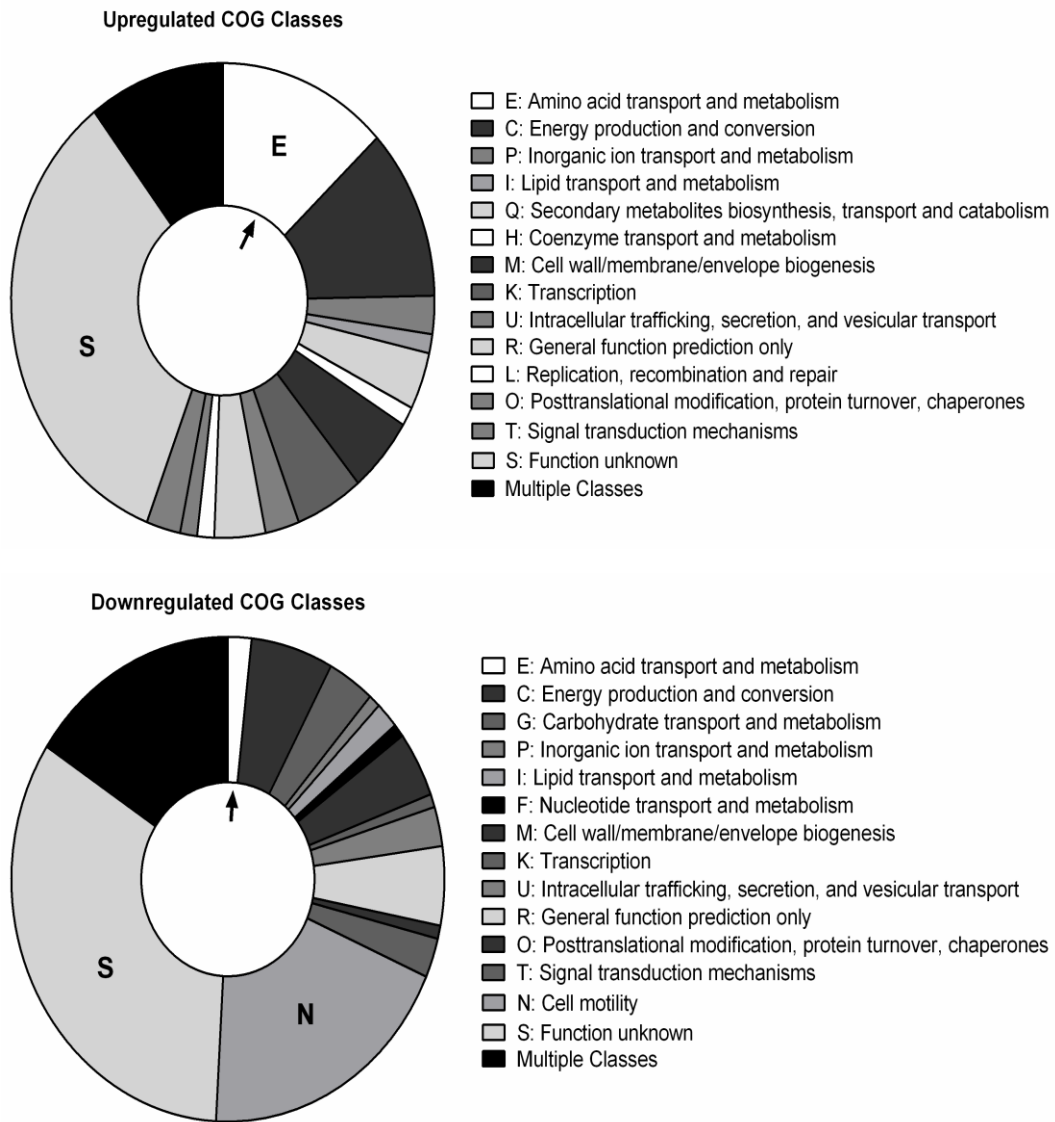


**Figure 21 Cluster of Orthologous Groups (COG) classification of differentially expressed genes in the *rpoN* mutant when grown in mucus. **A** Upregulated COG classes. **B**. Downregulated COG classes. Genes encoding motility proteins are classified into the COG class N. The most enriched COG class S is indicated within both charts. The first COG class in each chart is indicated by an arrow. Following COG classes are represented in a clockwise arrangement.**

**Genes repressed in the *rpoN* mutant when grown in minimal media supplemented with intestinal mucus.**

One hundred and fourteen features, all of which were annotated ORFs were found to be downregulated in the mutant when grown in mucus, 31 of which were hypothetical proteins (**Table 13, Figure 20 and Figure 21**). Downregulated gene clusters included the genes encoding for nitrogen response regulatory proteins and glutamine synthetase (VP0118-0121) and proteins involved in chemotaxis (VP2228-VP2231, VP2827, VPA0511, VPA0746, VPA1000, and VPA1449) (VP0689-0690, VP0775-0790, VP2234-2261, VP1376) and motility (VP0689-0690, VP0775-0790, VP2234-2261, VP1376). Four genes encoding the transmembrane chemoreceptors, methyl-accepting chemotaxis proteins (VP2827, VPA0511, VPA1000, VPA1449) were also downregulated in the mutant.

The polar flagella sigma factor *fliA* (VP2232) which was downregulated in glucose was also downregulated in mucus. The transcription factor DeoR (VP0358) was repressed and the DeoR family of regulators were shown to regulate several metabolic pathways in *E. coli* (Elgrably-Weiss et al. 2006). Genes encoding the outer membrane protein OmpA (VP0636, VPA1186) were also downregulated in mucus. Three genes encoding for both structural and secreted proteins of T6SS-2 (VPA1027, 1034, 1039) were downregulated in the *rpoN* mutant when grown on mucus. These included genes encoding for effector protein Hcp2 (VPA1027), the inner membrane proteins IcmF2 (VPA1039) and ImpC (VPA1034). The repression of *hcp2* was also validated by qPCR (**Figure 23 and Table 13**). The secretory protein Hcp2 (VPA1027)

was also downregulated in glucose with an l2fc of -2.28. The phage shock proteins *pspABC* (VP1173-1175) and *pspG* (VP2725) were also downregulated in in mucus.

Genes involved in metabolism that were downregulated in the *rpoN* mutant in mucus included a gene cluster involved in glyoxylate metabolism (VP1506, VP1510-1516), the C-4 dicarboxylate TRAP transport system *dctPQM* (VP0910-0912) and eight genes required for formate dehydrogenase synthesis (VP1506, VP1510-VP1515). ORF VP1703 that encodes an aldehyde dehydrogenase showed l2fc of -8.9. The polyhydroxyalkanoic acid synthase gene (VPA1202) was also downregulated. Polyhydroxyalkanoates (PHAs) are polyesters produced by bacteria to store excess nutrients. *Vibrio* sp. were shown to produce a high amount of PHA amounting up to 41% dry cell weight (Chien et al. 2007; Xiao and Jiao 2011).

#### **Genes differentially regulated in the *rpoN* mutant in both glucose and mouse intestinal mucus.**

Fifteen genes were upregulated in the *rpoN* mutant under both growth conditions examined (**Table 10, Table 12 and Figure 22**). Two T3SS-1 genes including VP1696 which encodes for the secretin VscC were upregulated under both conditions. The upregulation of T3SS-1 was confirmed by performing a qPCR validation (**Figure 23**). Previously we have shown that a deletion mutant of T3SS-1 had a slight but significant defect in colonization *in vivo* (Whitaker et al. 2012). Also upregulated in both conditions were the transcriptional regulator cold shock protein *cspA* and the virulence associated *vacB* gene.

Eighty-seven genes were down-regulated in the *rpoN* mutant under both growth conditions (**Table 11 and Table 13 and Figure 22**). These included, the nitrogen regulatory response genes (VP0118-0121), and genes encoding for motility and chemotaxis. Other gene regions of interest that were down-regulated under both conditions included the VP0081-VP0091 gene cluster OsmY (VP0081) was shown to be positively regulated by *rpoS* in *V. cholerae* (Dong and Schellhorn 2009; Zheng et al. 2015). In our analysis *rpoS* (VP2553) was also down-regulated under both conditions, albeit to a higher extent in glucose (12fc = -2.47) than in mucus (12fc = -0.88) conditions. Thus, the repression of *rpoS* may also have led to the repression of *osmY* in *V. parahaemolyticus*. Also downregulated under both conditions were the outer membrane protein OmpA, the phage shock proteins (*pspABC* and *pspG*). The T6SS-1 secreted protein Hcp1 was also found to be down-regulated under both conditions and was validated by qPCR (**Figure 23**). RpoN has been shown to be a positive regulator of *hcp1* and *hcp2* in *V. cholerae* (Dong and Mekalanos 2012) and seems to have a similar role in regulation in *V. parahaemolyticus*.

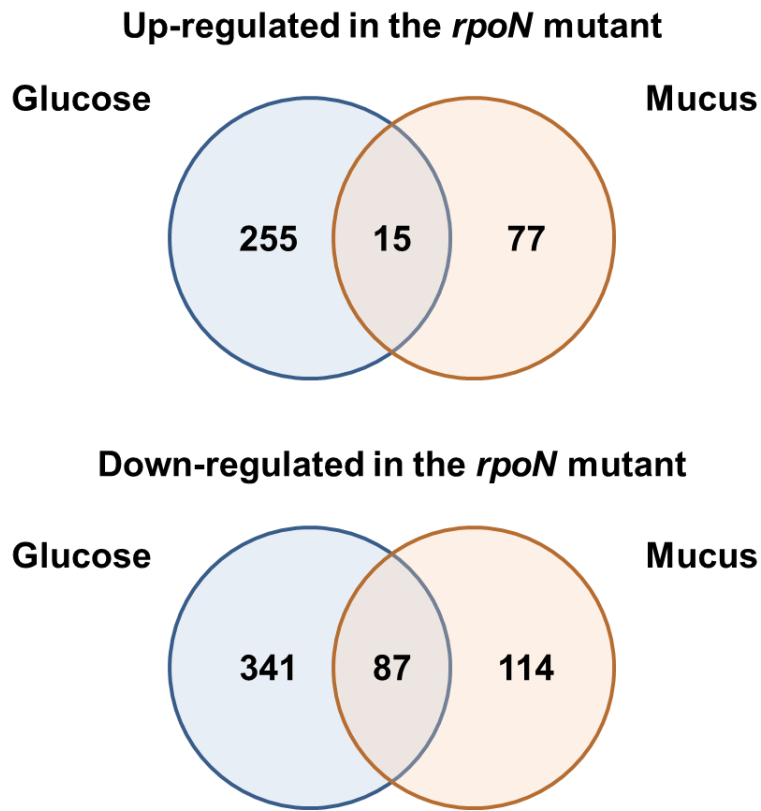


**Figure 22 Differentially Expressed Genes in the *rpoN* mutant.** Venn-diagrams showing number of Upregulated and Downregulated genes in the *rpoN* mutant in glucose and mucus. Number indicated in the intersection represent number of genes that are common to both conditions. Genes with a log<sub>2</sub> fold change of > 1 or < -1 and an adjusted *P* value of ≤ 0.0001 were considered as being differentially expressed between the mutant and the wild-type.

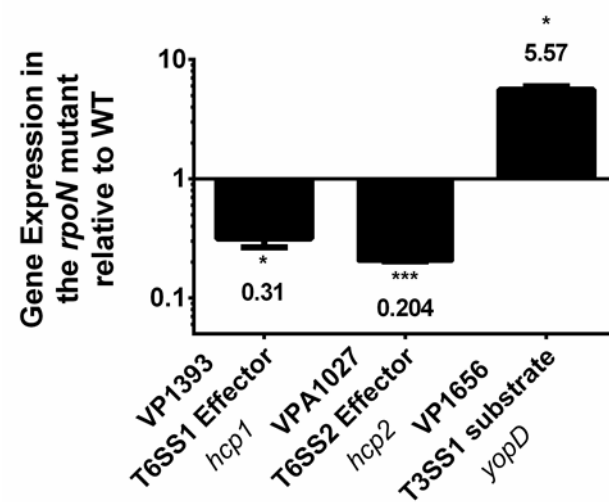


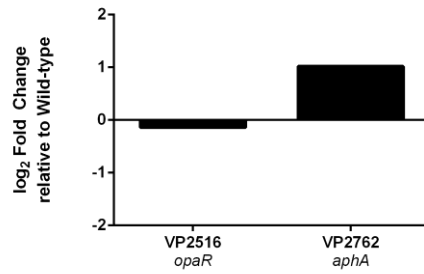
**Figure 23** qPCR Expression of Secretion System Effectors in the *rpoN* mutant grown in mouse intestinal mucus as sole carbon source. Bars represent the expression of *hcp1*, *hcp2* and *yopD* normalized to 16S rRNA in the *rpoN* mutant relative to wild-type.

**OpaR was not induced in the *rpoN* mutant under the conditions examined.**

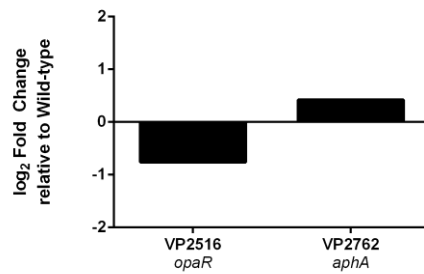
According to the quorum sensing pathway, deletion of *rpoN* should inhibit the *qrr* genes from being transcribed and result in the constitutive expression of HCD regulator OpaR and repression of LCD regulator AphA. However, the RNASeq expression patterns of the two regulators *opaR* and *aphA* were contrary to the expected expression pattern. The *opaR* (VP2516) gene was down-regulated in the *rpoN* mutant compared to wild-type (mucus l2fc = -0.76, glucose l2fc = -0.14) (**Figure 24 A-B**). The *aphA* (VP2762) gene was up-regulated in the *rpoN* mutant compared to wild-type (mucus l2fc = 0.42, glucose l2fc = 1.02) (**Figure 24 A - B**). The expression pattern in mucus was confirmed by qPCR analysis (**Figure 24 C**). We investigated this further

by examining expression analysis of the *qrr* genes. Interestingly, while the expression of *qrr1*, *qrr3*, *qrr4* and *qrr5* was either downregulated or showed no significant change compared to wild-type, the expression of *qrr2* was upregulated in the *rpoN* mutant (mucus l2fc = 3.57, glucose l2fc = 0.79) (**Figure 25 A-B**). qPCR analysis validated that *qrr2* was indeed highly upregulated in the *rpoN* mutant compared to wild-type (**Figure 25 C**). The observed expression was very different from the *qrr* expression pattern seen in the *luxO* mutant, in which *opaR* is up-regulated and *aphA* is down-regulated as expected by the QS pathway model. In *V. harveyi*, a species closely related to *V. parahaemolyticus*, Qrr2 was shown to be an important Qrr for LuxR repression (Tu and Bassler 2007). It will be interesting to study the promoter region of *qrr2* further to elucidate the reason behind its induction in the *rpoN* mutant and to determine whether this is the mechanism for the altered *opaR* gene expression in the *rpoN* mutant.

### A RNASeq Expression in Glucose



### B RNASeq Expression in Mucus



### C QPCR Validation of Mucus Expression

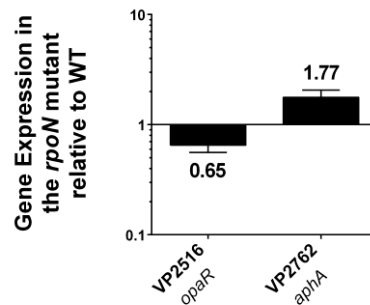
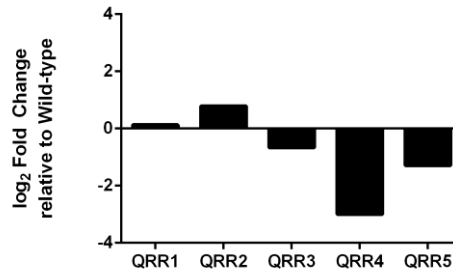
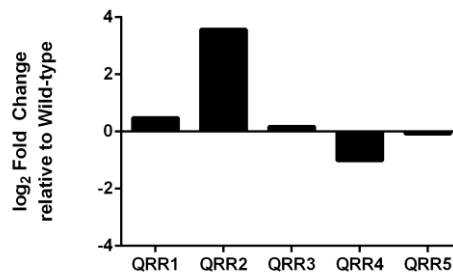


**Figure 24 Expression of Quorum Sensing Master Regulators.** (A) RNASeq expression values indicated as Log<sub>2</sub> Fold Change in the *rpoN* mutant compared to wild-type in glucose and (B) in mouse intestinal mucus (C) qPCR validation of the RNASeq expression in mucus. Bars represent the expression of *opaR* and *aphA* normalized to 16S rRNA in the *rpoN* mutant relative to wild-type.

### A RNASEq Expression in Glucose



### B RNASEq Expression in Mucus



### C qPCR Validation of Mucus Expression

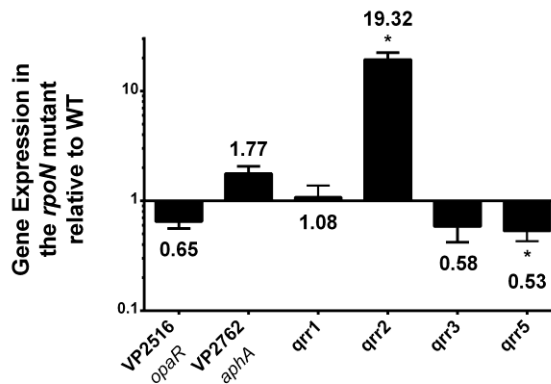


**Figure 25 Expression of Quorum Regulatory RNAs (*qrrs*).** (A) RNASEq expression values indicated as Log<sub>2</sub> Fold Change in the *rpoN* mutant compared to wild-type in glucose and (B) in mouse intestinal mucus (C) qPCR validation of the RNASEq expression in mucus. Bars represent the expression of *opaR*, *aphA*, *qrr1*, *qrr2*, *qrr3* and *qrr5* normalized to 16S rRNA in the *rpoN* mutant relative to wild-type.

### **OpaR binding sites in the promoter regions of ribosomal proteins.**

In order to determine the mechanism behind the upregulation of the genes encoding ribosomal proteins, we first performed bioinformatics analysis to identify putative binding sites for RpoN in the promoter regions of two major operons encoding 23 of the 54 ribosomal proteins in *V. parahaemolyticus*, VP00256-VP00266 and VP00267-VP00278. We did not find any putative RpoN binding sites in either regulatory region. Next, we performed bioinformatics analysis to identify putative binding sites for OpaR and AphA in the same regulatory regions. This analysis revealed no binding sites for AphA but revealed two putative binding sites for OpaR in the promoter regions of two ribosomal operons (**Table 14**), one of which was a strong putative binding site, the other much less so. Quorum sensing control of ribosomal and tRNA genes has been shown before in other Gram negative bacteria. An *E.coli luxS* mutant strain which is incapable of producing the autoinducer AI-2 molecules, showed faster growth rate compared to wild-type and genes upregulated in this mutant included ribosomal and tRNA genes (Sperandio et al. 2001). Based on this, we hypothesize that OpaR could be a negative regulator ribosomal proteins in *V. parahaemolyticus* and its repression in the *rpoN* mutant results in the upregulation of these genes.

**Table 8 Bacterial strains used in this study**

Strain	Genotype/ Strain Description	Reference
<i>Vibrio parahaemolyticus</i>		
RIMD2210633	O3:K6 clinical isolate, StrR	(Makino et al. 2003; Whitaker et al. 2010)
$\Delta rpoN$	RIMD2210633 $\Delta rpoN$ , StrR	(Whitaker, Richards, and Boyd 2014)

**Table 9 Primers used in this study**

Use and primer	Sequence (5'-3')	T <sub>m</sub>	Product size (bp)
<b>qPCR primers</b>			
VP2516For	TCA TGG AAA TCG CGT TAG AA	55	123
VP2516Rev	CTT CGC GAG TTG GGA AGT AG	58	
VP2762For	AGC CAC CAA CAA GTT TAC CG	59	140
VP2762Rev	CAT TCT CCA AGA GCG CTA CG	59	
<i>qrr1</i> For	CTC GGG TCA CCT AGC CAA CT	61	85
<i>qrr1</i> Rev	AAG AAG CCA ATA GGC AGT CG	58	
<i>qrr2</i> For	CTT AAG CCG AGG GTC ACC TA	59	95
<i>qrr2</i> Rev	ATA GCC AAC CGC AAT AAT CG	56	
<i>qrr3</i> For	CTT AAG CCG AGG GTC ACC TA	59	95
<i>qrr3</i> Rev	ATA GCC AAC CGC AAA GAG TG	50	
<i>qrr5</i> For	TCT AAG CCG AGG GTC ACC TA	59	95
<i>qrr5</i> Rev	AAA AGC CAA CCA CAA GGT GT	58	
VP1393For	CGG TGA AAC TCA AGG TCA CA	58	135
VP1393Rev	TGT GGA TCA CGT GGA ACA GT	59	
VPA1027For	ACC GAT TGT TGC TTC CTT GA	58	142
VPA1027Rev	TTG GAG TGT TGG TCG TGA AA	58	
VP1656For	CAC TTG GTA AAG CAG CGT CA	55	196

Table 1 Continued

VP1656Rev	TCA ATT AGA TGG GCC GAA AG	52	234
16sRNA_FWD	ACC GCC TGG GGA GTA CGG TC	66	
16sRNA_REV	TTG CGC TCG TTG CGG GAC TT	66	

**Table 10 Genes upregulated in the *rpoN* mutant in glucose**

Locus Tag	Common Name of Primary Target	baseMean	log2Fold Change	padj
EBG00000020300	tRNA-Tyr-1	144	1.6	1.00E-06
EBG00000020327	tRNA-Gln-6	139	1.7	4.36E-13
EBG00000020328	tRNA-Met-7	115	1.5	2.57E-12
EBG00000020336	tRNA-Arg-1	220	1.8	3.27E-09
EBG00000020337	tRNA-Thr-1	120	2.1	8.14E-16
EBG00000020347	tRNA-Thr-3	123	2.6	7.44E-11
EBG00000020348	tRNA-Ile-1	116	2.1	5.93E-14
EBG00000020352	tRNA-Pro-1	358	1.5	3.29E-07
EBG00000020353	tRNA-Gly-2	544	1.7	3.00E-09
EBG00000020361	tRNA-Gly-11	291	1.9	6.19E-22
EBG00000020381	tRNA-Ile-2	853	2.1	5.28E-18
EBG00000020382	tRNA-Ala-2	164	1.8	5.73E-13
EBG00000020383	tRNA-Thr-6	434	1.8	2.03E-35
EBG00000020424	tRNA-Ala-4	1025	1.7	7.01E-34
EBG00000020427	tRNA-Leu-11	283	1.5	4.08E-10
EBG00000020429	tRNA-Arg-11	812	1.5	2.03E-15
EBG00000020433	tRNA-Asn-4	111	2.2	2.31E-13
EBG00000020437	tRNA-Thr-2	137	1.6	8.19E-12
EBG00000020446	tRNA-Tyr-7	687	2.0	8.50E-17
svpa1191.1	Lysine riboswitch	749	1.9	7.67E-42
svpa1856.1	Glycine riboswitch	4511	2.1	1.03E-145
svpa1857.1	Glycine riboswitch	3298	2.3	1.79E-74

Table 2 Continued

svpa2205.1	MOCO_RNA_motif	187	1.5	7.31E-05
svpa2431.1	t44	1606	1.8	3.74E-18
svpa2576.1	S15	387	1.9	7.62E-32
svpa2583.1	rimP	3473	1.5	1.08E-12
VP0004	ribonuclease P	1105	1.8	2.95E-47
VP0005	50S ribosomal protein L34	1425	1.5	2.05E-27
VP0023	hypothetical protein	671	1.7	1.19E-44
VP0035	ketol-acid reductoisomerase	22745	2.3	4.75E-50
VP0057	hypothetical protein	462	2.1	4.60E-62
VP0111	hypothetical protein	986	3.2	7.76E-19
VP0112	methyltransferase-related protein	369	1.7	1.36E-35
VP0113	hypothetical protein	351	1.5	1.17E-27
VP0177	ribonuclease PH	1388	1.7	7.34E-86
VP0178	orotate phosphoribosyltransferase	1053	2.2	1.24E-21
VP0185	ribosomal protein L28	3610	2.0	5.08E-59
VP0186	50S ribosomal protein L33	2732	1.6	3.87E-27
VP0225	capsular polysaccharide biosynthesis protein CapF	573	1.9	3.01E-18
VP0226	rhamnosyl transferase	558	1.8	1.05E-16
VP0227	hypothetical protein	681	1.8	2.49E-22
VP0228	integral membrane protein	196	2.2	9.63E-13
VP0244	fructose 1,6-bisphosphatase II	309	1.5	6.79E-23
VP0255	50S ribosomal protein L31	1119	1.8	6.13E-17
VP0256	30S ribosomal protein S10	15784	2.0	5.89E-54

Table 3 Continued

VP0257	50S ribosomal protein L3	22042	2.1	1.57E-21
VP0258	50S ribosomal protein L4	14021	2.2	5.10E-23
VP0259	50S ribosomal protein L23	4644	2.2	8.06E-30
VP0260	50S ribosomal protein L2	21450	2.2	4.24E-23
VP0261	30S ribosomal protein S19	8082	2.2	3.89E-34
VP0262	50S ribosomal protein L22	9309	2.2	2.03E-51
VP0263	30S ribosomal protein S3	17466	2.2	1.64E-46
VP0264	50S ribosomal protein L16	13257	2.2	5.05E-40
VP0265	50S ribosomal protein L29	3743	2.2	1.83E-40
VP0266	ribosomal protein S17	8369	2.0	1.14E-63
VP0267	50S ribosomal protein L14	10874	1.6	9.18E-82
VP0268	50S ribosomal protein L24	11768	1.6	1.82E-186
VP0269	50S ribosomal protein L5	17798	1.5	4.17E-136
VP0270	30S ribosomal protein S14	8036	1.6	1.38E-77
VP0271	30S ribosomal protein S8	11121	1.6	1.68E-44
VP0272	50S ribosomal protein L6	13678	1.6	5.19E-35
VP0273	50S ribosomal protein L18	6260	1.7	5.00E-62
VP0274	30S ribosomal protein S5	10198	1.7	8.43E-49
VP0275	50S ribosomal protein L30	3410	1.7	1.49E-107

Table 4 Continued

VP0276	50S ribosomal protein L15	9923	1.7	3.59E-38
VP0277	preprotein translocase SecY	25184	1.5	3.67E-78
VP0282	DNA-directed RNA polymerase alpha subunit	23586	1.5	1.66E-42
VP0283	50S ribosomal protein L17	7950	1.6	1.29E-129
VP0287	ElaA protein	153	1.6	3.29E-17
VP0328	50S ribosomal protein L21	5718	1.6	7.01E-48
VP0329	50S ribosomal protein L27	6667	1.6	4.01E-59
VP0330	GTP1/Obg family protein	1648	1.9	7.06E-19
VP0357	hypothetical protein	260	1.7	9.29E-11
VP0405	DNA primase	2696	1.5	1.81E-80
VP0406	hypothetical protein	6943	1.7	6.54E-61
VP0407	30S ribosomal protein S21	2840	1.7	1.27E-40
VP0418	pho4 family protein	647	1.6	1.28E-43
VP0438	50S ribosomal protein L13	7454	2.0	3.70E-132
VP0439	30S ribosomal protein S9	2674	1.9	4.59E-70
VP0440	hypothetical protein	383	1.7	1.31E-33
VP0470	carbamoyl-phosphate synthase small subunit	11611	1.5	4.06E-16
VP0471	carbamoyl-phosphate synthase large subunit	31411	1.5	1.49E-21
VP0507	branched chain amino acid transport system II carrier protein	2132	2.0	6.53E-144
VP0562	hypothetical protein	649	1.7	1.49E-23
VP0566	ferredoxin	232	1.7	3.93E-25

Table 5 Continued

VP0567	protease	1404	1.8	1.47E-39
VP0587	S-adenosylmethionine:tRNA ribosyltransferase-isomerase	808	1.8	1.51E-69
VP0593	inositol monophosphate family protein	2897	2.2	3.69E-79
VP0605	hypothetical protein	639	1.5	3.46E-39
VP0615	exodeoxyribonuclease VII large subunit	2445	2.1	2.23E-129
VP0652	Sodium:dicarboxylate symporter GltP	429	1.6	1.93E-34
VP0666	phosphoribosylformylglycinamide synthase	3566	2.4	6.83E-189
VP0682	riboflavin synthase subunit beta	1341	1.8	8.96E-53
VP0691	thiamine biosynthesis protein ThiI	657	1.8	6.85E-40
VP0715	serine hydroxymethyltransferase	7127	2.3	1.31E-184
VP0733	hypothetical protein	1119	1.9	2.98E-62
VP0737	GTP-binding protein	1008	1.5	2.38E-53
VP0738	peptidyl-tRNA hydrolase	561	2.0	3.14E-57
VP0739	ribose-phosphate pyrophosphokinase	4067	2.1	4.70E-91
VP0762	glutamyl-tRNA synthetase	1268	1.5	4.97E-63
VP0861	arginyl-tRNA synthetase	2274	1.6	4.90E-40
VP0903	RhlE	129	1.5	4.06E-13
VP1008	outer membrane porin protein; locus of qsr prophage	2476	1.9	3.53E-127
VP1128	adenylosuccinate lyase	1545	1.6	8.80E-56

Table 6 Continued

VP1186	pseudouridine synthase Rlu family protein	109	1.8	2.26E-17
VP1210	50S ribosomal protein L25	1131	1.8	7.67E-81
VP1226	hypothetical protein	644	1.5	5.34E-39
VP1236	hypothetical protein	604	1.5	7.52E-08
VP1278	SpoOM-related protein	297	1.6	5.51E-24
VP1297	5'- phosphoribosylglycinam ide transformylase	334	1.6	3.04E-26
VP1318	flippase	176	3.0	1.15E-43
VP1319	hypothetical protein	144	1.7	5.33E-15
VP1479	multidrug efflux protein NorA	288	1.5	2.36E-25
VP1505	hypothetical protein	399	1.9	8.15E-49
VP1533	ATPase	494	2.0	2.37E-54
VP1600	hypothetical protein	2928	1.6	4.33E-44
VP1639	hypothetical protein	179	1.5	2.23E-17
VP1696	type III secretion protein YscC	124	1.6	7.41E-16
VP1698	hypothetical protein	267	1.5	3.14E-12
VP1708	6-phosphogluconate dehydrogenase	1700	1.7	2.97E-59
VP1709	6- phosphogluconolactonas e	484	1.5	5.15E-24
VP1710	glucose-6-phosphate 1- dehydrogenase	1213	1.5	1.56E-29
VP1741	sodium/alanine symporter	52817	2.4	4.37E-137
VP1764	transmembrane protein	426	1.6	1.15E-06
VP1879	serine transporter	420	1.9	2.70E-15
VP1889	cold shock transcriptional regulator CspA	5450	1.8	1.30E-20

Table 7 Continued

VP1890	virulence-associated protein VacB/RNase R	18334	2.0	5.41E-11
VP1900	aspartate aminotransferase	3492	1.7	1.26E-45
VP1916	amidase	297	1.7	1.79E-33
VP1917	hypothetical protein	395	2.4	4.90E-30
VP1918	hypothetical protein	312	2.1	1.61E-21
VP1919	hypothetical protein	547	2.4	1.00E-43
VP1920	iron-regulated protein A	1896	2.5	1.59E-203
VP1934	ribonucleotide-diphosphate reductase alpha subunit	2812	1.5	1.44E-27
VP1941	carboxynorspermidine dehydrogenase	514	1.7	9.14E-41
VP1980	hypothetical protein	606	1.5	7.01E-44
VP2031	cytidylate kinase	844	1.6	2.34E-39
VP2057	fatty acid/phospholipid synthesis protein	939	1.6	8.57E-64
VP2059	hypothetical protein	4087	1.6	3.66E-143
VP2063	sulfate permease family protein	974	2.1	2.09E-88
VP2072	Na <sup>+</sup> /H <sup>+</sup> -exchanging protein	1223	1.6	1.09E-69
VP2114	ribonuclease T	679	1.6	4.82E-58
VP2115	hypothetical protein	1614	1.7	9.12E-46
VP2160	rRNA (guanine-N1-)-methyltransferase	169	1.5	1.19E-17
VP2166	lactoylglutathione lyase	752	4.6	1.21E-116
VP2167	hypothetical protein	1644	5.2	7.32E-134
VP2185	amidophosphoribosyltransferase	1768	1.8	9.33E-43
VP2186	bacteriocin production protein	710	1.5	8.49E-44
VP2285	phosphoribosylaminoimidazole synthetase	911	2.1	3.81E-49

Table 8 Continued

VP2317	elongation factor Ts	7525	1.6	1.09E-114
VP2318	30S ribosomal protein S2	11301	1.6	7.21E-40
VP2396	LacI-family regulatory PurR	129	1.6	8.51E-17
VP2426	hypothetical protein	233	2.9	6.24E-32
VP2428	elongation factor EF-2	27692	1.6	7.38E-124
VP2445	lipid carrier protein	318	1.8	2.73E-09
VP2453	30S ribosomal protein S15	2574	1.9	3.79E-60
VP2456	translation initiation factor IF-2	10847	1.5	6.74E-68
VP2457	transcription elongation factor NusA	4856	1.8	1.37E-53
VP2458	hypothetical protein	1524	1.8	1.01E-111
VP2459	hypothetical protein	3053	1.7	5.46E-23
VP2489	iron(III) ABC transporter, ATP-binding protein	616	1.6	7.88E-47
VP2490	iron(III) ABC transporter, permease protein	644	2.0	1.01E-61
VP2491	iron(III) ABC transporter, periplasmic iron-compound-binding protein	2559	2.9	6.84E-200
VP2520	transcriptional regulator of pyruvate dehydrogenase PdhR	1356	2.7	8.95E-44
VP2522	nicotinate-nucleotide pyrophosphorylase	233	1.5	7.30E-22
VP2530	50S ribosomal protein L19	5054	2.3	1.03E-55
VP2531	tRNA (guanine-N(1)-)-methyltransferase	8201	2.2	9.82E-47
VP2532	16S rRNA-processing protein	7552	2.1	1.55E-67

Table 9 Continued

VP2533	30S ribosomal protein S16	2161	2.0	1.83E-30
VP2573	signal peptidase I	820	1.5	2.11E-49
VP2624	hypothetical protein	424	1.7	1.19E-42
VP2625	tRNA (guanine-N(7)-)-methyltransferase	361	1.7	1.72E-26
VP2654	aspartate carbamoyltransferase catalytic subunit	1186	1.5	1.62E-08
VP2737	50S ribosomal protein L9	8797	2.2	1.22E-91
VP2738	30S ribosomal protein S18	3222	2.2	1.08E-49
VP2739	primosomal replication protein N	3892	2.3	8.86E-107
VP2740	30S ribosomal protein S6	5494	2.3	9.98E-67
VP2771	elongation factor EF-2	9784	1.7	1.30E-80
VP2772	30S ribosomal protein S7	13889	1.8	4.09E-119
VP2773	30S ribosomal protein S12	9407	1.8	6.83E-65
VP2855	6-phosphofructokinase	6015	1.6	2.24E-09
VP2883	ribosomal protein L11 methyltransferase	437	1.6	6.88E-30
VP2884	NifR3/Smm1 family protein	1290	2.3	2.15E-148
VP2885	DNA-binding protein Fis	370	1.9	3.01E-47
VP2896	bifunctional phosphoribosylaminoimidazolecarboxamide formyltransferase/IMP cyclohydrolase	1522	2.7	7.02E-102
VP2898	phosphoribosylamine--glycine ligase	820	2.5	1.36E-91
VP2921	DNA-directed RNA polymerase beta' subunit	24224	1.5	3.51E-27

Table 10 Continued

VP2923	50S ribosomal protein L7/L12	7739	1.5	5.49E-36
VP2924	50S ribosomal protein L10	8258	2.0	8.95E-166
VP2925	50S ribosomal protein L1	11016	2.0	6.86E-65
VP2926	50S ribosomal protein L11	5479	2.1	1.32E-112
VP2930	elongation factor Tu	4375	1.7	6.39E-188
VP3004	hypothetical protein	387	2.1	9.47E-33
VP3037	phosphoribosylaminoimidazole carboxylase	899	1.8	5.47E-83
VP3064	multidrug resistance protein	1591	1.6	4.09E-79
VPA0127	cytochrome c-type protein YecK	733	2.0	1.52E-13
VPA0148	transcriptional regulator CpxR	176	2.5	2.94E-36
VPA0149	two-component system sensor kinase	258	2.9	1.60E-56
VPA0193	hypothetical protein	398	1.9	4.52E-35
VPA0247	hypothetical protein	623	1.6	1.16E-42
VPA0248	outer membrane protein OmpA	9301	1.5	1.52E-107
VPA0286	co-chaperonin GroES	205	2.3	1.29E-14
VPA0287	chaperonin GroEL	1440	2.2	7.87E-28
VPA0314	hypothetical protein	492	2.4	1.16E-31
VPA0356	glycine betaine transporter	371	2.1	8.87E-47
VPA0393	hypothetical protein	747	1.7	4.85E-13
VPA0407	hypothetical protein	1278	1.9	1.45E-46
VPA0415	hypothetical protein	223	2.2	4.07E-36
VPA0416	hypothetical protein	802	1.5	1.34E-27
VPA0512	hypothetical protein	2602	3.2	1.02E-248
VPA0522	hypothetical protein	103	1.8	1.25E-15

Table 11 Continued

VPA0551	hypothetical protein	293	1.5	3.22E-23
VPA0572	cation efflux system component	17892	1.5	4.69E-95
VPA0583	ATP-dependent RNA helicase	253	1.6	5.34E-20
VPA0590	ATP-dependent RNA helicase	932	1.5	9.36E-46
VPA0608	ATP-dependent RNA helicase DeaD	6518	2.9	3.63E-45
VPA0636	arginine ABC transporter, ATP-binding protein	5581	1.5	3.53E-133
VPA0656	cyclic nucleotide binding protein	145	1.8	5.03E-20
VPA0657	iron(III) ABC transporter, periplasmic iron-compound-binding protein	180	1.9	7.29E-26
VPA0658	iron(III) ABC transporter, permease protein	120	1.9	6.98E-20
VPA0660	iron(III) ABC transporter, ATP-binding protein	151	1.8	1.07E-21
VPA0701	oxalate/formate antiporter	149	1.8	2.31E-21
VPA0706	C4-dicarboxylate transporter, anaerobic	664	1.5	2.46E-08
VPA0747	MSHA pilin protein MshA	108	3.0	1.68E-29
VPA0784	peptide deformylase	118	1.8	9.74E-14
VPA0829	iron-containing alcohol dehydrogenase	916	2.1	5.92E-64
VPA0835	inosine-guanosine kinase	1097	1.9	7.93E-46
VPA0839	hypothetical protein	1005	2.1	2.88E-46
VPA0851	formate transporter 1	3766	4.1	2.97E-17

Table 12 Continued

VPA0857	hypothetical protein	651	3.3	1.99E-87
VPA0870	short-chain alcohol dehydrogenase family	1382	1.5	1.38E-07
VPA0882	heme transport protein HutA	233	1.7	5.36E-20
VPA0910	phage-related protein	440	1.8	5.72E-33
VPA0979	ferric aerobactin receptor precursor	559	3.1	1.02E-90
VPA0991	hypothetical protein	468	1.7	9.58E-15
VPA1166	chloride channel protein	340	1.8	1.67E-12
VPA1168	hypothetical protein	1693	2.3	7.48E-53
VPA1169	GTP cyclohydrolase I	992	1.5	6.06E-52
VPA1193	peptidase T	1956	1.6	7.08E-11
VPA1209	protein export protein SecD	348	1.6	3.17E-12
VPA1232	hypothetical protein	585	1.6	2.54E-46
VPA1242	cytosine permease/transport	160	1.7	1.44E-15
VPA1243	cytosine deaminase	332	1.6	1.53E-31
VPA1289	cold shock transcriptional regulator CspA	10131	1.8	5.20E-68
VPA1290	hypothetical protein	2201	1.9	3.93E-30
VPA1403	capsular polysaccharide biosynthesis glycosyltransferase	157	3.3	1.41E-41
VPA1406	exopolysaccharide biosynthesis protein	131	2.8	4.96E-18
VPA1434	hemolysin secretion ATP-binding protein	134	1.5	9.83E-15
VPA1435	iron(III) compound receptor	574	2.8	1.09E-99
VPA1468	ATP-dependent RNA helicase, DEAD box family	1983	1.7	3.14E-123
VPA1570	hypothetical protein	251	1.6	2.73E-20

Table 13 Continued

VPA1656	ferric vibrioferrin receptor	752	2.4	1.41E-52
VPA1658	hypothetical protein	146	2.0	1.07E-23
VPA1670	collagenase family protease	150	2.0	1.49E-09
VPA1701	transcriptional regulatory GntR family uxuR	913	1.6	1.86E-51

Table 11 Genes downregulated in the *rpoN* mutant in glucose

Locus Tag	Common Name of Primary Target	baseMean	log2Fold Change	padj
RASTmRNA33		2077	-1.7	9.28E-18
svpa172.1	CsrB	370347	-3.4	6.63E-52
svpa201.1	Qrr4	116	-3.0	1.30E-26
svpa3216.1	CsrB	266221	-1.9	7.12E-43
VP0026	hypothetical protein	8449	-5.4	0
VP0029	acetyl-CoA acetyltransferase	2113	-2.5	7.29E-103
VP0030	fatty oxidation complex, alpha subunit	3743	-2.7	4.19E-181
VP0052	hypothetical protein	722	-2.7	5.71E-71
VP0081	hyperosmotically inducible periplasmic protein	21338	-9.1	6.06E-222
VP0082	transmembrane protein	4466	-8.4	1.56E-189
VP0083	hypothetical protein	9154	-8.6	1.53E-294
VP0084	hypothetical protein	5217	-7.9	1.08E-197
VP0085	methylglyoxal synthase	3898	-7.3	1.62E-200
VP0086	hypothetical protein	3227	-6.7	1.29E-127
VP0087	hypothetical protein	7663	-9.0	2.62E-181
VP0088	hypothetical protein	5024	-8.4	5.90E-179
VP0089	hypothetical protein	4063	-8.2	2.25E-175
VP0090	hypothetical protein	974	-7.6	1.94E-125

Table 11 Continued

VP0091	permease protein	1412	-6.6	2.30E-249
VP0118	nitrogen regulation protein	286	-2.3	5.81E-36
VP0119	nitrogen regulation protein	573	-2.7	6.06E-122
VP0121	glutamine synthetase	25296	-4.0	5.51E-274
VP0149	hypothetical protein	4169	-3.1	8.22E-157
VP0162	hypothetical protein	9805	-2.6	3.90E-178
VP0163	TonB2 protein	4765	-2.7	3.00E-84
VP0164	TonB system transport protein ExbD2	2796	-2.9	9.12E-133
VP0165	TonB system transport protein ExbB2	4310	-2.8	2.29E-73
VP0166	TolR	12678	-3.0	2.10E-116
VP0167	hypothetical protein	8926	-3.1	1.77E-112
VP0168	hypothetical protein	50716	-3.1	3.34E-113
VP0170	transmembrane ABC transporter protein	1281	-1.7	1.77E-81
VP0171	peptide ABC transporter, permease protein	1393	-2.2	3.33E-39
VP0172	binding protein component of ABC transporter	3629	-2.0	4.77E-56
VP0173	oligopeptide ABC transporter, ATP-binding protein	2615	-1.8	5.14E-32
VP0174	oligopeptide ABC transporter, ATP-binding protein	1793	-1.5	6.32E-32
VP0304	hypothetical protein	903	-2.5	1.42E-112
VP0305	hypothetical protein	1712	-2.5	3.69E-23
VP0345	hypothetical protein	7024	-1.6	4.53E-86
VP0360	hypothetical protein	21855	-6.0	0
VP0361	two component response regulator transcription regulator protein	2552	-4.5	5.04E-115
VP0362	two component sensor protein	994	-3.3	1.77E-47
VP0379	ABC transporter substrate binding protein	11739	-1.9	2.15E-34
VP0384	hypothetical protein	162	-2.4	5.84E-28

Table 11 Continued

VP0422	potassium channel protein	236	-1.5	5.40E-27
VP0481	glutamate synthase, small subunit	4256	-2.4	1.53E-154
VP0482	glutamate synthase, large subunit	12373	-2.7	9.80E-160
VP0483	glutamate synthase, small subunit	14617	-1.7	2.23E-78
VP0484	glutamate synthase, large subunit	30948	-1.8	0
VP0492	ribonuclease activity regulator protein RraA	2819	-1.7	1.54E-45
VP0494	bifunctional aspartokinase I/homeserine dehydrogenase I	14425	-1.5	5.02E-22
VP0502	hypothetical protein	181	-1.7	9.14E-08
VP0583	malate synthase	6328	-3.5	2.70E-133
VP0584	isocitrate lyase	10430	-3.4	1.48E-213
VP0596	cysteine desulfurase	20780	-1.6	6.47E-52
VP0597	NifU-related protein	6763	-1.7	9.71E-82
VP0598	HesB family protein	5258	-1.5	6.51E-94
VP0623	D-amino acid dehydrogenase small subunit	295	-1.5	1.81E-22
VP0624	transcriptional regulator, LysR family	388	-2.4	1.80E-33
VP0634	hypothetical protein	570	-1.7	2.78E-34
VP0636	outer membrane protein A	1415	-5.8	0
VP0689	flagellar motor protein	261	-1.6	1.16E-18
VP0690	flagellar motor protein	473	-1.5	4.09E-35
VP0758	cation transport ATPase, E1-E2 family	31334	-1.6	5.08E-18
VP0767	hypothetical protein	461	-2.1	5.98E-37
VP0768	hypothetical protein	536	-4.3	2.27E-129
VP0769	hypothetical protein	286	-3.9	5.23E-60
VP0775	flagellar basal body protein	1799	-2.5	8.31E-110
VP0776	flagellar basal body rod protein	1502	-2.6	1.78E-55
VP0777	flagellar basal body rod modification protein	2312	-2.8	4.75E-54
VP0778	flagellar hook protein	4844	-2.7	3.41E-50

Table 11 Continued

VP0780	polar flagellar FlgF	333	-4.7	8.50E-114
VP0781	polar flagellar FlgG	234	-5.7	5.98E-73
VP0782	flagellar L-ring protein precursor	224	-4.3	2.17E-66
VP0783	flagellar P-ring protein precursor	379	-4.7	6.32E-92
VP0784	peptidoglycan hydrolase	372	-4.6	2.57E-111
VP0785	flagellar hook-associated protein	975	-6.4	2.75E-173
VP0786	flagellar hook-associated protein	601	-3.9	4.05E-59
VP0788	flagellin	1782	-4.4	2.78E-138
VP0790	flagellin	179	-4.7	1.41E-69
VP0826	asparagine synthetase B	8240	-1.5	3.08E-15
VP0834	hypothetical protein	427	-1.7	1.13E-28
VP0910	C4-dicarboxylate-binding periplasmic protein	438	-2.0	1.26E-62
VP0996	54 kDa polar flagellar sheath protein A	1158	-3.6	2.95E-256
VP0998	amino acid ABC transporter, ATP-binding protein	4697	-1.9	3.41E-130
VP0999	amino acid ABC transporter, periplasmic amino acid-binding protein	7813	-2.2	7.75E-105
VP1000	amino acid ABC transporter, permease protein	3529	-2.2	1.09E-92
VP1001	amino acid ABC transporter, permease protein	2277	-2.1	6.04E-170
VP1117	hypothetical protein	3374	-3.1	1.18E-34
VP1119	transcriptional regulator	193	-1.6	4.04E-17
VP1120	short chain dehydrogenase	244	-1.9	1.49E-31
VP1121	hypothetical protein	420	-2.0	1.83E-68
VP1122	hypothetical protein	245	-2.0	4.09E-44
VP1123	cyclopropane-fatty-acyl-phospholipid synthase	228	-1.9	1.36E-32
VP1137	ATP phosphoribosyltransferase	7294	-1.7	2.17E-59
VP1138	histidinol dehydrogenase	8273	-1.7	7.21E-33
VP1161	cytochrome c-type protein TorC	473	-1.5	5.34E-44

Table 11 Continued

VP1172	psp operon transcriptional activator	1326	-1.7	5.50E-56
VP1173	phage shock protein A	2862	-3.5	1.78E-147
VP1174	phage shock protein B	441	-3.1	6.19E-103
VP1175	phage shock protein C	1291	-2.8	4.90E-76
VP1229	Na <sup>+</sup> /H <sup>+</sup> -antiporter protein	370	-2.3	8.95E-71
VP1230	oxidoreductase, acyl-CoA dehydrogenase family	2847	-2.4	2.49E-53
VP1243	hypothetical protein	1595	-2.1	5.85E-48
VP1252	hypothetical protein	174	-1.5	8.74E-14
VP1265	hypothetical protein	164	-1.7	4.22E-11
VP1349	4-hydroxyphenylpyruvate dioxygenase	604	-2.8	1.17E-132
VP1350	oxidoreductase	469	-2.8	2.22E-113
VP1351	hypothetical protein	327	-2.8	5.06E-62
VP1513	formate dehydrogenase large subunit	570	-1.7	3.29E-55
VP1524	NAD-dependent deacetylase	3052	-1.7	2.63E-43
VP1620	amino acid ABC transporter, periplasmic amino acid-binding protein	11052	-3.8	4.21E-156
VP1621	amino acid ABC transporter, permease protein	3718	-3.9	1.82E-98
VP1622	amino acid ABC transporter, permease protein	2529	-4.1	1.32E-101
VP1623	amino acid ABC transporter, ATP-binding protein	3159	-3.7	1.47E-155
VP1634	agglutination protein	1243	-1.7	3.62E-96
VP1635	outer membrane protein	952	-1.6	5.42E-57
VP1644	PrpE protein	354	-2.0	3.94E-29
VP1645	hypothetical protein prpF	127	-2.4	1.45E-25
VP1646	aconitate hydratase citrate to isocitrate	320	-3.0	6.62E-59
VP1647	citrate synthase	919	-2.8	3.07E-138

Table 11 Continued

VP1648	carboxyphosphoenolpyruvate phosphonmutase	825	-3.3	1.02E-102
VP1649	transcriptional regulator, GntR family	802	-3.5	6.25E-213
VP1651	tricarboxylic transport TctC	10250	-7.4	6.53E-166
VP1652	tricarboxylic transport TctB	1299	-7.5	2.46E-208
VP1653	tricarboxylic transport TctA	4141	-7.1	0
VP1655	immunogenic protein	151	-2.3	5.28E-35
VP1703	aldehyde dehydrogenase	116	-1.7	1.12E-16
VP1704	sigma-54 dependent transcriptional regulator	141	-2.0	4.38E-25
VP1719	aspartate kinase	10722	-1.7	4.81E-22
VP1720	ectoine synthase	5232	-2.1	6.38E-25
VP1721	diaminobutyrate--2-oxoglutarate aminotransferase	15536	-2.2	1.43E-51
VP1722	L-2,4-diaminobutyric acid acetyltransferase	5306	-2.2	2.15E-35
VP1726	ABC superfamily (glycine/betaine/proline transport protein)	8236	-1.6	4.47E-43
VP1727	glycine betaine/L-proline transport system permease	4677	-2.1	2.35E-156
VP1728	ABC superfamily (glycine/betaine/proline transport protein)	6679	-1.9	6.27E-57
VP1745	lipid A biosynthesis lauroyl acyltransferase	959	-1.7	5.23E-15
VP1749	hypothetical protein	763	-2.0	2.47E-26
VP1751	homoserine O-succinyltransferase	8652	-2.2	2.26E-32
VP1752	fimbrial biogenesis and twitching motility protein	100	-1.8	5.71E-10
VP1771	Gamma-glutamyl-putrescine synthetase <i>puuA</i>	759	-2.5	1.55E-36
VP1772	Putrescine utilization symporter	661	-2.8	3.07E-49
VP1773	Agmatine deiminase <i>aguA</i>	476	-3.2	1.85E-62

Table 11 Continued

VP1774	N-carbamoylputrescine amidase <i>aguB</i>	591	-3.4	2.12E-96
VP1775	Gamma-glutamyl-putrescine oxidase <i>puuB</i>	1037	-3.3	1.28E-94
VP1776	gamma-glutamyl- aminobutyraldehyde dehydrogenase <i>PuuC</i>	264	-3.4	2.50E-61
VP1777	gamma-glutamyl-gamma- aminobutyraldehyde dehydrogenase <i>PuuC</i>	1061	-3.5	5.79E-249
VP1778	Putrescine utilization regulator <i>PuuR</i>	619	-3.8	7.09E-137
VP1779	glutamine amidotransferase <i>puuD</i>	696	-3.1	2.66E-75
VP1781	Gamma-glutamyl-putrescine synthetase <i>puuA</i>	1494	-3.6	8.00E-136
VP1782	Putrescine utilization symporter	2116	-3.8	7.06E-260
VP1842	RelB protein	356	-2.0	2.30E-29
VP1843	hypothetical protein	487	-1.7	1.79E-23
VP1913	hypothetical protein	320	-1.6	3.90E-33
VP1975	hypothetical protein	1491	-1.5	3.09E-34
VP1976	transcriptional activator MetR	13456	-1.9	1.17E-22
VP2025	hypothetical protein	8897	-1.8	9.70E-84
VP2040	hypothetical protein	1544	-1.8	2.25E-29
VP2078	ABC transporter, ATP-binding protein	556	-2.3	7.18E-29
VP2079	ABC transporter, permease protein	571	-2.7	9.00E-59
VP2080	ABC transporter substrate- binding protein	1413	-2.5	3.47E-84
VP2085	hypothetical protein	137	-2.6	1.42E-24
VP2111	sodium-type flagellar protein MotY	668	-2.6	1.15E-117
VP2119	hypothetical protein	161	-2.9	2.02E-41
VP2151	2,4-dienoyl-CoA reductase	1914	-2.3	1.45E-56

Table 11 Continued

VP2162	hypothetical protein	180	-2.4	1.05E-43
VP2208	fatty oxidation complex, alpha subunit	4998	-2.1	3.21E-85
VP2209	acetyl-CoA acetyltransferase	2548	-2.1	1.11E-88
VP2211	hypothetical protein	2935	-1.5	6.07E-40
VP2226	hypothetical protein	634	-1.6	1.25E-15
VP2227	Soj-like protein	609	-1.7	5.02E-21
VP2228	chemotaxis-specific methylesterase	1063	-1.9	4.97E-32
VP2229	chemotaxis protein CheA	3650	-2.0	1.01E-61
VP2230	chemotaxis protein CheZ	2325	-2.1	1.11E-91
VP2231	chemotaxis protein CheY	1574	-2.1	4.98E-115
VP2232	flagellar biosynthesis sigma factor FliA	2399	-2.9	1.23E-274
VP2233	flagellar biosynthesis protein FlhG	2873	-4.0	1.10E-231
VP2234	flagellar biosynthesis protein	3345	-6.4	0
VP2235	flagellar biosynthesis protein	1596	-4.8	6.43E-295
VP2241	flagellar motor switch protein	597	-1.7	2.41E-37
VP2242	flagellar motor switch protein	1234	-1.8	1.66E-49
VP2243	flagellar basal body-associated protein	547	-1.8	9.17E-56
VP2244	polar flagellar hook-length control protein FliK	1402	-3.6	3.90E-297
VP2247	flagellar assembly protein	555	-2.1	1.70E-46
VP2248	flagellar motor protein	1698	-2.5	6.77E-145
VP2249	flagellar M-ring protein	2281	-2.3	5.97E-122
VP2251	FlaM	946	-1.6	4.69E-20
VP2252	FlaL	545	-1.8	1.67E-53
VP2254	flagellar protein FliS	214	-4.3	3.67E-82
VP2256	flagellar hook-associated protein	2098	-4.2	0
VP2257	flagellar protein FlaG	1593	-4.1	7.24E-246
VP2258	flagellin	3547	-4.0	1.99E-229

Table 11 Continued

VP2259	Flagellin	588	-4.5	1.23E-179
VP2261	flagellin	270	-4.0	1.14E-74
VP2289	acyl-CoA dehydrogenase	1998	-2.1	1.86E-37
VP2327	hypothetical protein	290	-2.0	3.06E-27
VP2328	hypothetical protein	719	-2.0	2.56E-26
VP2357	transcriptional activator ChrR	618	-1.9	2.92E-66
VP2358	RNA polymerase sigma-70 factor	508	-2.0	2.26E-62
VP2359	hypothetical protein	160	-1.5	1.32E-20
VP2378	transcriptional regulator, LysR family	199	-1.6	3.30E-23
VP2388	aerobic glycerol-3-phosphate dehydrogenase	208	-1.9	1.88E-28
VP2425	long-chain-fatty-acid-CoA ligase	996	-3.2	1.45E-209
VP2492	ammonium transporter	492	-3.0	3.32E-29
VP2493	nitrogen regulatory protein P-II	149	-5.0	2.95E-47
VP2495	aconitate hydratase	34035	-1.9	1.09E-62
VP2553	RNA polymerase sigma factor RpoS	45809	-2.5	1.32E-97
VP2554	lipoprotein NlpD	16975	-1.7	2.93E-18
VP2594	hypothetical protein	1641	-1.5	2.86E-25
VP2596	LysE/YggA family protein	102	-1.8	3.78E-18
VP2652	arginine deiminase	703	-1.8	2.11E-30
VP2670	DNA-directed RNA polymerase subunit N	1875	-1.6	4.25E-43
VP2683	hypothetical protein	381	-1.9	2.62E-30
VP2714	aminotransferase, class V	1620	-1.6	1.69E-27
VP2725	phage shock protein G	101	-3.9	1.46E-42
VP2760	acetylornithine deacetylase	5257	-1.5	1.28E-60
VP2761	phosphoenolpyruvate carboxylase	17339	-1.9	1.89E-135
VP2763	5,10-methylenetetrahydrofolate reductase	51184	-1.5	2.30E-24
VP2764	bifunctional aspartate kinase II/homoserine dehydrogenase II	30986	-1.7	2.02E-15

Table 11 Continued

VP2765	cystathionine gamma-synthase	17186	-2.0	8.55E-29
VP2785	glutathione-regulated potassium-efflux system protein	1318	-1.8	1.49E-31
VP2786	glutathione-regulated potassium-efflux system ancillary protein	424	-1.6	2.67E-22
VP2810	hypothetical protein	705	-2.4	7.45E-75
VP2827	methyl-accepting chemotaxis protein	317	-3.4	1.03E-76
VP2868	hypothetical protein	5136	-6.9	0
VP2869	sodium/solute symporter	28523	-6.2	0
VP2870	hypothetical protein	1428	-3.0	3.23E-267
VP2871	hypothetical protein	394	-3.1	7.63E-104
VP2876	hypothetical protein	2665	-3.7	4.02E-228
VP2877	DNA polymerase III subunit epsilon	549	-2.9	3.44E-57
VP2878	acetyl-coenzyme A synthetase	18434	-3.6	1.94E-68
VP3012	hypothetical protein	775	-2.1	5.81E-13
VP3014	signal peptide protein	2035	-2.0	1.70E-22
VP3015	hypothetical protein	1139	-1.8	4.56E-16
VP3016	hypothetical protein	459	-2.3	1.65E-56
VP3017	transmembrane protein	264	-2.1	6.11E-25
VPA0009	two-component sensor	441	-2.2	8.25E-74
VPA0040	hypothetical protein	1057	-2.3	1.08E-21
VPA0103	hypothetical protein	252	-1.7	2.17E-18
VPA0104	ring-cleaving dioxygenase	243	-1.8	5.89E-25
VPA0118	transcriptional regulator	311	-1.6	2.08E-33
VPA0188	immunogenic protein	4546	-6.9	0
VPA0189	hypothetical protein	3721	-5.9	5.16E-299
VPA0190	transcriptional regulator	3304	-5.0	6.48E-165
VPA0196	hypothetical protein	3275	-1.5	1.60E-34
VPA0201	malate synthase	3224	-3.5	1.18E-155
VPA0206	hypothetical protein	1143	-2.5	5.40E-27

Table 11 Continued

VPA0207	bifunctional methionine sulfoxide reductase A/B protein	3835	-2.1	2.89E-20
VPA0213	hypothetical protein	2052	-3.3	3.15E-65
VPA0254	L-serine dehydratase 1	517	-1.7	2.99E-40
VPA0312	hypothetical protein	1207	-1.5	3.24E-14
VPA0320	lipoprotein	1247	-1.5	9.68E-30
VPA0343	membrane fusion protein	916	-2.2	6.51E-44
VPA0344	multidrug resistance protein	2237	-1.7	1.48E-17
VPA0345	hypothetical protein	506	-5.7	6.05E-133
VPA0381	transcription regulator	725	-3.0	2.74E-103
VPA0441	integral membrane protein	152	-2.0	4.92E-31
VPA0460	PAS factor	907	-1.8	1.73E-11
VPA0475	hypothetical protein	196	-2.9	2.01E-38
VPA0480	cation efflux system transmembrane protein	6047	-1.5	8.99E-16
VPA0481	cation efflux system transmembrane protein	2706	-1.5	3.62E-18
VPA0524	glutaredoxin-related protein	1467	-1.5	6.18E-10
VPA0548	protein F-related protein	304	-3.6	5.19E-80
VPA0554	methyl-accepting chemotaxis protein	688	-1.7	1.93E-40
VPA0562	chemotaxis transducer	1793	-3.5	3.34E-273
VPA0575	acetyl-CoA synthase	4496	-4.3	0
VPA0576	phenylalanine-4-hydroxylase	664	-4.0	2.96E-135
VPA0577	pterin-4-alpha-carbinolamine dehydratase	309	-3.7	4.72E-68
VPA0596	methyl-accepting chemotaxis protein	992	-2.7	1.12E-148
VPA0597	hypothetical protein	130	-3.0	7.19E-42
VPA0602	transcription activator NahR	462	-1.5	4.01E-31
VPA0647	pyruvate dehydrogenase E1 component, alpha subunit	142	-3.3	3.80E-51
VPA0694	hypothetical protein	189	-2.9	3.29E-49

Table 11 Continued

VPA0695	accessory colonization factor AcfA	241	-2.5	1.74E-55
VPA0699	hypothetical protein	710	-1.7	4.59E-29
VPA0768	catalase/oxidase	1689	-2.0	4.65E-108
VPA0788	outer membrane phospholipase A precursor	553	-2.0	2.34E-77
VPA0833	glucose-1-phosphate adenylyltransferase	115	-1.5	3.94E-15
VPA0859	lipase	5317	-3.9	0
VPA0860	long-chain fatty acid transport protein	1888	-4.5	0
VPA0914	hypothetical protein	199	-1.6	1.46E-12
VPA0943	AcrA/AcrE family protein	178	-1.5	1.60E-19
VPA0944	cation efflux system (AcrB/AcrD/AcrF family)	386	-1.9	3.46E-23
VPA0973	MFS family transport protein	744	-1.5	6.66E-27
VPA0984	uroporphyrin-III C- methyltransferase	1028	-1.7	1.49E-21
VPA0985	formate dehydrogenase	1380	-1.5	6.94E-17
VPA0986	nitrite reductase small subunit	665	-1.7	3.91E-43
VPA0998	hypothetical protein	537	-1.5	8.05E-20
VPA1008	hypothetical protein	12002	-4.2	3.91E-258
VPA1009	hypothetical protein	14089	-3.9	4.60E-248
VPA1027	hypothetical protein	134	-2.3	1.03E-20
VPA1045	hypothetical protein	1233	-1.6	4.20E-68
VPA1046	hypothetical protein	165	-2.3	1.53E-38
VPA1117	3-ketoacyl-(acyl-carrier-protein) reductase	436	-5.5	4.28E-91
VPA1118	3-hydroxyisobutyrate dehydrogenase	547	-5.6	3.63E-108
VPA1119	enoyl-CoA hydratase/isomerase	762	-6.2	4.75E-138
VPA1120	enoyl-CoA hydratase	588	-6.4	3.41E-135
VPA1121	acyl-CoA dehydrogenase	977	-6.2	3.25E-222
VPA1122	aldehyde dehydrogenase	3073	-5.9	0

Table 11 Continued

VPA1123	acyl-CoA thiolase	3230	-5.3	0
VPA1124	transcriptional regulator	1834	-3.2	1.14E-83
VPA1125	acyl-CoA dehydrogenase	2173	-3.3	2.86E-251
VPA1126	acyl-CoA carboxyltransferase beta chain	627	-3.9	2.09E-128
VPA1127	enoyl-CoA hydratase/isomerase	241	-4.1	4.90E-89
VPA1128	acyl-CoA carboxylase alpha chain	535	-4.2	2.25E-145
VPA1129	hydroxymethylglutaryl-CoA lyase	332	-3.5	3.00E-69
VPA1147	phenylacetate-CoA ligase	1404	-3.9	6.50E-129
VPA1148	high-affinity branched-chain amino acid transport ATP- binding protein	1094	-4.0	9.19E-82
VPA1149	hypothetical protein	1888	-4.0	2.49E-77
VPA1150	high-affinity branched-chain amino acid transport permease protein	1328	-3.8	1.11E-72
VPA1151	ABC transporter, membrane spanning protein	1721	-3.8	3.59E-150
VPA1152	long-chain-fatty-acid-CoA ligase	4025	-4.0	2.66E-134
VPA1153	high-affinity branched-chain amino acid transport ATP- binding protein	3004	-3.9	2.64E-243
VPA1155	electron transfer flavoprotein- ubiquinone oxidoreductase	15024	-3.4	8.03E-152
VPA1156	electron transfer flavoprotein, beta-subunit	2063	-2.8	7.17E-74
VPA1157	electron transfer flavoprotein, alpha-subunit	2924	-2.6	2.24E-62
VPA1158	acetyl-CoA synthase	578	-2.8	8.99E-132
VPA1186	outer membrane protein OmpA	2640	-1.6	2.37E-54
VPA1203	hypothetical protein	147	-1.5	2.18E-19
VPA1204	acetyl-CoA acetyltransferase	224	-1.9	5.36E-21
VPA1205	acetoacetyl-CoA reductase	174	-1.8	1.61E-29
VPA1262	hypothetical protein	1972	-1.5	5.58E-38

Table 11 Continued

VPA1266	ATP-dependent exoDNAse (exonuclease V), alpha subunit	730	-1.8	3.41E-76
VPA1267	hypothetical protein	210	-2.3	5.61E-48
VPA1268	hypothetical protein	390	-2.4	5.58E-69
VPA1269	hypothetical protein	1117	-2.6	7.20E-85
VPA1270	hypothetical protein	735	-2.8	8.84E-141
VPA1428	azurin	1067	-1.9	7.82E-33
VPA1449	methyl-accepting chemotaxis protein	480	-2.2	1.05E-26
VPA1469	outer membrane lipoprotein	7351	-1.6	1.37E-10
VPA1471	deoxyribodipyrimidine photolyase	874	-2.1	2.63E-49
VPA1472	transcriptional regulator, MerR family	1067	-2.1	4.30E-72
VPA1473	hypothetical protein	1327	-1.7	1.79E-17
VPA1515	two-component sensor histidine kinase	356	-2.5	1.44E-81
VPA1516	two-component response regulator	402	-1.8	6.06E-27
VPA1586	ferredoxin-NADP reductase	1816	-1.8	2.36E-19
VPA1615	outer membrane protein	545	-1.7	4.32E-49
VPA1637	hypothetical protein	205	-1.6	3.98E-27
VPA1646	recombinase	212	-1.9	1.47E-22
VPA1647	hypothetical multidrug resistance protein D	262	-1.9	2.72E-43
VPA1667	PTS system, glucose-specific IIBC component	191	-2.6	2.79E-45
VPA1749	hypothetical protein	384	-1.5	8.14E-35

**Table 12 Genes upregulated in the *rpoN* mutant in mouse intestinal mucus**

<b>Locus Tag</b>	<b>Function</b>	<b>baseMean</b>	<b>log2Fold Change</b>	<b>padj</b>
RASTm RNA31	hypothetical protein	462	1.48	5.27E-10
VP0008	amino acid ABC transporter, periplasmic amino acid-binding portion	712	2.05	3.88E-74
VP0284	hypothetical protein	797	1.6	8.97E-35
VP0292	sulfate adenylyltransferase subunit 2	472	1.8	4.25E-28
VP0293	sulfate adenylyltransferase subunit 1	679	1.55	2.73E-10
VP0648	DNA repair protein RecN	2142	1.51	3.51E-24
VP0652	GltP	705	2.86	8.95E-42
VP1273	histidine ammonia-lyase	950	1.51	1.60E-13
VP1329	fatty aldehyde dehydrogenase	389	1.55	3.64E-10
VP1330	proline racemase	155	1.69	2.42E-12
VP1331	D-amino acid dehydrogenase, small subunit	159	1.66	3.24E-19
VP1332	probable binding protein component of ABC transporter	318	1.86	1.04E-20
VP1334	hypothetical protein	132	2.04	8.83E-20
VP1335	probable dihydrodipicolinate synthetase	127	1.82	1.95E-15
VP1400	hypothetical protein	129	1.68	4.36E-16
VP1408	putative IcmF-related protein	350	2.15	1.37E-25
VP1409	hypothetical protein	138	2.91	1.61E-32
VP1645	hypothetical protein	421	1.57	1.73E-07
VP1646	aconitate hydratase	1168	1.92	2.47E-14
VP1651	putative tricarboxylic transport TctC	1042	2.2	5.20E-41
VP1652	putative tricarboxylic transport TctB	122	2.32	3.78E-10
VP1653	putative tricarboxylic transport TctA	713	2.72	6.43E-15

Table 12 Continued

VP1659	hypothetical protein	177	1.51	6.23E-12
VP1667	putative outer membrane protein PopN	148	2.36	9.07E-31
VP1668	type III secretion system ATPase	126	2.46	4.21E-24
VP1680	hypothetical protein	118	1.67	9.17E-08
VP1686	hypothetical protein	102	1.99	3.29E-12
VP1695	putative type III export protein PscD	127	1.98	1.26E-19
VP1696	putative type III secretion protein YscC	180	2.05	5.00E-29
VP1698	hypothetical protein	428	2.01	3.20E-51
VP1771	4-aminobutyrate aminotransferase	2195	2.09	2.99E-23
VP1772	succinate-semialdehyde dehydrogenase	1549	2.27	4.18E-23
VP1773	hypothetical protein	1078	2.35	4.72E-28
VP1774	putative carbon-nitrogen hydrolase	1197	1.95	1.17E-11
VP1775	putative oxidoreductase	2236	1.64	3.99E-27
VP1888	hypothetical protein	1125	2.51	4.73E-35
VP1889	cold shock transcriptional regulator CspA	5341	2.84	5.03E-35
VP1890	putative virulence-associated protein VacB/RNase R	22155	2.67	2.52E-77
VP1909	hypothetical protein	169	3.13	9.58E-40
VP1910	hypothetical protein	139	3.77	1.88E-45
VP1911	extracellular solute-binding protein, family 7	1417	4.01	3.79E-224
VP1917	hypothetical protein	175	1.54	1.54E-15
VP1918	hypothetical protein	146	1.67	7.71E-17
VP1919	hypothetical protein	213	2.04	2.82E-33
VP1920	putative iron-regulated protein A	540	1.94	3.91E-30
VP2329	efflux pump component MtrF	942	2.37	3.63E-104
VPA014 9	putative two-component system sensor kinase	139	1.68	2.54E-17
VPA022 6	lecithin-dependent hemolysin (LDH)	404	1.73	2.95E-23

Table 12 Continued

VPA024 2	hypothetical protein	540	1.98	9.84E-25
VPA024 3	putative virK protein	1231	2.04	8.93E-50
VPA025 1	transcriptional regulator, LysR family	201	1.94	1.40E-26
VPA031 8	putative outer membrane protein OmpV	5675	1.65	4.80E-22
VPA034 6	hypothetical protein	1497	1.48	0.0004663 4
VPA061 2	putative chemotaxis transducer	906	1.86	1.72E-36
VPA062 8	cytochrome o ubiquinol oxidase, subunit I	420	1.85	7.13E-18
VPA062 9	cytochrome o ubiquinol oxidase, subunit III	148	1.94	1.19E-21
VPA063 1	putative protoheme IX farnesyltransferase	201	2.01	4.32E-21
VPA081 0	hypothetical protein	1642	1.49	5.27E-15
VPA119 7	iron-sulfur cluster-binding protein NapF	456	2.15	3.93E-40
VPA119 8	NapD protein	305	1.66	5.27E-15
VPA119 9	periplasmic nitrate reductase	5672	1.48	1.23E-17
VPA127 8	hypothetical protein	479	1.81	1.65E-43
VPA127 9	diacylglycerol kinase	316	1.74	1.27E-19
VPA128 0	hypothetical protein	680	1.66	8.59E-27
VPA128 9	cold shock transcriptional regulator CspA	14868	1.5	6.05E-48
VPA129 0	hypothetical protein	1649	2.22	1.36E-26
VPA129 1	hypothetical protein	126	1.96	4.40E-09

Table 12 Continued

VPA140 3	putative capsular polysaccharide biosynthesis glycosyltransferase	214	2.61	1.02E-27
VPA140 4	hypothetical protein	164	2.57	1.28E-29
VPA140 6	putative exopolysaccharide biosynthesis protein	120	2.17	1.39E-21
VPA143 5	putative iron(III) compound receptor	249	2.09	1.50E-34
VPA146 2	methyl-accepting chemotaxis protein	137	2.08	3.82E-13
VPA151 1	ScrC (sensory box/GGDEF family protein) (involved in swarmer cell regulation)	439	1.76	4.04E-38
VPA151 2	ScrB (extracellular solute binding protein)	334	1.63	1.80E-30
VPA151 3	ScrA (aminotransferase)	1789	1.78	2.00E-44
VPA163 4	putrescine transport protein	114	1.94	5.73E-19
VPA163 5	ornithine decarboxylase, inducible	325	2.51	7.30E-43

**Table 13 Genes downregulated in the *rpoN* mutant in mouse intestinal mucus**

<b>Locus Tag</b>	<b>Common Name of Primary Target</b>	<b>baseMean</b>	<b>log2Fold Change</b>	<b>padj</b>
VP0052	hypothetical protein	722	-2.4	5.06E-68
VP0081	putative hyperosmotically inducible periplasmic protein	3859	-7.35	3.02E-291
VP0082	putative transmembrane protein	883	-6.58	7.32E-117
VP0083	hypothetical protein	1758	-6.06	8.74E-185
VP0084	hypothetical protein	922	-5.92	3.52E-138
VP0085	methylglyoxal synthase	628	-5.16	1.03E-102
VP0086	hypothetical protein	527	-5.16	2.74E-100
VP0087	hypothetical protein	1372	-7.14	6.66E-198
VP0088	hypothetical protein	1316	-6.79	5.12E-179
VP0089	hypothetical protein	969	-6.73	5.28E-164
VP0090	hypothetical protein	216	-5.77	9.59E-64
VP0091	putative permease protein	443	-4.93	1.07E-84
VP0118	nitrogen regulation protein	420	-2.77	4.27E-83
VP0119	nitrogen regulation protein	274	-1.95	1.03E-22
VP0121	glutamine synthetase	17074	-3.15	9.40E-136
VP0149	hypothetical protein	3467	-3.76	0
VP0358	transcriptional regulator, DeoR family	995	-2.09	7.14E-58
VP0359	D-fructose-6-phosphate amidotransferase	1833	-1.88	2.75E-14
VP0422	putative potassium channel protein	540	-1.72	1.03E-31
VP0636	putative outer membrane protein A	438	-3.68	7.61E-32
VP0689	flagellar motor protein	343	-1.98	4.13E-40
VP0690	flagellar motor protein	552	-1.71	2.16E-39
VP0767	hypothetical protein	429	-2.98	1.29E-78
VP0768	hypothetical protein	607	-5	8.74E-151
VP0769	hypothetical protein	315	-4.77	5.85E-92
VP0775	flagellar basal body protein	1926	-2.95	5.16E-109
VP0776	flagellar basal body rod protein	1731	-3.21	1.74E-80

Table 13 Continued

VP0777	flagellar basal body rod modification protein	2607	-3.3	4.62E-47
VP0778	flagellar hook protein	5237	-3.42	4.23E-94
VP0780	polar flagellar FlgF	389	-5.17	2.83E-105
VP0781	polar flagellar FlgG	298	-5.11	1.01E-84
VP0782	flagellar L-ring protein precursor	297	-4.7	7.30E-86
VP0783	flagellar P-ring protein precursor	447	-5	3.11E-115
VP0784	peptidoglycan hydrolase	350	-5.11	8.72E-96
VP0785	flagellar hook-associated protein	1116	-6.59	3.69E-190
VP0786	flagellar hook-associated protein	662	-4.77	9.48E-131
VP0788	flagellin	2486	-5.49	0
VP0790	flagellin	494	-6.51	4.24E-106
VP0910	C4-dicarboxylate-binding periplasmic protein	1883	-5.38	4.08E-225
VP0911	putative C4-dicarboxylate transport protein DctQ	297	-4.94	6.30E-58
VP0912	C4-dicarboxylate transport protein	813	-5.35	1.47E-109
VP0996	putative 54 kDa polar flagellar sheath protein A	1280	-4.89	1.86E-228
VP1173	phage shock protein A	11293	-5.57	9.09E-180
VP1174	phage shock protein B	1902	-5.25	1.24E-108
VP1175	phage shock protein C	5275	-5.73	7.33E-262
VP1176	putative multidrug resistance protein	771	-1.66	2.95E-20
VP1243	hypothetical protein	1698	-2.05	9.84E-47
VP1325	hypothetical protein	516	-1.57	6.22E-22
VP1376	putative chemotaxis protein CheY	549	-1.63	2.25E-13
VP1506	formate dehydrogenase accessory protein	300	-1.7	7.67E-10
VP1510	iron-sulfur cluster-binding protein	771	-4.13	1.78E-155
VP1511	putative formate dehydrogenase-specific chaperone	200	-3.8	2.91E-59
VP1512	hypothetical protein	165	-3.41	6.09E-48
VP1513	putative formate dehydrogenase large subunit	2132	-3.71	1.83E-274

Table 13 Continued

VP1514	formate dehydrogenase, iron-sulfur subunit	381	-3.55	5.03E-96
VP1515	formate dehydrogenase, cytochrome b556 subunit	567	-3.08	1.10E-79
VP1516	hypothetical protein	324	-2.72	2.16E-62
VP1634	agglutination protein	834	-1.95	1.25E-56
VP1635	putative outer membrane protein	579	-1.81	5.22E-41
VP1703	aldehyde dehydrogenase	18320	-8.94	0
VP2111	sodium-type flagellar protein MotY	454	-2.88	2.85E-92
VP2119	hypothetical protein	225	-4.45	3.02E-68
VP2162	hypothetical protein	218	-3.76	2.99E-60
VP2226	hypothetical protein	896	-1.74	9.11E-50
VP2227	Soj-like protein	882	-1.89	1.01E-60
VP2228	chemotaxis-specific methylesterase	1338	-1.92	9.40E-72
VP2229	chemotaxis protein CheA	3401	-2.1	2.12E-102
VP2230	chemotaxis protein CheZ	1440	-1.98	6.96E-26
VP2231	chemotaxis protein CheY	939	-2.01	1.09E-40
VP2232	flagellar biosynthesis sigma factor FliA	1128	-2.31	3.26E-60
VP2233	flagellar biosynthesis protein FlhG	1689	-3.57	5.15E-136
VP2234	flagellar biosynthesis protein	1824	-4.54	2.49E-227
VP2235	flagellar biosynthesis protein	1169	-3.38	1.06E-179
VP2244	polar flagellar hook-length control protein FliK	1124	-2.56	7.02E-88
VP2248	flagellar motor protein	1032	-1.55	8.00E-53
VP2249	flagellar M-ring protein	1429	-1.63	1.35E-40
VP2250	flagellar hook-basal body protein	549	-1.76	1.03E-50
VP2254	flagellar protein FliS	359	-4.96	5.07E-91
VP2255	polar flagellar rod protein FlaI	101	-4.13	1.18E-38
VP2256	flagellar hook-associated protein	3603	-5.22	0
VP2257	flagellar protein FlaG	3452	-5.28	1.28E-245
VP2258	flagellin	8895	-5.38	0
VP2259	flagellin	1408	-5.8	7.43E-230

Table 13 Continued

VP2261	Flagellin	418	-5.05	3.07E-79
VP2492	putative ammonium transporter	290	-3.09	3.68E-19
VP2683	hypothetical protein	611	-1.6	6.28E-48
VP2724	hypothetical protein	2381	-2.75	5.81E-233
VP2725	phage shock protein G	632	-6.22	1.03E-127
VP2810	hypothetical protein	789	-3.72	1.07E-151
VP2827	methyl-accepting chemotaxis protein	839	-3.44	1.42E-150
VPA0040	hypothetical protein	1116	-1.9	3.71E-87
VPA0128	biotin sulfoxide reductase	1486	-1.62	2.82E-16
VPA0188	immunogenic protein	270	-2.43	1.55E-49
VPA0189	hypothetical protein	195	-1.59	4.31E-13
VPA0345	hypothetical protein	2083	-7.68	1.69E-230
VPA0347	hypothetical protein	1052	-1.97	3.48E-23
VPA0367	spermidine/putrescine ABC transporter, periplasmic spermidine/putrescine-binding protein	1087	-1.75	5.13E-24
VPA0475	hypothetical protein	229	-2.26	4.62E-25
VPA0511	methyl-accepting chemotaxis protein	531	-1.6	4.35E-42
VPA0548	putative protein F-related protein	421	-4.7	3.65E-100
VPA0566	alcohol dehydrogenase	23624	-1.73	4.80E-14
VPA0746	chemotaxis protein CheV	492	-2.41	8.37E-67
VPA0973	putative MFS family transport protein	893	-1.57	3.51E-13

Table 13 Continued

VPA1000	methyl-accepting chemotaxis protein	226	-1.71	3.29E-23
VPA1027	hypothetical protein	338	-2.19	4.23E-33
VPA1034	hypothetical protein	132	-2.44	8.79E-19
VPA1039	hypothetical protein	239	-1.73	1.65E-17
VPA1186	outer membrane protein OmpA	7125	-1.56	1.66E-44
VPA1202	polyhydroxyalkanoic acid synthase	698	-1.96	3.29E-58
VPA1203	hypothetical protein	309	-2.3	2.73E-23
VPA1204	acetyl-CoA acetyltransferase	351	-2.45	3.60E-25
VPA1205	acetoacetyl-CoA reductase	265	-2.4	1.58E-41
VPA1449	methyl-accepting chemotaxis protein	691	-4.13	1.15E-150
VPA1637	hypothetical protein	459	-1.72	5.59E-11

**Table 14 Putative OpaR binding sites identified using the MOODS algorithm**

Operon	Function	OpaR Binding Site Prediction				
		Position (bp's) upstream of ATG		Log odds score	Probability	P-Value
		Start	End			
VP0256 - 0266	Ribosomal proteins <i>rpsJ, rplC, rplD, rplW,</i> <i>rplB, rpsS, rplV, rpsC,</i> <i>rplP, rpmC, rpsQ</i>	38	19	6.319	0.999	0.0003
		363	344	3.146	0.959	0.003
VP0267 - 0278	Ribosomal proteins <i>rplN, rplX, rplE, rpsN,</i> <i>rpsH, rplF, rplR, rpsE,</i> <i>rpmD, rplO, secY, rpmJ</i>	37	18	2.638	0.933	0.003

## Chapter 4

### **COMPLETE GENOME SEQUENCE OF *VIBRIO PARAHAEMOLYTICUS* ENVIRONMENTAL STRAIN UCM-V493.**

The work in this chapter was published in *Genome Announcements*.

#### **Complete genome sequence of *Vibrio parahaemolyticus* environmental strain UCM-V493.**

Kalburge, S.S., Polson, S.W., Boyd Crotty, K., Katz, L., Turnsek, M., Tarr, C.L.,  
Martinez-Urtaza, J., Boyd, E.F.

Genome Announc. 2014 Mar 13;2(2). pii: e00159-14. doi: 10.1128/genomeA.00159-14.

#### **Introduction**

*Vibrio parahaemolyticus* is a moderately halophilic, Gram-negative bacterium found in marine environments in association with plankton, fish and shellfish (Johnson et al. 2012; Joseph, Colwell, and Kaper 1982; Kaneko and Colwell 1973; Krantz, Colwell, and Lovelace 1969). *V. parahaemolyticus* is the leading bacterial cause for seafood related gastroenteritis with the CDC estimating 45,000 cases of infection yearly in the United States alone (Daniels et al. 2000; Krantz, Colwell, and Lovelace 1969; Naughton et al. 2009; Scallan et al. 2011; Su and Liu 2007). Pathogenic strains of *V. parahaemolyticus* are characterized by the presence of *tdh* and *trh* genes, coding for the Thermostable Direct Hemolysin (TDH) and TDH-related hemolysin (TRH) respectively (DePaola et al. 2003; Johnson et al. 2012; Johnson et al. 2009; Paranjpye

et al. 2012; Parvathi et al. 2006). The first complete genome sequence of a *V. parahaemolyticus* strain was announced for the pandemic clinical isolate RIMD2210633 (Makino et al. 2003). Genomic analysis on this strain revealed the presence of 7 genomic islands, VPai-1 to VPai-7, ranging between 10 kb and 81 kb in size (Hurley et al. 2006). Recently another complete genome sequence was reported for an extensively studied environmental isolate BB22OP. It was reported that this strain lacks 5 of the 7 genomic islands present in the clinical isolate (Jensen et al. 2013). Here we report the complete genome sequence of *V. parahaemolyticus* UCM-V493. This strain is an O2:K28 serovar isolated in 2002 from a sediment sample in Spain. It is *tdh* negative and *trh* negative strain and lacks all 7 genomic islands present in the clinical isolate (Hurley et al. 2006; Martinez-Urtaza et al. 2004).

### **Materials and Methods**

*Vibrio parahaemolyticus* UCM-V493 was grown at 37°C overnight in Luria-Bertani (LB) broth (Fisher Scientific, Fair Lawn, NJ) (pH 7) supplemented with streptomycin (200µg/ml) with the final NaCl (Fisher Scientific) concentration adjusted to 3%. Genomic DNA was isolated using GNOME DNA Isolation Kit (MP Biomedicals, Solon, OH). The genome was sequenced using PacBio SMRT sequencing technology. *De novo* sequence assembly was performed using the hierarchical genome assembly process (HGAP) on the PacBio SMRT portal and a coverage of 75X was obtained. Additional sequencing was performed using the Illumina MiSeq technology in order to assist in filling gaps. Assembly on the Illumina

sequence was performed using CG Pipeline and CLC Genomics workbench. Gaps were filled manually using MEGA 5 software.

## **Results and Discussion**

The UCM-493 genome is comprised of two circular chromosomes and a circular plasmid. Annotation was performed using MAKER2 and RAST server. Chromosome 1 is 3.446 MB and contains 3187 CDSs, chromosome 2 is 1.698 MB and contains 1557 CDSs and the plasmid is 88.5 KB and contains 116 CDSs.

UCM-V493 shares high homology with the clinical strain RIMD2210633; >80% of the CDSs are similar in both strains. But UCM-V493 genome shows high level of gene synteny as compared to the RIMD2210633. The strain is *tdh* negative and *trh* negative and lacks all seven pathogenicity islands (VPaI-1 to VPaI-7). Two novel prophage elements were identified in the UCM-V493 genome. The prophage element on chromosome 1 showed homology to filamentous phage VCY-phi found in environmental *V. cholerae* strains and the prophage element on chromosome 2 showed homology to filamentous phage VFJ of *V. cholerae*. A detailed comparative analysis of the UCM-V493 and the RIMD2210633 genomes will be published elsewhere.

**Nucleotide sequence accession numbers.** The complete, annotated genome sequence for *V. parahaemolyticus* strain UCM-V493 were deposited at NCBI under the accession numbers CP007004 (UCM-V493\_Chromosome\_1), CP007005 (UCM-V493\_Chromosome\_2) and CP007006 (UCM-V493\_pVPUCMV\_plasmid).

## Chapter 5

### **HIGH SALT PRE-ADAPTATION OF *VIBRIO PARAHAEMOLYTICUS* ENHANCES SURVIVAL TO LETHAL ENVIRONMENTAL STRESSES**

The work in this chapter was published in the *Journal of Food Protection*

#### **High-salt preadaptation of *Vibrio parahaemolyticus* enhances survival in response to lethal environmental stresses.**

Kalburge, S.S. Whitaker, W.B., Boyd, E.F.

J Food Prot. 2014 Feb;77(2):246-53. doi: 10.4315/0362-028X.JFP-13-241

#### **Introduction**

*Vibrio parahaemolyticus* is a Gram-negative, moderately halophilic bacterium found in the marine environment throughout the world (Joseph, Colwell, and Kaper 1982). In the United States, *V. parahaemolyticus* is present in high numbers during the warmer summer months and is isolated in association with plankton, fish and shellfish (Kaneko and Colwell 1973; Krantz, Colwell, and Lovelace 1969; Johnson et al. 2012). *V. parahaemolyticus* is a pathogen in various fish and shellfish but more importantly is the leading cause of bacterial seafood-related gastroenteritis worldwide (Krantz, Colwell, and Lovelace 1969; Nair et al. 2007; Daniels et al. 2000; Su and Liu 2007). Recent CDC data shows a 116% increase in foodborne illness caused by *Vibrio* sp. with a majority being attributed to *V. parahaemolyticus*. The CDC estimates 45,000 cases (90% confidence interval, 23,000-75,000) of *V. parahaemolyticus* yearly

in the United States. While other foodborne pathogens have either subsided or remained constant over time, *V. parahaemolyticus* infections are on a continuous rise (Scallan et al. 2011).

Bacteria commonly encounter various environmental stresses during their lifecycle. In order to counter environmental stresses, bacteria have developed a compendium of complex adaptive responses (Whitaker 2012). A unique defense mechanism in bacteria is their ability to induce stress resistance upon exposure to sub-lethal doses of a stress that subsequently permits its survival under lethal doses of the same stress (Whitaker 2012). Additionally, in some cases, adapting to a particular stress condition can provide cross-protection against other non-homologous stresses (Pichereau, Hartke, and Auffray 2000). This adaptive response mechanism of bacteria to the various environmental conditions can lead to an increase in survival and virulence, and thus an increase in risk associated with pathogenic bacteria in food (Abee and Wouters 1999; Yeung and Boor 2004; Huang and Wong 2012).

*Vibrio parahaemolyticus* is a moderate halophile and requires a minimum of 0.5% NaCl for growth. It has been shown to grow in media containing up to 10.5% NaCl, however the bacteria exhibits optimum growth at 3% NaCl (Naughton et al. 2009; Ongagna-Yhombi and Boyd 2013). Numerous *V. parahaemolyticus* serogroups are associated with disease, however, in 1995 an O3:K6 serogroup emerged in Southeast Asia causing large outbreaks and rapid hospitalizations (Wong et al. 1998). This new highly virulent O3:K6 strain is now globally disseminated and is referred to as the pandemic clone (Wong et al. 1998). The presence of the *tdh* gene, which

encodes Thermo Direct Hemolysin (TDH) is often used as a diagnostic tool to identify pathogenic isolates of *V. parahaemolyticus* and is found in all pandemic isolates (Boyd et al. 2008; DePaola et al. 2003; Hurley et al. 2006; Johnson et al. 2012; Johnson et al. 2009; Paranjpye et al. 2012; Parvathi et al. 2006). Pathogenic non pandemic isolates contained a TDH-related hemolysin (TRH) encoded by *trh*, and TRH positive strains predominately contain a urease gene cluster and are TDH negative (Boyd et al. 2008; DePaola et al. 2003; Hurley et al. 2006; Johnson et al. 2012; Johnson et al. 2009; Paranjpye et al. 2012; Parvathi et al. 2006). Neither TDH nor TRH are generally present in non-pathogenic isolates.

As a marine enteric pathogen, *V. parahaemolyticus* encounters a variety of salinity and temperature fluctuations; firstly in the marine environment, then during harvesting of the seafood it colonizes and finally during post-harvesting processing (Mahoney et al. 2010; Huang and Wong 2012; Johnson et al. 2012). Once inside the human host, the bacterium faces abiotic and biotic challenges including low pH stress from the acids present in the gastrointestinal tract (Huang and Wong 2012; Foster 1999). Previously it was demonstrated that the *toxRS* regulon in *V. parahaemolyticus* RIMD2210633, an O3:K6 pandemic strain, is essential for acid tolerance through its regulation of the outer membrane protein OmpU (Whitaker et al. 2012). Another acid resistant system present in *V. parahaemolyticus* is the lysine decarboxylase pathway (**Figure 26**) (Huang and Wong 2012; Foster 1999). Lysine decarboxylase (encoded by *cadA*) mediated acid resistance has been well characterized in *Escherichia coli*, *Salmonella enterica* serovar Typhimurium and *V. cholerae*. Under low pH conditions,

*cadA* is induced and mediates the conversion of the amino acid lysine to the basic product cadaverine. The decarboxylation reaction consumes protons and results in an increase in the pH of the media. The basic product cadaverine is excreted out of the bacteria by the lysine-cadaverine antiporter CadB (Merrell and Camilli 1999; Neely and Olson 1996; Samartzidou et al. 2003; Soksawatmaekhin et al. 2004; Tanaka et al. 2008). Mild acid exposure has been shown to enhance the survival of pathogens under lethal acid conditions known as the Acid Tolerance Response (ATR) and has been reported in *S. enterica* Typhimurium, *V. cholerae* and in *V. parahaemolyticus* (Foster and Hall 1990; Merrell and Camilli 1999; Tanaka et al. 2008; Yeung and Boor 2004; Chiang et al. 2012). We have previously shown that cells exposed to lethal acid stress show a greater defect in survival when grown at 1% NaCl as compared to 3% NaCl and that a short pre-adaptation phase at 3% NaCl rescues the cells and increases survival (Whitaker et al. 2010).

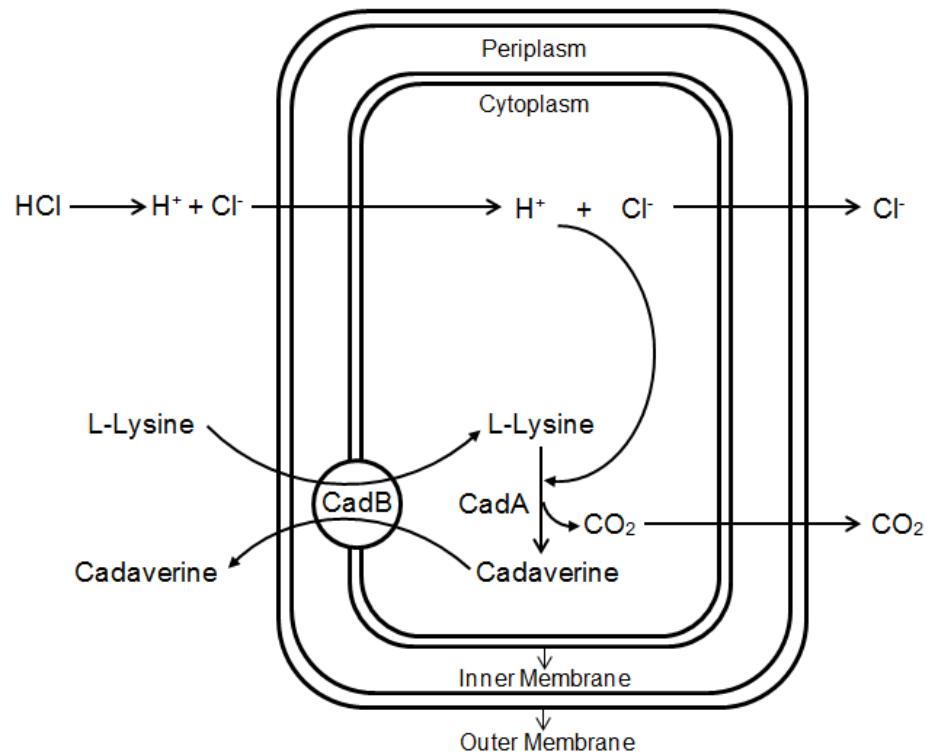


**Figure 26 The lysine decarboxylase pathway.** In acidic conditions, CadA (lysine decarboxylase) consumes a cytoplasmic proton in a decarboxylation reaction converting lysine to the basic product cadaverine, generating a pH gradient. CadB acts as a lysine-cadaverine antiporter transporting lysine into the cell and basic product cadaverine out of the cell. The pH of the external environment is increased by cadaverine.

In this study, the effect of a high salt pre-adaptation on the survival of *V. parahaemolyticus* strains subjected to lethal acid stress was examined. We demonstrated that high salt pre-adaptation for a short period significantly increased survival of the wild-type cells and that this increase in survival was not fully reliant on the lysine decarboxylase system. We also examined whether the general stress response was required for this response by examining a previously described *rpoS*

deletion mutant strain (Wong *et al.* 1998). We determined that the *rpoS* mutant behaved similar to wild-type. Next, we examined whether high salt pre-adaptation cross-protected against temperature stress and found increased survival of the bacteria at -20°C. To determine whether high salt pre-adaptation was a characteristic unique to *V. parahaemolyticus* we examined other less osmotolerant *Vibrio* species and showed that both *V. cholerae* and *V. vulnificus* exhibit increased survival under lethal acid conditions when pre-adapted to high salt but not to the same extent as *V. parahaemolyticus*.

## **Materials and Methods**

### **Bacterial strains, plasmids and growth conditions.**

All bacterial strains and plasmids used in the study are listed in **Table 15**. A streptomycin resistant strain of *V. parahaemolyticus* RIMD2210633 was used throughout this study (Whitaker *et al.* 2010). *Vibrio parahaemolyticus* was grown in Luria-Bertani (LB) broth (Fisher Scientific, Fair Lawn, NJ) (pH 7) supplemented with streptomycin (200µg/ml) with the final NaCl (Fisher Scientific) concentration adjusted to 1%, 3% or 6% as desired. All *E. coli* strains were grown in LB broth (pH 7) with the media being supplemented with 0.3mM diaminopimelic acid (DAP) (Sigma Aldrich, St. Louis, MO) for the DAP auxotroph *E. coli* β2155 λpir strain. All strains were grown aerobically (250 rpm) at 37°C.

### **Construction of the $\Delta cadA$ deletion mutant.**

Splicing by overlap extension (SOE) PCR coupled with homologous recombination (Horton et al. 1989) was used to create an in-frame non polar deletion mutation of the *cadA* gene (VP2890) in *V. parahaemolyticus* RIMD2210633. All of the primers used in this study are listed in **Table 16** and were purchased from Integrated DNA Technologies (Coralville, IA). The 1009-bp truncated version of the *cadA* gene was cloned into the pJet1.2 vector (Fermentas Life Sciences, Glen Burnie, MD), designated pJet1.2 $\Delta cadA$  and subsequently transformed into *E. coli* DH5 $\alpha$   $\lambda$ pir. The gene insert was removed from the pJet vector via restriction digest and ligated into the vector pDS132 and designated pDS $\Delta cadA$ . pDS $\Delta cadA$  was transformed into *E. coli*  $\beta$ 2155  $\lambda$ pir. pDS $\Delta cadA$  was then transferred into *V. parahaemolyticus* RIMD2210633 via conjugation through cross streaking on an LB DAP plate. To obtain the single-crossover mutant, colonies from this plate was transferred onto an LB plate supplemented with streptomycin (200 $\mu$ g/ml) and chloramphenicol (25 $\mu$ g/ml), selecting only for *V. parahaemolyticus* containing pDS $\Delta cadA$ . Exconjugate colonies were grown overnight in the absence of chloramphenicol and subsequently plated on sucrose plates to select for colonies that have lost the pDS $\Delta cadA$  insert. Double-crossover deletion mutants were confirmed by screening obtained colonies using the AD and flanking primers. Double crossovers were also sequenced (GENEWIZ DNA Sequencing Services) to confirm that the deletion was indeed in-frame.

### **Acid survivability assays.**

*Vibrio parahaemolyticus* RIMD2210633 and  $\Delta cadA$  survival under lethal acid stress conditions was determined by growing cells overnight in 5ml of LB broth (pH 7) with a final NaCl concentration of 3%. Overnight cultures were diluted 1:50 into fresh LB broth (3% NaCl, pH 7) and incubated aerobically at 37°C until cells reached mid-log phase (optical density at 595nm [OD<sub>595</sub>] of 0.4). The culture was then centrifuged (5,000 rpm for 10 min) to harvest the cells. The cells were resuspended either in 5ml acidified LB broth (pH4) or were subjected to an acid pre-adaptation phase. LB broth had a final salt concentration of 3% NaCl and was acidified to pH 4 or pH 5.5 using 1M HCl. Pre-adaptation of cells was done by exposing cells to LB broth that was adjusted to mild pH 5.5 for 30min at 37°C. After 30 min, cells were harvested by centrifugation (5,000 rpm for 10min) of the culture. Cells were then resuspended in the acidified LB broth pH 4. Resuspended cells were incubated at 37°C with aeration, and then serially diluted at 0, 20, 40 and 60 min and plated onto LB plates (1.5% Agar) supplemented with 3% NaCl. Plates were incubated at 37°C for 10 h, after which the CFU/ml was determined for each time point as a measure of survival.

### **High salinity pre-adapted acid survivability assays.**

To determine survival under lethal acid conditions with high salt adaptation, cells were grown to mid-log phase in LB 3% NaCl at 37°C from overnight cultures as described in the previous section. Upon reaching mid-log phase, cells were centrifuged

(5,000 rpm for 10 min) and harvested cells were subsequently subjected to high salt pre-adaptation phase for 60 min in LB 6% NaCl media. Cells were then centrifuged and resuspended in LB 3% NaCl acidified to pH 4 and were incubated at 37°C with aeration. Serial dilutions were performed at 0, 20, 40 and 60 min and cells were plated onto LB plates (1.5% Agar) supplemented with 3% NaCl. In order to examine the effect of prolonged exposure to high salt, cells were grown overnight to mid-log phase in LB 6% NaCl and then subjected to lethal acid stress in LB 3% NaCl. Cells were plated at 0, 20, 40 and 60 min as mentioned previously to determine CFU/ml and hence cell survival. The high salt pre-adapted acid survival assay was examined with *V. parahaemolyticus* strains; UCM V493 a sediment isolate lacking both the thermolysin gene *tdh* and TDH related hemolysin gene *trh* and AQ4235 a non-pandemic *trh* positive, urease positive clinical isolate which lacks the *tdh* gene (Horton et al. 1989).

#### **High salinity pre-adapted temperature survivability assays.**

To determine the effect of high salt adaptation on temperature stressed cells, the cells were grown overnight in LB 3% NaCl and to mid-log phase as previously mentioned. Cells were then resuspended in LB broth with either 3% NaCl or 6% NaCl and subjected to high temperature stress at 50°C for 60 min with cells being serially diluted and plated at 0, 20, 40 and 60 min. For cells being subjected to cold stress, resuspended cells were placed at -20°C for 24 h. Cells were serially diluted and then plated on LB plates supplemented 3% NaCl to determine cell survival.

### **High salinity pre-adapted acid survivability assays in other *Vibrio* species.**

Effect of high salt adaptation on survival under lethal acid stress was determined for *V. cholerae* N16961 and *V. vulnificus* YJ016. *Vibrio cholerae* and *V. vulnificus* were grown overnight in 5ml of LB broth pH 7 with a final NaCl concentration of 1% and 2% respectively. Overnight culture was diluted into 1:50 into fresh LB broth (1% NaCl or 2% NaCl, pH 7) and incubated aerobically at 37°C until cells reached mid-log phase as described previously. The culture was then centrifuged (5,000 rpm for 10 min) to harvest the cells. Both cultures were then subjected to high salt pre-adaptation phase for 60 min in LB 4% NaCl media. Pre-adapted cells were then tested for lethal acid survival in LB media with a final NaCl concentration of 1% or 2%, acidified to pH 4. Cells were plated at 0, 20, 40 and 60 min on LB plates supplemented with 1% or 2% NaCl. Plates were incubated at 37°C for 10 h. CFU/ml was determined for each time point and hence cell survival.

### **Statistical analysis.**

All the experiments were performed in triplicate with at least two biological replicates. *P* values for each data set were calculated using an unpaired Students t test (GraphPad Software, Inc. La Jolla, CA) with a 95% confidence interval.

## **Results**

**Pre-adaptation in mild acid condition increases survival under lethal acid stress conditions.** In order to confirm that a mild acid pre-adaptation phase increases

*V. parahaemolyticus* survival under lethal acid conditions, cells were pre-adapted at pH 5.5 prior to testing survival at pH 4 (Foster and Hall 1990; Merrell and Camilli 1999; Tanaka et al. 2008; Yeung and Boor 2004; Chiang et al. 2012). It was determined that the 30 min pre-adaptation phase significantly increased survival at 20 min post-lethal acidification in both the wild-type ( $P < 0.001$ ) and the isogenic  $\Delta cadA$  strain ( $P < 0.01$ ) compared to the survival of un-adapted cells (**Figure 27**). The wild-type continued to exhibit significantly increased survival at 40 min ( $P < 0.001$ ) and 60 min ( $P < 0.01$ ), while the  $\Delta cadA$  strain fell below the limit of detection ( $1 \times 10^{-6}$ ) by 40 min (**Figure 27**).

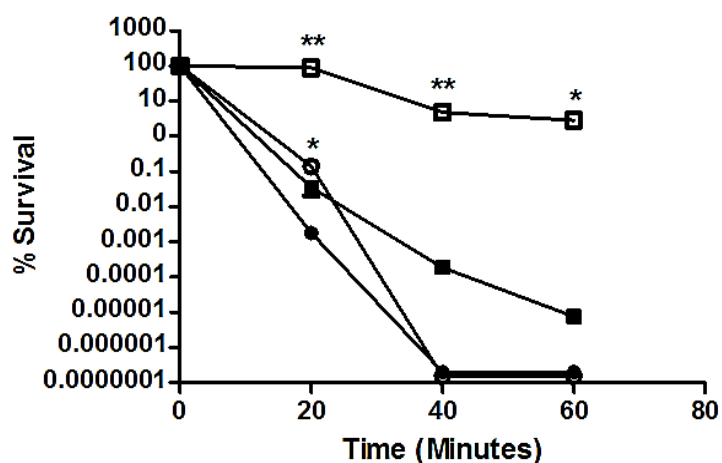


**Figure 27 Effect of lethal acid stress on the *cadA* deletion mutant.** Wild-type and  $\Delta cadA$  were grown up to mid-log phase in LB media containing 3% NaCl and then subjected to lethal acid stress in LB 3% NaCl media at pH 4 for 60 min. Closed squares indicate the wild-type strain un-adapted, open squares indicate the wild-type strain pre-adapted in acid, closed circles indicate the  $\Delta cadA$  strain un-adapted and open circles indicate the  $\Delta cadA$  strain pre-adapted in acid. Pre-adaptation for 30 min in LB 3% NaCl media at pH 5.5 prior to exposing the cells to lethal acid stress a significant increase in survival was seen. All survival assays were done in triplicate with at least two biological replicates. Error bars, indicating standard deviations, are too small to be observed. An unpaired Student t test was used to determine statistical differences between wild-type survival and  $\Delta cadA$  deletion mutant survival under lethal acid stress without pre-adaptation to mild acid conditions and with pre-adaptation. \*,  $P < 0.01$ ; \*\*,  $P < 0.001$ .

### High salt adaptation increases survival under lethal acid stress conditions.

In order to determine if an induction of osmotic stress can influence growth and survival under lethal acid stress conditions, we repeated the acid survival assays, this time with the addition of either a short-term (60 min pre-adaptation) or an extended exposure for 15-h in high salt conditions (LB media containing 6% NaCl pH 7). We determined that high salt pre-adaptation for 60 min significantly ( $P < 0.001$ ) increased

survival of both the wild-type *V. parahaemolyticus* RIMD2210633 and the isogenic  $\Delta cadA$  strain as compared to cells subjected to lethal acid stress without pre-adaptation (**Figure 28A**). To examine if prolonged exposure to high salt would magnify the protective effect on cell survival against acid stress, cells were grown overnight in LB media containing 6% NaCl at pH 7. Cells were then subjected to lethal acid stress in LB media containing 3% NaCl at pH 4. Exposure to high salt for an extended time further increased survival of the  $\Delta cadA$  strain at all three time points over the 60 min period with a limit of detection of  $1 \times 10^{-6}$  ( $P < 0.05$ ) (**Figure 28B**). In order to determine if other *V. parahaemolyticus* strains besides RIMD2210633 exhibited increased survival upon high salt pre-adaptation, we performed lethal acid survival assays on strains UCM V493 and AQ4235. The *trh* and urease positive strain AQ4235 showed a slightly significantly increase in survival at 20 min ( $P < 0.02$ ) compared to RIMD2210633 (**Figure 28C**). The environmental strain UCM V493, which is *tdh*, *trh* and urease negative, showed significantly reduced survival at 20 min ( $P < 0.005$ ), 40 min ( $P < 0.02$ ) and 60 min ( $P < 0.005$ ) compared to RIMD2210633 and AQ4235 (**Figure 28C**). These results suggest that high salt pre-adaptation cross-protects it against lethal acid stress and that this cross-protection is less dependent on the Cad system and that there are differences between clinical and environmental strains in the level of this response.

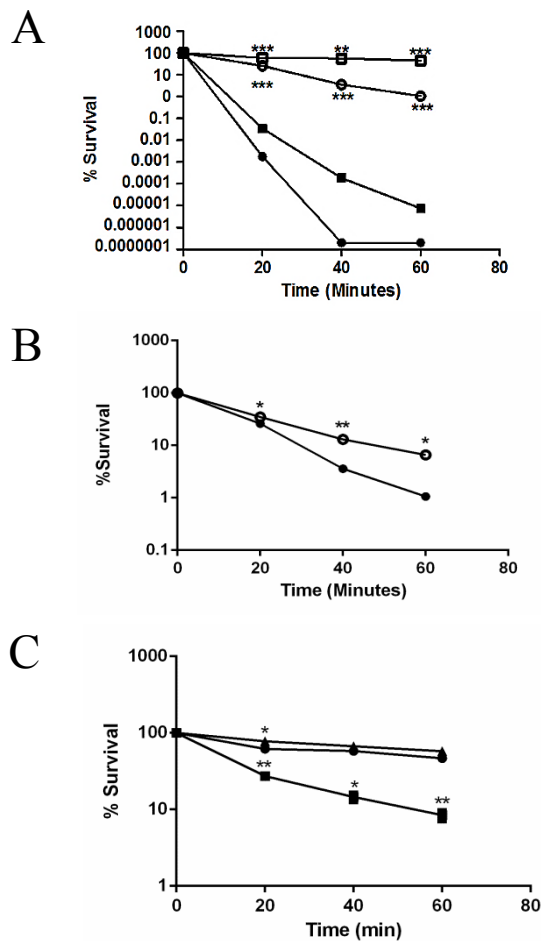


**Figure 28 Effect of high salt adaptation on survival in lethal acid stress.**

(A) Wild-type and  $\Delta cadA$  were grown up to mid-log phase in LB media containing 3% NaCl and then subjected to lethal acid stress in LB 3% NaCl media at pH 4 for 60 min or were first adapted to high salt for 60 min prior to acidification. Closed squares indicate the wild-type strain un-adapted, open squares indicate the wild-type strain pre-adapted in high salt, closed circles indicate the  $\Delta cadA$  strain un-adapted, and open circles indicate the  $\Delta cadA$  strain pre-adapted in high salt. Upon high salt pre-adaptation for 60 min in LB 6% NaCl media and then exposing the cells to lethal acid stress, a significant increase in survival was seen for both the wild-type and the mutant. (B)  $\Delta cadA$  grown overnight in LB media containing 6% NaCl exhibited a further increase in survival when subjected to lethal acid stress. Closed circles indicate  $\Delta cadA$  pre-adapted to high salt for 60 min and open circles indicate  $\Delta cadA$  pre-adapted to high salt overnight. An unpaired Student t test was used to determine statistical differences between wild-type survival and  $\Delta cadA$  survival under lethal acid stress without any pre-adaptation and with pre-adaptation to 6% salt concentration either for 60

min or overnight. \*,  $P < 0.05$ ; \*\*,  $P < 0.01$ ; \*\*\*,  $P < 0.001$  (C) Wild-type RIMD2210633, UCM V493 and AQ4235 cells were grown up to mid-log phase in LB media containing 3% NaCl and then subjected to lethal acid stress in LB 3% NaCl media at pH 4 for 60 min or were first adapted to high salt for 60 min prior to acidification. Closed circles indicate the RIMD2210633 strain, closed squares indicate the UCM V493 strain and closed triangles indicate the AQ4235 strain. An unpaired Student t test was used to determine statistical differences between survival of RIMD2210633 and UCM V493 or AQ4235 under lethal acid stress with pre-adaptation to 6% salt concentration either for 60 min. \*,  $P < 0.02$ ; \*\*,  $P < 0.005$ .

We next examined whether the general stress response sigma factor regulator RpoS plays a role in high salt pre-adaptation to lethal acid stress conditions. To accomplish this, we compared the wild-type RIMD2210633 strain to a previously described isogenic in-frame non-polar *rpoS* mutant under the same conditions described above (Boyd et al. 2008; DePaola et al. 2003; Hurley et al. 2006; Johnson et al. 2012; Johnson et al. 2009; Paranjpye et al. 2012; Parvathi et al. 2006). We found that the *rpoS* mutant showed similar survival to wild-type under the conditions examined indicating that it does not play a role in this phenotype (data not shown).

### **High salt concentration cross-protects against cold shock but does not protect against heat.**

Temperature stress is the other most common stress encountered by foodborne pathogens. To assess if high salt adaptation offered cross-protection against temperature stress, high salt adapted or un-adapted cells were subjected to cold shock at  $-20^{\circ}\text{C}$  for 24 h. Cells resuspended in media containing 6% NaCl showed significantly higher ( $P < 0.05$ ) survival at the end of 24 h (**Figure 29A**). In contrast,

pre-adaptation to high salt did not provide any cross-protection against cells that were subjected to high temperature stress at 50°C for 60 min (**Figure 29B**). High salt pre-adapted cells showed a significant reduction in number as compared to cells in LB media containing 3% NaCl ( $P < 0.05$ ) with the cells falling below the limit of detection of  $3.6 \times 10^{-5}$  at the end of the 20 min time point (**Figure 29B**).

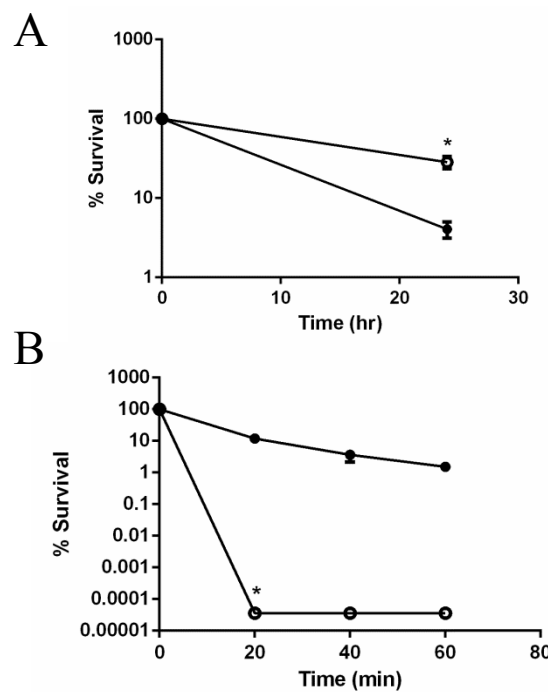


**Figure 29 Effect of high salt concentration on survival under high-temperature stress and cold stress.**

(A) Survival under cold stress was determined by subjecting cells to -20°C in either LB media containing 3% NaCl or 6% NaCl for 24 h. Closed circles indicate cells wild-type cells pre-adapted in 3% NaCl and open circles indicate wild-type cells pre-adapted in 6% NaCl. (B) To determine survivability under high temperature stress cells were subjected to 50°C in either LB media containing 3% NaCl or 6% NaCl for 60 min. Closed circles indicate cells wild-type cells pre-adapted in 3% NaCl and open circles indicate wild-type cells pre-adapted in 6% NaCl. An unpaired Student t test was used to determine statistical differences between wild-

type survival in LB media containing 3% NaCl and 6% NaCl under high temperature stress and cold stress. \*,  $P < 0.05$ .

**Increased survival under lethal acid stress upon high salt adaptation is consistent among other pathogenic *Vibrio* species.** In order to determine if an increase in survival under lethal acid stress is unique to *V. parahaemolyticus* or if it is exhibited in other pathogenic members of the *Vibrionaceae*, we performed lethal acid survival assays on *V. cholerae* N16961 and *V. vulnificus* YJ016. Both organisms showed significantly increased survival at 20 min ( $P < 0.04$ ) (**Figure 30A-B**) and additionally, *V. cholerae* showed a significant increase in survival at 40 min ( $P < 0.03$ ) and 60 min ( $P < 0.02$ ) (**Figure 30A**).

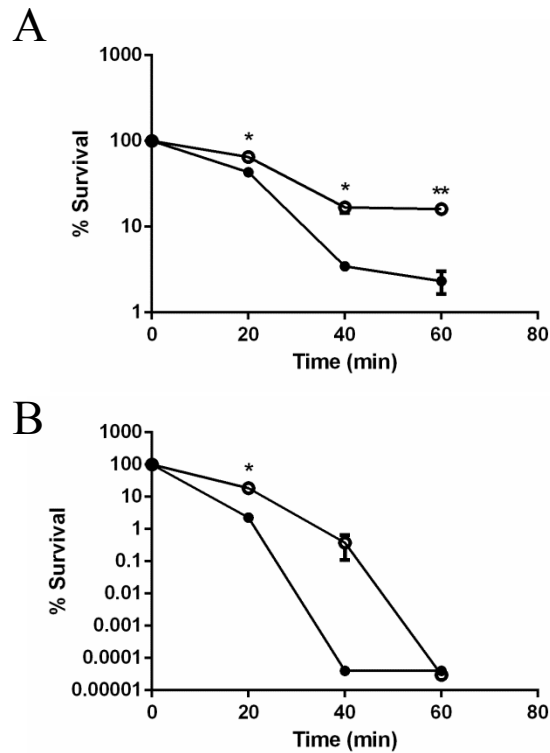


**Figure 30 Effect of high salt adaptation on the survival of other *Vibrio* species under lethal acid stress.** (A) *V. cholerae* N16961 cells were grown to mid-log phase in LB media containing 1% NaCl at pH 7 and then pre-adapted for 60 min in LB media containing 4% NaCl before being subjected to lethal acid stress in LB media containing 1% NaCl at pH 4 for 60 min. Closed circles indicate the un-adapted cells, open circles indicate the cells pre-adapted in high salt. (B) *V. vulnificus* YJ016 cells were grown to mid-log phase in LB media containing 2% NaCl at pH 7 and then pre-adapted for 60 min in LB media containing 4% NaCl before being subjected to lethal acid stress in LB media containing 2% NaCl at pH 4 for 60 min. Closed circles indicate the un-adapted cells, open circles indicate the cells pre-adapted in high salt. An unpaired Student t test was used to determine statistical differences between wild-type *Vibrio cholerae* N16961 and *Vibrio vulnificus* YJ016 survival under lethal acid stress without any pre-adaptation and with pre-adaptation to 4% salt concentration for 60 min. \*,  $P < 0.04$ ; \*\*,  $P < 0.02$ .

## Discussion

One of the main inducible systems for acid resistance in *V. parahaemolyticus* is the lysine dependent amino acid decarboxylase system or the Cad system (Tanaka et al. 2008; Whitaker et al. 2010). The *cadA* gene, which encodes lysine decarboxylase, has been shown to be induced during acid stress (Tanaka et al. 2008; Whitaker et al. 2010). A *cadA* in-frame non-polar deletion mutant was constructed and shown to be defective in survival under acid stress conditions when compared to wild-type as described previously (Tanaka et al. 2008). A pre-adaptation phase in mild-acid conditions was shown to increase survival of the wild-type RIMD2210633 and the  $\Delta cadA$  deletion mutant. This characteristic, known as the acid tolerance response (ATR), has been described in previous studies of the Cad system (Tanaka et al. 2008).

Survivability of *V. parahaemolyticus* starvation adapted cells has been examined and demonstrated to increase resistance to heat, acid and freeze-thaw conditions (Wong, Chang, and Chen 2004). In addition, it was demonstrated that low salinity adapted *V. parahaemolyticus* cells were cross-protected against low pH stress (Wong et al. 1998). In an effort to determine the role of high salinity adaptation on the acid tolerance response of *V. parahaemolyticus*, pre-adaptation in 6% NaCl followed by survival under lethal acid stress conditions was examined. It was found that both wild-type *V. parahaemolyticus* and the *cadA* deletion mutant show increased survival under lethal acid when pre-adapted in 6% NaCl. It was also found that an overnight exposure to 6% NaCl showed a further increase in survival of the *cadA* deletion

mutant. Taken together, these results indicate cross-protection between non-homologous stresses specifically induction of osmotic stress cross protects against lethal acid stress. It also suggests that lethal acid survival upon high salt adaptation is less dependent on the lysine decarboxylase pathway and that additional, as yet to be determined systems are playing a role in acid survival under these conditions. To investigate a possible mechanism behind the increased survival, we tested whether the alternative stress response sigma factor RpoS played a role. Previously, it has been demonstrated that an *rpoS* deletion mutant shows significant reduction in survival under acid stress, which is restored to wild-type levels upon mild acid pre-adaptation (Naughton et al. 2009; Ongagna-Yhombi and Boyd 2013). In this study, it was found that the *rpoS* deletion mutant survived acid stress similar to wild-type upon high salt pre-adaptation (data not shown). We also examined whether compatible solutes might play a role since upon osmotic shock, *V. parahaemolyticus* synthesizes both ectoine and betaine compatible solutes (Naughton et al. 2009; Ongagna-Yhombi and Boyd 2013). It was determined that neither ectoine nor betaine added to growth media provided cross-protection under lethal acid conditions (data not shown).

Interestingly, we found that there was variability among *V. parahaemolyticus* strains in the level of the per-adaptative response to lethal acid conditions. It was demonstrated that a clinical AQ4235 strain showed a slight increase in survival upon high salt pre-adaptation compared to RIMD2210633 whereas an environmental strain UCM V493 showed significantly reduced survival compared to the clinical isolates. Strain AQ4235 is a pre-pandemic O3:K6 isolate that encodes the *trh* gene, which

similar to *tdh* is a marker for virulence. Previously, it was demonstrated that *trh* strains are also predominantly urease positive as is AQ4235 (Iida et al. 1998; Iida et al. 1997; Okuda et al. 1997; Osawa et al. 1996). The role of urease in acid tolerance has been well established in *Helicobacter pylori* (Scott et al. 1998). We propose that urease activity in AQ4235 could be a contributing factor for the increased survival under acid stress conditions compared to RIMD2210633, which is urease negative. The UCM V493 environmental strain showed significantly reduced survival compared to the clinical isolates. We previously showed by PCR analysis that UCM V493 lacked seven large chromosomal regions that are present in RIMD2210633 and related pandemic isolates (Scott et al. 1998). However, these regions cannot account for the differences in survival since the seven regions are also absent from AQ4235 and related pre-pandemic pathogenic isolates (Scott et al. 1998). Therefore the difference noted in survival may be the result of additional regions absence from the unsequenced UCM V493 strain or differences in regulation of genes among the strains. Furthermore, we found that both *V. cholerae* N16961 and *V. vulnificus* YJ016 exhibited an increase in survival under lethal acid stress when pre-adapted with 4% NaCl. The increase in survival for these species was not as pronounced as seen in *V. parahaemolyticus* but was still significantly higher ( $P < 0.04$ ) than un-adapted cells. It has been previously demonstrated that low salinity pre-adapted *V. parahaemolyticus* cells did not have any increased protection against heat and cold stresses (Boyd et al. 2008; DePaola et al. 2003; Hurley et al. 2006; Johnson et al. 2012; Johnson et al. 2009; Paranjpye et al. 2012; Parvathi et al. 2006). In our studies, pre-adaptation in

high salinity conditions crossed protected cells to cold stress conditions. No such cross-protection was observed when cells were exposed to high temperature stress.

In summary, high salt adaptation of *V. parahaemolyticus* was demonstrated to cross-protect the organism and significantly increase its survival under lethal acid stress and cold temperature stress conditions. *Vibrio parahaemolyticus* generally encounters salt concentrations of 3.5% NaCl. However, salt levels can rise even further during the months of summer when higher temperatures lead to increased levels of evaporation (Mann 2000). CDC data shows a higher incidence of vibrios and *Vibrio* infections during the months of summer (Scallan et al. 2011). Wild-type *V. parahaemolyticus* survives significantly better under lethal stress conditions when adapted to high salt concentration, suggesting that the organism may be better adapted to evading the pH stress within the host. From a practical standpoint, our results have shown that prolonged exposure to high salt significantly increases the survival of the *cadA* deletion mutant under lethal acid stress, suggesting the acid tolerance response of the organism begins to function in a manner that is less dependent on the Cad system. We speculate that this data also suggests that *V. parahaemolyticus* present in oysters and other shellfish isolated from high salinity seawater may be better adapted to evade and survive the gastric pH barriers of the host. Our results also show that high salt adaptation increases the survival of the organism after freezing suggesting that if oysters and shellfish are frozen upon being obtained from high salinity seawater, it could possibly result in higher survival of *V. parahaemolyticus*. However our data also suggests that it may be possible to reduce *V. parahaemolyticus* levels in oysters and

shellfish obtained from high salt waters if subjected to high temperature (50°C) for more than 20 min.

**Table 15 Bacterial strains and plasmids used in this study**

Strain	Genotype	Reference
<b><i>Vibrio parahaemolyticus</i></b>		
RIMD2210633	O3:K6 clinical isolate	(Makino et al. 2003)
UCM V493	O2:K28 sediment isolate	(Martinez-Urtaza et al. 2004)
AQ4235	O3:K6 clinical isolate	(Wong et al. 2005)
$\Delta cadA$	RIMD2210633 $\Delta cadA$ (VP2890), Str <sup>R</sup>	This study
$\Delta rpoS$	RIMD2210633 $\Delta rpoS$ (VP2553), Str <sup>R</sup>	(Whitaker et al. 2010)
<b><i>Vibrio cholerae</i></b>		
N16961	O1, El Tor, VPI-2 <sup>+</sup> , Str <sup>R</sup>	(Heidelberg et al. 2000)
<b><i>Vibrio vulnificus</i></b>		
YJ016	SAC <sup>+</sup> SAT <sup>+</sup> ; clinical isolate	(Chen et al. 2003)
<b><i>Escherichia coli</i></b>		
$\beta 2155 \lambda_{pir}$	$\Delta dapA::erm_{pir}$ for bacterial conjugation	
$\beta 2155 \lambda_{pir} \Delta cadA$	$\beta 2155 \lambda_{pir}$ containing pDS132 $\Delta cadA$	This study
<b>Plasmids</b>		
pDS132	Suicide plasmid; Cm <sup>r</sup> ; SacB	(Philippe et al. 2004)
pDS132 $\Delta cadA$	pDS132 harboring truncated <i>cadA</i> (VP2890) gene	This study

**Table 16 Primers used in this study**

Use and primer	Sequence (5'-3')	T <sub>m</sub> (°C)	Product size (bp)
<b>Splice Overlap Extension PCR</b>			
SOEvp2890A	GCT GCC TTA CTT CTA CTC AAG C	59	449
SOEvp2890B	CTC AAG AGC AGC GTG AAG TTG	67	
SOEvp2890C	GGC ATC GTG GTT GAG AAA ACA	67	550
SOEvp2890D	TTG TTG GTA CAG ACC GTG GA	62	
SOEvp2890FLFor	AAC AGC ACA CGC ATC AGA C	56	1583
SOEvp2890FLRev	TCG GTG GAT GCG CAG TAT AG	57	

## Chapter 6

### **PERSPECTIVES AND FUTURE DIRECTIONS**

The findings in this dissertation demonstrate the role of quorum sensing regulators in metabolic fitness of *V. parahaemolyticus*. First, we examined single and double deletion mutants of the regulators *in vivo* to determine their role in host colonization. We then went on to reveal a correlation between the observed *in vivo* phenotype and cell metabolism. We proceeded to demonstrate a direct role for the high cell density quorum sensing master regulator OpaR in metabolism. We also investigated the regulon of sigma-54 RpoN, and uncovered likely reasons for the increased metabolic fitness of the strain.

#### **Quorum Sensing and Metabolism**

The RNA-Seq analysis of the *luxO* mutant revealed that about 60% of the genes that were downregulated in the *luxO* mutant were involved in metabolism and transport. Furthermore, we went on to identify OpaR binding sites in the regulatory regions of metabolic genes and confirmed binding to these regions. And although this finding along with supporting *in vitro* phenotypes from growth and competition experiments suggest that OpaR is a negative regulator of metabolism, this will need to be investigated further and confirmed. In order to determine if OpaR is indeed a negative regulator of metabolic gene clusters in *V. parahaemolyticus*, we will need to

perform an RNASeq analysis comparing the expression of metabolic genes in the *opaR* mutant to expression in an *opaR* over-expressing strain such as the *luxO* mutant. The transcriptome profile of both these strains will allow us to analyze whether deletion of *opaR* restores expression of the arabinose transport and metabolism gene cluster, which is downregulated in the *luxO* mutant. It would be also interesting to perform the same analysis on a *luxOopaR* double mutant. Our *in vivo* colonization revealed that deletion of *opaR* in the *luxO* mutant significantly increases its colonization ability and restores it to wild-type levels. Similarly, if indeed expression of metabolic genes is restored in the double mutant, it would provide additional confirmation of the negative regulation of these genes by OpaR. Additionally, we identified AphA binding sites in the regulatory regions of 9 metabolic gene clusters. The purification of AphA protein and subsequent binding assays will be helpful in confirming the predicted sites and providing insights into the role of AphA in metabolism.

Preliminary evidence from the environmental isolate UCM-V493 suggests that the strain possesses a significant metabolic advantage over the clinical isolate RIMD2210633. It will be interesting to assess the role of the quorum sensing regulators in metabolism in this strain. We have constructed deletion mutants of the two quorum sensing master regulators *opaR* and *aphA* in UCM-V493. We will need to characterize these mutants *in vitro*. It will be especially interesting to perform *in vitro* growth and competition experiments with the mutants in this strain and compare them to the phenotypes observed with the RIMD2210633 mutants.

### **Role of metabolism in *V. parahaemolyticus* *in vivo* colonization**

Previously published research from our group has showed that the super-colonizing *rpoN* mutant has increased metabolic fitness compared to wild-type (Whitaker, Richards, and Boyd 2014). This data combined with the findings of this dissertation, suggests a correlation between metabolic fitness *and in vivo* colonization fitness, making it a compelling study for the future. In order to determine the contribution of metabolic fitness of strains to their competitiveness *in vivo*, we will need to examine other global regulators of metabolism such as the cyclic AMP receptor protein, Crp and the nucleoid binding protein Fis, which are yet to be characterized in *V. parahaemolyticus*. *In vitro* and *in vivo* characterization of deletion mutants of these regulators will provide more insights into our understanding of the behavior of this bacteria inside its host from a metabolism standpoint. In addition to determining the importance of individual mucus sugars and the importance of their utilization to *in vivo* fitness, we will need to investigate the roles of individual proteins in the metabolic pathways. Since construction of deletion mutants of each protein would be impractical, due to the laborious, time-consuming and expensive nature of the procedure, we could use a high-throughput strategy to create and analyze mutants of these genes the using the Tn-seq procedure. The Tn-seq procedure has been previously used to construct *V. parahaemolyticus* transposon mutant libraries (Hubbard et al. 2016). Analyzing the *in vivo* fitness of insertion mutants of metabolism genes will provide insights into not only the role of metabolism in the fitness of the

bacteria but will assessing the fitness of mutants of specific sugars will also allow to determine the important sugars utilized by the bacteria *in vivo*.

### **Investigation of *V. parahaemolyticus* small RNAs**

In chapter 3 we showed that the quorum regulatory small RNA *qrr2* is significantly upregulated in the *rpoN* mutant. The reason for this upregulation is currently unknown and will need to be investigated further. It will be interesting to perform bioinformatics and biochemical analysis of the *qrr2* promoter region to identify the mechanism behind the transcription of the small RNA in the absence of *rpoN*. Our RNASeq analysis comparing the *luxO* mutant to the wild-type revealed that the Hfq-binding sRNA Spot 42 was upregulated in the *luxO* mutant. The *luxO* mutant was found to have a defect *in vivo* and in metabolic fitness compared to wild-type. In *E. coli*, Spot 42 plays an essential role as a regulator in carbohydrate metabolism and uptake, and its expression is activated by glucose and inhibited by CRP. Spot 42 was shown to be a negative regulator of metabolism of many sugars in both *E. coli* and *Vibrio (Allivibrio) salmonicida* (Beisel and Storz 2011, 2012; Hansen et al. 2012; Moller et al. 2002). It will be interesting to further investigate the role of spot 42 in *V. parahaemolyticus* and determine if it contributes to the metabolic defect seen in the *luxO* mutant. Another sRNA, VrrA was also found to be upregulated in the *luxO* mutant. In *V. cholerae*, studies showed that a *vrrA* mutant had a 5 fold increased ability to colonize infant mice (Song et al. 2008) suggesting that this small RNA is a negative regulator of colonization. It was shown that VrrA downregulates outer

membrane proteins, OmpA and OmpT, the stationary phase survival factor Vrp and biofilm matrix protein RbmC in *V. cholerae* (Sabharwal et al. 2015; Song, Sabharwal, and Wai 2010). Upregulation of this small RNA in the *luxO* mutant might lead to negative regulation of colonization and thereby lead to the defect observed with the mutant *in vivo*. It will be interesting to investigate a deletion mutant of the small RNA in the streptomycin treated adult mouse model.

## REFERENCES

- Abee, T., and J. A. Wouters. 1999. Microbial stress response in minimal processing. *Int. J. Food Microbiol.* 50 (1-2):65-91.
- Alam, M., S. Miyoshi, K. Tomochika, and S. Shinoda. 1997. *Vibrio mimicus* attaches to the intestinal mucosa by outer membrane hemagglutinins specific to polypeptide moieties of glycoproteins. *Infect Immun* 65 (9):3662-5.
- An, J. H., E. Goo, H. Kim, Y. S. Seo, and I. Hwang. 2014. Bacterial quorum sensing and metabolic slowing in a cooperative population. *Proc Natl Acad Sci U S A* 111 (41):14912-7.
- Bardill, J. P., X. Zhao, and B. K. Hammer. 2011. The *Vibrio cholerae* quorum sensing response is mediated by Hfq-dependent sRNA/mRNA base pairing interactions. *Mol Microbiol* 80 (5):1381-94.
- Bassler, B. L. 1999. How bacteria talk to each other: regulation of gene expression by quorum sensing. *Curr Opin Microbiol* 2 (6):582-7.
- Bassler, B. L., E. P. Greenberg, and A. M. Stevens. 1997. Cross-species induction of luminescence in the quorum-sensing bacterium *Vibrio harveyi*. *J Bacteriol* 179 (12):4043-5.
- Bassler, B. L., M. Wright, R. E. Showalter, and M. R. Silverman. 1993. Intercellular signalling in *Vibrio harveyi*: sequence and function of genes regulating expression of luminescence. *Mol Microbiol* 9 (4):773-86.
- Bassler, B. L., M. Wright, and M. R. Silverman. 1994. Sequence and function of LuxO, a negative regulator of luminescence in *Vibrio harveyi*. *Mol Microbiol* 12 (3):403-12.
- Beisel, C. L., and G. Storz. 2011. Discriminating tastes: physiological contributions of the Hfq-binding small RNA Spot 42 to catabolite repression. *RNA Biol* 8 (5):766-70.
- Beisel, C. L., and G. Storz. 2012. The base-pairing RNA spot 42 participates in a multioutput feedforward loop to help enact catabolite repression in *Escherichia coli*. *Mol Cell* 41 (3):286-97.

- Bhowmick, R., A. Ghosal, and N. S. Chatterjee. 2007. Effect of environmental factors on expression and activity of chitinase genes of vibrios with special reference to *Vibrio cholerae*. *J Appl Microbiol* 103 (1):97-108.
- Bhowmick, R., A. Ghosal, B. Das, H. Koley, D. R. Saha, S. Ganguly, R. K. Nandy, R. K. Bhadra, and N. S. Chatterjee. 2008. Intestinal adherence of *Vibrio cholerae* involves a coordinated interaction between colonization factor GbpA and mucin. *Infect Immun* 76 (11):4968-77.
- Boles, B. R., and L. L. McCarter. 2002. *Vibrio parahaemolyticus* scrABC, a novel operon affecting swarming and capsular polysaccharide regulation. *J Bacteriol* 184 (21):5946-54.
- Boyaci, H., T. Shah, A. Hurley, B. Kokona, Z. Li, C. Ventocilla, P. D. Jeffrey, M. F. Semmelhack, R. Fairman, B. L. Bassler, and F. M. Hughson. 2016. Structure, Regulation, and Inhibition of the Quorum-Sensing Signal Integrator LuxO. *PLoS Biol* 14 (5):e1002464.
- Boyd, E. F., M. R. Carpenter, N. Chowdhury, A. L. Cohen, B. L. Haines-Menges, S. S. Kalburge, J. J. Kingston, J. B. Lubin, S. Y. Ongagna-Yhombi, and W. B. Whitaker. 2015. Post-Genomic Analysis of Members of the Family Vibrionaceae. *Microbiol Spectr* 3 (5).
- Boyd, E. F., A. L. Cohen, L. M. Naughton, D. W. Ussery, T. T. Binnewies, O. C. Stine, and M. A. Parent. 2008. Molecular analysis of the emergence of pandemic *Vibrio parahaemolyticus*. *BMC Microbiol* 8:110.
- Bremer, H., and P.P. Dennis. 1996. Modulation of chemical composition and other parameters of the cell by growth rate In *Escherichia coli and Salmonella typhimurium: Cellular and Molecular Biology*, edited by H. J. e. al. Washington DC: ASM.
- Broberg, C. A., L. Zhang, H. Gonzalez, M. A. Laskowski-Arce, and K. Orth. 2010. A *Vibrio* effector protein is an inositol phosphatase and disrupts host cell membrane integrity. *Science* 329 (5999):1660-2.
- Brondijk, T. H., D. Fiegen, D. J. Richardson, and J. A. Cole. 2002. Roles of NapF, NapG and NapH, subunits of the *Escherichia coli* periplasmic nitrate reductase, in ubiquinol oxidation. *Mol Microbiol* 44 (1):245-55.
- Brutinel, E. D., C. A. Vakulskas, and T. L. Yahr. 2009. Functional domains of ExsA, the transcriptional activator of the *Pseudomonas aeruginosa* type III secretion system. *J Bacteriol* 191 (12):3811-21.

- Burdette, D. L., J. Seemann, and K. Orth. 2009. *Vibrio* VopQ induces PI3-kinase-independent autophagy and antagonizes phagocytosis. *Mol Microbiol* 73 (4):639-49.
- Burdette, D. L., M. L. Yarbrough, and K. Orth. 2009. Not without cause: *Vibrio parahaemolyticus* induces acute autophagy and cell death. *Autophagy* 5 (1):100-2.
- Bush, M., and R. Dixon. 2012. The role of bacterial enhancer binding proteins as specialized activators of sigma54-dependent transcription. *Microbiol Mol Biol Rev* 76 (3):497-529.
- Carpenter, M. R., S. Rozovsky, and E. F. Boyd. 2015. Pathogenicity Island Cross Talk Mediated by Recombination Directionality Factors Facilitates Excision from the Chromosome. *J Bacteriol* 198 (5):766-76.
- CDC. 2016. 2015 Food Safety Report: Centers for Disease Control and Prevention.
- Ceccarelli, D., N. A. Hasan, A. Huq, and R. R. Colwell. 2013. Distribution and dynamics of epidemic and pandemic *Vibrio parahaemolyticus* virulence factors. *Front Cell Infect Microbiol* 3:97.
- Chang, D. E., D. J. Smalley, D. L. Tucker, M. P. Leatham, W. E. Norris, S. J. Stevenson, A. B. Anderson, J. E. Grissom, D. C. Laux, P. S. Cohen, and T. Conway. 2004. Carbon nutrition of *Escherichia coli* in the mouse intestine. *Proc Natl Acad Sci U S A* 101 (19):7427-32.
- Chao, M. C., J. R. Pritchard, Y. J. Zhang, E. J. Rubin, J. Livny, B. M. Davis, and M. K. Waldor. 2013. High-resolution definition of the *Vibrio cholerae* essential gene set with hidden Markov model-based analyses of transposon-insertion sequencing data. *Nucleic Acids Res* 41 (19):9033-48.
- Chapon-Herve, V., M. Akrim, A. Latifi, P. Williams, A. Lazdunski, and M. Bally. 1997. Regulation of the xcp secretion pathway by multiple quorum-sensing modulons in *Pseudomonas aeruginosa*. *Mol Microbiol* 24 (6):1169-78.
- Chen, C. Y., K. M. Wu, Y. C. Chang, C. H. Chang, H. C. Tsai, T. L. Liao, Y. M. Liu, H. J. Chen, A. B. Shen, J. C. Li, T. L. Su, C. P. Shao, C. T. Lee, L. I. Hor, and S. F. Tsai. 2003. Comparative genome analysis of *Vibrio vulnificus*, a marine pathogen. *Genome Res.* 13 (12):2577-87.

- Chiang, M. L., C. C. Chou, H. C. Chen, Y. T. Tseng, and M. J. Chen. 2012. Adaptive acid tolerance response of *Vibrio parahaemolyticus* as affected by acid adaptation conditions, growth phase, and bacterial strains. *Foodborne Pathog Dis* 9 (8):734-40.
- Chien, C. C., C. C. Chen, M. H. Choi, S. S. Kung, and Y. H. Wei. 2007. Production of poly-beta-hydroxybutyrate (PHB) by *Vibrio* spp. isolated from marine environment. *J Biotechnol* 132 (3):259-63.
- Chugani, S., B. S. Kim, S. Phattarasukol, M. J. Brittnacher, S. H. Choi, C. S. Harwood, and E. P. Greenberg. 2012. Strain-dependent diversity in the *Pseudomonas aeruginosa* quorum-sensing regulon. *Proc Natl Acad Sci U S A* 109 (41):E2823-31.
- Clamp, J. R., G. Fraser, and A. E. Read. 1981. Study of the carbohydrate content of mucus glycoproteins from normal and diseased colons. *Clin Sci (Lond)* 61 (2):229-34.
- Coburn, B., I. Sekirov, and B. B. Finlay. 2007. Type III secretion systems and disease. *Clin Microbiol Rev* 20 (4):535-49.
- Cohen, P. S., and D. C. Laux. 1995. Bacterial adhesion to and penetration of intestinal mucus *in vitro*. *Methods Enzymol* 253:309-14.
- Colwell, R. R., J. Kaper, and S. W. Joseph. 1977. *Vibrio cholerae*, *Vibrio parahaemolyticus*, and other vibrios: occurrence and distribution in Chesapeake Bay. *Science* 198 (4315):394-6.
- Conway, T., and P. S. Cohen. 2015. Commensal and Pathogenic *Escherichia coli* Metabolism in the Gut. *Microbiol Spectr* 3 (3).
- Conway, T., K. A. Krogfelt, and P. S. Cohen. 2004. The Life of Commensal *Escherichia coli* in the Mammalian Intestine. *EcoSal Plus* 1 (1).
- Corazziari, E. S. 2009. Intestinal mucus barrier in normal and inflamed colon. *J Pediatr Gastroenterol Nutr* 48 Suppl 2:S54-5.
- Daniels, N. A., L. MacKinnon, R. Bishop, S. Altekruse, B. Ray, R. M. Hammond, S. Thompson, S. Wilson, N. H. Bean, P. M. Griffin, and L. Slutsker. 2000. *Vibrio parahaemolyticus* infections in the United States, 1973-1998. *J. Infect. Dis.* 181 (5):1661-6.
- Daniels, N. A., Shafie, A. 2000. A review of pathogenic *Vibrio* infections for clinicians. *Infect Med* 17:665-685.

- Davenport, P. W., J. L. Griffin, and M. Welch. 2015. Quorum Sensing Is Accompanied by Global Metabolic Changes in the Opportunistic Human Pathogen *Pseudomonas aeruginosa*. *J Bacteriol* 197 (12):2072-82.
- De Silva, R. S., G. Kovacicova, W. Lin, R. K. Taylor, K. Skorupski, and F. J. Kull. 2005. Crystal structure of the virulence gene activator AphA from *Vibrio cholerae* reveals it is a novel member of the winged helix transcription factor superfamily. *J Biol Chem* 280 (14):13779-83.
- DePaola, A., J. Ulaszek, C. A. Kaysner, B. J. Tenge, J. L. Nordstrom, J. Wells, N. Puhr, and S. M. Gendel. 2003. Molecular, serological, and virulence characteristics of *Vibrio parahaemolyticus* isolated from environmental, food, and clinical sources in North America and Asia. *Appl Environ Microbiol* 69 (7):3999-4005.
- Donaldson, G. P., S. M. Lee, and S. K. Mazmanian. 2015. Gut biogeography of the bacterial microbiota. *Nat Rev Microbiol* 14 (1):20-32.
- Dong, T. G., and J. J. Mekalanos. 2012. Characterization of the RpoN regulon reveals differential regulation of T6SS and new flagellar operons in *Vibrio cholerae* O37 strain V52. *Nucleic Acids Res* 40 (16):7766-75.
- Dong, T., and H. E. Schellhorn. 2009. Global effect of RpoS on gene expression in pathogenic *Escherichia coli* O157:H7 strain EDL933. *BMC Genomics* 10:349.
- Dong, T., R. Yu, and H. Schellhorn. 2011. Antagonistic regulation of motility and transcriptome expression by RpoN and RpoS in *Escherichia coli*. *Mol Microbiol* 79 (2):375-86.
- Drapeau, G. R., and R. A. Macleod. 1963. Nutrition and Metabolism of Marine Bacteria. Xii. Ion Activation of Adenosine Triphosphatase in Membranes of Marine Bacterial Cells. *J Bacteriol* 85:1413-9.
- Elgrably-Weiss, M., E. Schlosser-Silverman, I. Rosenshine, and S. Altuvia. 2006. DeoT, a DeoR-type transcriptional regulator of multiple target genes. *FEMS Microbiol Lett* 254 (1):141-8.
- Enos-Berlage, J. L., Z. T. Guvener, C. E. Keenan, and L. L. McCarter. 2005. Genetic determinants of biofilm development of opaque and translucent *Vibrio parahaemolyticus*. *Mol Microbiol* 55 (4):1160-82.
- Erzberger, J. P., and J. M. Berger. 2006. Evolutionary relationships and structural mechanisms of AAA+ proteins. *Annu Rev Biophys Biomol Struct* 35:93-114.

- Fabich, A. J., S. A. Jones, F. Z. Chowdhury, A. Cernosek, A. Anderson, D. Smalley, J. W. McHargue, G. A. Hightower, J. T. Smith, S. M. Autieri, M. P. Leatham, J. J. Lins, R. L. Allen, D. C. Laux, P. S. Cohen, and T. Conway. 2008. Comparison of carbon nutrition for pathogenic and commensal *Escherichia coli* strains in the mouse intestine. *Infect Immun* 76 (3):1143-52.
- Farmer, J.J.I. 2006. The family *Vibrionaceae*. In *The Prokaryotes*. New York: Springer.
- Farmer, J.J.I., and F.W. Hickman-Brenner. 2006. The genera *Vibrio* and *Photobacterium*. In *The Prokaryotes*. New York: Springer.
- Finn, R., T. Ahmad, E. T. Coffey, D. J. Brayden, A. W. Baird, and A. Boyd. 2013. Translocation of *Vibrio parahaemolyticus* across an *in vitro* M cell model. *FEMS Microbiol Lett* 350 (1):65-71.
- Foster, J. W. 1999. When protons attack: microbial strategies of acid adaptation. *Curr. Opin. Microbiol.* 2 (2):170-4.
- Foster, J. W., and H. K. Hall. 1990. Adaptive acidification tolerance response of *Salmonella typhimurium*. *J. Bacteriol.* 172 (2):771-8.
- Francke, C., T. Groot Kormelink, Y. Hagemeyer, L. Overmars, V. Sluijter, R. Moezelaar, and R. J. Siezen. 2011. Comparative analyses imply that the enigmatic Sigma factor 54 is a central controller of the bacterial exterior. *BMC Genomics* 12:385.
- Freeman, J. A., and B. L. Bassler. 1999. A genetic analysis of the function of LuxO, a two-component response regulator involved in quorum sensing in *Vibrio harveyi*. *Mol Microbiol* 31 (2):665-77.
- Fujino, T., T. Miwatani, Y. Takeda, S. Shinoda, and A. Yoshihara. 1972. Characterization of *Vibrio parahaemolyticus* isolated in the USA. *Biken J* 15 (4):223-8.
- Fujino, T., Okuno, Y., Nakada, D., Aoyama, A., Fukai, K., Mukai, T., and Veho, T. 1953. On the bacteriological examination of shirasu food poisoning. *Medical Journal Osaka Univ* 4:299-304.
- Fuqua, C., and E. P. Greenberg. 1998. Self perception in bacteria: quorum sensing with acylated homoserine lactones. *Curr Opin Microbiol* 1 (2):183-9.

- Fuqua, C., M. R. Parsek, and E. P. Greenberg. 2001. Regulation of gene expression by cell-to-cell communication: acyl-homoserine lactone quorum sensing. *Annu Rev Genet* 35:439-68.
- Fuqua, C., S. C. Winans, and E. P. Greenberg. 1996. Census and consensus in bacterial ecosystems: the LuxR-LuxI family of quorum-sensing transcriptional regulators. *Annu Rev Microbiol* 50:727-51.
- Fuqua, W. C., S. C. Winans, and E. P. Greenberg. 1994. Quorum sensing in bacteria: the LuxR-LuxI family of cell density-responsive transcriptional regulators. *J Bacteriol* 176 (2):269-75.
- Gallegos, M. T., R. Schleif, A. Bairoch, K. Hofmann, and J. L. Ramos. 1997. Arac/XylS family of transcriptional regulators. *Microbiol Mol Biol Rev* 61 (4):393-410.
- Gode-Potratz, C. J., D. M. Chodur, and L. L. McCarter. 2010. Calcium and iron regulate swarming and type III secretion in *Vibrio parahaemolyticus*. *J Bacteriol* 192 (22):6025-38.
- Gode-Potratz, C. J., and L. L. McCarter. 2011. Quorum sensing and silencing in *Vibrio parahaemolyticus*. *J Bacteriol* 193 (16):4224-37.
- Gonzalez-Gil, G., P. Bringmann, and R. Kahmann. 1996. FIS is a regulator of metabolism in *Escherichia coli*. *Mol Microbiol* 22 (1):21-9.
- Goo, E., J. H. An, Y. Kang, and I. Hwang. 2015. Control of bacterial metabolism by quorum sensing. *Trends Microbiol* 23 (9):567-76.
- Goo, E., C. D. Majerczyk, J. H. An, J. R. Chandler, Y. S. Seo, H. Ham, J. Y. Lim, H. Kim, B. Lee, M. S. Jang, E. P. Greenberg, and I. Hwang. 2012. Bacterial quorum sensing, cooperativity, and anticipation of stationary-phase stress. *Proc Natl Acad Sci U S A* 109 (48):19775-80.
- Gray, K. M., L. Passador, B. H. Iglewski, and E. P. Greenberg. 1994. Interchangeability and specificity of components from the quorum-sensing regulatory systems of *Vibrio fischeri* and *Pseudomonas aeruginosa*. *J Bacteriol* 176 (10):3076-80.
- Gu, D., H. Liu, Z. Yang, Y. Zhang, and Q. Wang. 2016. Chromatin Immunoprecipitation Sequencing Technology Reveals Global Regulatory Roles of Low-Cell-Density Quorum-Sensing Regulator AphA in the Pathogen *Vibrio alginolyticus*. *J Bacteriol* 198 (21):2985-2999.

- Guvener, Z. T., and L. L. McCarter. 2003. Multiple regulators control capsular polysaccharide production in *Vibrio parahaemolyticus*. *J Bacteriol* 185 (18):5431-41.
- Haines-Menges, B., W. B. Whitaker, and E. F. Boyd. 2014. Alternative sigma factor RpoE is important for *Vibrio parahaemolyticus* cell envelope stress response and intestinal colonization. *Infect Immun* 82 (9):3667-77.
- Haines-Menges, B. 2015. Functional analysis of the role of alternative sigma factors in *Vibrio parahaemolyticus* host pathogen interactions, Biological Sciences, University of Delaware, Newark.
- Ham, H., and K. Orth. 2012. The role of type III secretion system 2 in *Vibrio parahaemolyticus* pathogenicity. *J Microbiol* 50 (5):719-25.
- Hammer, B. K., and B. L. Bassler. 2003. Quorum sensing controls biofilm formation in *Vibrio cholerae*. *Mol Microbiol* 50 (1):101-4.
- Hansen, G. A., R. Ahmad, E. Hjerde, C. G. Fenton, N. P. Willassen, and P. Haugen. 2012. Expression profiling reveals Spot 42 small RNA as a key regulator in the central metabolism of *Vibrio salmonicida*. *BMC Genomics* 13:37.
- Hanzelka, B. L., A. M. Stevens, M. R. Parsek, T. J. Crone, and E. P. Greenberg. 1997. Mutational analysis of the *Vibrio fischeri* LuxI polypeptide: critical regions of an autoinducer synthase. *J Bacteriol* 179 (15):4882-7.
- Hao, B., Z. L. Mo, P. Xiao, H. J. Pan, X. Lan, and G. Y. Li. 2012. Role of alternative sigma factor 54 (RpoN) from *Vibrio anguillarum* M3 in protease secretion, exopolysaccharide production, biofilm formation, and virulence. *Appl Microbiol Biotechnol* 97 (6):2575-85.
- Hardman, A. M., G. S. Stewart, and P. Williams. 1998. Quorum sensing and the cell-cell communication dependent regulation of gene expression in pathogenic and non-pathogenic bacteria. *Antonie Van Leeuwenhoek* 74 (4):199-210.
- Hastings, J. W., and K. H. Nealson. 1977. Bacterial bioluminescence. *Annu Rev Microbiol* 31:549-95.
- Hayashi, M., Y. Nakayama, and T. Unemoto. 2001. Recent progress in the Na(+)-translocating NADH-quinone reductase from the marine *Vibrio alginolyticus*. *Biochim Biophys Acta* 1505 (1):37-44.

- He, G., R. A. Shankar, M. Chzhan, A. Samouilov, P. Kuppusamy, and J. L. Zweier. 1999. Noninvasive measurement of anatomic structure and intraluminal oxygenation in the gastrointestinal tract of living mice with spatial and spectral EPR imaging. *Proc Natl Acad Sci U S A* 96 (8):4586-91.
- Heidelberg, J. F., J. A. Eisen, W. C. Nelson, R. A. Clayton, M. L. Gwinn, R. J. Dodson, D. H. Haft, E. K. Hickey, J. D. Peterson, L. Umayam, S. R. Gill, K. E. Nelson, T. D. Read, H. Tettelin, D. Richardson, M. D. Ermolaeva, J. Vamathevan, S. Bass, H. Qin, I. Dragoi, P. Sellers, L. McDonald, T. Utterback, R. D. Fleishmann, W. C. Nierman, O. White, S. L. Salzberg, H. O. Smith, R. R. Colwell, J. J. Mekalanos, J. C. Venter, and C. M. Fraser. 2000. DNA sequence of both chromosomes of the cholera pathogen *Vibrio cholerae*. *Nature* 406 (6795):477-83.
- Henke, J. M., and B. L. Bassler. 2004. Quorum sensing regulates type III secretion in *Vibrio harveyi* and *Vibrio parahaemolyticus*. *J Bacteriol* 186 (12):3794-805.
- Henke, J. M., and B. L. Bassler. 2004. Three parallel quorum-sensing systems regulate gene expression in *Vibrio harveyi*. *J Bacteriol* 186 (20):6902-14.
- Henkin, T. M. 2008. Riboswitch RNAs: using RNA to sense cellular metabolism. *Genes Dev* 22 (24):3383-90.
- Hibbing, M. E., C. Fuqua, M. R. Parsek, and S. B. Peterson. 2010. Bacterial competition: surviving and thriving in the microbial jungle. *Nat Rev Microbiol* 8 (1):15-25.
- Hiyoshi, H., T. Kodama, T. Iida, and T. Honda. 2010. Contribution of *Vibrio parahaemolyticus* virulence factors to cytotoxicity, enterotoxicity, and lethality in mice. *Infect Immun* 78 (4):1772-80.
- Honda, T., Iida, T., Akeda, Y., and Kodama, T. 2008. Sixty years of *Vibrio parahaemolyticus* research. *Microbe* 3:462-466.
- Hondo, S., I. Goto, I. Minematsu, N. Ikeda, N. Asano, M. Ishibashi, Y. Kinoshita, N. Nishibuchi, T. Honda, and T. Miwatani. 1987. Gastroenteritis due to Kanagawa negative *Vibrio parahaemolyticus*. *Lancet* 1 (8528):331-2.
- Horton, R. M., H. D. Hunt, S. N. Ho, J. K. Pullen, and L. R. Pease. 1989. Engineering hybrid genes without the use of restriction enzymes: gene splicing by overlap extension. *Gene* 77 (1):61-8.
- Huang, W. S., and H. C. Wong. 2012. Characterization of low salinity stress in *Vibrio parahaemolyticus*. *J. Food Prot.* 75 (2):231-7.

- Hubbard, T. P., M. C. Chao, S. Abel, C. J. Blondel, P. Abel Zur Wiesch, X. Zhou, B. M. Davis, and M. K. Waldor. 2016. Genetic analysis of *Vibrio parahaemolyticus* intestinal colonization. *Proc Natl Acad Sci U S A* 113 (22):6283-8.
- Hurley, C. C., A. Quirke, F. J. Reen, and E. F. Boyd. 2006. Four genomic islands that mark post-1995 pandemic *Vibrio parahaemolyticus* isolates. *BMC Genomics* 7:104.
- Iida, T., K. S. Park, O. Suthienkul, J. Kozawa, Y. Yamaichi, K. Yamamoto, and T. Honda. 1998. Close proximity of the *tdh*, *trh* and *ure* genes on the chromosome of *Vibrio parahaemolyticus*. *Microbiology* 144 ( Pt 9):2517-23.
- Iida, T., O. Suthienkul, K. S. Park, G. Q. Tang, R. K. Yamamoto, M. Ishibashi, K. Yamamoto, and T. Honda. 1997. Evidence for genetic linkage between the *ure* and *trh* genes in *Vibrio parahaemolyticus*. *J Med Microbiol* 46 (8):639-45.
- Ishikawa, T., P. K. Rompikuntal, B. Lindmark, D. L. Milton, and S. N. Wai. 2009. Quorum sensing regulation of the two *hcp* alleles in *Vibrio cholerae* O1 strains. *PLoS One* 4 (8):e6734.
- Iwamoto, M., T. Ayers, B. E. Mahon, and D. L. Swerdlow. 2010. Epidemiology of seafood-associated infections in the United States. *Clin Microbiol Rev* 23 (2):399-411.
- Jaques, S., and L. L. McCarter. 2006. Three new regulators of swarming in *Vibrio parahaemolyticus*. *J Bacteriol* 188 (7):2625-35.
- Jennifer, Y.H., Olga, L.H., Patricia M.G., Duc J.V., Alicia B.C. 2016. Infection with Pathogens Transmitted Commonly Through Food and the Effect of Increasing Use of Culture-Independent Diagnostic Tests on Surveillance — Foodborne Diseases Active Surveillance Network, 10 U.S. Sites, 2012–2015: Centers for Disease Control and Prevention.
- Jensen, R. V., S. M. Depasquale, E. A. Harbolick, T. Hong, A. L. Kernell, D. H. Kruchko, T. Modise, C. E. Smith, L. L. McCarter, and A. M. Stevens. 2013. Complete Genome Sequence of Prepandemic *Vibrio parahaemolyticus* BB22OP. *Genome Announc* 1 (1).
- Ji, G., R. C. Beavis, and R. P. Novick. 1995. Cell density control of staphylococcal virulence mediated by an octapeptide pheromone. *Proc Natl Acad Sci U S A* 92 (26):12055-9.

- Johnson, C. N., J. C. Bowers, K. J. Griffitt, V. Molina, R. W. Clostio, S. Pei, E. Laws, R. N. Paranjpye, M. S. Strom, A. Chen, N. A. Hasan, A. Huq, N. F. Noriea, 3rd, D. J. Grimes, and R. R. Colwell. 2012. Ecology of *Vibrio parahaemolyticus* and *Vibrio vulnificus* in the coastal and estuarine waters of Louisiana, Maryland, Mississippi, and Washington (United States). *Appl Environ Microbiol* 78 (20):7249-57.
- Johnson, C. N., A. R. Flowers, V. C. Young, N. Gonzalez-Escalona, A. DePaola, N. F. Noriea, 3rd, and D. J. Grimes. 2009. Genetic relatedness among tdh+ and trh+ *Vibrio parahaemolyticus* cultured from Gulf of Mexico oysters (*Crassostrea virginica*) and surrounding water and sediment. *Microb Ecol* 57 (3):437-43.
- Joly, N., N. Zhang, M. Buck, and X. Zhang. 2012. Coupling AAA protein function to regulated gene expression. *Biochim Biophys Acta* 1823 (1):108-16.
- Joseph, S. W., R. R. Colwell, and J. B. Kaper. 1982. *Vibrio parahaemolyticus* and related halophilic Vibrios. *Crit Rev Microbiol* 10 (1):77-124.
- Jovanovic, G., C. Engl, A. J. Mayhew, P. C. Burrows, and M. Buck. 2010. Properties of the phage-shock-protein (Psp) regulatory complex that govern signal transduction and induction of the Psp response in *Escherichia coli*. *Microbiology* 156 (Pt 10):2920-32.
- Kalburge, S. S., W. B. Whitaker, and E. F. Boyd. 2014. High-salt preadaptation of *Vibrio parahaemolyticus* enhances survival in response to lethal environmental stresses. *J Food Prot* 77 (2):246-53.
- Kaneko, T., and R. R. Colwell. 1973. Ecology of *Vibrio parahaemolyticus* in Chesapeake Bay. *J Bacteriol* 113 (1):24-32.
- Kawagishi, I., M. Nakada, N. Nishioka, and M. Homma. 1997. Cloning of a *Vibrio alginolyticus rpoN* gene that is required for polar flagellar formation. *J Bacteriol* 179 (21):6851-4.
- Kelly, A., M. D. Goldberg, R. K. Carroll, V. Danino, J. C. Hinton, and C. J. Dorman. 2004. A global role for Fis in the transcriptional control of metabolism and type III secretion in *Salmonella enterica* serovar Typhimurium. *Microbiology* 150 (Pt 7):2037-53.
- Kernell Burke, A., L. T. Guthrie, T. Modise, G. Cormier, R. V. Jensen, L. L. McCarter, and A. M. Stevens. 2015. OpaR controls a network of downstream transcription factors in *Vibrio parahaemolyticus* BB22OP. *PLoS One* 10 (4):e0121863.

- Kim, D., Y. H. Kim, J. Jang, J. H. Yeom, J. W. Jun, S. Hyun, and K. Lee. 2016. Functional Analysis of *Vibrio vulnificus* Orthologs of *Escherichia coli* RraA and RNase E. *Curr Microbiol* 72 (6):716-22.
- Kirn, T. J., B. A. Jude, and R. K. Taylor. 2005. A colonization factor links *Vibrio cholerae* environmental survival and human infection. *Nature* 438 (7069):863-6.
- Klemm, P., and M. A. Schembri. 2000. Bacterial adhesins: function and structure. *Int J Med Microbiol* 290 (1):27-35.
- Klose, K. E., and J. J. Mekalanos. 1998. Differential regulation of multiple flagellins in *Vibrio cholerae*. *J Bacteriol* 180 (2):303-16.
- Klose, K. E., and J. J. Mekalanos. 1998. Distinct roles of an alternative sigma factor during both free-swimming and colonizing phases of the *Vibrio cholerae* pathogenic cycle. *Mol Microbiol* 28 (3):501-20.
- Klose, K. E., V. Novik, and J. J. Mekalanos. 1998. Identification of multiple sigma54-dependent transcriptional activators in *Vibrio cholerae*. *J Bacteriol* 180 (19):5256-9.
- Korhonen, J., P. Martinmaki, C. Pizzi, P. Rastas, and E. Ukkonen. 2009. MOODS: fast search for position weight matrix matches in DNA sequences. *Bioinformatics* 25 (23):3181-2.
- Kovacikova, G., W. Lin, and K. Skorupski. 2003. The virulence activator AphA links quorum sensing to pathogenesis and physiology in *Vibrio cholerae* by repressing the expression of a penicillin amidase gene on the small chromosome. *J Bacteriol* 185 (16):4825-36.
- Krachler, A. M., H. Ham, and K. Orth. 2011. Outer membrane adhesion factor multivalent adhesion molecule 7 initiates host cell binding during infection by gram-negative pathogens. *Proc Natl Acad Sci U S A* 108 (28):11614-9.
- Krantz, G. E., R. R. Colwell, and E. Lovelace. 1969. *Vibrio parahaemolyticus* from the blue crab *Callinectes sapidus* in Chesapeake Bay. *Science* 164 (885):1286-7.
- Kuo, A., N. V. Blough, and P. V. Dunlap. 1994. Multiple N-acyl-L-homoserine lactone autoinducers of luminescence in the marine symbiotic bacterium *Vibrio fischeri*. *J Bacteriol* 176 (24):7558-65.

- Lange, R., M. Barth, and R. Hengge-Aronis. 1993. Complex transcriptional control of the sigma s-dependent stationary-phase-induced and osmotically regulated *osmY* (*csi-5*) gene suggests novel roles for Lrp, cyclic AMP (cAMP) receptor protein-cAMP complex, and integration host factor in the stationary-phase response of *Escherichia coli*. *J Bacteriol* 175 (24):7910-7.
- LaRock, C. N., J. Yu, A. R. Horswill, M. R. Parsek, and F. C. Minion. 2013. Transcriptome analysis of acyl-homoserine lactone-based quorum sensing regulation in *Yersinia pestis* [corrected]. *PLoS One* 8 (4):e62337.
- Leatham, M. P., S. J. Stevenson, E. J. Gauger, K. A. Krogfelt, J. J. Lins, T. L. Haddock, S. M. Autieri, T. Conway, and P. S. Cohen. 2005. Mouse intestine selects nonmotile *flhDC* mutants of *Escherichia coli* MG1655 with increased colonizing ability and better utilization of carbon sources. *Infect Immun* 73 (12):8039-49.
- Lee, M., J. H. Yeom, S. H. Sim, S. Ahn, and K. Lee. 2009. Effects of *Escherichia coli* RraA orthologs of *Vibrio vulnificus* on the ribonucleolytic activity of RNase E *in vivo*. *Curr Microbiol* 58 (4):349-53.
- Lenz, D. H., M. B. Miller, J. Zhu, R. V. Kulkarni, and B. L. Bassler. 2005. CsrA and three redundant small RNAs regulate quorum sensing in *Vibrio cholerae*. *Mol Microbiol* 58 (4):1186-202.
- Lenz, D. H., K. C. Mok, B. N. Lilley, R. V. Kulkarni, N. S. Wingreen, and B. L. Bassler. 2004. The small RNA chaperone Hfq and multiple small RNAs control quorum sensing in *Vibrio harveyi* and *Vibrio cholerae*. *Cell* 118 (1):69-82.
- Letchumanan, V., K. G. Chan, and L. H. Lee. 2014. *Vibrio parahaemolyticus*: a review on the pathogenesis, prevalence, and advance molecular identification techniques. *Front Microbiol* 5:705.
- Lilley, B. N., and B. L. Bassler. 2000. Regulation of quorum sensing in *Vibrio harveyi* by LuxO and sigma-54. *Mol Microbiol* 36 (4):940-54.
- Liu, H., S. Srinivas, X. He, G. Gong, C. Dai, Y. Feng, X. Chen, and S. Wang. 2013. Quorum Sensing in *Vibrio* and its Relevance to Bacterial Virulence. *J Bacteriol Parasitol* 4: 172 (3).
- Liu, Y. W., K. Denkmann, K. Kosciow, C. Dahl, and D. J. Kelly. 2013. Tetrathionate stimulated growth of *Campylobacter jejuni* identifies a new type of bi-functional tetrathionate reductase (TsdA) that is widely distributed in bacteria. *Mol Microbiol* 88 (1):173-88.

- Livny, J., X. Zhou, A. Mandlik, T. Hubbard, B. M. Davis, and M. K. Waldor. 2014. Comparative RNA-Seq based dissection of the regulatory networks and environmental stimuli underlying *Vibrio parahaemolyticus* gene expression during infection. *Nucleic Acids Res* 42 (19):12212-23.
- Ma, L., Y. Zhang, X. Yan, L. Guo, L. Wang, J. Qiu, R. Yang, and D. Zhou. 2012. Expression of the type VI secretion system 1 component Hcp1 is indirectly repressed by OpaR in *Vibrio parahaemolyticus*. *ScientificWorldJournal* 2012:982140.
- Maddocks, S. E., and P. C. Oyston. 2008. Structure and function of the LysR-type transcriptional regulator (LTTR) family proteins. *Microbiology* 154 (Pt 12):3609-23.
- Mahoney, J. C., M. J. Gerding, S. H. Jones, and C. A. Whistler. 2010. Comparison of the pathogenic potentials of environmental and clinical *Vibrio parahaemolyticus* strains indicates a role for temperature regulation in virulence. *Appl Environ Microbiol* 76 (22):7459-65.
- Makino, K., K. Oshima, K. Kurokawa, K. Yokoyama, T. Uda, K. Tagomori, Y. Iijima, M. Najima, M. Nakano, A. Yamashita, Y. Kubota, S. Kimura, T. Yasunaga, T. Honda, H. Shinagawa, M. Hattori, and T. Iida. 2003. Genome sequence of *Vibrio parahaemolyticus*: a pathogenic mechanism distinct from that of *V. cholerae*. *Lancet* 361 (9359):743-9.
- Maltby, R., M. P. Leatham-Jensen, T. Gibson, P. S. Cohen, and T. Conway. 2013. Nutritional basis for colonization resistance by human commensal *Escherichia coli* strains HS and Nissle 1917 against *E. coli* O157:H7 in the mouse intestine. *PLoS One* 8 (1):e53957.
- Mann, K.H. 2000. *Ecology of coastal waters, with implications for management*. Blackwell Publishing, Hoboken, N.J.
- Mao, F., P. Dam, J. Chou, V. Olman, and Y. Xu. 2009. DOOR: a database for prokaryotic operons. *Nucleic Acids Res* 37 (Database issue):D459-63.
- Martin, M., R. Showalter, and M. Silverman. 1989. Identification of a locus controlling expression of luminescence genes in *Vibrio harveyi*. *J Bacteriol* 171 (5):2406-14.

- Martinez-Urtaza, J., A. Lozano-Leon, A. DePaola, M. Ishibashi, K. Shimada, M. Nishibuchi, and E. Liebana. 2004. Characterization of pathogenic *Vibrio parahaemolyticus* isolates from clinical sources in Spain and comparison with Asian and North American pandemic isolates. *J Clin Microbiol* 42 (10):4672-8.
- McCarter, L. L. 1998. OpaR, a homolog of *Vibrio harveyi* LuxR, controls opacity of *Vibrio parahaemolyticus*. *J Bacteriol* 180 (12):3166-73.
- McLaughlin, J. B., A. DePaola, C. A. Bopp, K. A. Martinek, N. P. Napolilli, C. G. Allison, S. L. Murray, E. C. Thompson, M. M. Bird, and J. P. Middaugh. 2005. Outbreak of *Vibrio parahaemolyticus* gastroenteritis associated with Alaskan oysters. *N Engl J Med* 353 (14):1463-70.
- Merrell, D. S., and A. Camilli. 1999. The *cadA* gene of *Vibrio cholerae* is induced during infection and plays a role in acid tolerance. *Mol. Microbiol.* 34 (4):836-49.
- Miller, M. B., and B. L. Bassler. 2001. Quorum sensing in bacteria. *Annu Rev Microbiol* 55:165-99.
- Miller, M. B., K. Skorupski, D. H. Lenz, R. K. Taylor, and B. L. Bassler. 2002. Parallel quorum sensing systems converge to regulate virulence in *Vibrio cholerae*. *Cell* 110 (3):303-14.
- Millikan, D. S., and E. G. Ruby. 2003. FlrA, a sigma54-dependent transcriptional activator in *Vibrio fischeri*, is required for motility and symbiotic light-organ colonization. *J Bacteriol* 185 (12):3547-57.
- Milton, D. L. 2006. Quorum sensing in vibrios: complexity for diversification. *Int J Med Microbiol* 296 (2-3):61-71.
- Miyamoto, C. M., P. V. Dunlap, E. G. Ruby, and E. A. Meighen. 2003. LuxO controls luxR expression in *Vibrio harveyi*: evidence for a common regulatory mechanism in *Vibrio*. *Mol Microbiol* 48 (2):537-48.
- Miyamoto, C. M., and E. A. Meighen. 2006. Involvement of LuxR, a quorum sensing regulator in *Vibrio harveyi*, in the promotion of metabolic genes: *argA*, *purM*, *lysE* and *rluA*. *Biochim Biophys Acta* 1759 (6):296-307.
- Miyamoto, Y., T. Kato, Y. Obara, S. Akiyama, K. Takizawa, and S. Yamai. 1969. *In vitro* hemolytic characteristic of *Vibrio parahaemolyticus*: its close correlation with human pathogenicity. *J Bacteriol* 100 (2):1147-9.

- Moisi, M., C. Jenul, S. M. Butler, A. New, S. Tutz, J. Reidl, K. E. Klose, A. Camilli, and S. Schild. 2009. A novel regulatory protein involved in motility of *Vibrio cholerae*. *J Bacteriol* 191 (22):7027-38.
- Moller, T., T. Franch, C. Udesen, K. Gerdes, and P. Valentin-Hansen. 2002. Spot 42 RNA mediates discoordinate expression of the E. coli galactose operon. *Genes Dev* 16 (13):1696-706.
- Moncada, D. M., S. J. Kammanadiminti, and K. Chadee. 2003. Mucin and Toll-like receptors in host defense against intestinal parasites. *Trends Parasitol* 19 (7):305-11.
- Nair, G. B., T. Ramamurthy, S. K. Bhattacharya, B. Dutta, Y. Takeda, and D. A. Sack. 2007. Global dissemination of *Vibrio parahaemolyticus* serotype O3:K6 and its serovariants. *Clin Microbiol Rev* 20 (1):39-48.
- Naughton, L. M., S. L. Blumerman, M. Carlberg, and E. F. Boyd. 2009. Osmoadaptation among *Vibrio* species and unique genomic features and physiological responses of *Vibrio parahaemolyticus*. *Appl. Environ. Microbiol.* 75 (9):2802-10.
- Neely, M. N., and E. R. Olson. 1996. Kinetics of expression of the *Escherichia coli* cad operon as a function of pH and lysine. *J. Bacteriol.* 178 (18):5522-8.
- Neutra, M. R., and J. F. Forstner. 1987. Gastrointestinal mucus: synthesis, secretion and function. In *Physiology of the gastrointestinal tract*, edited by L.R.Johnson. New York: Raven Press.
- Ng, W. L., and B. L. Bassler. 2009. Bacterial quorum-sensing network architectures. *Annu Rev Genet* 43:197-222.
- Ng, W. L., L. Perez, J. Cong, M. F. Semmelhack, and B. L. Bassler. 2012. Broad spectrum pro-quorum-sensing molecules as inhibitors of virulence in vibrios. *PLoS Pathog* 8 (6):e1002767.
- Nishibuchi, M., A. Fasano, R. G. Russell, and J. B. Kaper. 1992. Enterotoxigenicity of *Vibrio parahaemolyticus* with and without genes encoding thermostable direct hemolysin. *Infect Immun* 60 (9):3539-45.
- Novick, R. P., and E. Geisinger. 2008. Quorum sensing in staphylococci. *Annu Rev Genet* 42:541-64.

- Novick, R. P., S. J. Projan, J. Kornblum, H. F. Ross, G. Ji, B. Kreiswirth, F. Vandenesch, and S. Moghazeh. 1995. The agr P2 operon: an autocatalytic sensory transduction system in *Staphylococcus aureus*. *Mol Gen Genet* 248 (4):446-58.
- Nudler, E., and A. S. Mironov. 2004. The riboswitch control of bacterial metabolism. *Trends Biochem Sci* 29 (1):11-7.
- O'Boyle, N., and A. Boyd. 2014. Manipulation of intestinal epithelial cell function by the cell contact-dependent type III secretion systems of *Vibrio parahaemolyticus*. *Front Cell Infect Microbiol* 3:114.
- O'Boyle, N., B. Houeix, M. Kilcoyne, L. Joshi, and A. Boyd. 2013. The MSHA pilus of *Vibrio parahaemolyticus* has lectin functionality and enables TTSS-mediated pathogenicity. *Int J Med Microbiol* 303 (8):563-73.
- O'Toole, R., D. L. Milton, P. Horstedt, and H. Wolf-Watz. 1997. RpoN of the fish pathogen *Vibrio (Listonella) anguillarum* is essential for flagellum production and virulence by the water-borne but not intraperitoneal route of inoculation. *Microbiology* 143 ( Pt 12):3849-59.
- Okuda, J., M. Ishibashi, E. Hayakawa, T. Nishino, Y. Takeda, A. K. Mukhopadhyay, S. Garg, S. K. Bhattacharya, G. B. Nair, and M. Nishibuchi. 1997. Emergence of a unique O3:K6 clone of *Vibrio parahaemolyticus* in Calcutta, India, and isolation of strains from the same clonal group from Southeast Asian travelers arriving in Japan. *J Clin Microbiol* 35 (12):3150-5.
- Ongagna-Yhombi, S.Y., and E. F. Boyd. 2013. The biosynthesis of the osmoprotectant ectoine but not glycine-betaine is critical for the survival of osmotically stressed *Vibrio parahaemolyticus* cells. *Applied Environ. Microbio.*
- Osawa, R., T. Okitsu, H. Morozumi, and S. Yamai. 1996. Occurrence of urease-positive *Vibrio parahaemolyticus* in Kanagawa, Japan, with specific reference to presence of thermostable direct hemolysin (TDH) and the TDH-related-hemolysin genes. *Appl Environ Microbiol* 62 (2):725-7.
- Paranjpye, R., O. S. Hamel, A. Stojanovski, and M. Liermann. 2012. Genetic diversity of clinical and environmental *Vibrio parahaemolyticus* strains from the Pacific Northwest. *Appl Environ Microbiol* 78 (24):8631-8.
- Park, K. S., T. Ono, M. Rokuda, M. H. Jang, K. Okada, T. Iida, and T. Honda. 2004. Functional characterization of two type III secretion systems of *Vibrio parahaemolyticus*. *Infect Immun* 72 (11):6659-65.

- Parvathi, A., H. S. Kumar, A. Bhanumathi, M. Ishibashi, M. Nishibuchi, and I. Karunasagar. 2006. Molecular characterization of thermostable direct haemolysin-related haemolysin (TRH)-positive *Vibrio parahaemolyticus* from oysters in Mangalore, India. *Environ Microbiol* 8 (6):997-1004.
- Pfaffl, M. W. 2001. A new mathematical model for relative quantification in real-time RT-PCR. *Nucleic Acids Res* 29 (9):e45.
- PHAC. 2015. Public Health Notice - Outbreak of *Vibrio parahaemolyticus* linked to raw shellfish: Public Health Agency of Canada.
- Phadtare, S., and M. Inouye. 2004. Genome-wide transcriptional analysis of the cold shock response in wild-type and cold-sensitive, quadruple-csp-deletion strains of *Escherichia coli*. *J Bacteriol* 186 (20):7007-14.
- Philippe, N., J. P. Alcaraz, E. Coursange, J. Geiselmann, and D. Schneider. 2004. Improvement of pCVD442, a suicide plasmid for gene allele exchange in bacteria. *Plasmid* 51 (3):246-55.
- Pichereau, V., A. Hartke, and Y. Auffray. 2000. Starvation and osmotic stress induced multiresistances. Influence of extracellular compounds. *Int. J. Food Microbiol.* 55 (1-3):19-25.
- Pineyro, P., X. Zhou, L. H. Orfe, P. J. Friel, K. Lahmers, and D. R. Call. 2010. Development of two animal models to study the function of *Vibrio parahaemolyticus* type III secretion systems. *Infect Immun* 78 (11):4551-9.
- Pizzi, C., P. Rastas, and E. Ukkonen. 2011. Finding significant matches of position weight matrices in linear time. *IEEE/ACM Trans Comput Biol Bioinform* 8 (1):69-79.
- Pompeani, A. J., J. J. Irgon, M. F. Berger, M. L. Bulyk, N. S. Wingreen, and B. L. Bassler. 2008. The *Vibrio harveyi* master quorum-sensing regulator, LuxR, a TetR-type protein is both an activator and a repressor: DNA recognition and binding specificity at target promoters. *Mol Microbiol* 70 (1):76-88.
- Popham, D. L., D. Szeto, J. Keener, and S. Kustu. 1989. Function of a bacterial activator protein that binds to transcriptional enhancers. *Science* 243 (4891):629-35.
- Potter, L. C., P. Millington, L. Griffiths, G. H. Thomas, and J. A. Cole. 1999. Competition between *Escherichia coli* strains expressing either a periplasmic or a membrane-bound nitrate reductase: does Nap confer a selective advantage during nitrate-limited growth? *Biochem J* 344 Pt 1:77-84.

- Prouty, M. G., N. E. Correa, and K. E. Klose. 2001. The novel sigma54- and sigma28-dependent flagellar gene transcription hierarchy of *Vibrio cholerae*. *Mol Microbiol* 39 (6):1595-609.
- Qadri, F., M. S. Alam, M. Nishibuchi, T. Rahman, N. H. Alam, J. Chisti, S. Kondo, J. Sugiyama, N. A. Bhuiyan, M. M. Mathan, D. A. Sack, and G. B. Nair. 2003. Adaptive and inflammatory immune responses in patients infected with strains of *Vibrio parahaemolyticus*. *J Infect Dis* 187 (7):1085-96.
- Ralph, A., and B. J. Currie. 2007. *Vibrio vulnificus* and *V. parahaemolyticus* necrotising fasciitis in fishermen visiting an estuarine tropical northern Australian location. *J Infect* 54 (3):e111-4.
- Ramos, J. L., M. Martinez-Bueno, A. J. Molina-Henares, W. Teran, K. Watanabe, X. Zhang, M. T. Gallegos, R. Brennan, and R. Tobes. 2005. The TetR family of transcriptional repressors. *Microbiol Mol Biol Rev* 69 (2):326-56.
- Reen, F. J., and E. F. Boyd. 2005. Molecular typing of epidemic and nonepidemic *Vibrio cholerae* isolates and differentiation of *V. cholerae* and *V. mimicus* isolates by PCR-single-strand conformation polymorphism analysis. *J Appl Microbiol* 98 (3):544-55.
- Reitzer, L., and B. L. Schneider. 2001. Metabolic context and possible physiological themes of sigma(54)-dependent genes in *Escherichia coli*. *Microbiol Mol Biol Rev* 65 (3):422-44, table of contents.
- Reyes, E. D., P. L. Patidar, L. A. Uranga, A. S. Bortoletto, and S. L. Lusetti. 2010. RecN is a cohesin-like protein that stimulates intermolecular DNA interactions *in vitro*. *J Biol Chem* 285 (22):16521-9.
- Ritchie, J. M., H. Rui, X. Zhou, T. Iida, T. Kodoma, S. Ito, B. M. Davis, R. T. Bronson, and M. K. Waldor. 2012. Inflammation and disintegration of intestinal villi in an experimental model for *Vibrio parahaemolyticus*-induced diarrhea. *PLoS Pathog* 8 (3):e1002593.
- Rombel, I., A. North, I. Hwang, C. Wyman, and S. Kustu. 1998. The bacterial enhancer-binding protein NtrC as a molecular machine. *Cold Spring Harb Symp Quant Biol* 63:157-66.
- Rutherford, S. T., and B. L. Bassler. 2012. Bacterial quorum sensing: its role in virulence and possibilities for its control. *Cold Spring Harb Perspect Med* 2 (11).

- Rutherford, S. T., J. C. van Kessel, Y. Shao, and B. L. Bassler. 2011. AphA and LuxR/HapR reciprocally control quorum sensing in vibrios. *Genes Dev* 25 (4):397-408.
- Sabharwal, D., T. Song, K. Papenfort, and S. N. Wai. 2015. The VrrA sRNA controls a stationary phase survival factor Vrp of *Vibrio cholerae*. *RNA Biol* 12 (2):186-96.
- Saenz, H. L., V. Augsburg, C. Vuong, R. W. Jack, F. Gotz, and M. Otto. 2000. Inducible expression and cellular location of AgrB, a protein involved in the maturation of the staphylococcal quorum-sensing pheromone. *Arch Microbiol* 174 (6):452-5.
- Salmond, G. P., B. W. Bycroft, G. S. Stewart, and P. Williams. 1995. The bacterial 'enigma': cracking the code of cell-cell communication. *Mol Microbiol* 16 (4):615-24.
- Salomon, D., H. Gonzalez, B. L. Updegraff, and K. Orth. 2013. *Vibrio parahaemolyticus* type VI secretion system 1 is activated in marine conditions to target bacteria, and is differentially regulated from system 2. *PLoS One* 8 (4):e61086.
- Salomon, D., J. A. Klimko, and K. Orth. 2014. H-NS regulates the *Vibrio parahaemolyticus* type VI secretion system 1. *Microbiology* 160 (Pt 9):1867-73.
- Samartzidou, H., M. Mehrazin, Z. Xu, M. J. Benedik, and A. H. Delcour. 2003. Cadaverine inhibition of porin plays a role in cell survival at acidic pH. *J. Bacteriol.* 185 (1):13-9.
- Sawabe, T., K. Kita-Tsukamoto, and F. L. Thompson. 2007. Inferring the evolutionary history of vibrios by means of multilocus sequence analysis. *J Bacteriol* 189 (21):7932-6.
- Sawabe, T., Y. Ogura, Y. Matsumura, G. Feng, A. R. Amin, S. Mino, S. Nakagawa, R. Kumar, Y. Fukui, M. Satomi, R. Matsushima, F. L. Thompson, B. Gomez-Gil, R. Christen, F. Maruyama, K. Kurokawa, and T. Hayashi. 2013. Updating the *Vibrio* clades defined by multilocus sequence phylogeny: proposal of eight new clades, and the description of *Vibrio tritonius* sp. nov. *Front Microbiol* 4:414.
- Scallan, E., R.M. Hoekstra, F.J. Angulo, R.V. Tauxe, M.A. Widdowson, S.L. Roy, J.L. Jones, and P. M. Griffin. 2011. Foodborne Illness Acquired in the United States—Major Pathogens. *Emerging Infectious Diseases* 17 (1):7-15.

- Schaefer, A. L., D. L. Val, B. L. Hanzelka, J. E. Cronan, Jr., and E. P. Greenberg. 1996. Generation of cell-to-cell signals in quorum sensing: acyl homoserine lactone synthase activity of a purified *Vibrio fischeri* LuxI protein. *Proc Natl Acad Sci U S A* 93 (18):9505-9.
- Schuster, M., C. P. Lostroh, T. Ogi, and E. P. Greenberg. 2003. Identification, timing, and signal specificity of *Pseudomonas aeruginosa* quorum-controlled genes: a transcriptome analysis. *J Bacteriol* 185 (7):2066-79.
- Scott, D. R., D. Weeks, C. Hong, S. Postius, K. Melchers, and G. Sachs. 1998. The role of internal urease in acid resistance of *Helicobacter pylori*. *Gastroenterology* 114 (1):58-70.
- Shao, Y., and B. L. Bassler. 2012. Quorum-sensing non-coding small RNAs use unique pairing regions to differentially control mRNA targets. *Mol Microbiol* 83 (3):599-611.
- Shao, Y., L. Feng, S. T. Rutherford, K. Papenfort, and B. L. Bassler. 2013. Functional determinants of the quorum-sensing non-coding RNAs and their roles in target regulation. *EMBO J* 32 (15):2158-71.
- Shingler, V. 1996. Signal sensing by sigma 54-dependent regulators: derepression as a control mechanism. *Mol Microbiol* 19 (3):409-16.
- Showalter, R. E., M. O. Martin, and M. R. Silverman. 1990. Cloning and nucleotide sequence of luxR, a regulatory gene controlling bioluminescence in *Vibrio harveyi*. *J Bacteriol* 172 (6):2946-54.
- Skorupski, K., and R. K. Taylor. 1999. A new level in the *Vibrio cholerae* ToxR virulence cascade: AphA is required for transcriptional activation of the tcpPH operon. *Mol Microbiol* 31 (3):763-71.
- Soksawatmaekhin, W., A. Kuraishi, K. Sakata, K. Kashiwagi, and K. Igarashi. 2004. Excretion and uptake of cadaverine by CadB and its physiological functions in *Escherichia coli*. *Mol. Microbiol.* 51 (5):1401-12.
- Song, T., F. Mika, B. Lindmark, Z. Liu, S. Schild, A. Bishop, J. Zhu, A. Camilli, J. Johansson, J. Vogel, and S. N. Wai. 2008. A new *Vibrio cholerae* sRNA modulates colonization and affects release of outer membrane vesicles. *Mol Microbiol* 70 (1):100-11.
- Song, T., D. Sabharwal, and S. N. Wai. 2010. VrrA mediates Hfq-dependent regulation of OmpT synthesis in *Vibrio cholerae*. *J Mol Biol* 400 (4):682-8.

- Sperandio, V., A. G. Torres, J. A. Giron, and J. B. Kaper. 2001. Quorum sensing is a global regulatory mechanism in enterohemorrhagic *Escherichia coli* O157:H7. *J Bacteriol* 183 (17):5187-97.
- Stecher, B., and W. D. Hardt. 2011. Mechanisms controlling pathogen colonization of the gut. *Curr Opin Microbiol* 14 (1):82-91.
- Stevens, A. M., and E. P. Greenberg. 1997. Quorum sensing in *Vibrio fischeri*: essential elements for activation of the luminescence genes. *J Bacteriol* 179 (2):557-62.
- Stewart, V., Y. Lu, and A. J. Darwin. 2002. Periplasmic nitrate reductase (NapABC enzyme) supports anaerobic respiration by *Escherichia coli* K-12. *J Bacteriol* 184 (5):1314-23.
- Strom, L., H. B. Lindroos, K. Shirahige, and C. Sjogren. 2004. Postreplicative recruitment of cohesin to double-strand breaks is required for DNA repair. *Mol Cell* 16 (6):1003-15.
- Studer, S. V., M. J. Mandel, and E. G. Ruby. 2008. AinS quorum sensing regulates the *Vibrio fischeri* acetate switch. *J Bacteriol* 190 (17):5915-23.
- Studholme, D. J., and R. Dixon. 2003. Domain architectures of sigma54-dependent transcriptional activators. *J Bacteriol* 185 (6):1757-67.
- Su, Y. C., and C. Liu. 2007. *Vibrio parahaemolyticus*: a concern of seafood safety. *Food Microbiol* 24 (6):549-58.
- Sun, F., Y. Zhang, L. Wang, X. Yan, Y. Tan, Z. Guo, J. Qiu, R. Yang, P. Xia, and D. Zhou. 2012. Molecular characterization of direct target genes and cis-acting consensus recognized by quorum-sensing regulator AphA in *Vibrio parahaemolyticus*. *PLoS One* 7 (9):e44210.
- Sun, S., Q. X. Tay, S. Kjelleberg, S. A. Rice, and D. McDougald. 2015. Quorum sensing-regulated chitin metabolism provides grazing resistance to *Vibrio cholerae* biofilms. *ISME J* 9 (8):1812-20.
- Swift, S., N. J. Bainton, and M. K. Winson. 1994. Gram-negative bacterial communication by N-acyl homoserine lactones: a universal language? *Trends Microbiol* 2 (6):193-8.
- Syed, K. A., S. Beyhan, N. Correa, J. Queen, J. Liu, F. Peng, K. J. Satchell, F. Yildiz, and K. E. Klose. 2009. The *Vibrio cholerae* flagellar regulatory hierarchy controls expression of virulence factors. *J Bacteriol* 191 (21):6555-70.

- Tanaka, Y., B. Kimura, H. Takahashi, T. Watanabe, H. Obata, A. Kai, S. Morozumi, and T. Fujii. 2008. Lysine decarboxylase of *Vibrio parahaemolyticus*: kinetics of transcription and role in acid resistance. *J. Appl. Microbiol.* 104 (5):1283-93.
- Tena, D., M. Arias, B. T. Alvarez, C. Mauleon, M. P. Jimenez, and J. Bisquert. 2010. Fulminant necrotizing fasciitis due to *Vibrio parahaemolyticus*. *J Med Microbiol* 59 (Pt 2):235-8.
- Thompson, C. C., A. C. Vicente, R. C. Souza, A. T. Vasconcelos, T. Vesth, N. Alves, Jr., D. W. Ussery, T. Iida, and F. L. Thompson. 2009. Genomic taxonomy of Vibrios. *BMC Evol Biol* 9:258.
- Thompson, F. L., D. Gevers, C. C. Thompson, P. Dawyndt, S. Naser, B. Hoste, C. B. Munn, and J. Swings. 2005. Phylogeny and molecular identification of vibrios on the basis of multilocus sequence analysis. *Appl Environ Microbiol* 71 (9):5107-15.
- Thompson, J. R., M. A. Randa, L. A. Marcelino, A. Tomita-Mitchell, E. Lim, and M. F. Polz. 2004. Diversity and dynamics of a north atlantic coastal Vibrio community. *Appl Environ Microbiol* 70 (7):4103-10.
- Thorvaldsdottir, H., J. T. Robinson, and J. P. Mesirov. 2013. Integrative Genomics Viewer (IGV): high-performance genomics data visualization and exploration. *Brief Bioinform* 14 (2):178-92.
- Toffano-Nioche, C., A. N. Nguyen, C. Kuchly, A. Ott, D. Gautheret, P. Bouloc, and A. Jacq. 2012. Transcriptomic profiling of the oyster pathogen *Vibrio splendidus* opens a window on the evolutionary dynamics of the small RNA repertoire in the *Vibrio* genus. *RNA* 18 (12):2201-19.
- Tokuda, H., M. Sugawara, and T. Unemoto. 1982. Roles of Na<sup>+</sup> and K<sup>+</sup> in alpha-aminoisobutyric acid transport by the marine bacterium *Vibrio alginolyticus*. *J Biol Chem* 257 (2):788-94.
- Tu, K. C., and B. L. Bassler. 2007. Multiple small RNAs act additively to integrate sensory information and control quorum sensing in *Vibrio harveyi*. *Genes Dev* 21 (2):221-33.
- Unemoto, T., and M. Hayashi. 1979. NADH: quinone oxidoreductase as a site of Na<sup>+</sup>-dependent activation in the respiratory chain of marine *Vibrio alginolyticus*. *J Biochem* 85 (6):1461-7.

- Uzureau, S., J. Lemaire, E. Delaive, M. Dieu, A. Gaigneaux, M. Raes, X. De Bolle, and J. J. Letesson. 2010. Global analysis of quorum sensing targets in the intracellular pathogen *Brucella melitensis* 16 M. *J Proteome Res* 9 (6):3200-17.
- van Kessel, J. C., S. T. Rutherford, Y. Shao, A. F. Utria, and B. L. Bassler. 2013. Individual and combined roles of the master regulators AphA and LuxR in control of the *Vibrio harveyi* quorum-sensing regulon. *J Bacteriol* 195 (3):436-43.
- van Kessel, J. C., L. E. Ulrich, I. B. Zhulin, and B. L. Bassler. 2013. Analysis of activator and repressor functions reveals the requirements for transcriptional control by LuxR, the master regulator of quorum sensing in *Vibrio harveyi*. *MBio* 4 (4).
- Vogel, J., and B. F. Luisi. 2011. Hfq and its constellation of RNA. *Nat Rev Microbiol* 9 (8):578-89.
- Wagner, V. E., D. Bushnell, L. Passador, A. I. Brooks, and B. H. Iglewski. 2003. Microarray analysis of *Pseudomonas aeruginosa* quorum-sensing regulons: effects of growth phase and environment. *J Bacteriol* 185 (7):2080-95.
- Wang, L., Y. Ling, H. Jiang, Y. Qiu, J. Qiu, H. Chen, R. Yang, and D. Zhou. 2013. AphA is required for biofilm formation, motility, and virulence in pandemic *Vibrio parahaemolyticus*. *Int J Food Microbiol* 160 (3):245-51.
- Wang, L., D. Zhou, P. Mao, Y. Zhang, J. Hou, Y. Hu, J. Li, S. Hou, R. Yang, R. Wang, and J. Qiu. 2013. Cell density- and quorum sensing-dependent expression of type VI secretion system 2 in *Vibrio parahaemolyticus*. *PLoS One* 8 (8):e73363.
- Waters, C. M., and B. L. Bassler. 2005. Quorum sensing: cell-to-cell communication in bacteria. *Annu Rev Cell Dev Biol* 21:319-46.
- Waters, C. M., and B. L. Bassler. 2006. The *Vibrio harveyi* quorum-sensing system uses shared regulatory components to discriminate between multiple autoinducers. *Genes Dev* 20 (19):2754-67.
- Waters, L. S., and G. Storz. 2009. Regulatory RNAs in bacteria. *Cell* 136 (4):615-28.
- Weiss, D. S., J. Batut, K. E. Klose, J. Keener, and S. Kustu. 1991. The phosphorylated form of the enhancer-binding protein NTRC has an ATPase activity that is essential for activation of transcription. *Cell* 67 (1):155-67.

- Whitaker, W. B., M. A. Parent, A. Boyd, G. P. Richards, and E. F. Boyd. 2012. The *Vibrio parahaemolyticus* ToxRS regulator is required for stress tolerance and colonization in a novel orogastric streptomycin-induced adult murine model. *Infect Immun* 80 (5):1834-45.
- Whitaker, W. B., M. A. Parent, L. M. Naughton, G. P. Richards, S. L. Blumerman, and E. F. Boyd. 2010. Modulation of responses of *Vibrio parahaemolyticus* O3:K6 to pH and temperature stresses by growth at different salt concentrations. *Appl Environ Microbiol* 76 (14):4720-9.
- Whitaker, W. B., G. P. Richards, and E. F. Boyd. 2014. Loss of Sigma Factor RpoN Increases Intestinal Colonization of *Vibrio parahaemolyticus* in an Adult Mouse Model. *Infect Immun* 82 (2):544-56.
- Whitaker, W. B.; Boyd, E.F. 2012. Adaptations to environmental changes: stress response mechanisms among *Vibrio* species. In *Stress response in microbiology*, edited by J. M. Requena. Poole, UK.: Horizon Scientific Press.
- Winson, M. K., M. Camara, A. Latifi, M. Foglino, S. R. Chhabra, M. Daykin, M. Bally, V. Chapon, G. P. Salmond, B. W. Bycroft, and et al. 1995. Multiple N-acyl-L-homoserine lactone signal molecules regulate production of virulence determinants and secondary metabolites in *Pseudomonas aeruginosa*. *Proc Natl Acad Sci U S A* 92 (20):9427-31.
- Wolfe, A. J., D. S. Millikan, J. M. Campbell, and K. L. Visick. 2004. *Vibrio fischeri* sigma54 controls motility, biofilm formation, luminescence, and colonization. *Appl Environ Microbiol* 70 (4):2520-4.
- Wong, H. C., C. N. Chang, and M. Y. Chen. 2004. Effects of heat, acid, and freeze-thaw challenges on survival of starved *Vibrio parahaemolyticus* in minimal salt medium, tryptic soy broth, and filtered oyster homogenate medium. *J Food Prot* 67 (6):1243-6.
- Wong, H. C., C. H. Chen, Y. J. Chung, S. H. Liu, T. K. Wang, C. L. Lee, C. S. Chiou, M. Nishibuchi, and B. K. Lee. 2005. Characterization of new O3:K6 strains and phylogenetically related strains of *Vibrio parahaemolyticus* isolated in Taiwan and other countries. *J Appl Microbiol* 98 (3):572-80.
- Wong, H. C., P. Y. Peng, J. M. Han, C. Y. Chang, and S. L. Lan. 1998. Effect of mild acid treatment on the survival, enteropathogenicity, and protein production in *Vibrio parahaemolyticus*. *Infect. Immun.* 66 (7):3066-71.

- Xiao, N., and N. Jiao. 2011. Formation of polyhydroxyalkanoate in aerobic anoxygenic phototrophic bacteria and its relationship to carbon source and light availability. *Appl Environ Microbiol* 77 (21):7445-50.
- Yang, M., E. M. Frey, Z. Liu, R. Bishar, and J. Zhu. 2010. The virulence transcriptional activator AphA enhances biofilm formation by *Vibrio cholerae* by activating expression of the biofilm regulator VpsT. *Infect Immun* 78 (2):697-703.
- Yeung, P. S., and K. J. Boor. 2004. Effects of acid stress on *Vibrio parahaemolyticus* survival and cytotoxicity. *J. Food Prot.* 67 (7):1328-34.
- Yildiz, F. H., and K. L. Visick. 2009. Vibrio biofilms: so much the same yet so different. *Trends Microbiol* 17 (3):109-18.
- Yu, Y., H. Yang, J. Li, P. Zhang, B. Wu, B. Zhu, Y. Zhang, and W. Fang. 2012. Putative type VI secretion systems of *Vibrio parahaemolyticus* contribute to adhesion to cultured cell monolayers. *Arch Microbiol* 194 (10):827-35.
- Zhang, L., P. J. Murphy, A. Kerr, and M. E. Tate. 1993. Agrobacterium conjugation and gene regulation by N-acyl-L-homoserine lactones. *Nature* 362 (6419):446-8.
- Zhang, Y., Y. Qiu, Y. Tan, Z. Guo, R. Yang, and D. Zhou. 2012. Transcriptional regulation of *opaR*, *qrr2-4* and *aphA* by the master quorum-sensing regulator OpaR in *Vibrio parahaemolyticus*. *PLoS One* 7 (4):e34622.
- Zhang, Y., L. Zhang, S. Hou, X. Huang, F. Sun, and H. Gao. 2016. The Master Quorum-Sensing Regulator OpaR is Activated Indirectly by H-NS in *Vibrio parahaemolyticus*. *Curr Microbiol* 73 (1):71-6.
- Zheng, X., Y. Ji, X. Weng, and X. Huang. 2015. RpoS-dependent expression of OsmY in *Salmonella enterica* serovar typhi: activation under stationary phase and SPI-2-inducing conditions. *Curr Microbiol* 70 (6):877-82.
- Zhou, D., X. Yan, F. Qu, L. Wang, Y. Zhang, J. Hou, Y. Hu, J. Li, S. Xin, J. Qiu, R. Yang, and P. Mao. 2013. Quorum sensing modulates transcription of *cpsQ-mfpABC* and *mfpABC* in *Vibrio parahaemolyticus*. *Int J Food Microbiol* 166 (3):458-63.
- Zhou, X., M. E. Konkel, and D. R. Call. 2010. Regulation of type III secretion system 1 gene expression in *Vibrio parahaemolyticus* is dependent on interactions between ExsA, ExsC, and ExsD. *Virulence* 1 (4):260-72.
- Zhou, X., D. H. Shah, M. E. Konkel, and D. R. Call. 2008. Type III secretion system 1 genes in *Vibrio parahaemolyticus* are positively regulated by ExsA and negatively regulated by ExsD. *Mol Microbiol* 69 (3):747-64.

Zhu, J., M. B. Miller, R. E. Vance, M. Dziejman, B. L. Bassler, and J. J. Mekalanos. 2002. Quorum-sensing regulators control virulence gene expression in *Vibrio cholerae*. *Proc Natl Acad Sci U S A* 99 (5):3129-34.

## Appendix A

### **EFFECT OF LOW SALT ON LETHAL ACID STRESS SURVIVAL OF *VIBRIO PARAHAEMOLYTICUS*.**

Work in this appendix examines the effect of low pH acid stress on *V. parahaemolyticus* using media supplemented with low salt concentration (1% NaCl). *V. parahaemolyticus* RIMD2210633 and  $\Delta cadA$  strains were grown overnight in 5ml of LB broth (pH 7) with a final NaCl concentration of 1%. Overnight cultures were diluted 1:50 into fresh LB broth (1% NaCl, pH 7) and incubated aerobically at 37°C until cells reached mid-log phase (optical density at 595nm [OD<sub>595</sub>] of 0.4). The culture was then centrifuged (5,000 rpm for 10 min) to harvest the cells. The cells were resuspended either in 5ml acidified LB broth (pH4). LB broth had a final salt concentration of 1% and was acidified to pH 4 using 1M HCl. In cases where cells were preadapted, cells were exposed to LB broth with varying salt concentrations and/ or was adjusted to mild pH 5.5 for 30 min at 37°C. After 30 min, cells were harvested by centrifugation (5,000 rpm for 10min) of the culture. Cells were then resuspended in the acidified LB broth pH 4. Resuspended cells were incubated at 37°C with aeration, and then serially diluted at 0, 20, 40 and 60 min and plated onto LB plates (1.5% Agar) supplemented with 3% NaCl. Plates were incubated at 37°C for 10 h, after which the CFU/ml was determined for each time point as a measure of survival. The data demonstrated that salt pre-adaptation alone did not improve cell survivability but

3% NaCl preadaptation combined with mild acid preadaptation did improve survival of cells at the 20 min time point (**Figure 31 and Figure 32**).

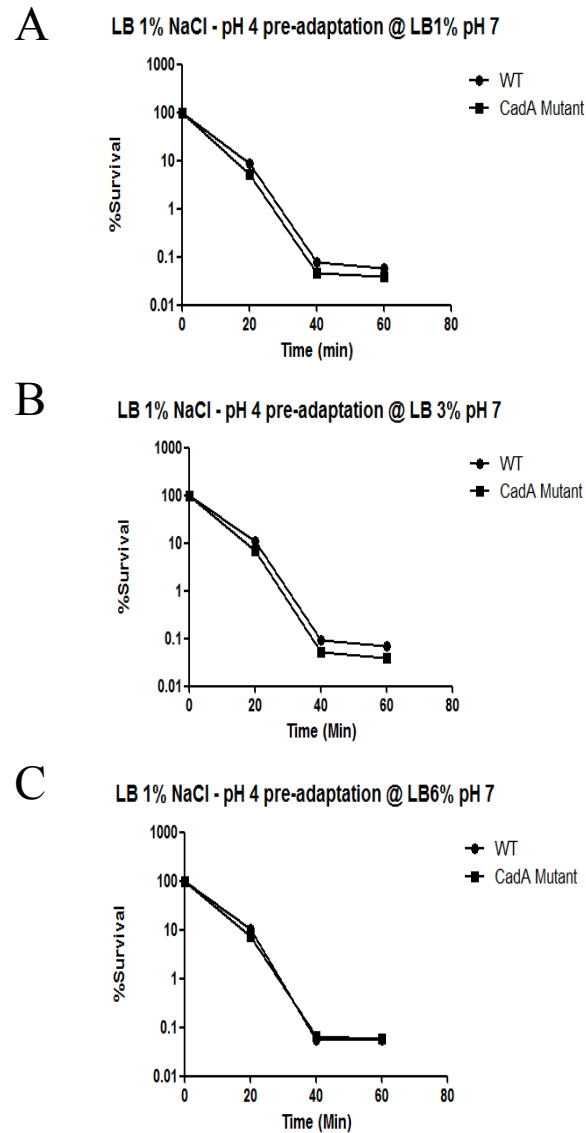


**Figure 31** Effect of low salt, lethal acid stress on *V. parahaemolyticus* cells pre-adapted in LB media supplemented with (A) 1% NaCl (B) 3% NaCl and (C) 6% NaCl

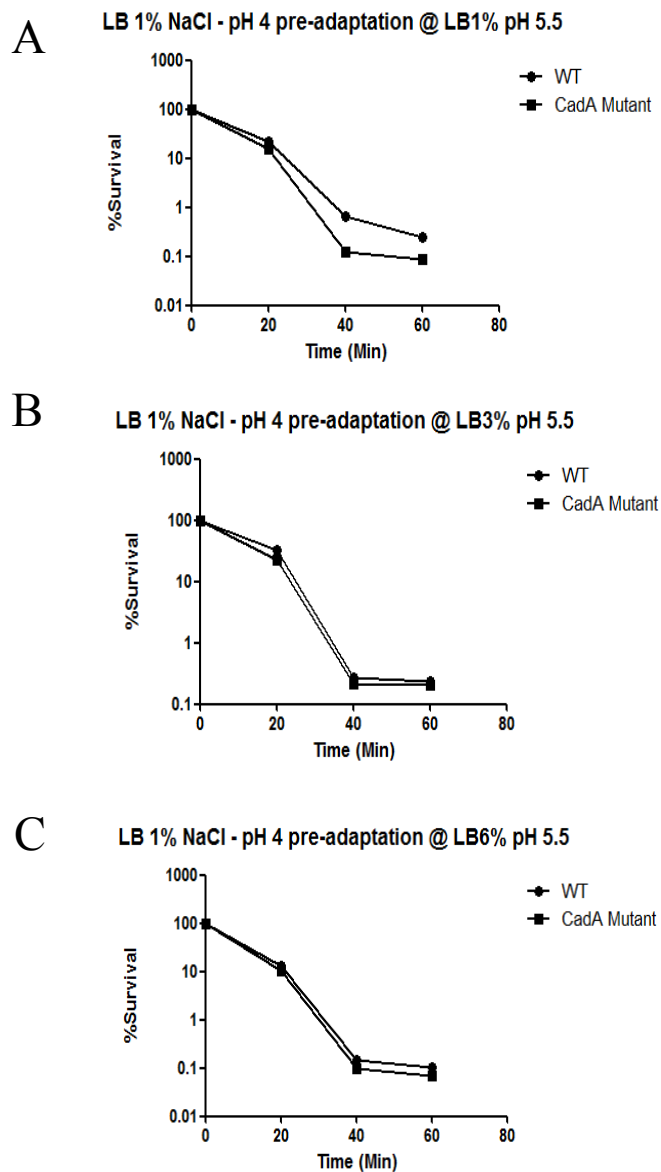


**Figure 32** Effect of low salt, lethal acid stress on *V. parahaemolyticus* cells pre-adapted in LB media acidified to mild acid pH 5.5 and supplemented with (A) 1% NaCl (B) 3% NaCl and (C) 6% NaCl

## Appendix B

### **EFFECT OF ORGANIC ACID AND BILE STRESS ON *VIBRIO PARAHAEMOLYTICUS*.**

Work in this appendix examines the effect of low pH acid stress on *V. parahaemolyticus* using acetic acid and lactic acid. *V. parahaemolyticus* RIMD2210633 and  $\Delta cadA$  strains were grown overnight in 5ml of LB broth (pH 7) with a final NaCl concentration of 3%. Overnight cultures were diluted 1:50 into fresh LB broth (3% NaCl, pH 7) and incubated aerobically at 37°C until cells reached mid-log phase (optical density at 595nm [OD<sub>595</sub>] of 0.4). The culture was then centrifuged (5,000 rpm for 10 min) to harvest the cells. The cells were resuspended either in 5ml acidified LB broth (pH4). LB broth had a final salt concentration of 1%, 3% or 6% NaCl and was acidified to pH 4 using acetic acid or lactic acid. Resuspended cells were incubated at 37°C with aeration, and then serially diluted at 0, 20, 40 and 60 min and plated onto LB plates (1.5% Agar) supplemented with 3% NaCl. Plates were incubated at 37°C for 10 h, after which the CFU/ml was determined for each time point as a measure of survival (Figure 30). To examine the effects of bile stress, mid-log phase cells were resuspended in LB broth supplemented with 3% NaCl and 15% bile salts. Resuspended cells were incubated at 37°C with aeration, and then serially diluted at 0, 20, 40 and 60 min and plated onto LB plates (1.5% Agar) supplemented with 3% NaCl. Plates were incubated at 37°C for 10 h, after which the CFU/ml was

determined for each time point as a measure of survival. Deletion of *cadA* does not lead to any additional defect under acetic acid stress but does lead to an additional defect compared to wild-type in lactic acid (**Figure 33**). CadA also does not contribute to bile stress survival. The mutant shows no additional defect compared to wild-type (**Figure 34**).

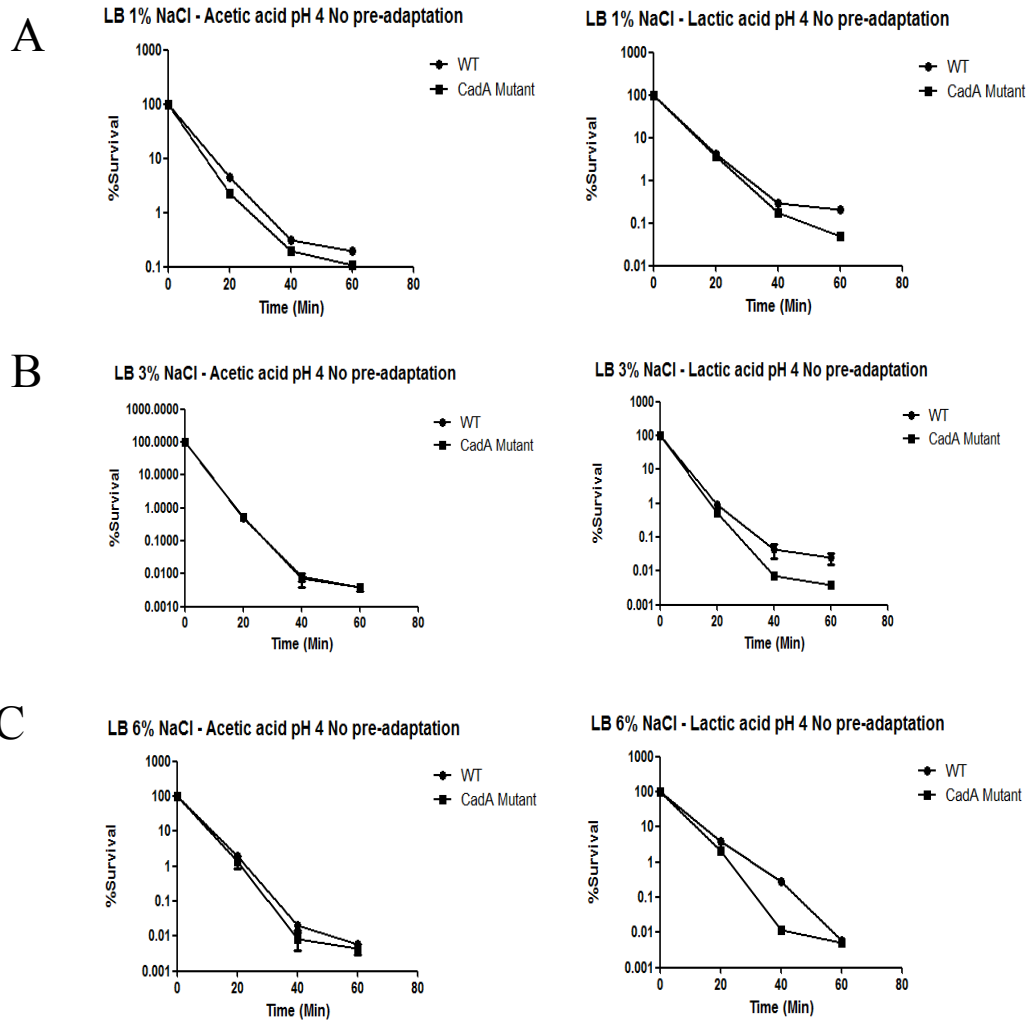


**Figure 33** Effect of lethal organic acid stress on *V. parahaemolyticus*. Survival in LB media acidified to pH 4 using acetic acid (left) and lactic acid (right) supplemented with (A) 1% NaCl (B) 3% NaCl and (C) 6% NaCl

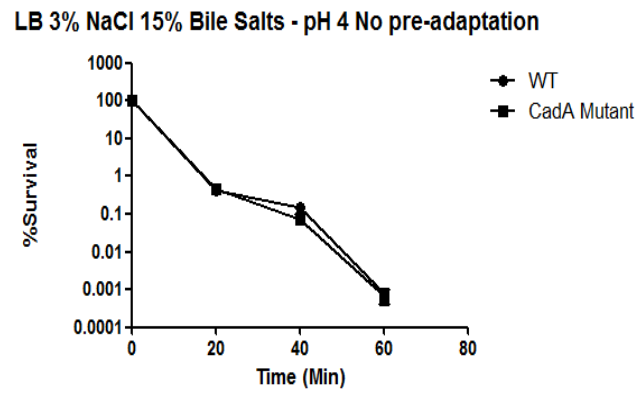


**Figure 34** Effect of bile salt stress on *V. parahaemolyticus*. Survival in LB media supplemented with 3% NaCl and 15% bile salts

## Appendix C

### GROWTH IN HIGH SALT PROVIDES COMPETITIVE ADVANTAGE *IN VIVO*

Previously, we had observed that high salt pre-adaptation of *V. parahaemolyticus* improves survival of the bacteria against environmental stresses. We wanted to determine if growth in high salt would provide a competitive advantage to the bacteria *in vivo*. We performed an *in vivo* competition assay using the streptomycin pre-treated adult mouse model for colonization. We competed cells grown in LB 6% NaCl against the WBWlacZ strain grown in LB 3% NaCl media. We found that cells grown in high salt were able to out-compete the WBWlacZ strain with an average CI of 1.97 *in vivo* (Figure 35).

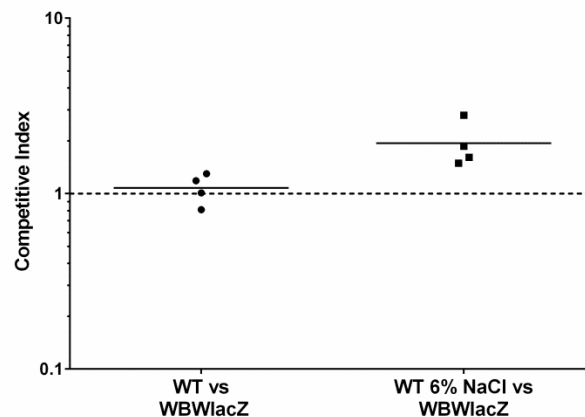


**Figure 35** *In vivo* competition assay between WBWlacZ and WT RIMD2210633 and WBWlacZ and WT RIMD2210633 grown in 6% NaCl.

## Appendix D

### **IN VIVO COLONIZATION ABILITY OF ENVIRONMENTAL ISOLATE UCM-V493 AND GALACTOSE UTILIZATION IN THE STRAIN**

Previously we had examined that *V. parahaemolyticus* environmental isolate UCM-V493 was able to out-compete the canonical clinical isolate RIMD2210633 in the streptomycin-pre-treated adult mouse model in a 24 hour colonization competition assay. We wanted to determine whether the environmental isolate would be able to out-compete the clinical isolate over a sustained period or if the clinical strain would be able to recover. To that end, we performed an *in vivo* persistence competition assay across four days. Fecal pellets were collected at various time points from the mice. The fecal pellets were resuspended in PBS, homogenized and plated to determine the CFU/g of each strain and the competitive index. We found that UCM-V493 outcompeted the RIMD2210633 lacZ knock-in strain WBWlacZ with a CI of 1.5, 2.8, 5.6, 11.9, 16.4, 9.6 respectively over the 6 h, 12h, 1d, 2d, 3d and 4d time-points (**Figure 36**).

We had also previously observed that the UCM-V493 strain had a significantly different growth profile on various carbon sources compared to RIMD2210633. We wanted to further examine the role of galactose, a carbon source that UCM-V493 utilized more efficiently. We constructed a mutant of the galactokinase (*galK*) gene in

order to use it in competition assays with WBWlacZ. The growth profile of the galK mutant strain is shown in **Figure 37**.

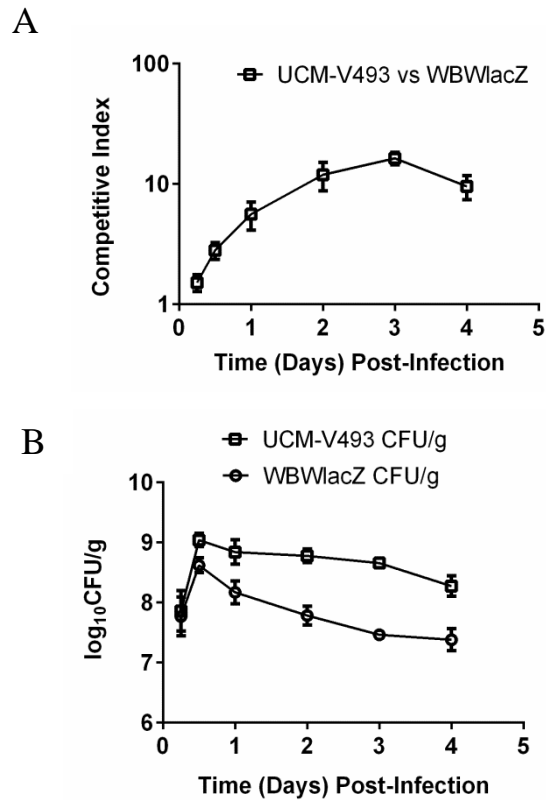


**Figure 36** *In vivo* persistence competition assay of UCM-V493 vs WBWlacZ. (A) Fecal pellets were collected from the mice at indicated intervals, weighed, homogenized and plated on X-gal plates to determine the CI. Competitive index (CI) was calculated as  $CI = \frac{\text{ratio out (UCM-V493/WBWlacZ)}}{\text{ratio in (UCM-V493/WBWlacZ)}}$ . (B) Data is represented as log-transformed CFU/g for UCM-V493 vs WBWlacZ.

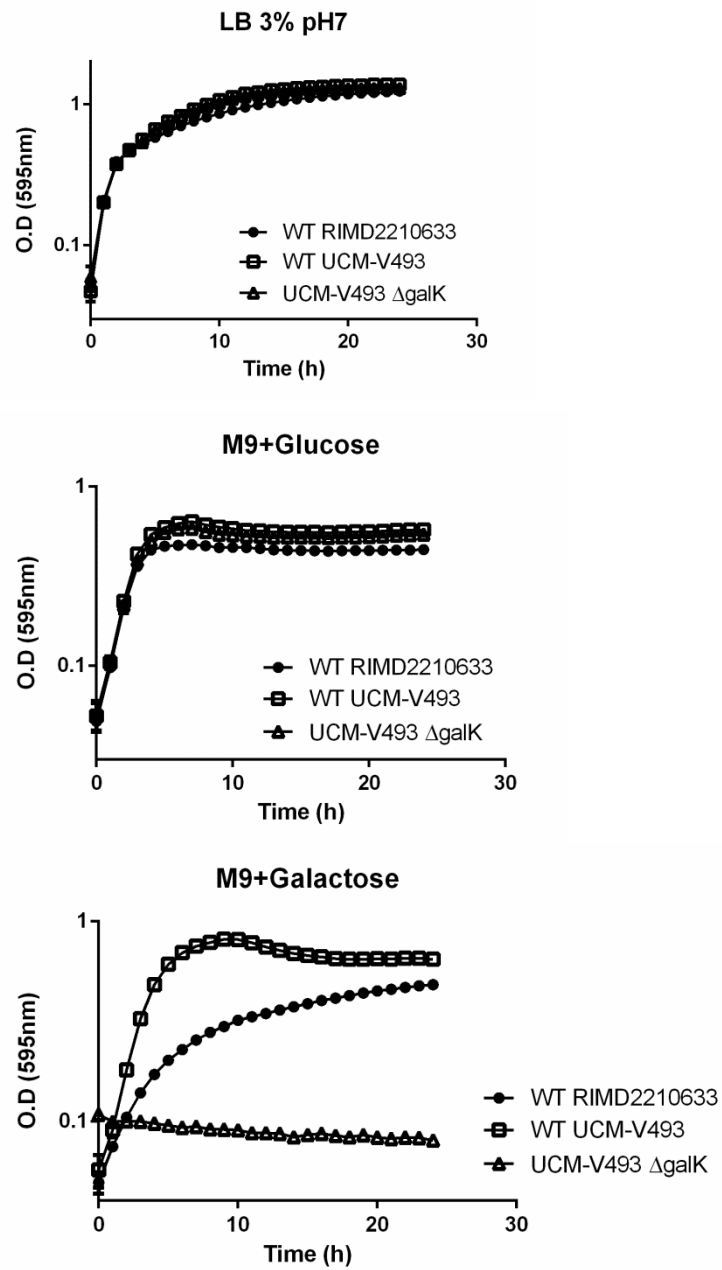


**Figure 37** Growth of RIMD2210633, UCM-V493 and UCM-V493 $\Delta$ galK on LB, M9 glucose and M9 galactose.

**Table 17 Primers used in this study**

<b>Primer</b>	<b>Sequence (5' – 3')</b>	<b>T<sub>m</sub></b>	<b>Product Size (bp)</b>
SOEVP2398A	TCT AGA TGA GCG CAA CAA CAC TTC AC	61	459
SOEVP2398B	TCG ATG CGC GAT GAT TTC	50	
SOEVP2398C	GAA ATC ATC GCG CAT CGA GAA TTC GTC CAC TGC GTT ACC	67	454
SOEVP2398D	GAG CTC TTC ATG GTG GGC TAC GAA AT	61	
SOEVP2398FLF	CAC CGT GCA GTG AGT TTT CA	53	1920
SOEVP2398FLR	CGA TGA GCA ACG AGA CGA T	53	

## Appendix E

### ADDITIONAL IN VITRO AND IN SILICO ANALYSIS OF *VIBRIO PARAHAEMOLYTICUS* QUORUM SENSING MUTANTS

Data in this appendix include additional *in vitro* characterization performed on the quorum sensing mutants that were not included in Chapter 2 of the dissertation.

#### Biofilm formation among QS regulator mutants

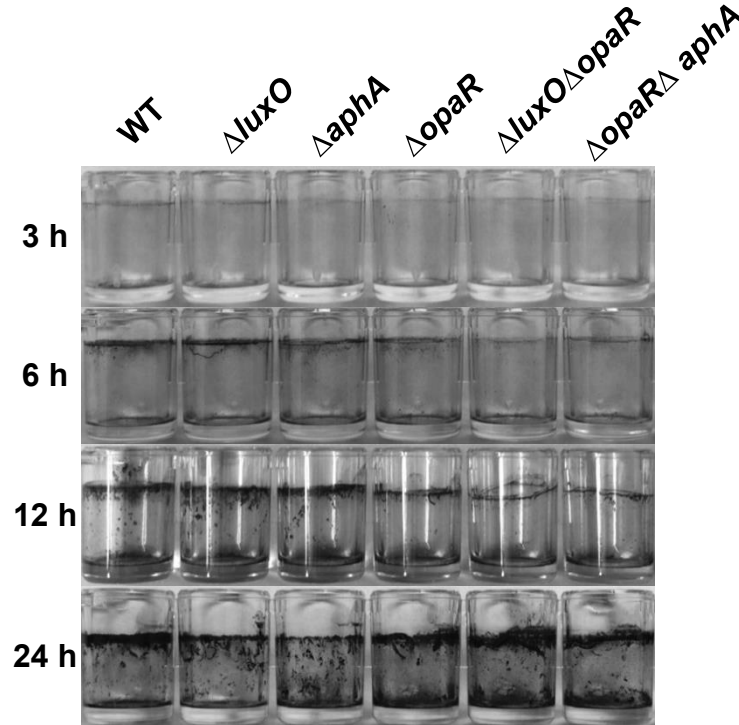
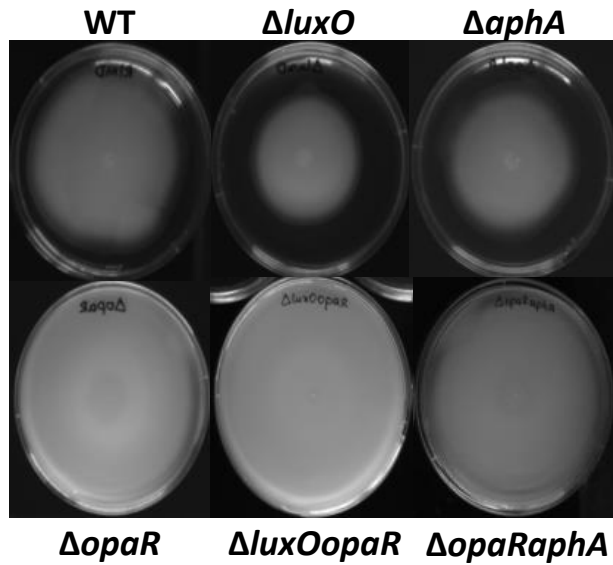


**Figure 38** Analysis of biofilm formation using the crystal violet assay. Strains were grown in 96 well strip plates statically for 24 h in LB 3% NaCl. After 24 h culture was decanted, wells were washed and crystal violet dye was added to each well. Crystal violet stained biofilm rings were imaged after 30 min of crystal violet staining at RT.

**A. Swimming motility**



**B. Swarming motility**

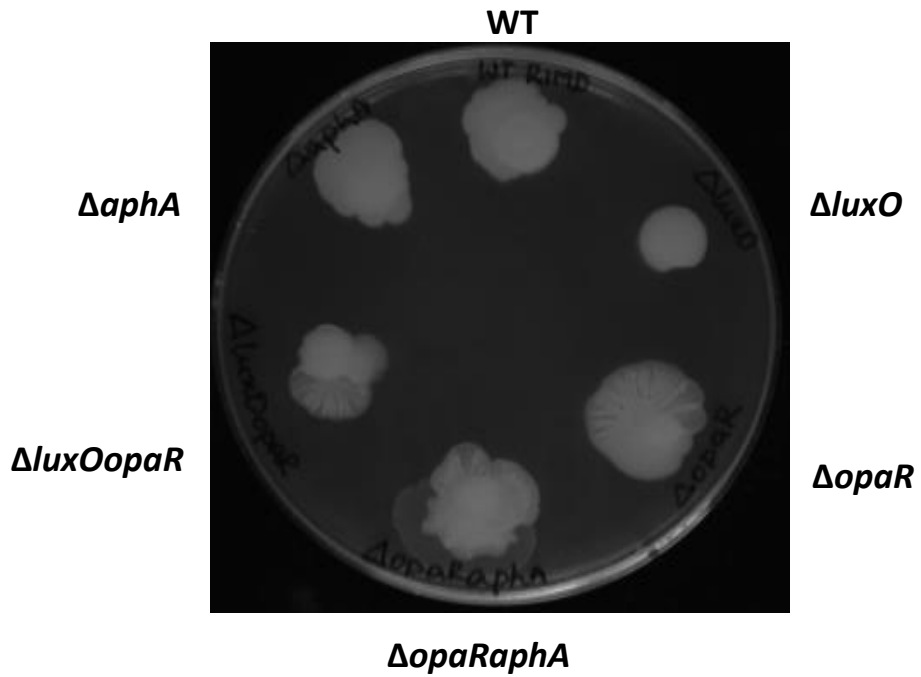
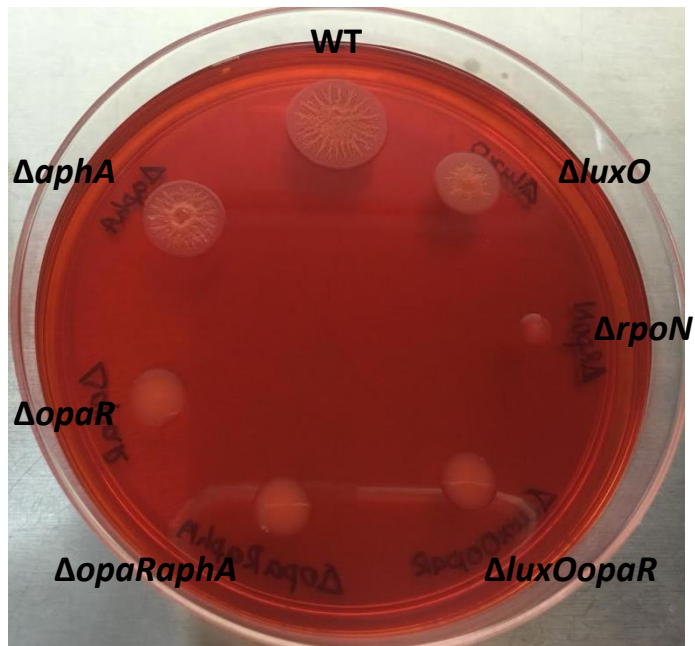


**Figure 39 Analysis of motility of the quorum sensing mutants.**

(A) Swimming motility studied using LB 2% NaCl 0.3% Agar plates. Images were taken after 18 h of incubation at 37°C (B) Swarming motility

was studied using HI 2% NaCl 1.5% Agar plates. Images were taken after 48 h of incubation at 30°C

### A. CPS Production in quorum sensing mutants



### B. CPS production in complemented strains

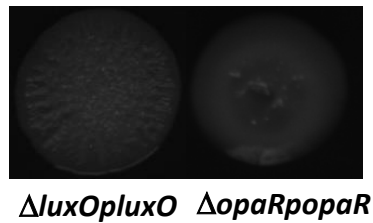


**Figure 40** Analysis of Capsule Polysaccharide (CPS) production using the Congo red assay. (A) Color image of CPS production observed for quorum sensing mutants on Congo red plate. Single colony images can be seen in Chapter 2. (B) CPS production observed in complemented strains of *luxO* and *opaR*. Complementation of *opaR* partially restores CPS production in the strain.

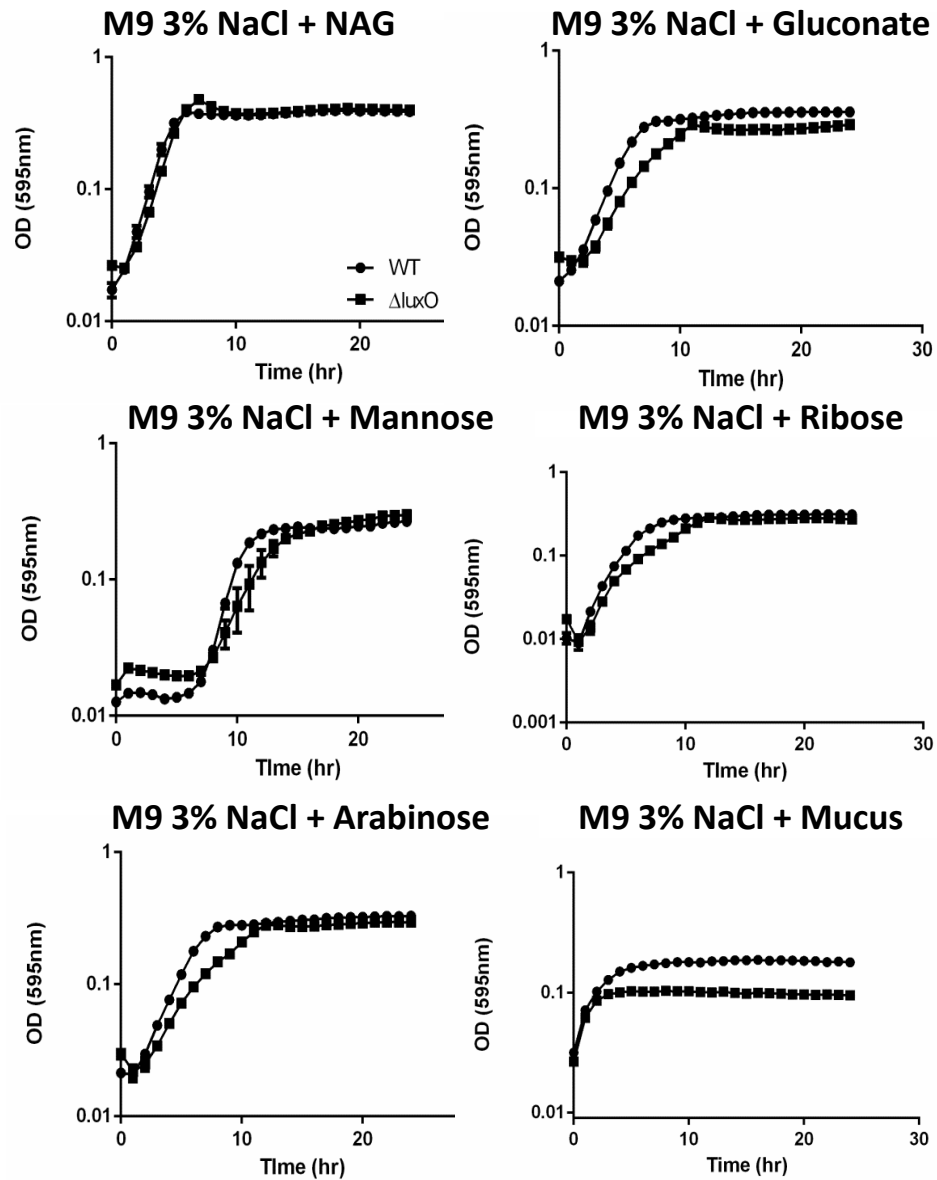


**Figure 41 Growth analysis of the  $\Delta luxO$  mutant in mucus and individual mucus components.** Strains were grown overnight in M9 3% NaCl 10mM glucose medium. Overnight cultures were centrifuged washed and then diluted 1:40 in M9 medium supplemented with 30  $\mu\text{g/ml}$  cecal mucus or 10mM of individual sugar. Strains were grown in 96 well plates at 37°C with intermittent shaking for 60s every hour. OD<sub>595</sub> was measured using a plate reader.

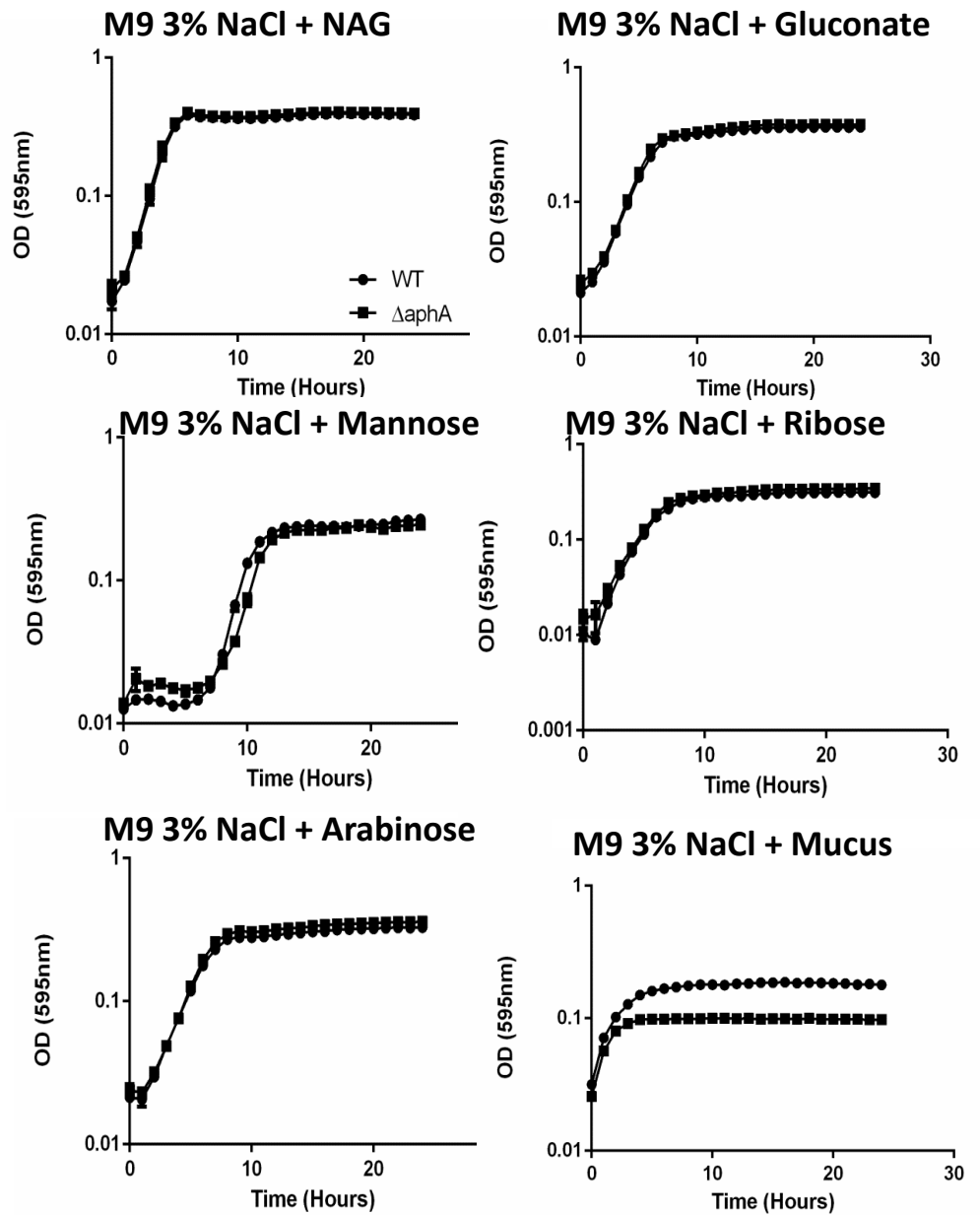


**Figure 42 Growth analysis of the  $\Delta aphA$  mutant in mucus and individual mucus components.**

Strains were grown overnight in M9 3% NaCl 10mM glucose medium. Overnight cultures were centrifuged washed and then diluted 1:40 in M9 medium supplemented with 30  $\mu$ g/ml cecal mucus or 10mM of individual

sugar. Strains were grown in 96 well plates at 37°C with intermittent shaking for 60s every hour. OD<sub>595</sub> was measured using a plate reader.

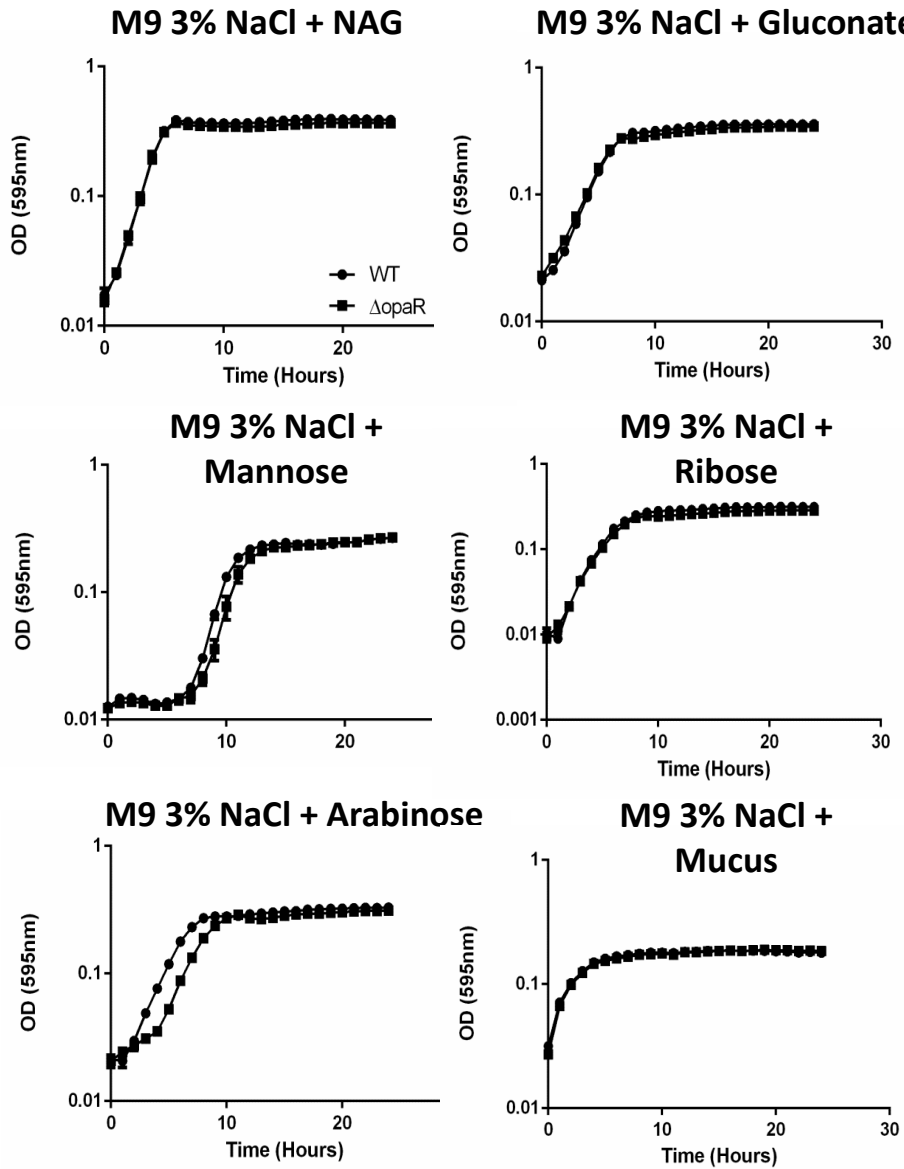


**Figure 43 Growth analysis of the  $\Delta opaR$  mutant in mucus and individual mucus components.**

Strains were grown overnight in M9 3% NaCl 10mM glucose medium. Overnight cultures were centrifuged washed and then diluted 1:40 in M9 medium supplemented with 30  $\mu$ g/ml cecal mucus or 10mM of individual

sugar. Strains were grown in 96 well plates at 37°C with intermittent shaking for 60s every hour. OD<sub>595</sub> was measured using a plate reader.

### Doubling times in mucus and mucus components

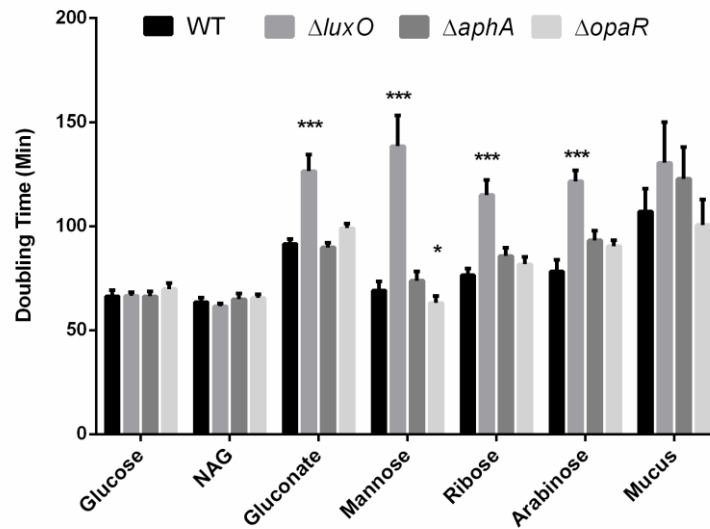


**Figure 44 Doubling times of strains grown in mucus and individual mucus components.** Doubling times of *V. parahaemolyticus* *luxO*, *aphA* and *opaR* mutants grown in mucus and individual mucus sugars. *P* values were calculated using an unpaired Student's t-test with a 95% confidence interval. Asterisks denote significant differences in doubling times between the mutant strains and the wild-type. \*, *P* < 0.05, \*\*, *P* < 0.005, \*\*\*, *P* = 0.0001

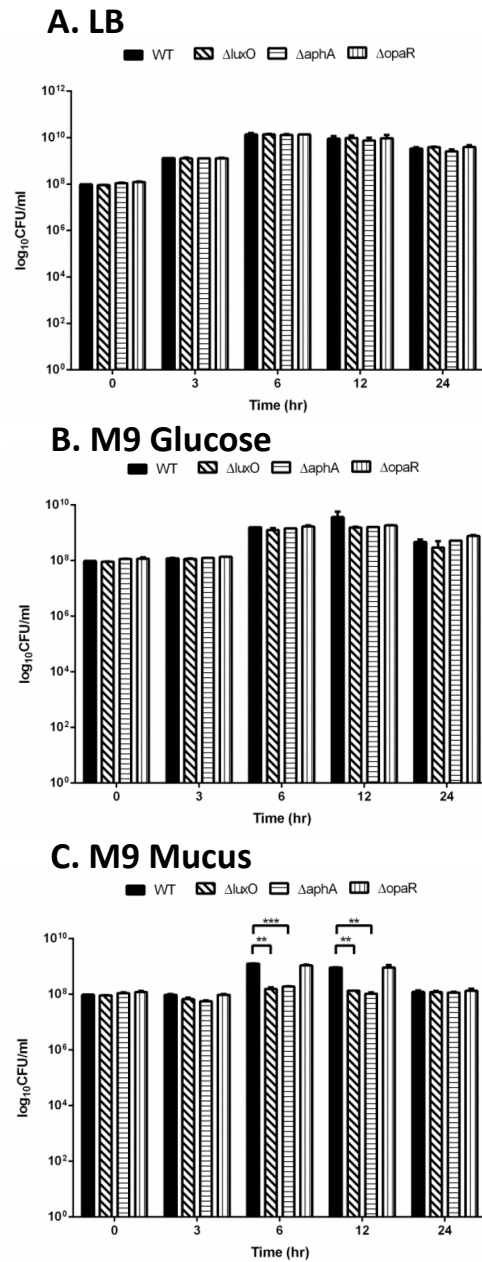


**Figure 45 Colony Forming Units (CFUs) counts for *V. parahaemolyticus*.** CFU counts for WT and QS mutants in (A) LB (B) M9 + Glucose (C) M9 + Mucus. *P* values were calculated using an unpaired Student's *t*-test with a 95% confidence interval. Asterisks denote significant differences in CFU/ml between the mutant strains and the wild-type. \*\*,  $P < 0.001$ , \*\*\*,  $P < 0.0005$

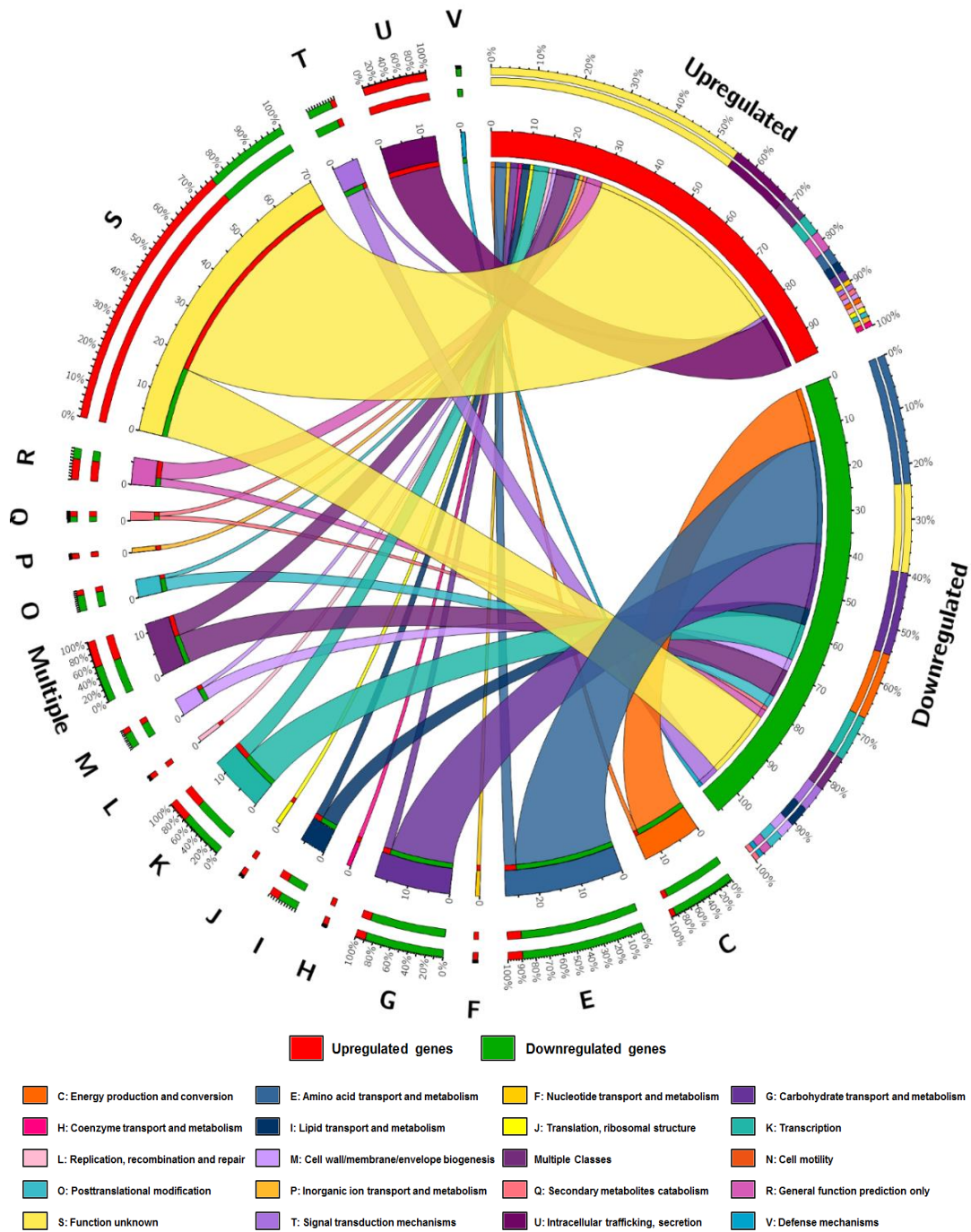
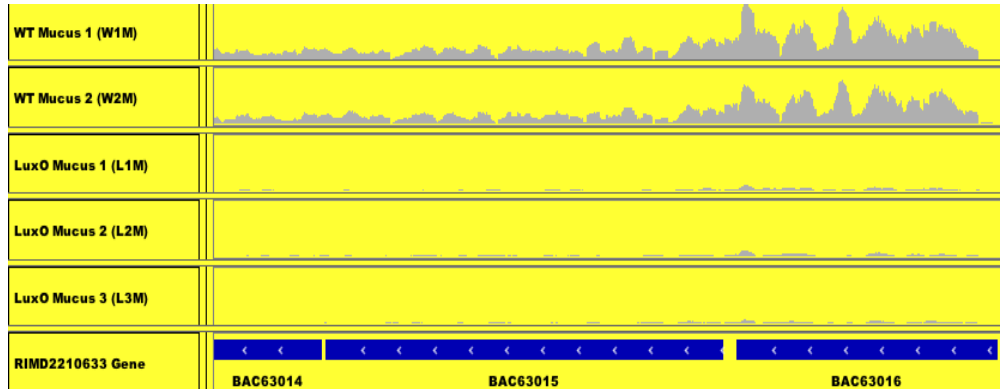
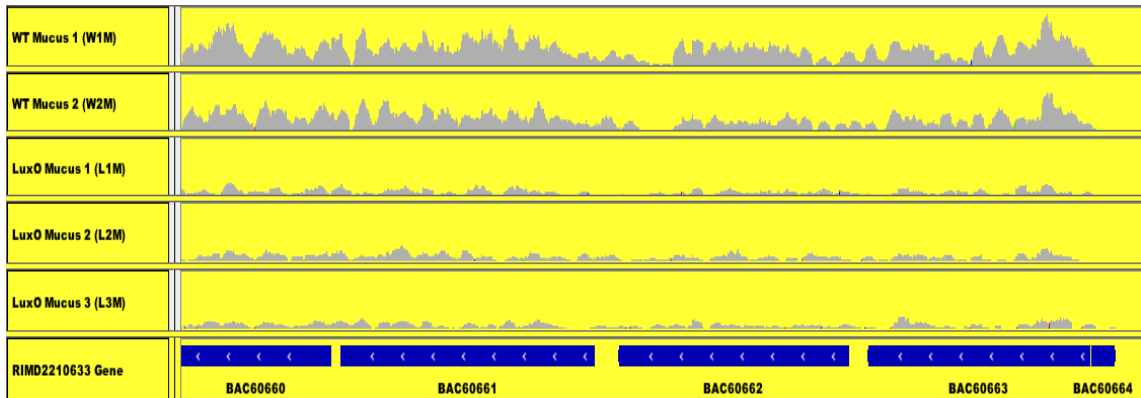


**Figure 46 COG Classification of differentially expressed genes between the *luxO* mutant and the wild-type cells grown in mucus.** Segments of the Circos Plot occur in a clockwise manner. The first two segments indicated in Red and Green represent the sum total of Upregulated and Downregulated genes respectively. Each following colored segment represents each COG class and is labelled with the letter assigned for the COG class. The size of the colored segment is representative of the number of differentially expressed genes within the segment. Colored COG classes are linked to the Red and Green segments by Ribbons. The size of the ribbon indicates the number of up or downregulated genes within each class. The outermost segment for the Upregulated and Downregulated genes indicates the percentage of genes represented by each COG class. The outermost segment for each COG class indicates the percentage of up or downregulated genes within each COG class.

### Downregulated arabinose gene cluster in *luxO* mutant



### Downregulated galactose gene cluster in *luxO* mutant



### Downregulated arginine biosynthesis gene cluster in *luxO* mutant

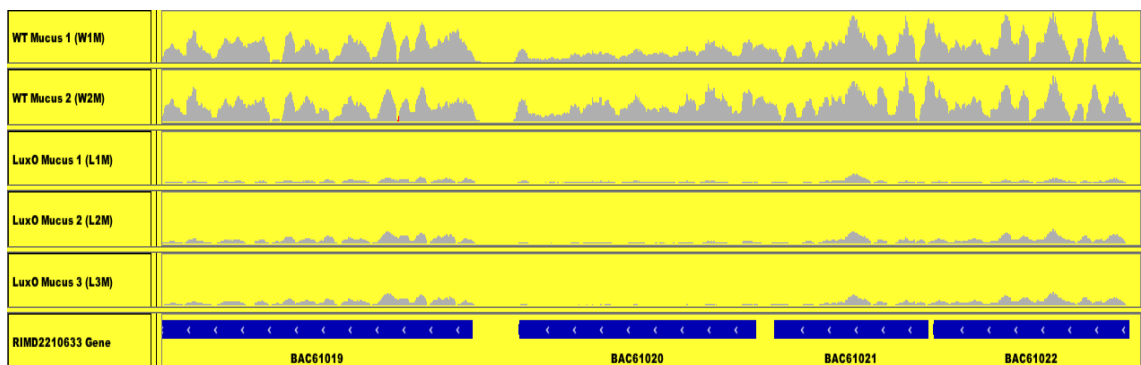
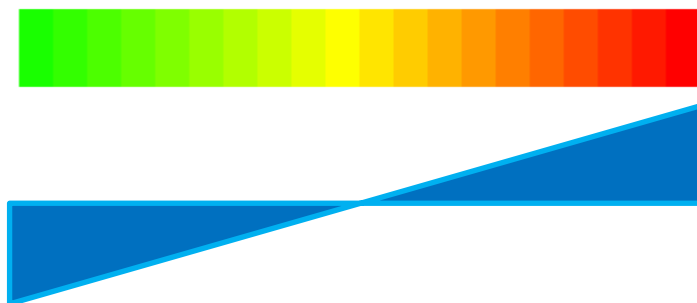
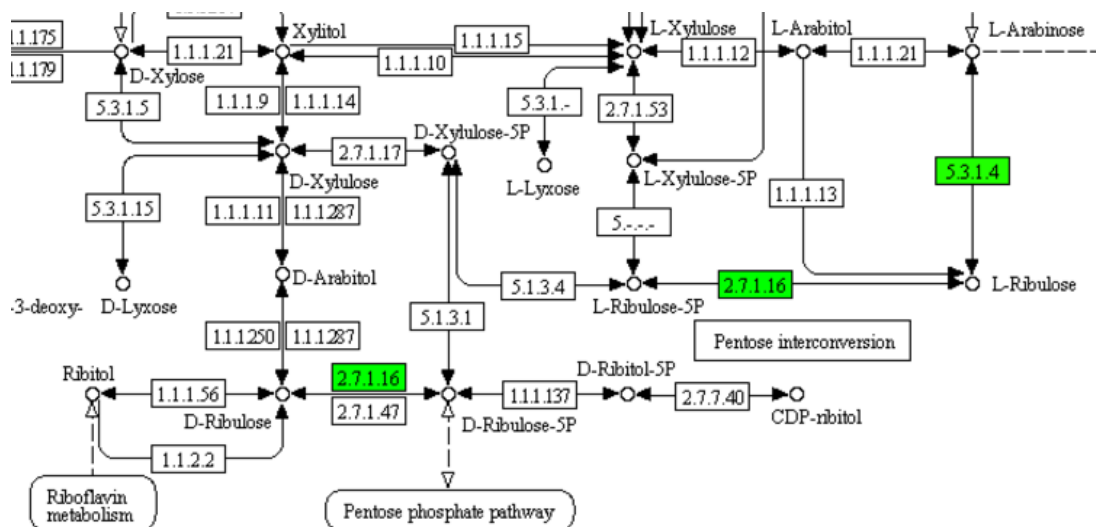


**Figure 47 Coverage across downregulated gene clusters.** Coverage plots obtained from IGV showing the comparison of coverage across the arabinose, galactose and arginine biosynthesis gene clusters in the wild-type (top two panels) and the *luxO* mutant (bottom two panels)

## Arabinose transport



## Arabinose metabolism



## Expression level

**Figure 48** Pathway analysis using KEGG colorizer. The KEGG pathway colorizer was used to represent expression. As indicated above, Green indicates downregulated genes and Red indicates upregulated genes. The downregulated arabinose transport and metabolism genes are colored green.

**Table 18 Biolog phenotype microarray data for wild-type and quorum sensing mutants.**

*P* values were calculated using an unpaired Student's *t*-test with a 95% confidence interval. Asterisks denote significant differences in AUC between the mutant strains and the wild-type. \*, *P* < 0.05, \*\*, *P* < 0.01, \*\*\*, *P* < 0.001, NS = Not Significant

Carbon Source	Area Under the Curve (AUC)								Average AUC				Statistics were performed using an Unpaired Student's <i>t</i> -Test on Graphpad software		
	WT		$\Delta luxO$		$\Delta aphA$		$\Delta opaR$		WT	$\Delta luxO$	$\Delta aphA$	$\Delta opaR$	Significant dif from WT? (P-val)		
	BR1	BR2	BR1	BR2	BR1	BR2	BR1	BR2					$\Delta luxO$	$\Delta aphA$	$\Delta opaR$
Maltotriose	12.36	11.57	11.21	11.40	10.06	10.07	11.04	11.12	11.97	11.31	10.06	11.08	NS	*	NS
$\alpha$ -D-Glucose	11.69	11.38	10.65	10.70	9.23	9.39	10.97	10.87	11.54	10.67	9.31	10.92	*	**	NS
$\alpha$ -Cyclodextrin	11.11	11.36	10.22	11.47	10.94	10.84	9.90	10.05	11.23	10.84	10.89	9.97	NS	NS	*
D-Trehalose	9.87	9.79	9.45	9.35	7.44	7.31	7.58	7.48	9.83	9.40	7.37	7.53	*	***	***
$\gamma$ -Cyclodextrin	9.68	9.81	9.03	9.95	9.98	9.01	8.53	8.61	9.75	9.49	9.49	8.57	NS	NS	**
Maltose	9.11	8.80	8.22	8.52	8.02	7.48	7.76	7.90	8.95	8.37	7.75	7.83	NS	NS	*
N-Acetyl-D-glucosamine	8.46	8.92	8.93	8.60	6.55	7.54	7.94	7.72	8.69	8.76	7.05	7.83	NS	NS	NS
D-Mannitol	8.70	8.43	7.64	7.79	6.89	8.54	6.64	6.52	8.57	7.71	7.71	6.58	*	NS	**
Dextrin	8.77	8.17	7.94	9.26	7.73	7.81	7.99	8.21	8.47	8.60	7.77	8.10	NS	NS	NS
D-Mannose	8.36	8.17	7.66	7.79	6.61	6.19	6.67	6.70	8.26	7.73	6.40	6.69	*	*	**
D-Glucose-6-Phosphate	7.54	7.68	5.90	5.72	4.74	5.15	7.35	7.31	7.61	5.81	4.95	7.33	**	**	NS

Table 18 Continued

<b>Inosine</b>	7.30	7.82	6.16	5.71	6.30	6.10	6.70	6.85	7.56	5.94	6.20	6.78	*	*	NS
D-Fructose	7.35	7.37	8.78	9.45	7.31	7.44	6.62	6.54	7.36	9.11	7.38	6.58	*	NS	**
<b><math>\beta</math>-cyclodextrin</b>	7.11	7.19	4.98	5.13	6.02	5.63	6.90	6.47	7.15	5.05	5.82	6.68	**	*	NS
L-Arabinose	6.06	7.30	6.54	6.50	5.78	5.68	4.80	4.79	6.68	6.52	5.73	4.80	NS	NS	NS
Glycogen	6.69	6.38	7.06	6.88	5.91	4.94	6.44	6.42	6.54	6.97	5.42	6.43	NS	NS	NS
<b>L-Glutamine</b>	5.70	6.85	4.19	3.80	3.10	3.25	4.45	4.92	6.27	3.99	3.18	4.69	NS	*	NS
D-Gluconic Acid	5.21	6.32	4.82	4.91	3.79	6.74	5.03	5.05	5.77	4.86	5.26	5.04	NS	NS	NS
<b>D-Fructose-6-Phosphate</b>	5.46	6.07	5.32	5.13	3.19	3.74	5.48	5.72	5.76	5.22	3.47	5.60	NS	*	NS
Fumaric Acid	5.41	5.60	4.70	4.84	4.13	2.79	4.51	4.77	5.50	4.77	3.46	4.64	*	NS	*
Glycerol	5.42	5.58	4.20	4.25	2.70	3.97	3.79	3.53	5.50	4.22	3.34	3.66	**	NS	**
$\beta$ -Methyl-D-Glucoside	5.41	5.27	4.41	4.35	3.50	3.39	4.41	4.58	5.34	4.38	3.45	4.49	**	**	*
L-Malic Acid	5.14	5.37	4.35	4.38	3.83	3.64	4.35	4.46	5.25	4.37	3.74	4.41	*	**	*
D-Lactic Acid Methyl Ester	5.05	5.22	4.41	4.44	4.14	4.45	4.45	4.20	5.14	4.42	4.29	4.32	*	*	*
<b>Glycyl-L-Aspartic Acid</b>	5.28	4.93	0.00	0.00	0.46	0.47	4.63	5.15	5.10	0.00	0.46	4.89	**	**	NS
Adenosine	5.01	5.08	4.24	3.88	4.24	3.93	4.46	4.62	5.05	4.06	4.09	4.54	*	*	*
<b>2-Deoxy Adenosine</b>	4.44	5.19	3.00	2.89	3.31	2.96	4.24	4.16	4.81	2.94	3.14	4.20	*	NS	NS
<b>L-Aspartic Acid</b>	4.35	4.58	0.94	0.96	1.90	2.41	4.84	5.16	4.46	0.95	2.15	5.00	**	*	NS
<b>D-Ribose</b>	4.69	4.04	6.53	6.90	1.54	2.29	4.45	4.23	4.36	6.71	1.92	4.34	*	*	NS
L-Proline	4.57	4.13	3.68	3.85	4.38	3.20	3.98	4.30	4.35	3.77	3.79	4.14	NS	NS	NS

Table 18 Continued

L-Glutamic Acid	3.65	4.62	2.85	2.59	3.19	3.19	3.72	3.59		4.13	2.72	3.19	3.66		NS	NS	NS
Hydroxy-L-Proline	3.97	3.95	2.89	3.38	3.61	4.42	3.69	3.75		3.96	3.13	4.01	3.72		NS	NS	*
D,L-Malic Acid	3.95	3.83	2.54	3.05	2.56	2.51	2.39	2.53		3.89	2.79	2.53	2.46		NS	**	**
Uridine	3.75	3.88	3.74	3.70	3.01	3.02	3.20	3.22		3.81	3.72	3.02	3.21		NS	**	*
<b>Succinic Acid</b>	3.54	3.90	2.57	2.32	2.76	3.05	3.61	3.37		3.72	2.44	2.90	3.49		*	NS	NS
D-Galactose	3.42	3.60	3.47	3.08	3.75	3.57	3.22	3.19		3.51	3.27	3.66	3.20		NS	NS	NS
Thymidine	3.28	3.47	3.04	2.87	2.77	2.60	2.59	2.51		3.38	2.95	2.68	2.55		NS	*	*
D-Glucuronic Acid	2.86	3.41	2.75	2.86	2.08	2.65	2.80	2.91		3.13	2.80	2.36	2.86		NS	NS	NS
Pyruvic Acid	2.55	3.46	1.73	2.12	2.05	1.91	2.41	2.67		3.01	1.92	1.98	2.54		NS	NS	NS
<b>Putrescine</b>	3.04	2.95	2.42	2.54	3.19	3.08	2.29	2.95		3.00	2.48	3.14	2.62		*	NS	NS
<b>Glycyl-L-Glutamic Acid</b>	3.19	2.77	0.08	0.00	0.16	0.19	3.09	3.16		2.98	0.04	0.18	3.12		**	**	NS
$\alpha$ -Keto-Glutaric Acid	2.71	3.21	1.52	1.96	2.16	2.41	2.71	3.13		2.96	1.74	2.29	2.92		NS	NS	NS
<b>L-Threonine</b>	3.09	2.78	0.81	0.53	3.06	2.64	3.18	3.41		2.93	0.67	2.85	3.30		**	NS	NS
D-Alanine	2.92	2.91	1.73	1.93	2.23	2.38	2.31	2.29		2.92	1.83	2.31	2.30		**	*	***
<b>L-Alanyl-Glycine</b>	3.01	2.72	0.42	0.38	0.87	1.02	3.13	3.27		2.87	0.40	0.95	3.20		**	**	NS
L-Lactic Acid	2.97	2.68	2.08	2.49	2.36	2.12	2.69	2.62		2.82	2.29	2.24	2.66		NS	NS	NS
<b>Tween 40</b>	2.69	2.89	1.20	1.31	3.18	1.83	3.95	2.50		2.79	1.25	2.51	3.23		**	NS	NS
Bromo Succinic Acid	2.54	2.60	2.14	2.13	1.48	1.28	1.78	1.87		2.57	2.14	1.38	1.83		**	**	**

Table 18 Continued

L-Asparagine	2.29	2.65	2.60	2.07	2.97	2.97	2.36	2.54		2.47	2.33	2.97	2.45		NS	NS	NS
Inulin	3.61	1.31	2.92	1.22	1.18	1.45	2.05	2.40		2.46	2.07	1.31	2.22		NS	NS	NS
<b>L-Serine</b>	2.42	2.41	0.81	0.45	1.76	1.83	2.55	2.78		2.41	0.63	1.79	2.67		*	**	NS
L-Alanine	2.45	2.37	1.87	1.69	2.55	2.82	1.98	1.81		2.41	1.78	2.69	1.90		*	NS	*
Pectin	1.85	2.45	3.32	2.82	3.01	2.85	2.67	3.94		2.15	3.07	2.93	3.31		NS	NS	NS
<b>Methyl Pyruvate</b>	2.18	1.98	2.28	2.24	1.34	1.40	1.87	1.86		2.08	2.26	1.37	1.86		NS	*	NS
<b>Tween 80</b>	2.09	1.98	1.03	1.06	1.38	1.19	2.03	2.01		2.04	1.04	1.28	2.02		**	*	NS
D,L- $\alpha$ -Glycerol-Phosphate	1.85	2.12	1.73	1.65	1.70	1.76	1.83	2.18		1.98	1.69	1.73	2.00		NS	NS	NS
D-Malic Acid	1.77	1.98	1.61	1.73	1.63	1.40	1.15	1.11		1.88	1.67	1.52	1.13		NS	NS	*
<b>Glycyl-L-Proline</b>	1.76	1.71	0.30	0.05	0.30	0.34	1.85	1.99		1.74	0.18	0.32	1.92		**	***	NS
Gelatin	1.63	1.83	2.75	3.94	2.90	2.87	1.70	2.22		1.73	3.34	2.88	1.96		NS	**	NS
<b>Tween 20</b>	1.69	1.57	0.66	0.60	1.32	0.60	2.27	2.11		1.63	0.63	0.96	2.19		**	NS	*
<b><math>\alpha</math>-Hydroxyl Glutaric Acid-<math>\gamma</math>-Lactone</b>	1.72	1.44	0.00	0.20	1.51	2.05	1.88	2.06		1.58	0.10	1.78	1.97		*	NS	NS
L-Arginine	1.64	1.52	0.80	1.12	1.58	1.45	1.88	1.93		1.58	0.96	1.51	1.90		NS	NS	*
L-Histidine	1.65	1.41	1.72	1.70	1.54	1.69	1.79	2.10		1.53	1.71	1.62	1.95		NS	NS	NS
<b>L-Ornithine</b>	1.61	1.41	0.78	0.71	0.90	0.83	2.00	2.18		1.51	0.75	0.87	2.09		*	*	NS
Dulcitol	1.43	1.53	0.98	0.91	1.16	1.21	1.10	1.09		1.48	0.95	1.18	1.09		*	*	*
Chondroitin Sulfate C	1.42	1.52	1.35	1.31	1.28	1.34	1.11	1.29		1.47	1.33	1.31	1.20		NS	NS	NS
Glycine	1.51	1.35	1.11	1.76	1.21	1.37	1.55	1.73		1.43	1.43	1.29	1.64		NS	NS	NS

Table 18 Continued

Acetic Acid	1.30	1.34	1.23	1.54	0.98	1.20	1.11	1.35		1.32	1.38	1.09	1.23		NS	NS	NS
<b>D-Cellobiose</b>	1.09	1.01	0.31	0.36	0.49	0.43	1.14	0.99		1.05	0.33	0.46	1.06		**	**	NS
$\alpha$ -D-Lactose	0.99	1.07	0.34	1.02	0.50	0.78	0.79	0.85		1.03	0.68	0.64	0.82		NS	NS	NS
L-Leucine	2.41	0.00	4.28	0.00	1.00	0.00	0.00	0.00		1.20	2.14	0.50	0.00		NS	NS	NS

**Table 19 Summary of quorum sensing biolig data.** Numbers indicate carbon sources with significant difference in AUC compared to wild-type.

Summary	
Defective in $\Delta luxO$	<b>33</b>
Defective in $\Delta aphA$	<b>30</b>
Defective in $\Delta opaR$	<b>22</b>
Defective in $\Delta luxO$ only	<b>7</b>
Defective in $\Delta aphA$ only	<b>5</b>
Defective in $\Delta opaR$ only	<b>6</b>
Defective in $\Delta luxO$ and $\Delta aphA$ only	<b>13</b>
Defective in $\Delta luxO$ and $\Delta opaR$ only	<b>4</b>
Defective in $\Delta aphA$ and $\Delta opaR$ only	<b>3</b>
Defective in $\Delta luxO$ , $\Delta aphA$ and $\Delta opaR$	<b>9</b>
Grows better in $\Delta luxO$	<b>2</b>
Grows better in $\Delta aphA$	<b>1</b>
Grows better in $\Delta opaR$	<b>2</b>
Grows better in $\Delta luxO$ only	<b>2</b>
Grows better in $\Delta aphA$ only	<b>1</b>
Grows better in $\Delta opaR$ only	<b>2</b>
Grows better in $\Delta luxO$ and $\Delta aphA$ only	<b>0</b>
Grows better in $\Delta luxO$ and $\Delta opaR$ only	<b>0</b>
Grows better in $\Delta aphA$ and $\Delta opaR$ only	<b>0</b>
Grows better in $\Delta luxO$ , $\Delta aphA$ and $\Delta opaR$	<b>0</b>

## Appendix F

### **RNASEQ EXPRESSION ANALYSIS OF THE WILD-TYPE AND THE *LUXO* MUTANT IN GLUCOSE.**

*Vibrio parahaemolyticus* wild-type and mutant strains were grown for 4 h in LB 3% NaCl and then diluted 1:50 into M9 medium supplemented with glucose and grown statically at 37°C for 90 min. Total RNA was extracted from cells obtained by centrifugation at the end of 90 mins using Trizol extraction method and sequencing was performed using ribosomal RNA depleted samples as detailed in Chapter 2 and Chapter 3. Data was obtained from a single biological replicate of the *luxO* mutant and two biological replicates of the wild-type. Each sample was sequenced twice yielding two technical replicates for each biological replicate. Differential expression analysis revealed that 97 genes were upregulated and 121 genes were downregulated in the *luxO* mutant compared to wild-type (**Figure 49 and Table 20 and Table 21**).

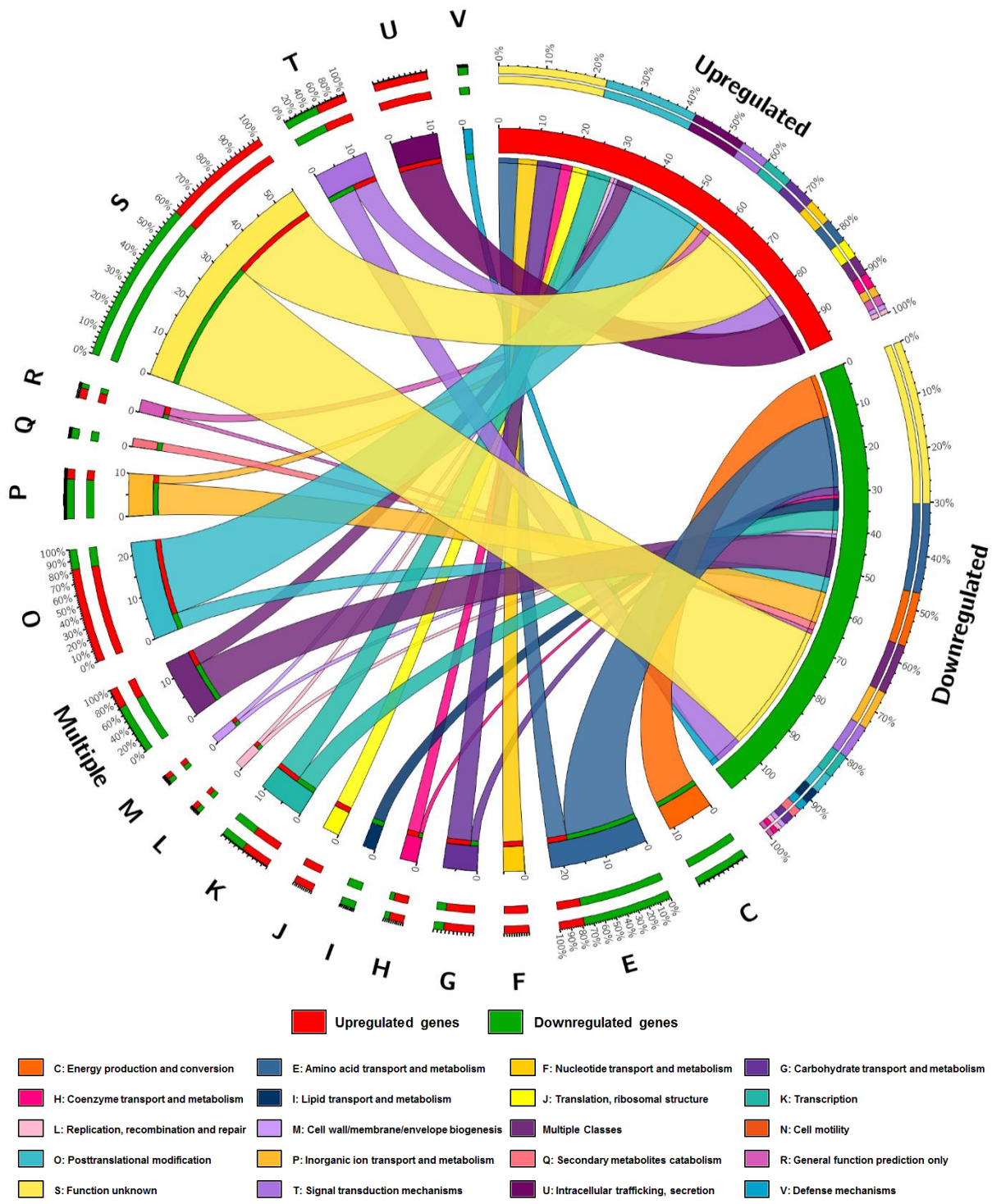


**Figure 49 COG Classification of differentially expressed genes between the *luxO* mutant and the wild-type cells grown in glucose.** Segments of the Circos Plot occur in a clockwise manner. The first two segments indicated in Red and Green represent the sum total of Upregulated and Downregulated genes respectively. Each following colored segment represents each COG class and is labelled with the letter assigned for the COG class. The size of the colored segment is representative of the number of differentially expressed genes within the segment. Colored COG classes are linked to the Red and Green segments by Ribbons. The size of the ribbon indicates the number of up or downregulated genes within each class. The outermost segment for the Upregulated and Downregulated genes indicates the percentage of genes represented by each COG class. The outermost segment for each COG class indicates the percentage of up or downregulated genes within each COG class.

**Table 20 Genes upregulated in the *luxO* mutant in glucose**

<b>Locus Tag</b>	<b>Common Name of Primary Target</b>	<b>baseMean</b>	<b>log2Fold Change</b>	<b>padj</b>
VP0018	16 kDa heat shock protein A	2277.82	1.55	1.90E-25
VP0070	oligopeptidase A	5413.44	1.16	5.47E-12
VP0130	Hsp33-like chaperonin	836.94	1.16	1.48E-35
VP0131	hypothetical protein	334.79	1.14	1.23E-12
VP0150	hypothetical protein	1572.62	1.56	7.76E-49
VP0178	orotate phosphoribosyltransferase	419.30	1.01	1.60E-05
VP0228	putative integral membrane protein	91.26	1.04	0.001522237
VP0249	ATP-dependent protease ATP-binding subunit	6043.94	1.35	6.01E-20
VP0250	ATP-dependent protease peptidase subunit	1436.39	1.38	7.16E-32
VP0433	protease DO	5092.66	1.05	5.35E-09
VP0467	translocase	8389.23	1.21	4.64E-41
VP0468	mutator MutT protein	153.76	1.31	9.73E-12
VP0472	hypothetical protein	27.92	1.07	0.000920474
VP0561	ClpB protein	12957.44	1.32	7.78E-15
VP0562	hypothetical protein	436.09	1.48	5.11E-30
VP0590	protein export protein SecD	640.61	1.22	2.89E-19
VP0591	protein export protein SecF	480.23	1.02	4.42E-15
VP0651	GrpE	1033.67	1.36	8.31E-26
VP0653	molecular chaperone DnaK	17700.55	1.50	3.82E-136
VP0654	DnaJ protein	3760.72	1.05	2.08E-06
VP0806	hypothetical protein	1461.61	1.35	1.76E-66
VP0821	heat shock protein 90	3410.16	1.78	4.40E-36
VP0831	PTS system, N-acetylglucosamine-specific IIBC component	350.42	1.00	2.14E-15
VP0916	trigger factor	5100.64	1.57	3.76E-114
VP0919	ATP-dependent protease LA	20678.03	1.03	2.86E-35
VP0962	hypothetical protein	2963.61	2.01	4.97E-137
VP1242	hypothetical protein	584.53	1.26	1.07E-08
VP1408	putative IcmF-related protein	191.09	1.15	3.54E-13

Table 20 Continued

VP1438	DnaK-related protein	1012.27	2.30	1.22E-129
VP1439	DnaK-related protein	2082.56	1.67	1.26E-72
VP1440	hypothetical protein	428.92	1.17	1.74E-24
VP1443	hypothetical protein	426.59	1.12	5.46E-22
VP1704	sigma-54 dependent transcriptional regulator	316.07	1.40	3.65E-22
VP1719	aspartate kinase	20808.15	1.19	1.30E-14
VP1720	ectoine synthase	10324.41	1.08	9.27E-09
VP1721	diaminobutyrate--2-oxoglutarate aminotransferase	31874.80	1.20	1.04E-29
VP1722	L-2,4-diaminobutyric acid acetyltransferase	9855.71	1.01	4.87E-20
VP1754	hypothetical protein	571.16	1.04	1.34E-12
VP1810	hypothetical protein	72.75	1.14	0.000233039
VP1812	hypothetical protein	1894.41	1.79	2.04E-31
VP1850	putative acetyltransferase	131.44	1.21	1.75E-08
VP1851	hypothetical protein	495.20	1.24	1.68E-30
VP1921	GTP cyclohydrolase II protein	1130.53	1.11	7.93E-37
VP1968	sensor protein LuxN	355.41	1.09	4.88E-13
VP2000	putative ribosomal-protein-alanine N-acetyltransferase	31.64	1.09	0.000378731
VP2001	hypothetical protein	39.02	1.00	0.000849239
VP2002	hypothetical protein	74.35	1.15	1.67E-06
VP2003	hypothetical protein	92.26	1.30	3.95E-08
VP2021	hypothetical protein	56.17	1.01	0.000292284
VP2038	transcriptional regulator, ROK family	232.04	1.28	1.06E-17
VP2098	phosphorelay protein	2135.52	3.19	2.50E-136
VP2177	recombination protein RecR	927.74	1.36	1.00E-48
VP2178	hypothetical protein	634.85	1.05	6.61E-26
VP2283	uracil permease	515.30	1.23	1.68E-30
VP2324	hypothetical protein	751.46	1.51	7.01E-42
VP2325	hypothetical protein	232.83	1.27	1.24E-10
VP2516	OpaR	2975.71	1.61	9.26E-52
VP2537	S-ribosylhomocysteinase	1255.59	1.31	3.19E-09

Table 20 Continued

VP2538	hypothetical protein	1112.06	1.37	7.53E-26
VP2539	glutamate--cysteine ligase	3205.22	1.21	1.41E-17
VP2610	hypothetical protein	722.96	1.13	5.27E-29
VP2611	glutathione synthetase	1585.16	1.34	3.99E-45
VP2612	hypothetical protein	507.64	1.36	1.17E-25
VP2613	Holliday junction resolvase-like protein	261.51	1.17	5.75E-17
VP2654	aspartate carbamoyltransferase catalytic subunit	900.57	1.35	4.20E-09
VP2655	aspartate carbamoyltransferase regulatory subunit	553.50	1.21	2.46E-06
VP2830	hypothetical protein	304.23	1.46	7.78E-27
VP2831	export protein SecB	1453.91	2.06	2.04E-121
VP2851	chaperonin GroEL	5814.98	2.05	6.53E-115
VP2852	co-chaperonin GroES	627.05	2.31	2.16E-79
VPA0166	putative outer membrane protein	19590.77	1.88	1.23E-42
VPA0182	putative C4-dicarboxylate transport sensor protein	118.20	1.53	1.41E-15
VPA0183	C4-dicarboxylate transport transcriptional regulatory protein	197.67	1.42	1.20E-15
VPA0286	co-chaperonin GroES	132.22	1.97	2.54E-24
VPA0287	chaperonin GroEL	716.37	1.54	1.00E-55
VPA0606	putative AraC-type regulatory protein	62.74	1.12	2.08E-05
VPA0658	iron(III) ABC transporter, permease protein	64.26	1.15	8.43E-06
VPA1032	hypothetical protein	30.44	1.24	0.000236973
VPA1033	hypothetical protein	62.17	1.17	3.95E-06
VPA1034	hypothetical protein	133.39	1.48	1.09E-11
VPA1035	hypothetical protein	42.77	1.63	8.73E-09

Table 20 Continued

VPA1039	hypothetical protein	239.71	1.06	5.77E-11
VPA1040	hypothetical protein	59.46	1.31	3.08E-06
VPA1041	hypothetical protein	74.57	1.44	1.12E-09
VPA1220	sensor protein LuxQ	1000.76	1.07	2.18E-32
VPA1255	hypothetical protein	7458.00	2.33	8.05E-125
VPA1400	maltose ABC transporter, permease protein	221.59	1.63	2.47E-24
VPA1401	periplasmic maltose-binding protein	668.49	1.15	1.85E-16
VPA1457	GGDEF family protein	49.53	1.06	7.51E-05
VPA1496	prolyl endopeptidase	2567.80	1.29	1.36E-13
VPA1503	CsuE	92.19	1.02	1.70E-06
VPA1618	glycogen branching enzyme	301.21	1.12	8.93E-18
VPA1619	4-alpha-glucanotransferase	373.45	1.15	4.66E-16
VPA1620	maltodextrin phosphorylase	879.51	1.34	8.45E-30
VPA1648	hypothetical protein	574.03	1.20	3.05E-17
VPA1651	putative methyl-accepting chemotaxis protein	326.06	1.23	1.14E-16
VPA1685	putative lactoylglutathione lyase	79.32	1.02	1.67E-05

**Table 21 Genes downregulated in the *luxO* mutant in glucose**

<b>Locus Tag</b>	<b>Common Name of Primary Target</b>	<b>baseMean</b>	<b>log2FoldChange</b>	<b>padj</b>
VP0006	amino acid ABC transporter, ATP-binding protein	551.88	-1.86	1.01E-57
VP0007	amino acid ABC transporter, permease protein	400.27	-1.50	3.04E-35
VP0008	amino acid ABC transporter, periplasmic amino acid-binding portion	1838.39	-2.19	1.16E-35
VP0060	putative multidrug transmembrane resistance signal peptide protein	369.47	-1.69	1.24E-30
VP0061	putative multidrug transmembrane resistance signal peptide protein	523.09	-1.53	5.81E-27
VP0084	hypothetical protein	5486.89	-1.07	1.37E-06
VP0086	hypothetical protein	3353.37	-1.08	4.15E-06
VP0291	uroporphyrin-III C-methyltransferase	3861.33	-2.34	6.67E-142
VP0292	sulfate adenylyltransferase subunit 2	4728.21	-2.21	1.55E-259
VP0293	sulfate adenylyltransferase subunit 1	6793.68	-2.25	5.98E-183
VP0295	putative sodium/sulfate symporter	1315.23	-2.18	3.48E-37
VP0296	adenylylsulfate kinase	420.30	-1.70	1.52E-12
VP0341	hypothetical protein	327.56	-1.23	9.77E-17
VP0360	hypothetical protein	16532.43	-4.49	0
VP0361	putative two component response regulator transcription regulator protein	1909.14	-3.79	2.11E-95
VP0362	putative two component sensor protein	742.25	-2.76	8.12E-33
VP0379	putative ABC transporter substrate binding protein	9651.40	-1.23	3.68E-25
svpa509.1	Thr_leader	544.24	-1.05	1.02E-06
VP0494	bifunctional aspartokinase I/homoserine dehydrogenase I	11334.92	-1.15	7.49E-28
VP0495	homoserine kinase	3532.05	-1.01	2.87E-15
VP0540	putative carbon starvation protein A	6499.94	-1.80	3.29E-45
VP0704	lipoprotein YaeC	5519.10	-1.44	8.43E-44

Table 21 Continued

VP0705	ABC transporter, permease protein	2249.21	-1.30	1.68E-16
VP0706	ABC transporter, ATP-binding protein	4156.76	-1.39	7.40E-28
EBG00000 020394	tRNA-Leu-7	143.80	-1.37	2.42E-10
VP0757	hypothetical protein	3460.62	-3.04	3.57E-142
VP0758	cation transport ATPase, E1-E2 family	19577.03	-2.97	0
VP0797	cysteine synthase A	6750.85	-1.65	6.91E-45
VP0826	asparagine synthetase B	6567.83	-1.07	2.07E-08
VP0935	hypothetical protein	142.47	-1.90	4.36E-14
svpa996.1	ffs	3685.47	-1.39	1.12E-24
rfam_sRN A_1	Bacteria_small_SRP	3685.47	-1.39	1.12E-24
VP0994	formate acetyltransferase	9378.58	-1.30	1.23E-81
VP0995	hypothetical protein	2045.29	-1.20	8.22E-46
VP1027	hypothetical protein	429.53	-1.08	1.27E-10
EBG00000 020408	tRNA-Ser-1	767.74	-1.21	0.000257 38
VP1103	alanine dehydrogenase	1637.98	-1.21	2.73E-23
VP1213	hypothetical protein	728.95	-1.03	1.16E-18
VP1264	hypothetical protein	2663.35	-1.30	8.27E-13
VP1351	hypothetical protein	304.94	-1.12	1.54E-10
VP1447	putative anaerobic dimethyl sulfoxide reductase, subunit A	1122.99	-2.21	6.43E-119
VP1448	anaerobic dimethyl sulfoxide reductase, subunit B	283.50	-2.30	1.33E-40
VP1449	putative anaerobic dimethyl sulfoxide reductase, chain C	331.33	-1.95	1.14E-18
VP1450	putative component of anaerobic dehydrogenase	206.93	-1.58	6.00E-11
VP1451	putative ferredoxin-type protein NapF	123.90	-1.96	2.14E-17
VP1514	formate dehydrogenase, iron-sulfur subunit	75.91	-1.02	1.77E-05
svpa1856.1	Glycine riboswitch	941.56	-1.05	2.55E-29

Table 21 Continued

VP1745	lipid A biosynthesis lauroyl acyltransferase	635.87	-2.26	3.36E-32
VP1751	homoserine O-succinyltransferase	7424.95	-1.25	2.99E-20
VP1966	proton/glutamate symporter	407.85	-1.66	3.54E-38
VP1975	hypothetical protein	1123.34	-1.33	8.77E-28
VP1976	transcriptional activator MetR	11177.54	-1.24	3.02E-32
VP2099	LuxO repressor protein	987.00	-2.14	7.62E-11
VP2121	alcohol dehydrogenase/acetaldehyde dehydrogenase	37300.12	-1.42	2.57E-54
VP2210	RNA polymerase sigma-70 factor	1424.02	-1.60	1.90E-47
VP2211	hypothetical protein	2110.75	-1.67	1.14E-103
VP2266	hypothetical protein	1236.75	-1.64	1.75E-28
VP2334	hypothetical protein	2431.45	-1.11	1.59E-62
VP2337	sodium-dependent transporter	877.77	-1.02	8.21E-10
VP2493	nitrogen regulatory protein P-II	148.59	-1.23	2.60E-08
EBG00000 020343	tRNA-Ser-3	2888.35	-1.02	0.003022 557
EBG00000 020310	5Sc	10967.72	-1.06	2.66E-09
EBG00000 020444	tRNA-Leu-13	71.54	-1.58	5.34E-11
VP2720	phosphoadenosine phosphosulfate reductase	2500.79	-1.68	1.97E-31
VP2721	sulfite reductase (NADPH) hemoprotein beta-component	8489.55	-2.03	1.16E-118
VP2722	sulfite reductase (NADPH) flavoprotein alpha-component	9095.14	-2.00	2.87E-246
VP2762	AphA	1133.68	-1.33	2.66E-57
VP2763	5,10-methylenetetrahydrofolate reductase	39226.22	-1.29	4.73E-40
VP2764	bifunctional aspartate kinase II/homoserine dehydrogenase II	25904.67	-1.03	6.22E-22
VP2765	cystathionine gamma-synthase	14746.36	-1.12	4.85E-28
VP2869	sodium/solute symporter	30614.91	-1.07	1.23E-62
VP2870	hypothetical protein	1379.69	-1.01	1.12E-10
VP2876	hypothetical protein	2684.63	-1.04	1.10E-17

Table 21 Continued

VP2878	acetyl-coenzyme A synthetase	18222.96	-1.15	3.84E-36
VP3014	putative signal peptide protein	1554.64	-1.76	4.95E-96
VP3015	hypothetical protein	853.46	-1.66	8.98E-52
VP3016	hypothetical protein	372.91	-1.61	3.36E-39
VP3017	putative transmembrane protein	203.48	-1.63	7.03E-15
VPA0067	hypothetical protein	231.13	-1.24	4.13E-14
VPA0068	GGDEF family protein	460.68	-1.28	7.62E-29
VPA0128	biotin sulfoxide reductase	419.03	-1.17	1.68E-12
VPA0185	putative branched chain amino acid transporter	473.86	-1.09	2.07E-06
svpa201.1	Qrr4	83.38	-2.61	4.00E-21
VPA0206	hypothetical protein	918.78	-1.77	6.97E-32
VPA0207	bifunctional methionine sulfoxide reductase A/B protein	2914.56	-1.85	4.84E-73
VPA0251	transcriptional regulator, LysR family	126.46	-1.36	1.67E-12
VPA0312	hypothetical protein	969.76	-1.00	1.93E-08
VPA0345	hypothetical protein	517.60	-1.19	1.52E-12
VPA0479	hypothetical protein	2606.50	-1.48	4.42E-25
VPA0480	putative cation efflux system transmembrane protein	4237.41	-1.66	3.23E-23
VPA0481	putative cation efflux system transmembrane protein	1914.82	-1.72	5.75E-36
VPA0482	putative outer membrane cation efflux protein	3456.48	-1.96	7.89E-103
VPA0483	hypothetical protein	716.92	-1.74	3.18E-36
VPA0484	hypothetical protein	6867.60	-1.96	1.57E-68
VPA0507	hypothetical protein	37.59	-2.29	1.33E-14
VPA0510	hypothetical protein	62.07	-1.06	0.000115325
VPA0524	glutaredoxin-related protein	1097.49	-1.42	4.04E-58
VPA0636	arginine ABC transporter, ATP-binding protein	1619.30	-1.04	4.69E-46
VPA0637	arginine ABC transporter, periplasmic arginine-binding protein	2589.40	-1.12	1.59E-25

Table 21 Continued

VPA0638	arginine ABC transporter, permease protein	1570.11	-1.03	1.04E-13
VPA0639	arginine ABC transporter, permease protein	1310.45	-1.02	1.97E-10
VPA0640	putative protocatechuate 3,4-dioxygenase beta chain protein	130.12	-1.09	3.71E-07
VPA0699	hypothetical protein	595.95	-1.01	1.53E-10
VPA0706	C4-dicarboxylate transporter, anaerobic	171.35	-1.13	7.72E-11
VPA0717	putative transcriptional regulator, LysR family	210.98	-1.75	2.25E-29
QRR5	Quorum Regulatory RNA 5	73.75	-2.76	8.14E-25
VPA0854	hypothetical protein	896.35	-1.04	8.19E-22
VPA0933	hypothetical protein	2331.67	-1.58	1.90E-25
VPA1012	cytochrome c554	329.49	-1.61	4.30E-17
VPA1123	putative acyl-CoA thiolase	3467.04	-1.00	3.84E-21
VPA1195	nitrate/nitrite response regulator protein	583.39	-1.18	4.35E-15
VPA1196	nitrate/nitrite sensor protein NarQ	1627.70	-1.46	1.56E-49
VPA1272	hypothetical protein	2119.11	-1.17	9.34E-11
VPA1462	methyl-accepting chemotaxis protein	464.48	-1.87	2.19E-47
VPA1515	putative two-component sensor histidine kinase	310.60	-1.31	4.42E-21
VPA1516	putative two-component response regulator	315.79	-1.35	2.02E-16
VPA1576	putative transmembrane protein	80.27	-1.77	7.85E-15
VPA1610	hypothetical protein	3726.26	-1.24	4.97E-12
VPA1615	putative outer membrane protein	432.15	-1.31	1.96E-30
svpa1729.1	Qrr2	42.58	-2.05	9.88E-13
VPA1667	PTS system, glucose-specific IIBC component	166.57	-1.31	2.28E-12

## Appendix G

### ROLE OF QUORUM SENSING IN OSMOTIC STRESS RESPONSE IN *VIBRIO PARAHAEMOLYTICUS*

RNASeq analysis revealed that the ectoine biosynthesis gene cluster (VP1722-1719) was upregulated in the *luxO* mutant compared to wild-type. We performed bioinformatics analysis to determine if OpaR and/ or AphA bind to osmotic stress response gene clusters.

**Table 22 Putative binding sites in the Ectoine biosynthesis regulatory region identified using the MOODS algorithm.** Start and End indicate number of base pairs upstream of the ATG start codon.

Protein	Ectoine promoter Binding Site Prediction						
	Binding (Yes/No)	Start	End	Log odds score	Odds	Probability	P-Value
OpaR	Y	166	147	3.691	40.100	0.976	0.003
		151	132	3.164	23.671	0.959	0.004
AphA	N						
BetI	Y	20	1	5.374	215.806	0.995	0.0005
		168	149	2.974	19.572	0.951	0.003
		50	31	2.966	19.420	0.951	0.003

**Table 23 Putative OpaR binding sites identified using the MOODS algorithm.**  
Start and End indicate number of base pairs upstream of the ATG start codon.

Gene		OpaR Binding Site Prediction						
		Binding (Yes/No)	Start	End	Log odds score	Odds	Probability	P-Value
VP1456	BCCT1	Y	107	88	0.826	2.284	0.695	0.009
VP1723	BCCT2	Y	184	165	1.786	5.963	0.856	0.008
VP1726	ProX	Y	275	256	3.893	49.046	0.980	0.002
			279	260	3.184	24.147	0.960	0.003
			75	56	3.254	25.892	0.963	0.003
			233	214	2.515	12.361	0.925	0.005
VP1905	BCCT3	Y	160	141	3.203	24.611	0.961	0.003
			141	122	3.252	25.853	0.963	0.003
			215	196	2.944	19.000	0.950	0.004
VP1906	CosR	Y	274	255	3.252	25.853	0.963	0.003
			255	236	3.203	24.611	0.961	0.003
			200	181	2.944	19.000	0.950	0.04
VPA0356	BCCT4	Y	112	93	2.550	12.807	0.928	0.004
			104	85	1.979	7.236	0.879	0.005
VPA1114	BetI	Y	36	17	6.651	773.712	0.999	0.0002
			213	194	2.819	16.756	0.944	0.003
			109	90	3.207	24.699	0.961	0.003
			505	486	2.159	8.660	0.896	0.005
VPA1115	BetB	Y/N	209	190	1.664	5.280	0.841	0.004
VIBHAR_BetI	VH_BetI	Y	598	579	7.822	2495.689	1.000	0.0001
			337	318	8.510	4962.128	1.000	0.0001
			36	17	6.263	524.775	0.998	0.0003
VP2516	OpaR	Y	146	127	9.942	20783.818	1.000	0.00001
			65	46	10.677	43329.978	1.000	0.00001

**Table 24 Putative Apha binding sites identified using the MOODS algorithm.**  
 Start and End indicate number of base pairs upstream of the ATG start codon.

Gene		Apha Binding Site Prediction						
		Binding (Yes/No)	Start	End	Log odds score	Odds	Probability	P-Value
VP1456	BCCT1	Y	41	22	2.928	18.690	0.949	0.0004
VP1723	BCCT2	Y	94	75	0.107	1.112	0.527	0.002
VP1726	ProX	Y	218	199	1.961	7.108	0.877	0.0007
VP1905	BCCT3	Y	192	173	2.416	11.199	0.918	0.0004
VP1906	CosR	N						
VPA0356	BCCT4	N						
VPA1114	BetI	Y	542	523	6.185	485.544	0.998	0.00006
VPA1115	BetB	Y/N	386	367	0.568	1.765	0.638	0.0008
VIBHAR_BetI	VH_BetI	N						
VP2516	OpaR	Y	98	79	18.230	82606588.563	1.000	2E-10

**Table 25 Putative BetI binding sites identified using the MOODS algorithm.**  
Start and End indicate number of base pairs upstream of the ATG start codon.

Gene		BetI Binding Site Prediction						
		Binding (Yes/No)	Start	End	Log odds score	Odds	Probability	P-Value
VP1456	BCC T1	Y	125	106	2.520	12.424	0.926	0.004
VP1723	BCC T2	N						
VP1726	ProX	Y	219	200	4.938	139.488	0.993	0.0006
			319	300	4.240	69.433	0.986	0.0009
VP1905	BCC T3	Y	192	173	2.238	9.375	0.904	0.005
VP1906	CosR	N	201	182	2.238	9.375	0.904	0.005
VPA0356	BCC T4	Y	46	27	2.935	18.820	0.950	0.003
VPA1114	BetI	Y	38	19	7.192	1328.825	0.999	0.00008
			245	226	3.527	34.038	0.971	0.002
			415	396	2.519	12.420	0.925	0.004
			305	286	2.059	7.836	0.887	0.005
VPA1115	BetB	Y/N	416	397	2.019	7.531	0.883	0.004
VIBHAR_BetI	VH_BetI	Y	38	19	6.915	1007.533	0.999	0.0001
			166	147	3.446	31.372	0.969	0.002
			236	217	2.544	12.729	0.927	0.004
			600	581	1.999	7.378	0.881	0.005

## Appendix H

### BACTERIOPHAGE f237 IS REGULATED BY QUORUM SENSING

RNASeq analysis revealed the genes of the f237 bacteriophage region were highly upregulated in the *luxO* mutant. Bioinformatics analysis revealed that OpaR binds upstream of orf 8 in the phage gene cluster (**Table 26**).

**Table 26 Putative OpaR binding sites identified using the MOODS algorithm.** Start and End indicate number of base pairs upstream of the ATG start codon.

ORF	RefSeq Definition	OpaR Binding Site Prediction						
		Binding (Yes/No)	Start	End	Log odds score	Odds	Probability	P-Value
VP1550	Hypothetical protein	N						
VP1561	Bacteriophage f237 ORF8	Y	44	25	6.017	410.227	0.998	0.0002
			32	13	3.139	23.090	0.958	0.002
			48	29	2.739	15.473	0.939	0.002
			137	118	2.110	8.250	0.892	0.003
			52	33	1.570	4.808	0.828	0.004
			148	129	1.400	4.056	0.802	0.004
			35	16	0.898	2.456	0.711	0.005

## Appendix I

### IMPORTANT *VIBRIO CHOLERAE* COLONIZATION FACTOR, GbpA DOES NOT PLAY A ROLE IN *VIBRIO PARAHAEMOLYTICUS IN VIVO* COLONIZATION

#### Introduction

*Vibrio parahaemolyticus* is Gram-negative marine bacterium and is the leading cause for seafood-related gastroenteritis worldwide (Joseph, Colwell, and Kaper 1982; Su and Liu 2007). Disease is caused by consumption of contaminated shellfish and typically results in nausea, vomiting, fever and diarrhea (Daniels 2000; Hondo et al. 1987; McLaughlin et al. 2005; Qadri et al. 2003). Inside the human host, *V. parahaemolyticus* the enterocytes lining the intestinal tract that serves as the primary attachment sites for the bacteria (Finn et al. 2013). The mechanism of how the bacteria adhere to these attachment sites and colonize their host is poorly understood. Studies *in vitro*, have implied the possible role of the mannose-sensitive haemagglutinin (MSHA) pilus and multivalent adhesion molecule 7 (MAM7) in adhesion and host colonization (Krachler, Ham, and Orth 2011; O'Boyle et al. 2013). Other *in vitro* studies also implicated the role of the type VI secretion system I in adhesion but this was shown not to be expressed at *in vivo* temperature of 37°C (Salomon et al. 2013; Yu et al. 2012).

Many pathogenic bacteria express proteinaceous surface adhesins that enable attachment to host mucosal surfaces in the respiratory, urinary or gastrointestinal tracts (Klemm and Schembri 2000). The mucus layer in mammalian intestines is composed mainly of a complex, high-molecular-weight glycoprotein called as mucin (Neutra 1987). Several enteric pathogens have been shown to adhere to mucin oligosaccharides (Moncada, Kammanadiminti, and Chadee 2003). In the *Vibrio* genus, mucin has been shown to act as receptor for the adherence of bacteria (Alam et al. 1997; Bhowmick et al. 2008). *V. cholerae* has been shown to bind to N-acetyl-D-glucosamine (GlcNAc) residues in mucin (Bhowmick et al. 2008). Interestingly, GlcNAc, a monomer of chitin, forms a bulk of the sugars present in intestinal mucin (Moncada, Kammanadiminti, and Chadee 2003). *V. cholerae* expresses an adhesin designated as the GlcNAc-binding protein A (GbpA) that allows the bacteria to attach to the residues in mucin and thus acts as an important colonization factor in this bacterium (Bhowmick, Ghosal, and Chatterjee 2007; Bhowmick et al. 2008; Kirn, Jude, and Taylor 2005). A deletion mutant strain of *gbpA* in *V. cholerae* was defective in colonization of infant mice with a 6.3 fold reduction in colonization ability compared to the wild-type (Bhowmick et al. 2008). In *V. parahaemolyticus*, GbpA has been shown to be regulated by the surface sensing regulon which also regulates the type III secretion system 1, an important virulence factor in this bacterium (Gode-Potratz and McCarter 2011). Considering that the gene was being expressed along with other virulence factors, we hypothesized that *gbpA* might be an important colonization factor in *V. parahaemolyticus*.

Here we constructed a *gbpA* deletion mutant in *V. parahaemolyticus* and examined its role in *in vivo* colonization using the streptomycin pre-treated adult mouse model. Contrary to what we initially hypothesized, we found that the *gbpA* deletion mutant was not out-competed by the wild-type and thus implying no role of *gbpA* in colonization in our model.

## **Materials and Methods**

### **Bacterial strains, media and culture conditions.**

All the strains and plasmids used in this study are listed in **Table 27**. A streptomycin-resistant strain of *V. parahaemolyticus* O3:K6 clinical isolate RIMD2210633 was used throughout this study (Whitaker et al. 2012; Whitaker et al. 2010). For the *in vivo* competition experiment a  $\beta$ -galactosidase-positive strain of RIMD2210633, named WBWlacZ was used, which was previously shown to behave identical to wild-type *in vitro* and *in vivo* (Haines-Menges, Whitaker, and Boyd 2014; Whitaker et al. 2012; Whitaker, Richards, and Boyd 2014). Unless stated otherwise, all *V. parahaemolyticus* strains were grown at 37°C with aeration in LB containing 3% NaCl (Fischer Scientific, Pittsburgh, PA) or M9 medium (Sigma Aldrich, St. Louis, MO) supplemented with glucose. For genetic manipulations, an *Escherichia coli* diaminopimelic acid (DAP) auxotroph  $\beta$ 2155  $\lambda$ pir was used. The *E. coli*  $\beta$ 2155  $\lambda$ pir strain was cultured in medium supplemented with 0.3 mM DAP (Sigma Aldrich). When required, antibiotics were added to the growth mediums at the following concentrations: streptomycin, 200  $\mu$ g/ml; chloramphenicol, 25  $\mu$ g/ml.

### **Construction of *V. parahaemolyticus* RIMD2210633 *gfpA* deletion mutant.**

An in-frame nonpolar deletion mutant of the *gfpA* gene (VPA1598) was constructed using splicing by overlap extension (SOE) PCR and homologous recombination (Horton et al. 1989) as previously described (Kalburge, Whitaker, and Boyd 2014). Primers were designed to the *gfpA* gene using the *V. parahaemolyticus* RIMD2210633 genome sequence as the template. All primers used in the study are listed in **Table 28**. A 75-bp truncated version of 1464-bp *gfpA* gene was obtained. The mutant was confirmed by PCR and verified to be in-frame by sequencing.

### **Motility and biofilm assays.**

Swarming motility assays for lateral flagella expression were performed using HI plates incubated at 30°C for 60 h. Biofilm formation was examined using the crystal violet assay with plates incubated statically at 37°C for 24 h.

### ***In vivo* competition assays.**

All experiments involving mice were approved by the University of Delaware Institutional Animal Care and Use Committee. Male C57BL/6 mice, aged 6 to 10 wk were housed under specific-pathogen-free conditions in standard cages in groups (4 per group) and provided standard mouse feed and water *ad libitum*. Streptomycin pre-treatment and inoculations were performed as previously described (Haines-Menges, Whitaker, and Boyd 2014; Whitaker et al. 2012; Whitaker, Richards, and Boyd 2014). Briefly, mice were fasted for 4 h and then administered 20 mg streptomycin per

animal orogastrically and then food and water were returned 24 h before bacterial inoculations by oral gavage. Water was returned immediately upon inoculation and food was returned 2 h post-infection. The *V. parahaemolyticus* strain used for *in vivo* experiments is the  $\beta$ -galactosidase knock-in designated WBWlacZ, which allows for a blue: white colony selection (Haines-Menges, Whitaker, and Boyd 2014; Whitaker et al. 2012; Whitaker, Richards, and Boyd 2014). Overnight cultures were diluted 1:50 with LB streptomycin media and grown for 4 h at 37°C with aeration. An aliquot of the 4 h culture was pelleted, washed in PBS and resuspended in fresh PBS to a final concentration of  $\sim 1 \times 10^{10}$  CFU/ml. A  $\sim 1 \times 10^{10}$  CFU/ml with a ratio of 1:1 CFU of mutant: WBWlacZ was used. Each inoculum was serially diluted and plated on LB plates to determine the administered dose. The mice were sacrificed 24 h post infection and the gastrointestinal tract was harvested in 8 ml of sterile PBS, homogenized mechanically, serially diluted and plated on LB plates containing 40 mg/ml X-gal at 37°C overnight. The competitive index (CI) was determined with the following equation:  $CI = \text{ratio out}_{(\text{mutant/wild-type})} / \text{ratio in}_{(\text{mutant/wild-type})}$ . A CI >1 indicates that the test strain has the ability to out-compete the wild-type strain, while a CI of <1 indicates that the test strain is less fit than the wild-type strain. An *in vitro* competition assay in LB was performed simultaneously with the *in vivo* assays using the same inoculum.

## Results and Discussion

### ***ΔgfpA* mutant behaves similar to wild-type *in vitro*.**

An in-frame deletion mutant of *gfpA* was constructed using SOE-PCR and homologous recombination. The mutant strain was grown under optimal growth conditions to demonstrate that deletion of the gene does not cause any overall growth defects. The mutant strain grew similar to wild-type in both LB and M9 minimal medium supplemented with glucose (**Figure 50A**). Next we performed *in vitro* characterization of the mutant, testing for motility and biofilm formation. The mutant showed similar motility profile to the wild-type on swarming plates (**Figure 50B**). The mutant also produced biofilm to same extent as wild-type (**Figure 50C**).

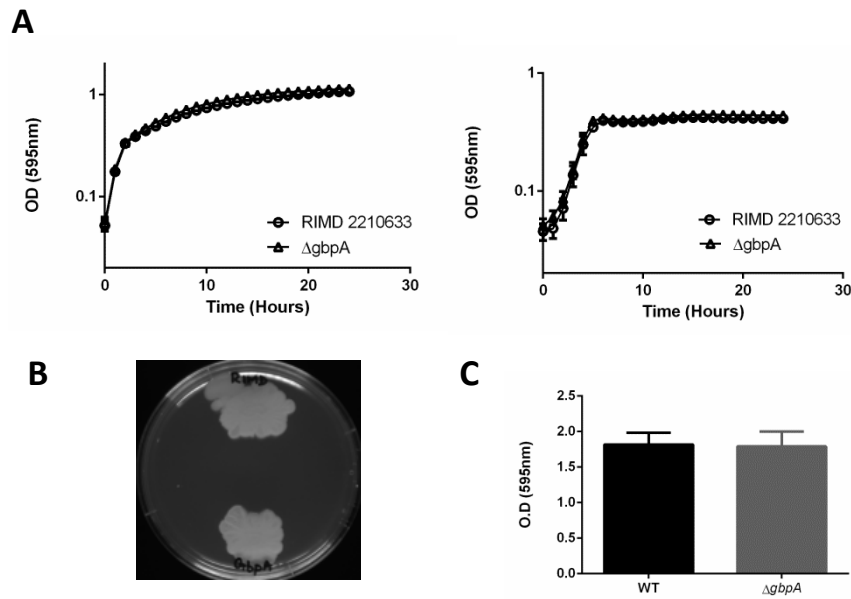


**Figure 50** *In vitro* characterization of the *gbpA* deletion mutant. (A) Growth in LB and M9 minimal medium supplemented with glucose (B) Swarming motility (C) Biofilm formation

**Deletion of *gbpA* does not cause any defect in *in vivo* colonization.**

GbpA has been shown to be a significant adhesin in *V. cholerae*. Deletion of *gbpA* resulted in a significant reduction in the ability of *V. cholerae* cells to colonize the intestine in a mouse model (Bhowmick et al. 2008). In a recent paper comparing expression of *V. parahaemolyticus* genes in LB and cecal fluid, *gbpA* was upregulated over 3-fold in cecal fluid suggesting a possible role of the protein *in vivo* (Livny et al. 2014). In order to determine if *gbpA* played a similar role as an adhesin in *V. parahaemolyticus*, we performed an *in vivo* competition experiment between the wild-type and the *gbpA* deletion mutant. Interestingly, we did not see any effect of the

deletion on *in vivo* colonization (**Figure 51**). The average *in vivo* competitive index was found to be 0.99. GbpA in *V. parahaemolyticus* shares a 70% amino acid homology with the *V. cholerae* GbpA. Interestingly, only 82% of the chitin binding domain is conserved between both proteins. It will be interesting to examine if this difference in amino acid content is contributing to the lack of an observable phenotype *in vivo*.

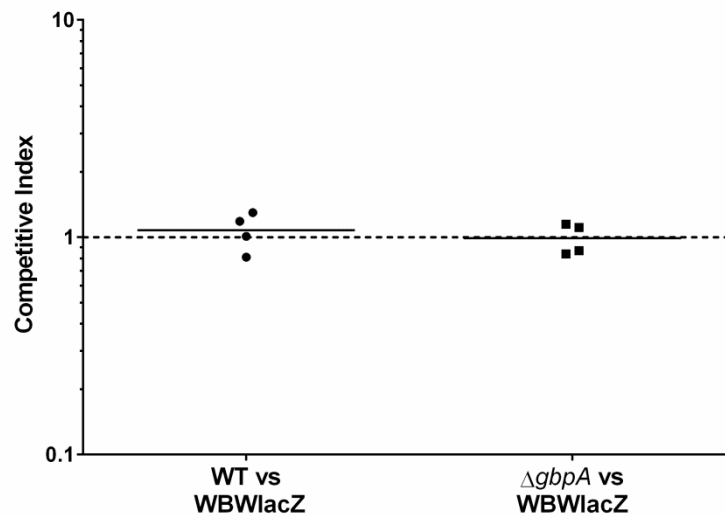


**Figure 51** *In vivo* colonization competition using streptomycin pre-treated adult mouse model. Competition assay was performed between  $\Delta gbpA$  and WBWlacZ.

## Conclusions

Chitin binding protein GbpA is an important colonization factor in *Vibrio cholerae*. Here for the first time, we demonstrate that in closely related species *V. parahaemolyticus*, GbpA does not seem to play any role in *in vivo* colonization. Our findings reveal that the loss of GbpA does not result in any observable growth defect in an adult mouse model of colonization. Interestingly, we found that the proteins share only 82% homology in the conserved functional domain between *V. cholerae* and *V. parahaemolyticus*.

**Table 27 Bacterial strains and plasmids used in this study**

Strain	Genotype	Reference
<i>Vibrio parahaemolyticus</i>		
RIMD2210633	O3:K6 clinical isolate, StrR	(Makino et al. 2003; Whitaker et al. 2010)
WBWlacZ	RIMD2210633, StrR, lacZ	(Whitaker et al. 2012)
SSKA1598	RIMD2210633 $\Delta gbpA$ (VPA1598)	This study
<i>Escherichia coli</i>		
$\beta 2155 \lambda_{pir}$	$\Delta dapA::erm$ pir for bacterial conjugation	
$\beta 2155 \lambda_{pir} \Delta gbpA$	$\beta 2155 \lambda_{pir}$ containing pDS132 $\Delta gbpA$	This study
Plasmids		
pDS132	Suicide plasmid; CmR; SacB	(Philippe et al. 2004)
pDS132 $\Delta gbpA$	pDS132 harboring truncated <i>gbpA</i> (VPA1598)	This study

**Table 28 Primers used in this study**

<b>Primer</b>	<b>Sequence (5' – 3')</b>	<b>T<sub>m</sub></b>	<b>Product Size (bp)</b>
SOEVPA1598A	TCT AGA CAC TTC CCC CTC ATC AGT GT	61	485
SOEVPA1598B	GGC AAC GAG CGA TTT ATT A	50	
SOEVPA1598C	TAA TAA ATC GCT CGT TGC CAC AGG CTC ACA CTG GGA AAT	67	456
SOEVPA1598D	GAG CTC ACA TCA CGG TTG TGC TAT CG	61	
SOEVPA1598FLF	AAT GTC ACG GCA AAC ATT CA	53	3114
SOEVPA1598FLR	TGA TTT TGC GAT TGG TGT GT	53	

## Appendix J

### CHARACTERIZATION OF *VIBRIO PARAHAEMOLYTICUS* TYPE 6 SECRETION SYSTEM MUTANTS *IN VITRO* AND *IN VIVO*

Work in this appendix examines mutant strains of the T6SSs in *V. parahaemolyticus*. The T6SS effector protein mutants,  $\Delta hcp1$ ,  $\Delta hcp2$  and  $\Delta hcp1\Delta hcp2$ , were constructed by the Orth laboratory in the POR1 ( $\Delta tdhA5$ ) background of the canonical strain RIMD2210633 (Salomon et al. 2013). Growth analysis of the strains demonstrated that the T6SS double mutant,  $\Delta hcp1\Delta hcp2$  exhibited a significant defect in minimal media supplemented with mouse intestinal mucus (**Figure 52**). An *in vitro* competition assay between the T6SS double mutant and the WBWlacZ strain resulted in the double mutant being out-competed by the wild-type with an average CI of 0.49 (**Figure 53**). An *in vivo* persistence colonization competition assay between the T6SS double mutant and the WBWlacZ strain yielded inconclusive results from five mice. No T6SS double mutant colonies were recovered from the mice. The T6SS system is an antibacterial system that has been shown in *V. parahaemolyticus* to be involved in intra-species virulence (Salomon et al. 2013). We suspect that the wild-type strain is virulent towards the double mutant in a competition experiment resulting in the double mutant being out-competed by the wild-type. It will be interesting to repeat the *in vivo* assay as a single inoculum instead of a competition to understand the role of T6SSs in *V. parahaemolyticus in vivo* colonization.

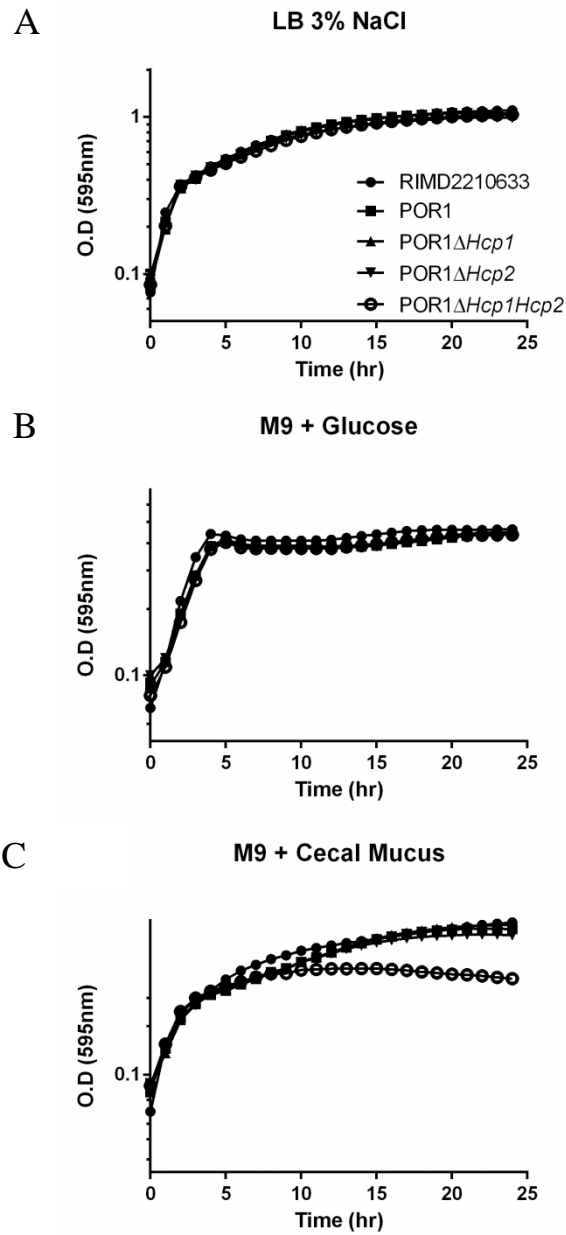


**Figure 52** Growth analysis of the T6SS mutants in (A) LB 3% NaCl (B) M9 minimal media supplemented with 10mM glucose and (C) M9 minimal media supplemented with 30  $\mu$ g/ml cecal mucus

*In vitro* competition assays in LB

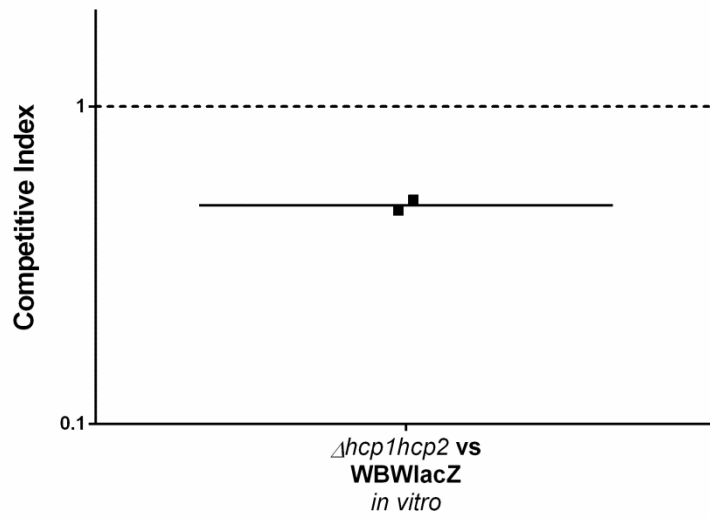


**Figure 53** *In vitro* colonization competition assay between  $POR1\Delta hcp1\Delta hcp2$  and  $WBWlacZ$

## Appendix K

### RNASEQ ANALYSIS STEP-BY-STEP PROTOCOL

#### **Before Sequencing**

RNaseq experiments should be typically performed with 3 biological replicates (or at least 2 biological replicates). It is advisable to perform two technical replicates for each RNA library. Review these papers while designing the experiment and deciding on the number of replicates.

“RNA-seq differential expression studies: more sequence or more replication?” - Liu et al 2013

“A survey of best practices for RNA-seq data analysis” - Conesa et al 2016

**RNA Isolation** – If following the Trizol extraction method make sure to read all of the manufacturer’s guidelines before performing the procedure. Always read notes provided by manufacturer for troubleshooting problems.

Prior to Ribozero rRNA depletion ensure that you have retained enough DNase treated RNA for cDNA synthesis. This RNA can be used for validations of your sequence data.

Also ensure that you retain some Ribozero treated RNA for additional cDNA synthesis for further validation.

#### **After Sequencing**

Immediately after completion of sequencing, ensure that you have obtained all the information from the Sequencing core about the Kits used for clustering, library preparation, and sequencing. Make note of the chemistry and protocol followed. This information is essential to publish the data and also to make comparisons to past or future RNASeq experiments.

### **RNASeq data analysis**

#### **Step 1: Obtaining the sequence file**

Download the file ilab solutions. Usually is a compressed folder containing fastq files as tarballs (.tar.gz). Decompress the tarball to get the fastq files (.fastq).

The .fastq file is the short-read sequence data obtained from the Illumina sequencing.

#### **Step 2: Checking quality of the sequences**

We check the quality of the fastq sequence file using the FastQC tool. This tool is available to be downloaded as on Java Runtime Environment with a simple UI.

Download link for FastQC:

[\(http://www.bioinformatics.babraham.ac.uk/projects/fastqc/\)](http://www.bioinformatics.babraham.ac.uk/projects/fastqc/)

FastQC is a quality control tool for high throughput sequence data.

Below are the important parameters to observe in the FastQC report to assess the quality of the sequencing output:

Per base sequence quality: Quality scores should be high throughout the sequence length. > 20 is considered good quality. Poor quality read positions can be trimmed in the next step and the positions should be noted.

Per sequence quality score: The sequence reads should form a tight distribution of high quality (Just one peak should be seen)

Per base sequence content: An even distribution of all four bases (A, T, G, C) without any bias for a particular base.

Sequence duplication levels: Indicates uniqueness of sequences in the library. Ideally < 10% duplication needs to be seen for the sequencing file, indicating highly unique sequences. But duplication levels will often times be really high and you will need to observe the next parameter to understand this.

Overrepresented sequences: Sequences that occur multiple times in the library are listed. The program checks to see if the sequence is a known contaminant such as an “Illumina primer”. If not the possible source will list “No Hit”. Although time consuming and laborious, copy all overrepresented sequences into an excel file and blast to the genome to make note of the gene that the sequences hit. The high expression of the particular gene will be determined by the end of the analysis. We can then conclude if the gene is truly “highly expressed” or if this overrepresentation is an artifact of the sequencing process.

Make note of all discrepancies such as poor quality bases, location of these bases and overrepresented sequences.

### **Step 3: Adapter clipping and quality trimming using FastX toolkit**

**Input:** Raw .fastq file

**Output:** .fastq file that is trimmed for quality and devoid of adapter sequences and poor quality reads. This file is then used to map to reference

The FASTX-Toolkit is a collection of command line tools for Short-Reads

FASTA/FASTQ files preprocessing. ([hannonlab.cshl.edu/fastx\\_toolkit/](http://hannonlab.cshl.edu/fastx_toolkit/) )

Based on our FastQC report above we will use the following tools to process our fastq files

FASTQ Clipper – Removes Illumina Sequencing adapters

FASTQ Trimmer – Shortening reads to remove barcodes/ bad quality bases/ noise

FASTQ Quality Trimmer – Discards reads below specified minimum quality

Note: Parameters to be used for the above tools are decided based on the FastQC reports.

#### **Step 4: Mapping reads to reference**

**Input:** .fastq file and .fa file (reference fasta file)

**Output:** .sam file (alignment file)

Download the fasta file of the reference from the database. Available at

<http://bacteria.ensembl.org/index.html>

Save the fasta file in the same working directory as the fastq file.

We use the BWA (Burrows-Wheeler Aligner) software package for mapping against the reference.

<http://bio-bwa.sourceforge.net/>

Mapping using BWA results in a Sequence Alignment Map (SAM) file which will be used to generate read counts for genes.

#### **Step 5: Deduplication of SAM files**

If duplicate reads are a big concern from the FastQC report, we will remove the duplicate reads from our alignment file in this step.

First we will convert the SAM file (human readable) into the binary BAM format (for further computation) using SAMtools (<http://samtools.sourceforge.net/>)

**Input:** .sam

**Output:** .bam

Next we will remove duplicate reads using the MarkDuplicates tool from the Picard tools package (<http://broadinstitute.github.io/picard/>)

**Input:** .bam

**Output:** dedup.bam (deduplicated BAM file)

Convert the deduplicated BAM file to a SAM file using SAMtools

**Input:** dedup.bam (deduplicated BAM file)

**Output:** dedup.sam

### **Step 6: Obtaining raw read counts for genes**

Download the gtf for the reference genome from

<http://bacteria.ensembl.org/index.html>

The gtf (Gene Transfer Format) file contains information about gene structure such as position in the genome and strand information.

Raw reads are then obtained using a HTSeq python package using a Count tool.

<http://www-huber.embl.de/users/anders/HTSeq/doc/overview.html>

Raw read counts can then be saved onto an Excel file for further processing.

### **Step 7: Differential gene expression analysis**

DESeq2 - Estimate variance-mean dependence in count data from high-throughput sequencing assays and test for differential expression based on a model using the negative binomial distribution.

<http://bioconductor.org/packages/release/bioc/html/DESeq2.html>

**Other analysis:**

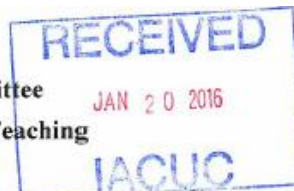
Functional analysis using Blast2GO – Using gene ontologies to identify functional gene systems that are differentially expressed. (<https://www.blast2go.com/>)

RNA-Rocket – RNA-Seq analysis meant for bacterial pathogens.

(<http://rnaseq.pathogenportal.org/>)

**Appendix L**  
**ANIMAL WORK APPROVAL**

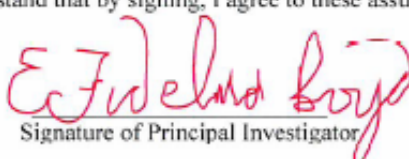
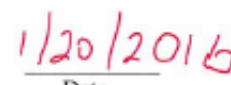
University of Delaware  
Institutional Animal Care and Use Committee  
Application to Use Animals in Research and Teaching



Title of Protocol: <b>Studies of <i>Vibrio species</i> pathogenesis</b>	
AUP Number: 1169-2016-0	← (4 digits only — if new, leave blank)
Principal Investigator: <b>Dr. E. Fidelma Boyd</b>	
Common Name: Mouse	
Genus Species: <i>Mus musculus</i>	
Pain Category: <i>(please mark one)</i>	
<b>USDA PAIN CATEGORY: <i>(Note change of categories from previous form)</i></b>	
<b>Category</b>	<b>Description</b>
<input type="checkbox"/> B	Breeding or holding where NO research is conducted
<input type="checkbox"/> C	Procedure involving momentary or no pain or distress
<input type="checkbox"/> D	Procedure where pain or distress is alleviated by appropriate means (analgesics, tranquilizers, euthanasia etc.)
<input checked="" type="checkbox"/> E	Procedure where pain or distress cannot be alleviated, as this would adversely affect the procedures, results or interpretation

<b>Official Use Only</b>	
IACUC Approval Signature:	
Date of Approval:	3-1-16

**Principal Investigator Assurance**

1. I agree to abide by all applicable federal, state, and local laws and regulations, and UD policies and procedures.
2. I understand that deviations from an approved protocol or violations of applicable policies, guidelines, or laws could result in immediate suspension of the protocol and may be reportable to the Office of Laboratory Animal Welfare (OLAW).
3. I understand that the Attending Veterinarian or his/her designee must be consulted in the planning of any research or procedural changes that may cause more than momentary or slight pain or distress to the animals.
4. I declare that all experiments involving live animals will be performed under my supervision or that of another qualified scientist. All listed personnel will be trained and certified in the proper humane methods of animal care and use prior to conducting experimentation.
5. I understand that emergency veterinary care will be administered to animals showing evidence of discomfort, ailment, or illness.
6. I declare that the information provided in this application is accurate to the best of my knowledge. If this project is funded by an extramural source, I certify that this application accurately reflects all currently planned procedures involving animals described in the proposal to the funding agency.
7. I assure that any modifications to the protocol will be submitted to by the UD-IACUC and I understand that they must be approved by the IACUC prior to initiation of such changes.
8. I understand that the approval of this project is for a maximum of one year from the date of UD-IACUC approval and that I must re-apply to continue the project beyond that period.
9. I understand that any unanticipated adverse events, morbidity, or mortality must be reported to the UD-IACUC immediately.
10. I assure that the experimental design has been developed with consideration of the three Rs: reduction, refinement, and replacement, to reduce animal pain and/or distress and the number of animals used in the laboratory.
11. I assure that the proposed research does not unnecessarily duplicate previous experiments. ( <i>Teaching Protocols Exempt</i> )
12. I understand that by signing, I agree to these assurances.   Signature of Principal Investigator   Date

**NAMES OF ALL PERSONS WORKING ON THIS PROTOCOL**

I certify that I have read this protocol, accept my responsibility and will perform only those procedures that have been approved by the IACUC.

Name	Signature
1. Dr. E. Fidelma Boyd	
2. Sai Kalburge	
3. Abish Regmi	
4. Nathan McDonald	
5.	
0. Click here to enter text.	
7. Click here to enter text.	
8. Click here to enter text.	
9. Click here to enter text.	
10. Click here to enter text.	
11. Click here to enter text.	
12. Click here to enter text.	
13. Click here to enter text.	
14. Click here to enter text.	

## Appendix M

### PERMISSIONS RIGHTS LINK

Permission for published work in Chapter 4 – “Complete genome sequence of *Vibrio parahaemolyticus* environmental strain UCM-V493.” published in Genome Announcements.

Exerpt from “Permissions and Commercial Reprints” section of the Journal

“Copyright of all material published in Genome Announcements remains with the authors. The authors grant the American Society for Microbiology a nonexclusive license to publish their work if it is accepted. Upon publication, the work becomes available to the public to copy, distribute, or display under a Creative Commons Attribution 4.0 International license.”

Permission for published work in Chapter 5 – “High-salt preadaptation of *Vibrio parahaemolyticus* enhances survival in response to lethal environmental stresses.” published in Journal of Food Protection.

Exerpt from “Copyright, Open Access and Permissions Policy” document of Journal

“Authors who wish to use their published paper in their thesis or dissertation may do so without requesting permission.”